# Applied Optics

September
1963

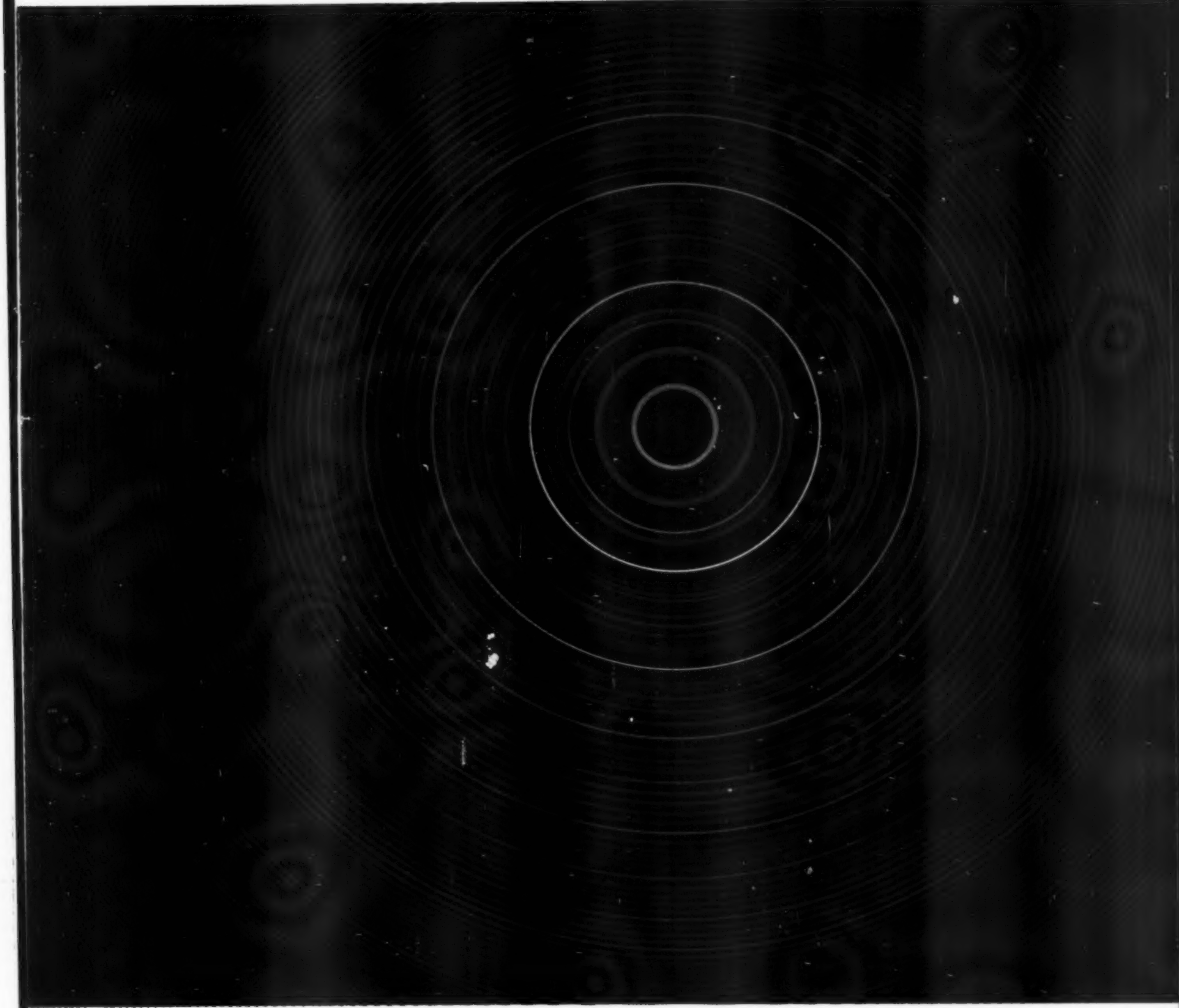

## SPECTROSCOPIC INSTRUMENTATION

Effective Jan. 1, 1965. All back issues and single copies are sold at $3.00 per copy.

*The Barnes*

**PEAC™ PHOTOELECTRIC AUTOCOLLIMATOR**

*for ultra-precise, automatic monitoring of angular position*

- Resolution better than 0.1 second of arc
- Repeatability better than 0.5 second of arc
- Angular measuring range of 1000 seconds
- Features both direct measurement and closed-loop control operation
- Available for single- or dual-axis operation
- Built-in visual alignment feature

CALL OR WRITE FOR BULLETIN 23-100

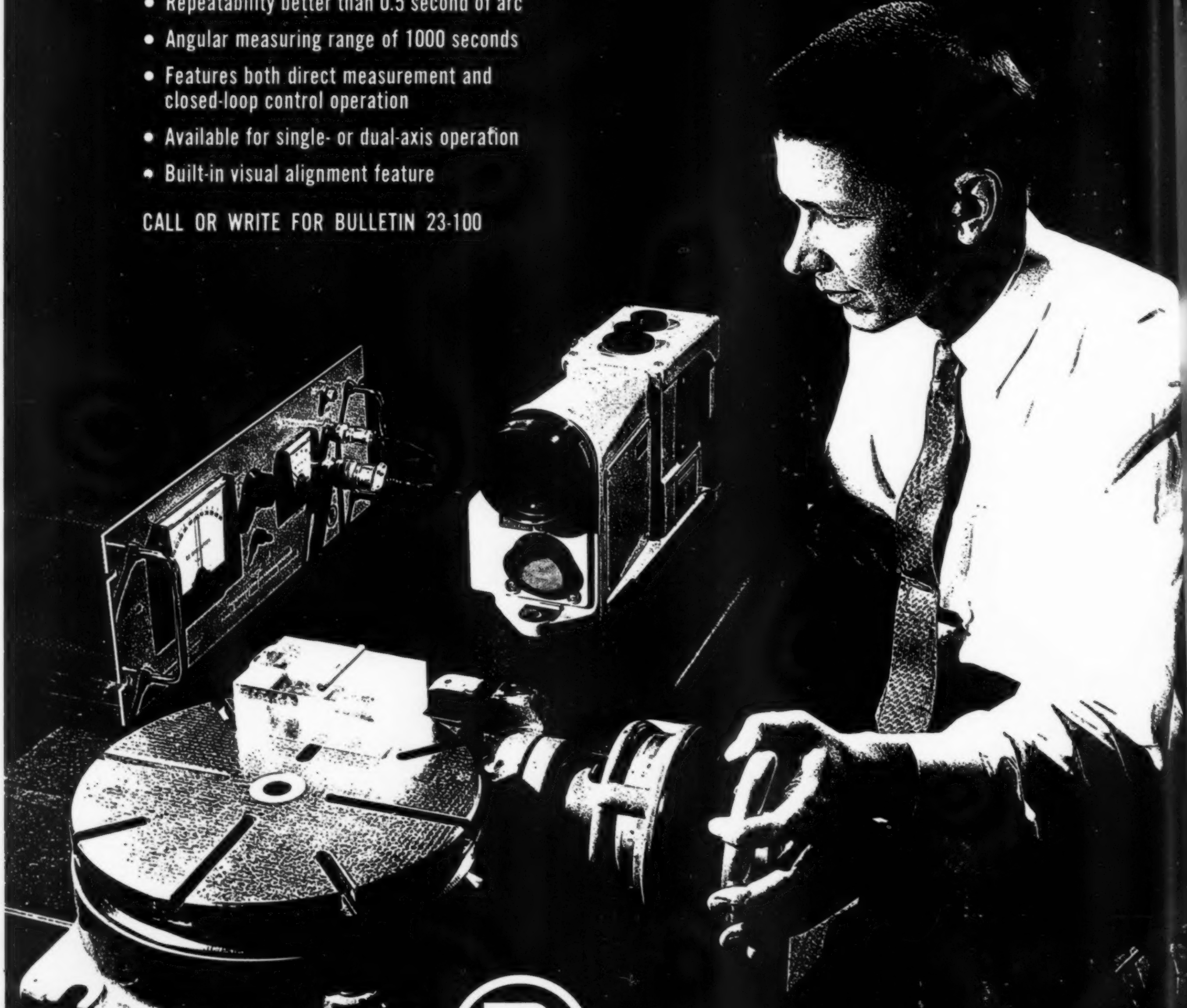

Barnes Engineering Company

Defense and Space Division

30 Commerce Road Stamford, Connecticut
Telephone: (203) 348-5381 TWX: (203) 327-0840

# Applied Optics

VOLUME 2
NUMBER 9
SEPTEMBER
1963

A monthly publication of the
Optical Society of America

**John N. Howard,** Editor

**Mary E. Warga,** Feature Editor

**Patricia R. Wakeling,** Managing Editor

**COVER:** Fabry-Perot etalon rings (Haidinger fringes) from a low-voltage cadmium arc, with a screen interposed to produce a uniform object field. If this were a moving picture and if the air pressure between the etalon plates were altered with the time, as in each etalon of the poly-etalon pressure-swept interferometric optical spectrometer, the ring diameters would change with the time, and light passing through a central aperture would yield a record of the spectrum. Spacer 10 mm. Camera $f$ = 80 mm. Picture by F. E. Barmore and F. L. Roesler © 1963 Design, Inc. Color reproduction through the generosity of Engis Equipment Company, Hilger and Watts Limited, and George W. Gates and Company.

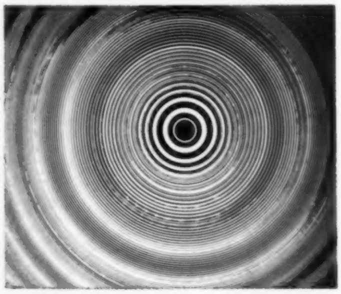

Published monthly by the Optical Society of America, Inc., in cooperation with the American Institute of Physics, at 20th and Northampton Streets, Easton, Pa. Editorial and advertising offices: 1155 16th St. N.W., Washington, D.C. 20036 202-Di7-4131 Supported in part by a grant from the National Science Foundation. Subscription rates: $6.00 to OSA members, $8.00 other AIP Societies' members; nonmembers and libraries: $10.00 per year. Single copies $2.00. Second class postage paid at Easton, Pa. © Copyright 1963 by the Optical Society of America.

873 **The PEPSIOS Purely Interferometric High-Resolution Scanning Spectrometer. I. The Pilot Model**—J. E. Mack, D. P. McNutt, F. L. Roesler, and R. Chabbal

887 **Infrared Transmission of the Atmosphere to Solar Radiation**—David M. Gates and Walter J. Harrop

899 **Microspectrophotometry**—J. J. Wolken and G. K. Strother

909 **Spectrographie Infrarouge à Haute Résolution: Application à l'Étude de Quelques Molécules Simples**—Ph. Arcas, C. Haeusler, C. Joffrin, C. Meyer, Nguyen van Thanh, and P. Barchewitz

919 **The Spectroscopy of Shock-Excited Powdered Solids**—R. W. Nicholls, W. H. Parkinson, and E. M. Reeves

931 **An Atomic Absorption Spectrophotometer**—Herbert L. Kahn and Walter Slavin

937 **Beer's Law and the Optimum Transmittance in Absorption Measurements**—Harold K. Hughes

947 **Absorption Coefficients of Krypton in the 600 to 886 Å Wavelength Region**—R. E. Huffman, Y. Tanaka, and J. C. Larrabee

955 **Performance of Curved Crystals in the Range 3 to 12 Å**—J. L. Jones, K. W. Paschen, and J. B. Nicholson

963 **Predisperser for High-Resolution Grating Spectrographs**—Joseph Reader, Louis C. Marquet, and Sumner P. Davis

969 **A Two-Wavelength Two-Frequency Ratio Recording Infrared Spectrometer Analyzer**—A. M. Bartz and H. D. Ruhl

## DEPARTMENTS

977 **Letters to the Editor**

**Far-Infrared Absorption of Ruby at Liquid Helium Temperature**—Armand Hadni

**Feasibility of a Reflector Coronagraph**—H. Zirin and G. Newkirk, Jr.

885 **Books**

946 **From the Editor**

962 **Meeting Reports**

973 **Of Optics and Opticists**

978 **Optical Activities in Industry**

ENGINEERS
SCIENTISTS

# Instrumentation for Nuclear Environmental Measurements

Throughout our career — dating back to the initial development of strobe flash technology by Messrs. Edgerton, Germeshausen and Grier at M.I.T. in the early Thirties — E G & G has pursued a broadening capability in pulsed energy.

Today, E G & G provides a full range of pulsed energy capabilities, embracing basic and applied research, components, instruments, integrated packages and entire systems.

Our capability spectrum ranges from projects ROVER, PLOWSHARE and VELA to underwater exploration, nucleonics and instrumentation, and a growing line of industrial products.

Pulsed light technology at E G & G is an area of immediate and long-range interest. Applications are being explored with range from reliable small boat distress signal lights to the potentialities of electronic flash systems for orbitai rendezvous. Comprehensive laboratory, testing and manufacturing facilities support and complete this capability.

Typically involved for the

## PHYSICIST and ELECTRO-OPTICAL ENGINEER are:

- Studies of physics and phenomenology of nuclear environments leading to the design and development of instrumentation utilizing photomultiplier tubes, photo tubes and solid state light measurement equipment and associated electronic recording apparatus.
- Problems relating to optical and electronic calibration devices and optical design as adjuncts to systems development.
- Utilization of optical darkroom techniques and technology including the use of spectrophotometers, standard light sources and narrow band interference filters.

## ELECTRONIC ENGINEERS

will find varied design problems relating to the fabrication and circuitry coupled with optical components for signal transmission and processing. Preferably, the Electronic Engineer will have a background in the design of:

- **Low-level recording schemes**
- **Photomultiplier circuits**
- **Photocell circuits**

You will have the opportunity to follow the design through systems development in our laboratories. You will also be directly involved in the operation of this equipment and the analysis and evaluation of the data brought forth.

*Respond in confidence*
*by mail to:*
*MR. SCOTT CARSON*

***EDGERTON, GERMESHAUSEN & GRIER, INC.*** EG&G

**95 Brookline Avenue • Boston 15, Massachusetts**

An equal opportunity employer

# *INTERFEROMETRIC CONTROL... KEY TO QUALITY LEADERSHIP*

## for Bausch & Lomb Certified Precision Diffraction Gratings

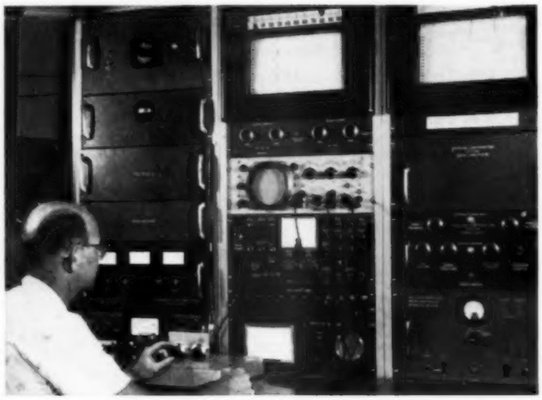

**EVERY STEP OF THE WAY** ... the testing of master grating blanks, coatings, groove shapes, diamond and grating carriage motion, and quality of masters and replicas ... is under the most rigid INTERFEROMETRIC control. You are assured of the highest precision standards and finest quality gratings you can buy. Since 1950, reliance on INTERFEROMETRIC control has been the key to the high resolving power, low ghosts and high efficiency which have made Bausch & Lomb Diffraction Gratings world famous ... and preferred by all major manufacturers of spectroscopic instruments.

There are 672 different sizes and types of plane reflectance, transmission and concave gratings that cover a range of wavelengths from 10A (x-rays) to $10^7$A (far infrared). We can also produce special types for your unusual requirements. Any size up to 200 x 350mm (8″ x 14″) is currently available. (Again, larger sizes can be obtained on special order.)

Our subterranean laboratory, built within layers of solid rock, offers stability, cleanliness and a unique capacity to supply gratings in even large quantities ... within reasonable delivery requirements.

Thirteen years of pioneering experience in developing and supplying gratings to astronomers, spectroscopists, instrument manufacturers, and other scientists has given Bausch & Lomb engineers the extensive knowledge and unequaled know-how that can assist you with your grating problems. Write to Bausch & Lomb Incorporated, 77145 Bausch Street, Rochester 2, N. Y., for the new Catalog D-261 for prices, uses, characteristics and details on the theory and mechanics of diffraction gratings ... it's the most comprehensive gratings catalog available anywhere.

**BAUSCH & LOMB**

In Canada, write Bausch & Lomb Optical Co., Ltd., Dept. 771, Scientific Instrument Division, 16 Grosvenor Street, Toronto 5, Canada

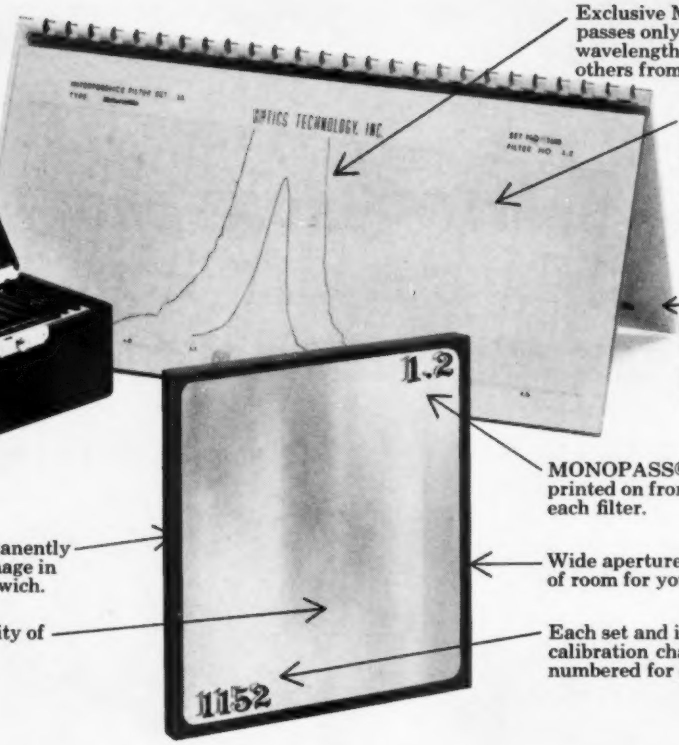

Every set of these filters comes in a leatherette felt-lined box.

Exclusive MONOPASS design passes only a narrow band of wavelengths, rejecting all others from X-band to X-ray.

Calibration charts assure pinpoint accuracy. Spectrophotometer traces include 10:1 scale expansion for each individual filter.

Each chart is laminated in heavy plastic and permanently bound into a rugged volume.

MONOPASS® wavelength printed on front side of each filter.

Coatings are permanently sealed against damage in durable glass sandwich.

Wide aperture gives you plenty of room for your experiments.

Excellent uniformity of transmission over entire surface.

Each set and its companion calibration charts are numbered for easy reference.

# CALIBRATED FILTER SETS FOR IMMEDIATE DELIVERY

## VISIBLE SPECTRUM SETS

5A/Four neutral density filters covering the entire visible spectrum, with density ratings of .5, 1, 2, and 3. Set comes complete with calibration tables. $95.

10A/Ten MONOPASS filters which isolate principal lines such as K, Ca, Hg, etc., from 404 to 706 millimicrons. Essential for flame chemical analysis. Four neutral density filters, a linear spectral "wedge" filter, and book of calibration charts are included. $395.

12A/Ten MONOPASS filters uniformly spaced from 400 millimicrons to 700 millimicrons, as well as four neutral density filters and a linear spectral "wedge" filter. Calibration charts are also included in price. $395.

*We also offer complete custom service for LASER technology. Reflectors to your specifications. Coatings on your substrates. We're at your service. Delivery normally within two weeks.*

## INFRARED SETS

15A/Ten MONOPASS filters spaced 0.1 micron apart between 0.8 and 1.7 microns. Individually drawn calibration charts accompany each boxed set. $450.

20A/Ten interference filters on 1" diameter substrates, mounted in convenient plastic holders, spaced at every 0.1 micron between 1.8 and 2.7 microns. Complete calibration charts included. These filters are blocked past 3.2 microns (lead sulphide cut-off) on the long end and to X-ray on the short end. $450.

## PLUS: RUBY LASER SET 50A

This specially designed set includes seven all-dielectric mirrors and beam-splitters at several values of attenuation. Each is designed and manufactured to withstand high LASER energies without deterioration. Also included are a MONOPASS filter at 694 millimicron ruby wavelength and complete calibration chart for set. $395.

**R&D positions available for scientists and engineers in classical and modern optics. Contact Personnel Department.**

**OPTICS TECHNOLOGY, INC**

248 HARBOR BOULEVARD
BELMONT, CALIFORNIA
LYtell 1-0358 (AC 415)

For additional information, write OTI or your nearest OTI representative: New England, H. J. Schuft Co.; New York, Metropolitan: E. C. Smith and Assoc.; New York, Upstate: E. W. Stone Co.; Mid-Atlantic: C. E. Snow Co.; So. California: Abbott Instrument & Engineering; Southwest & Mountain States: Southwestern Engineering & Equipment Co.; Europe: HVL, Brussels; Other export: Henley and Co., New York, N. Y.

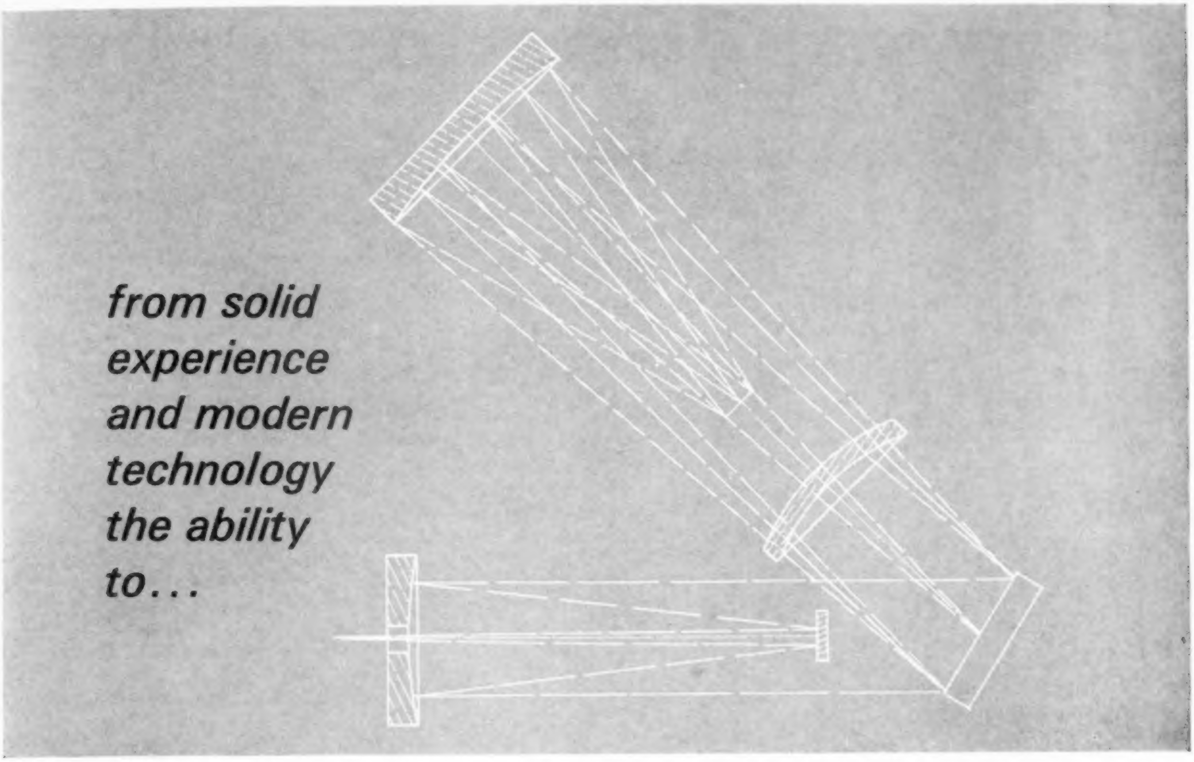

# SOLVE YOUR OPTICS PROBLEMS

Modern electronic computer techniques have made it possible to simulate an optical system in every detail. Multiple ray traces produce a spot diagram from which energy distribution for a spot anywhere in the image surface may be derived. Bolometric energy distribution over a wave length region of interest can be calculated and the contribution due to a particular aberration identified. All this (and a great deal more) is accomplished with our IBM 1620, with amazing rapidity and accuracy.

We, also, are currently engaged with several other firms in a co-operative endeavor to develop a program for the 7090 which will automatically optimize the optical parameters for over-all system performance. The first stages of the program have been tested successfully and completion is scheduled for the near future.

Sounds marvelous? It is – but – machines have no imagination, no experience in "working" glass, no knowledge of what makes a practical optical system. Such things are for men.

In the hands of a man with skill and imagination even a desk calculator produced results, slowly to be sure, by modern standards, and with greater approximation. Today's powerful mathematical machines have multiplied his efforts a thousand fold and made possible a degree of accuracy and sophistication unforeseen a few years back.

The attributes peculiar to the man, imagination, skill, experience are now more necessary and valuable than ever.

Perhaps you have need for the talents of our optical design and engineering staff. We will be happy to tackle your systems or instrumentation problem . . . U-V, I-R, or anywhere between.

We can do the whole job from design to a complete prototype instrument, if you like.

**The experience, imagination, skill, and talents of our staff are at your service at all times. For consultation or quotation, write, wire or telephone: DIRECTOR OF RESEARCH . . .**

FERSON OPTICS, INC.
P. O. BOX 398 / OCEAN SPRINGS, MISSISSIPPI
TELEPHONE 875-5422 (Area Code 601)

OPTIC SYSTEMS FOR AMERICA'S FUTURE

# spectroscopy

**ANALYSIS INSTRUMENTATION 1963**

edited by Dr. L. Fowler, R. D. Eanes, and T. J. Kehoe

An expertly written book drawing upon the skills of leaders in analytical and process instrumentation to present an up-to-the-minute picture of the current state of development of this fast-growing field, including a number of startling new instruments and systems never before reported. *272 pages, $12.50*

**IR – THEORY AND PRACTICE OF INFRARED SPECTROSCOPY**

by Dr. Herman A. Szymanski and Dr. Nelson L. Alpert

A unique text providing complete coverage of all aspects of infrared spectroscopy, from basic theoretical principles to the very latest practical applications. The instrument chapter, written by Dr. Alpert, deals with general principles of IR instrumentation applicable to present and future developments. The text, amply supplemented by illustrations, charts, and all-new high-resolution spectra, includes a chapter devoted to "The Spectral Library" describing documentation, abstracting and reference services. *300 pages, $10.00*

**INFRARED BAND HANDBOOK**

by Dr. Herman A. Szymanski, Chairman, Chem. Dept., Canisius College

Over 8500 band positions of organic and inorganic compounds tabulated according to wavenumber of their IR spectral absorption bands. Data retrieval time is cut since all compounds with absorption at a given wavelength are listed sequentially, and the formula cross index lists all bands produced by compounds. Completely referenced. Sample pages upon request.

*approx. 500 pages, $35.00; annual supplements, $7.50*

**DEVELOPMENTS IN APPLIED SPECTROSCOPY, Volumes 1-3**

*Proceedings of the Annual Mid-America Spectroscopy Symposia sponsored by the Society for Applied Spectroscopy*

A convenient and comprehensive guide to the latest research and developments in the field. Complete contents upon request.

Volume 1: edited by W. D. Ashby, Picker X-Ray Corp. *270 pages, $9.00*

Volume 2: edited by J. R. Ferraro, Argonne National Laboratory, and J. S. Ziomek, Martin-Marietta Corp. *448 pages, $16.00*

Volume 3: edited by J. E. Forrette and E. Lanterman, Borg-Warner Corp. *in preparation*

**PROGRESS IN INFRARED SPECTROSCOPY, Volumes 1 and 2**

*Proceedings of the Annual Infrared Spectroscopy Institutes, Canisius College*

Volume 1: Instrumentation (*all* spectral regions) and instrument design; group theory; analytical applications of UV, visible, near-IR absorption spectroscopy; inorganic IR spectroscopy; high-resolution instrumentation; KBr disk techniques; quantitative analysis; Raman spectroscopy; incorporation of NMR spectroscopy into the IR laboratory. Includes all discussions and a very extensive bibliography. *452 pages, $16.00*

Volume 2: Compact, expert surveys of specialized phases of contemporary spectroscopic methods: Far infrared, Raman, polarized infrared, inorganic infrared, near infrared, ultraviolet and visible, theoretical, instrumentation. *in preparation*

**INTERPRETED INFRARED SPECTRA**

prepared by Dr. Herman A. Szymanski

Some 300 IR spectra of all common classes of organic compounds have been marked to identify the structural groups causing typical absorption peaks. Of wider application than correlation tables, as interfering and related bands can be seen at a glance. *est. 150 pages, about $7.50*

**RESEARCH ON SPECTROSCOPY AND LUMINESCENCE**

A series documenting original research carried out at the P.N. Lebedev Institute of Physics, Acad. Sci. USSR. Extensive bibliographies. Translated from Russian.

1. Calculation of Wave Functions and Oscillator Strengths of Complex Atoms, by L. A. Vainshtein. *50 pages, $12.50*
2. On the Broadening and Shift of Spectral Lines in the Plasma of a Gaseous Discharge, by M. A. Mazing. *66 pages, $15.00*
3. On Excitation Spectra in Spark Discharges, by N. K. Sukhodrev. *52 pages, $12.50*
4. The Radioluminescence Yield of Organic Substances, by Z. A. Chizhikova. *50 pages, $12.50*

*special set price (parts 1-4): $40.00*

further information and complete catalogs on request

**PLENUM PRESS** 227 West 17th Street, New York 11, New York

Professor Arthur Schawlow of Stanford University, with W. E. Bell of Spectra-Physics, evaluates the Model 130 CW gas laser as an educational tool.

## COMPACT LASER FITS MOST BRIEFCASES, MOST BUDGETS

When you compare the Model 130 with other CW gas lasers — our own Models 112 and 115 included — you may wonder how it is possible to get so much laser into so small a package (approx. 10 lbs., 13″ long) at such a reasonable cost ($1525).

Part of the secret is that the Model 130 is d-c excited and self-contained; it operates without the need for a bulky r-f power source. But equally significant is the fact that Spectra-Physics has developed, through the experience of making almost all the commercial CW gas lasers now in use, the ability to make them smaller and less costly without sacrificing quality.

Designed for the lecture platform and the laboratory, the new Spectra-Physics Model 130 gas laser generates a 6328Å beam of coherent light in the confocal configuration. With it you can perform all the important classical optical experiments. In addition, the Model 130 affords you a capability not available in any laser of comparable price: the ability to operate in the hemispherical configuration, providing complete spatial coherence in a single phase wavefront.

**ONE YEAR WARRANTY.** When you buy a Spectra-Physics Model 130, (or a model with more sophisticated performance capabilities for advanced laboratory work), you can expect it to serve you well. To insure sustained performance, every laser we make is backed, plasma tube included, by a full year's warranty. Write for details on Models 130, 115, and 112. Address us at 1255 Terra Bella Ave., Mountain View 5, Calif. (or call collect [415] 961-2550).

Spectra-Physics

**OPTOmechanisms'** / **OPTO WAVE DIGITIZER**

*automatic measuring interferometer for distances and angles*

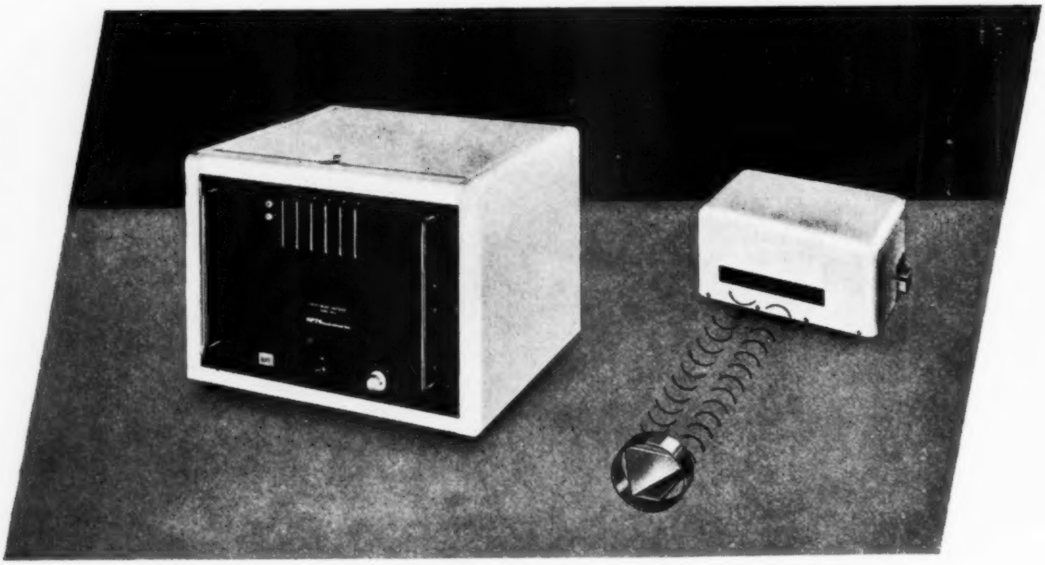

The OPTO WAVE DIGITIZER is an automatic measuring interferometer . . . a device utilizing light waves as a standard of measurement. The instrument is capable of measuring angles to 0.05 seconds and distances to 0.1 micron. The simplicity of its automated visual digital readout when used with machine tools, measuring tables, and inspection-test equipment, will reduce measuring time to fractions of conventional methods.

In Photographic Interpretation on film for data reduction to computers, the automatic readout may be recorded on hard copy . . . punched tape . . . or punched card.

The measuring interferometer generates optical fringes . . . the number of which determines distance travelled.

A unique method of mounting the optics assures stability of measurement. The split phase, three photomultiplier detection produces highly accurate reversible sensing of fringes. The light waves are counted between the tetrahedral prism, mounted on the moving body whose location it is desired to determine, and the sensor. This exciting development opens the door to new concepts of measurement and unprecedented accuracy of angular and linear measurement.

OPTOmechanisms Inc.

**OPTOmechanisms Inc.**

ENGINEERS HILL, PLAINVIEW, L. I., N. Y. GE 3-8100
TWX: CODE 516 433 9690

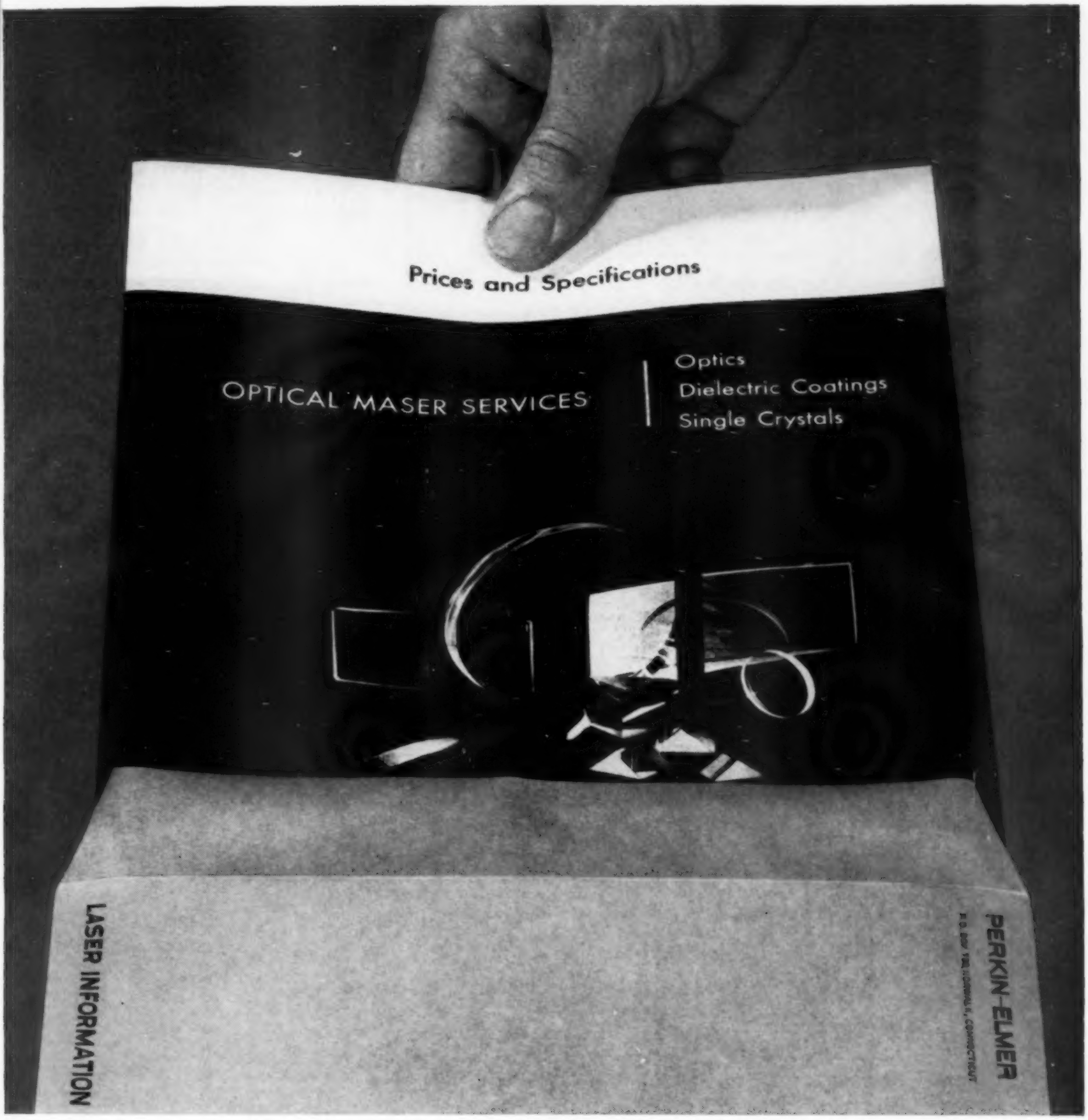

HANDY GUIDE TO
**OPTICS FOR LASERS**
WRITE OR PHONE FOR YOUR COPY

Here in one compact catalog you will find detailed specifications and prices on Perkin-Elmer's comprehensive optical maser services. Included are such data as coating transmission curves, material transmission characteristics and typical dimensional tolerances.

These and other products are available in quantity for research or production programs:

**Interferometer Flats** 1.0", 1.5" and 2.0" diameter. Surface: 1/10 to 1/200 wave. BK-7 or Quartz.

**Spherical Mirrors** 1.0", 1.5" and 2.0" diameter. 1M, 2M, 3M, 4M, 5M, 10M, 25M, 50M radius of curvature. BK-7 or Quartz.

**Windows** 1.0", 1.5" and 2.0" diameter. Standard or Brewster's angle. BK-7 or Quartz.

**Dielectric Coating** Durable, minimum loss, specified reflectivities for the full spectrum of laser research and development.

**Solid State Laser Materials** Tungstate, Molybdate, Sapphire, Garnet, Emerald, Fluoride, Glass.

**Special Optics** Trihedral and 90° prisms with deviation within 2 seconds.

**Gas Laser and Accessories** He-Ne laser with D.C. excitation. Compact, lightweight, suitable for laboratory research, military systems or industrial processes. Series V mounts accommodate complete line of adaptive optical accessories. Provides continuous wave, coherent, visible or IR output.

Please direct your request for "Prices and Specifications—Optical Maser Services" to Perkin-Elmer Corporation, Optical Maser Marketing, Norwalk, Connecticut. Phone (203) 847-0411

PERKIN-ELMER

**FROM**

1

**TINY SPECTROMETERS**

FIXED POSITION
RANGE 1,900A – 10,000A

**TO**

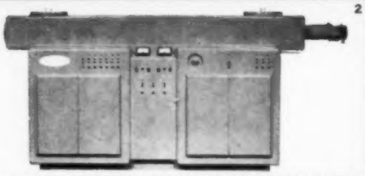

2

**LARGE LABORATORY INSTRUMENTS**

3 METER HIGH RESOLUTION SCANNING
MONOCHROMATOR CZERNY-TURNER
RANGE 1,000A – 6,000A*

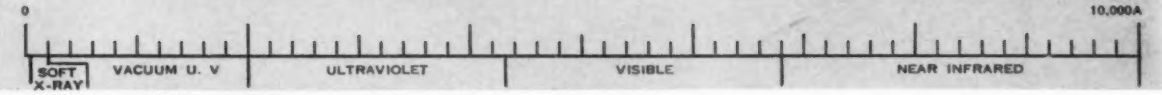

## McPherson offers a complete line of instruments to study the spectral range from soft X-ray to near infrared

3

.5 METER VACUUM U. V. SCANNING MONOCHROMATOR CZERNY-TURNER
RANGE 1,000A – 6,500A*

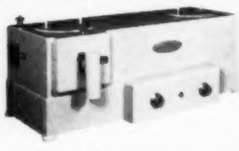

4

1 METER SCANNING MONOCHROMATOR CZERNY-TURNER
RANGE 2,000A – 10,000A*

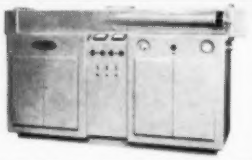

5

2 METER COMBINATION SPECTROGRAPH AND SCANNING MONOCHROMATOR, EAGLE
RANGE 300A – 6,800A*

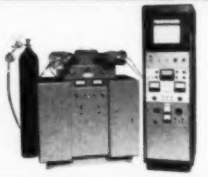

6

.5 METER SCANNING MONOCHROMATOR SEYA-NAMIOKA
RANGE 300A – 6,000A*

These instruments represent a partial list of the standard spectrometers manufactured by McPherson.

**The range and resolution of these instruments may be increased by interchanging gratings.*

7

NORMAL INCIDENCE ROCKET SPECTROGRAPH FIXED POSITION, RANGE 300A – 3,000A*

8

2 METER GRAZING INCIDENCE VACUUM U. V. SCANNING MONOCHROMATOR, ROWLAND CIRCLE
RANGE 50A – 2,000A*

9

1 METER SCANNING MONOCHROMATOR SEYA AND NORMAL INCIDENCE
RANGE 300A – 6,000A*

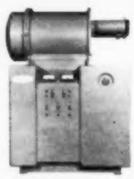

10

1 METER NORMAL INCIDENCE SCANNING MONOCHROMATOR ROWLAND CIRCLE, RANGE 300A – 6,000A*

11

1 METER NORMAL INCIDENCE SCANNING MONOCHROMATOR McPHERSON TYPE
RANGE 300A – 6,000A*

12

2 METER GRAZING INCIDENCE VACUUM U. V. SPECTROGRAPH, FIXED POSITION
RANGE 50A – 2,000A*

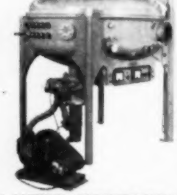

13

1 METER SPECTROGRAPH FIXED POSITION
RANGE 500A – 4,000A*

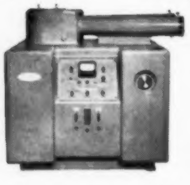

14

1 METER SCANNING MONOCHROMATOR SEYA-NAMIOKA
RANGE 300A – 6,000A*

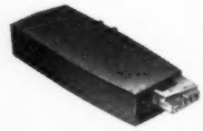

15

GRAZING INCIDENCE ROCKET SPECTROGRAPH
RANGE 50A – 2,000A*

We welcome the opportunity to quote on standard or special instruments designed to meet your exact needs, and recommend that you consult us early in your planning stage.

McPherson INSTRUMENT CORP.
530 MAIN STREET ACTON, MASS.
COlonial 3-7733

HORIZONTAL MICROMETER
FOCUSING LENS
IMAGE PLANE
BEAM SPLITTER
EYEPIECE
LAMP
FOCUSING ADJUSTMENT
OBJECTIVE LENS

# New dual-micrometer alignment telescope

**Kollmorgen Model K122 provides micrometer readings of two-plane displacements as small as 0.001-inch at distances up to 100 feet (0.0005-inch at closer ranges).**

**Exclusive linear optical micrometers** . . . for independently measuring vertical and horizontal displacements from line of sight . . . make the Model K122 more accurate than any other commercially available alignment telescope.

**Why so accurate?** Because a unique direct-coupled system is employed. It makes displacement of the instrument's line of sight exactly linear with displacement of the micrometer lenses. Results? Full instrument accuracy over the entire measuring range. No angular errors as with tilting plates. No tolerance build-up as with complex indirect mechanisms. No intersection errors between the two axes as with single-micrometer instruments.

**Virtually error-free focusing from zero to infinity** is another superior feature of the K122. Its focusing lens rides on precision ways. Line of sight is never displaced by refocusing as with conventional sliding tube arrangements.

**Wide adjustment range!** One revolution of each micrometer dial corresponds to a line-of-sight displacement of 0.025 inch. Total dial travel . . . 8 revolutions . . . spans the measuring range of ±0.100 inch.

**A versatile instrument!** In addition to providing displacement data for aligning and positioning applications, the Model K122 has autocollimator capabilities. An optional eyepiece with built-in light source adapts the instrument either for "finding" purposes or for measuring large angles in the auto-reflection mode.

**Informative 12-page bulletin** contains complete data on the Model K122 and other new Kollmorgen optical tooling instruments: Single and Dual-Axis Autocollimators, Dual-Axis Automatic Autocollimator, non-measuring Alignment Telescope, Pointing Interferometer, and all required accessories. Write to Director of Instrument Sales today for this bulletin, specifying whether you want early demonstrations.

K C
**KOLLMORGEN**
CORPORATION
NORTHAMPTON, MASSACHUSETTS

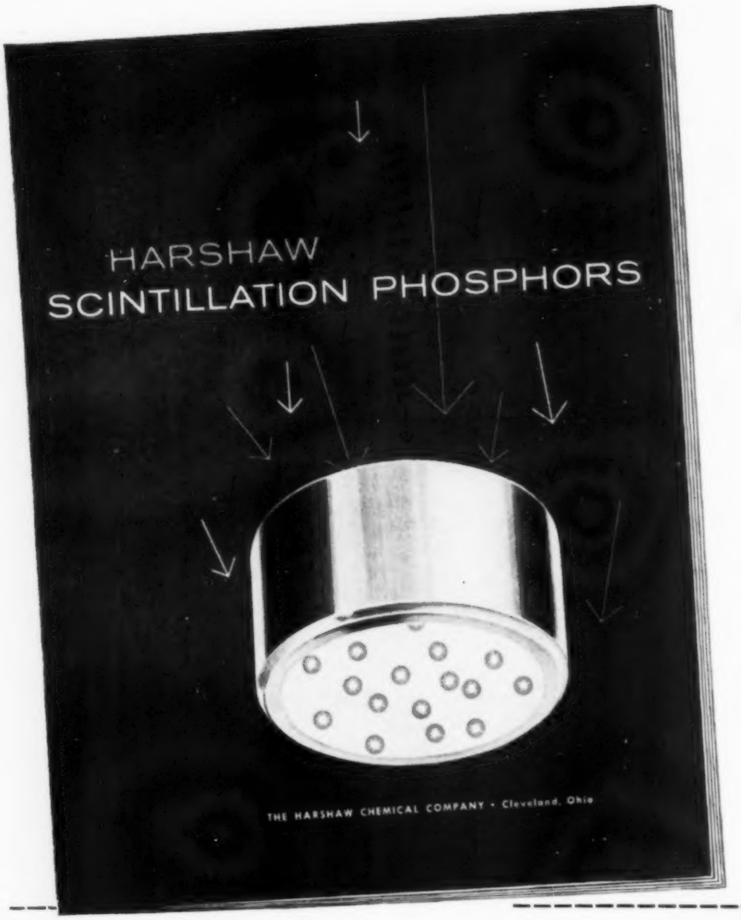
HARSHAW
SCINTILLATION PHOSPHORS
THE HARSHAW CHEMICAL COMPANY • Cleveland, Ohio

Write for this
free 56-page book

**HARSHAW SCINTILLATION PHOSPHORS**

Presents definitive article on characteristics and properties of scintillation phosphors with special emphasis on NaI(Tl). A general discussion of scintillation counting is augmented with many appropriate tables, efficiency curves, and typical gamma ray spectra. Gives specifications and drawings of Harshaw mounted phosphors, and lists miscellaneous other phosphors available from Harshaw. We will be pleased to send you a copy.

*Also available . . . Free 36-page book . . .*

**HARSHAW SYNTHETIC OPTICAL CRYSTALS**

Discusses in detail various Harshaw crystals used for infrared and ultra-violet optics. Includes many pertinent graphs. Ask for your copy today.

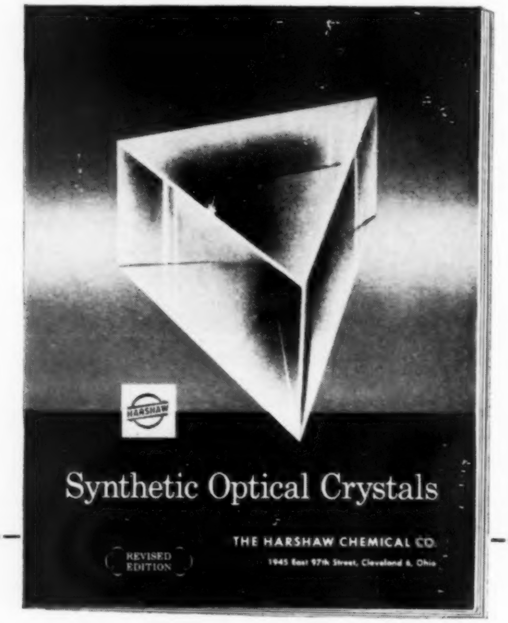
HARSHAW
Synthetic Optical Crystals
THE HARSHAW CHEMICAL CO.
1945 East 97th Street, Cleveland 6, Ohio
REVISED EDITION

CRYSTAL-SOLID STATE DIVISION
**THE HARSHAW CHEMICAL CO.**
1945 EAST 97th STREET • CLEVELAND 6, OHIO

# The PEPSIOS Purely Interferometric High-Resolution Scanning Spectrometer. I. The Pilot Model

J. E. Mack, D. P. McNutt, F. L. Roesler, and R. Chabbal

A description is given of the design principles, structure, and use of the PEPSIOS (trade mark) spectrometer, a versatile, easily portable, purely interferometric, high resolution short-range scanning instrument consisting essentially of an interference filter and several simultaneously pressure-swept Fabry–Perot etalons in series. In the study of a continuum, where it was necessary to isolate a single order, it has exhibited a luminosity $10^2$ as great as that of a comparable modern grating-etalon combination instrument at the same resolution and is considerably lighter, smaller, and mechanically more stable. Although designed primarily for the photoelectric measurement of the total flux through an axial zone, the instrument has the property of producing a two-dimensional spatially resolved image at high spectroscopic resolution.

## I. General and Historical

This paper describes the PEPSIOS* spectrometer, an instrument with a high luminosity-resolution product and a short but easily alterable scanning range, that utilizes an interference filter and several Fabry-Perot etalons to isolate its spectral passband. (In one sense the term "purely interferometric" in the title may be misleading: the essential all-interferometric property of the PEPSIOS instrument is its independence of grating and prism dispersion for blocking out neighboring spectral elements; it is convenient, however, to use sheet filters with chemical absorbers in order to eliminate the far side bands of the interference filter that may lie in regions passed by the lenses and windows and detected by the photomultiplier or other sensor.)

Many of the items of general principle, and some of the details, covered in this paper may be found in a fuller context in papers from Laboratoire Aimé Cotton[1-9] and from the Bellevue International Colloquium on Recent Progress in Interference Spectroscopy.[10]

### Interference Spectroscopy without Auxiliary Dispersion

Although pure interference spectroscopy is not new,[11] the high spectroscopic resolution characteristic of interference methods has always been achieved in series with prism or grating monochromators, except for a few instances[12-15] that we shall not try to list exhaustively.

### The Polyetalon

Years after the capability of the polyetalon for affording the combination of high resolution and great free spectral range (Sec. IIC) had been outlined in principle,[16] practical photographic spectroscopy with two interference units in series with a prism was introduced in 1917 by Houston[17] with two etalons and by Gehrcke and Lau[18] with two Lummer plates. A system of three etalons in series with a grating has been used by Series.[19]

### Vernier Spacing Ratios

Although in two-etalon spectroscopy one of the spacings has almost always been several times as wide as the other, it is well known[6] that a "vernier" ratio (a ratio of nearly unity) is just as useful in extending the effective free spectral range (Sec. IIC).

### Dielectric Multilayers

The recent emergence of transparent dielectric multilayers has made possible the production of etalons with transmittances unprecedentedly near to unity.

---

The authors are with the Department of Physics, University of Wisconsin, Madison, Wisconsin. R. Chabbal's permanent address is Laboratoires de Bellevue, Bellevue (Seine-et-Oise), France.

Received 16 February 1963.

This work was supported in part by a grant from the National Science Foundation and in part by the Research Committee of the Graduate School from funds supplied by the Wisconsin Alumni Research Foundation.

* Trade mark.

### Maximum Luminosity-Resolution Product

Although fair general quantitative comparisons are not easy to make among the different types of instruments, the luminosity-resolution product of an etalon with dielectric multilayer coatings is considerably greater than that of a comparable prism or grating[4] and is limited, not by the reflectance of the coatings, as in the case of metallic coatings, but by the flatness of the plates.

### Axial Fringe

Of the interference fringes of equal inclination (Haidinger fringes) produced by a pair of plane-parallel plates, it has been customary until recently, especially in photographic spectroscopy, to neglect the central fringe, that is, the light falling very near the axis where the dispersion increases without limit, and to measure the fringes for a few orders farther out. Following the work of Meissner,[20] the use of the central fringe, with the advantage of the simplicity of its axial disk geometry that makes it especially suitable for photomultiplier work, has become widespread.[2]

### Photoelectric Recording

From the time of the invention of the Fabry-Perot etalon[21] and the Lummer-Gehrcke plate[22] until quite recently, almost all interference spectroscopy was visual or photographic. In the past two decades, as a consequence of the remarkable enhancement in the sensitivity of photoelectric devices and especially photomultipliers, photoelectric recording has progressively usurped the place of photography in spectroscopy. Generally in photoelectric, unlike photographic, spectroscopy the spectral elements are sensed sequentially in time, or *scanned*. Photoelectric scanning spectrometers designed for the use of one or two etalons in series with a grating have recently been made and used successfully.[7,9,23]

### Pressure Scanning

Many systems have been used or proposed for the scanning of etalons,[10] including the movement of the plates by thermal expansion of the spacer,[24] electromagnetic attraction,[25] magnetostriction,[26] piezoelectricity, bellows action under pressure, and precision screw drives. Jackson and Kuhn[27] used the variation of the refractive index $n$ of the ambient gas by changing the pressure as a means of controlling the (static) optical path in polyetalon photographic spectroscopy. The extension of this means to pressure scanning, i.e., to varying the ambient gas pressure instead of the geometry of the etalon with the time, has been by far the simplest and most widely used scanning method. Pressure changes in a perfect gas effect the synchronous scanning of etalons and other dispersive elements.[28]

### Two-Dimensional Spatially Resolved Images

Whereas slit monochromators produce essentially one-dimensional images, a few devices with moderate spectral resolution, such as the interference filter and the Lyot filter, have been used to produce two-dimensional images that can be used directly, for instance, in spectroheliocinematography.

### The PEPSIOS Spectrometer

The PEPSIOS spectrometer is a high-resolution instrument incorporating, among others, all the properties listed at the heads of the foregoing nine paragraphs. For the pilot model described below it was decided to use three etalons and aim for an actual resolution with the moderate value of $3.5 \times 10^5$, in order to allow a direct comparison of properties between the PEPSIOS instrument and a Bellevue-type pressure-scanned instrument that has been used routinely with that resolution in both absorption and emission. The latter instrument consists of an Ebert-Fastie grating monochromator and one or two etalons, simultaneously pressure swept. The PEPSIOS spectrometer has turned out to be, by a considerable factor, the lighter, smaller, less expensive, mechanically more stable of the two. For the study of an absorption spectrum (in this case, the solar spectrum) the PEPSIOS instrument has been found to be superior in luminosity (cf. Sec. IIB) by a factor of the order of $10^2$; in the extreme case of an emission spectrum consisting of only a few lines, where the need for isolating a single order is less urgent or absent, the advantage may vanish.

A modified polyetalon, whose highest resolution member is a spherical Fabry-Perot[29] (not mentioned further in this paper), promises to be the ultimate instrument in the limit of very high resolution. No further improvement in luminosity-resolution product can be foreseen except through the gradual improvement in the quality of etalon surfaces and through the reduction of absorption in dielectric coatings.

## II. The Ideal Polyetalon

Here those aspects of the ideal polyetalon are treated that are requisite to the subsequent discussion of the PEPSIOS spectrometer.

### A. Properties of An Ideal Etalon

An ideal etalon may be defined as an etalon whose transmittance is given by the Airy function

$$\mathcal{A} = [1 + 4R(1 - R)^{-2}\sin^2(2\pi n l \sigma \cos\theta)]^{-1}, \qquad (1)$$

where $R$ is the reflectance of the coatings, $l$ the uniform spacing between (parallel, perfectly flat) plates, $n$ the refractive index of the medium between the plates, $\sigma$ the wavenumber of the incident light, and $\theta$ the angle of incidence. If $\mathcal{A}$ is plotted as a function of any one of the quantities $n$, $l$, $\sigma$, or $\cos\theta$, one obtains a regular series of peaks consisting of one peak whenever $2nl\sigma \cos\theta = m$, where $m$ is an integer called the *order*. In discussing an axial-fringe spectrometer, it is natural to consider $\mathcal{A}$ as a function of $\sigma$ only, with the other quantities fixed. In this case, the separation between peaks is the *free spectral range* $Q(n,\theta)$, where

$$Q(n,\theta) \equiv (2nl \cos\theta)^{-1}. \quad (2a)$$

For almost all purposes in the study of axial-fringe instruments, $\cos\theta$ is nearly 1 and $Q(n,\theta)$ may be replaced by the *nominal free spectral range* $Q$, where

$$Q \equiv (2l)^{-1}. \quad (2b)$$

The *half-intensity width* $\delta_{1/2}\sigma$, which may be loosely called the *resolving limit*, is the total width of a peak at half-intensity. The *finesse* $N$ is defined as

$$N \equiv Q/\delta_{1/2}\sigma. \quad (3a)$$

For an etalon with ideally flat plates, $N$ depends only upon the reflectance of the coatings and is called the *reflective finesse*, $N_R$, which can easily be shown from Eq. (1) to be

$$N_R = \pi R^{1/2}/(1 - R). \quad (3b)$$

The ratio of the maximum to the minimum transmittance is called the *contrast* $C$, which for perfectly flat plates is

$$C = (1 + R)^2/(1 - R)^2. \quad (4)$$

## B. The Etalon as a Spectrometer

If an etalon is illuminated by a broad monochromatic source, a system of rings is formed in the focal plane of a lens placed behind it. In order that it may be used as a spectrometer, the light bundle must be restricted in angular width by a diaphragm placed in the focal plane of the collimating or telescope lens and, in the general case of a heterochromatic source, a single order must be isolated by the restriction of the spectral range of the incident light to less than $2Q$ with the aid of an auxiliary monochromator, which may be an interference filter. For the present purpose, the aperture in the diaphragm is a hole centered on axis so as to restrict the bundle to an angular diameter $\beta$ about normal incidence, determined by the required resolution in Eq. (7).

This spectrometer is characterized by its resolution, luminosity, and filtrage.

The *theoretical resolution* $\mathcal{R}_t$ is obtained when $\beta \rightarrow 0$; under the assumption that the spectral range of the incident light is restricted by a rectangular function, it can be shown from Eq. (3) to be

$$\mathcal{R}_t \equiv \sigma/\delta_{1/2}\sigma = N_R\, \sigma/Q. \quad (5)$$

The *luminosity* $\mathcal{L}$ is a measure of the flux transmitted by the spectrometer from a source of unit luminance to the detector. For an etalon, it is[4]

$$\mathcal{L} = \tau S \Omega = \pi \tau S \beta^2/4, \quad (6)$$

where $S$ is the area of an etalon plate, $\tau$ a transmittance, and $\Omega( = \pi\beta^2/4)$, the solid angle of the bundle illuminating the etalon.

Clearly it is desirable that $\beta$ be as large as possible, so long as the resolution, which depends in a complicated way upon $\beta$ and $N$, is not seriously reduced. It was shown by Jacquinot[4] that a satisfactory compromise yielding $\mathcal{R} = 0.7\ \mathcal{R}_t$ is achieved by taking $\beta$ as the angular diameter of a ring, defined by its half-intensity points, with zero internal radius, i.e., of a disk. Then, since $\beta = 2\theta$,

$$\frac{1}{\mathcal{R}_t} = \frac{\delta_{1/2}\sigma}{\sigma} = \frac{\delta(\cos\theta)}{\cos\theta} = \frac{\theta^2}{2} = \frac{\beta^2}{8}$$

$$\beta = 2(2/\mathcal{R}_t)^{1/2}. \quad (7)$$

Equations (6) and (7), incidentally, illustrate the constancy of the luminosity-resolution product:

$$\mathcal{L}\mathcal{R}_t = 2\pi S\tau. \quad (8)$$

The *filtrage* $\mathfrak{F}$ (French, "f.f.i."[5]) of a spectrometer is a measure of the effectiveness of the instrument in isolating a spectral element from a continuous source and is defined as the ratio of the "useful" energy, $U$ (that is, the energy transmitted within the half-intensity width), to the total energy, $E$, received at the detector:

$$\mathfrak{F} \equiv U/E = \int_{\delta_{1/2}\sigma} T(\sigma)\mathcal{A}(\sigma)d\sigma \bigg/ \int_0^\infty T(\sigma)\mathcal{A}(\sigma)d\sigma, \quad (9)$$

where $T(\sigma)$ is the instrumental function of the auxiliary monochromator characterizing the spectral quality of the light passed from a white source. If $T(\sigma)$ is a rectangular function of width $Q$, then $\mathfrak{F} = 0.5$.[5] The definition of $\mathfrak{F}$ is in some degree arbitrary, through the arbitrary choice of $U$.

## C. The Polyetalon Spectrometer

### *Method of Isolation*

In order to make a spectrometer using only a small number, $M$, of etalons and one or more auxiliary sheet filters, it is necessary to put in series with an etalon (say, the widest spaced one), a train of $M - 1$ other etalons whose function is to isolate a single peak common to all the etalons by suppressing all the neighboring "parasitic" orders within the spectral range transmitted by the filter system comprising the coarse auxiliary monochromator.

If the effect of multiple reflection between etalons is negligible (but see Sec. IIIG) the transmittance $\mathcal{A}'(\sigma - \sigma_0)$ of the etalon train with spacings $l_1, l_2, \ldots l_M$ is the product of the transmittances of the individual etalons:

$$\mathcal{A}'(\sigma - \sigma_0) = \mathcal{A}_1(\sigma - \sigma_0)\mathcal{A}_2(\sigma - \sigma_0)\ldots\mathcal{A}_M(\sigma - \sigma_0), \quad (10)$$

where $\mathcal{A}_j(\sigma - \sigma_0)$ is the transmittance of an etalon with spacing $l_j$ adjusted to have a peak at $\sigma = \sigma_0$; thus the transmittance of the spectrometer as a whole is $\mathcal{A}'(\sigma - \sigma_0)$ times the transmittance of the filter system.

The isolation of a single order is accomplished by the judicious choice of spacing ratios in the etalon train. Since the contrast, Eq. (4), is always finite, the parasitic orders are never completely suppressed but are transmitted with the main peak as *ghosts*. The only ghosts that need to be given special attention are the stronger ones arising from the near coincidence of the peaks from two or more etalons. The occurrence and the suppression of ghosts are richly illustrated in Fig. 1 below.

### *Length of the Etalon Train*

The number of etalons needed to isolate a single order with a given resolution depends upon the finesse of the etalons and the resolution of the interference filter, $\mathcal{R}_f$. There is no exact theory, but it is approximately true that the resolution of an instrument can be increased[4] by a factor somewhat less than $N$, say about $N/2$, by the addition of an etalon of finesse $N$ to the optical train. Therefore, there must be a sufficient number, $M$, of etalons in the train to satisfy

$$(N/2)^M \gtrsim \mathcal{R}/\mathcal{R}_f. \tag{11}$$

With the practical values $N = 30$, $\mathcal{R}_f = 500$, Eq. (11) suggests that in the current state of the technology a train of two etalons should suffice for $\mathcal{R}$ values up to about $10^5$; three, to somewhat over $10^6$; and four, to about $2 \times 10^7$. (But notice that the shortness of the sweeping range reduces the usefulness of the instrument for work at low $R$, and that, as might be expected, a train of three or more etalons allows much greater freedom in the avoidance of ghosts than a train of two; so the two-etalon PEPSIOS instrument will probably not have much practical value except in very special circumstances.)

### *Resolution of a Polyetalon*

The resolution of a polyetalon spectrometer is of the same order of magnitude as that of the widest-spaced etalon in the train. However, because of the multiplication of Airy ordinates the actual resolution is increased by a gain factor that depends upon $M$ and the spacing ratios, and may be as high as 2 for a series of three etalons with nearly equal spacings (cf. Sec. IIID).

### *Luminosity of a Polyetalon*

The luminosity of a polyetalon, like that of a single etalon, is determined by Eq. (6). Therefore, the luminosity of an ideal polyetalon is the same as for a single etalon of the same resolving power. (In practice, however, the transmittance $\tau$ is considerably reduced; cf. Sec. IIIC.)

### *Filtrage of a Polyetalon*

While the filtrage for a polyetalon is defined in the same way as for a single etalon, the concept is subtler in the case of pure polyetalon spectroscopy. In the case of a single etalon it was calculated under the assumption that the free spectral range $Q$ was absolutely isolated, as by a monochromator with slits, so that there was no light incident on the etalon outside the free spectral range; in the case of a polyetalon it must be calculated taking into account the finite transmittance of the etalon everywhere. A beginning has been made on the theory of the filtrage of a polyetalon system[5] with the quite favorable result that so long as the gain in free spectral range occasioned by the addition of each etalon is less than the finesse $N$ by an appreciable factor, the value of the filtrage can be in the neighborhood of 0.5. Thus if a polyetalon spectrometer were used on a spectrum consisting of a continuum lacking only a sharply defined band of width $\delta_{1/2}\sigma$, the minimum relative intensity shown in the dark band would be in the neighborhood of 50%; but with a wider dark band, the PEPSIOS pilot model has actually achieved a background as low as 4% (see Fig. 5).

### *Selection of Spacing Ratios*

The goal in the selection of spacing ratios is to make the spacings effectively incommensurable, i.e., to prevent all the peaks of any one etalon, except the selected common peak, from coinciding with any of the peaks of any other. However, because of the finite width of the Airy peak, there exist exact or nearly exact coincidences in the case of any two etalons, some of which contribute intolerably strong ghosts, so the goal of incommensurability is unattainable and the relative spacings of the etalons are chosen in practice so that within the spectral band passed by the auxiliary filter system, the peaks of any etalon shall fall far enough from the strong ghosts of the other $M - 1$ etalons in the train to reduce them to unimportance. In principle, the free spectral range of the train may be extended without limit by the addition of more etalons.

Clearly, the relative strength of any particular ghost, and, therefore, in general, the choice of spacing ratios, depends upon the finesse.

Although several methods for systematically choosing spacing ratios for a polyetalon series to allow the indefinite extension of the free spectral range have been discussed in some detail,[6] no complete set of rules for the selection of optimum ratios has been developed. Indeed, what one means by optimum ratios may well depend upon such things as the particular problem to be studied or the method of scanning the spectrometer. Nevertheless, an attempt has been made at a beginning toward a systematic selection of a satisfactory set of ratios. A later paper in this series will deal with the evaluation of an effective filtrage through integration of the transmittance in the complex plane.

Consider the transmittance functions, Eq. (1), of the first two etalons, $E_1$ and $E_2$ in a train. Assume that after $p$ peaks of the first and $q$ peaks of the second there is an exact coincidence. Then the spacing ratio is $p/q$. The separation of the $k$th peaks of $E_1$ and $E_2$ expressed as a fraction of an order of $E_2$ is $k(p - q)/p$. The residual or ghost strength at the $k$th peak of $E_1$ is, therefore, approximately

$$\mathcal{A}_2(\sigma_0 - \sigma_k) = \mathcal{A}[Q_2k(p - q)/p], \tag{12}$$

where $\mathcal{A}$ is again the Airy function and $Q_2$ is the free spectral range of $E_2$. Since $\mathcal{A}_2(\sigma)$ is symmetric and has the period $Q_2$, one may write:

$$\mathcal{A}_2(\sigma - \sigma_p) = \mathcal{A}\{Q_2[k(p - q)/p - I_k]\} = \mathcal{A}\{Q_2f_k\}, \tag{13}$$

where $I_k$ is the integer nearest to $k(p - q)/p$ and the *fractional order difference* $f_k$ is $k(p - q)/p - I_k$; thus, $|f_k| \leqslant {}^1/_2$. Also,

$$\begin{aligned}\mathcal{A}\{Q_2k(p - q)/p\} = \mathcal{A}\{Q_2k[(p - q)/p - 1]\} &= \\ \mathcal{A}\{-Q_2kq/p\} &= \mathcal{A}\{Q_2kq/p\},\end{aligned} \tag{14}$$

or the action on the peaks of an etalon by a second etalon whose $q$th peak falls on the $p$th of the first is the same as the action of one whose $(p - q)$th peak falls on the $p$th peak. These rules allow the construction of a concise table for a train of three etalons, whose rows designate the $k$th peak of the widest etalon, whose columns designate the value of $q$, and whose entries are the fractional order differences $f_k$. The table can be searched to find two values $q_2$ and $q_3$ such that at least one of the values $f_k$ in every row is larger than about $N^{-1}$. The scheme can be extended to a train of four or more etalons.

For the pilot model of the PEPSIOS spectrometer, such a search was made for the case $p = 100$, a convenient number and a reasonable one since it is considerably in excess of $N$. Those ratios which appeared promising were fed into a digital computer programmed to calculate the strength of each ghost, the filtrage, and the finesse. Pilot model ratios 100:93:59 (or better, 100:93:~59, see next paragraph) were chosen for a transmittance curve with low ghost intensity and with the strongest ghosts quite far from the main peak, where the filter cutoff would reduce them. The set of ratios chosen is not claimed to be the optimum set, but as expected, the computed finesse and filtrage were reasonably high. See Fig. 1, overleaf, for a practical test of these ratios.

In order to approach the above-mentioned goal of incommensurability, and especially to avoid strong ghosts at the $p$th order of the widest etalon and integral multiples thereof, the actual values of about $(M - 1)/2$ of the ratios $p/q_j$ ought to be biased by amounts of the order of $N^{-2}$ from the commensurable ones reached by the above-outlined procedure (cf. Secs. IIID,E and especially Fig. 1 overleaf for an example). The exact value of the best bias in any case should be chosen to minimize the effect of the particular ghosts that occur.

Equation (14) shows that all the spacing ratios for a polyetalon can always be chosen to be between 0.5 and 1. For a given widest spacing, such vernier ratios yield higher resolution than more disparate ratios and may, in practice, be more convenient: for instance, the pressure change required for a given static alignment in wavenumber is inversely proportional to the spacing, and thicker spacers are sturdier than thinner ones.

## III. The Real Polyetalon

Within certain practical limits set by the degree of imperfection of the various optical elements, the behavior of a real etalon is like that of an ideal one. The nature and effects of these limits are discussed in the following paragraphs.

### A. Reflectance of Coatings

Even in practice, dielectric multilayers can be made with reflectance exceedingly close to 1. Consequently, the reflectance of a pair of etalon plates need not be considered among the factors contributing to the degradation of the passband of the PEPSIOS instrument.

### B. Absorptance of Coatings

Absorption in the reflecting layers limits the peak transmittance of a single etalon to

$$\tau = [1 - A/(1 - R)]^2, \tag{15a}$$

where $A = 1 - T - R$ is the absorptance of a layer, and reduces the luminosity of a system of $M$ similarly coated etalons by the factor $\tau^M$ [but cf. Eq. (16b)]. A representative value of $\tau$, which we obtain in the laboratory for a pair of good seven-layer ZnS–$Na_3AlF_6$ coatings, is 0.7.

### C. Plate Flatness

The deviation of optical flats from perfect planeness, the defect that currently places the most severe limitations upon the over-all quality of a polyetalon system, imposes a limit upon the finesse of an etalon which is reached when different area elements of the etalons transmit different wavelengths due to differences in plate spacing among the several elements, and which can be expressed through a relationship that depends upon the exact shapes of the surfaces[3]: for the study of the spectrum in the neighborhood of wavelength $\lambda$ with one plane and one spherical surface, the finesse cannot have a value greater than the *surface-limited finesse* $N_D = \lambda/2d$, where $d$ is the maximum departure of the spherical surface from flatness. In practice, this value of $N_D$

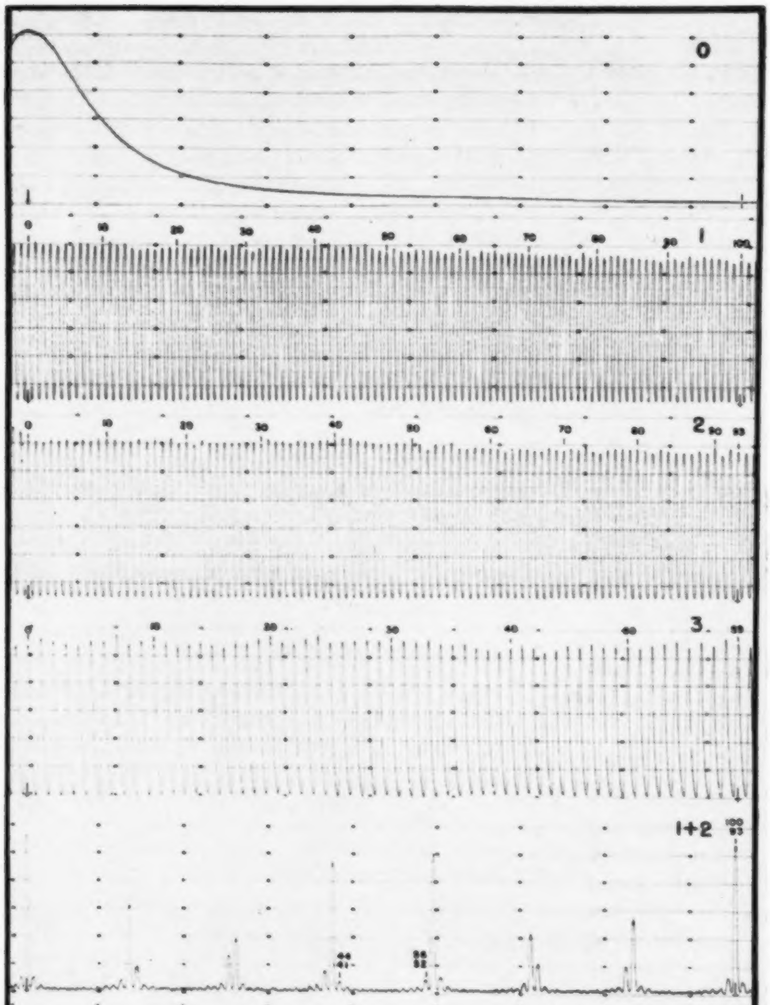

Fig. 1. Monochromatization in the PEPSIOS spectrometer by suppression of parasitic light, Secs. IIC, IIID, IIIE. The source is a continuum and the light arbitrarily selected for "$\sigma_0$", i.e., for transmission, is yellow light in the neighborhood of the sodium resonance doublet. The light from the source was sent through a filter to make the amplitudes of the peaks approximately uniform. The large digits stand for elements in the train: 0 for the interference filter, with $\delta_{1/2}\sigma = 30$ K $= 11$ Å; 1 for an etalon with $l_1 = 3.000$ mm; 2 for an etalon with $l_2 = 0.930\ l_1 = 2.790$ mm; 3 for an etalon with $l_3 = 0.5897\ l_1 = 1.769$ mm. The small digits stand for interference order numbers, measured from $\sigma_0$. For each trace, after an initial tuning to maximize the transmittance of $\sigma_0$, the pressure in each chamber was kept static and the transmitted light analyzed by means of a grating monochromator; since the grating had an inferior resolution, the traces show the positions, but not the shapes, of the peaks; they are not PEPSIOS spectrometer traces. In trace "1 + 2", the near equality in amplitude between orders 0, 0 and 100, 93 and the symmetry of the intervening ghost pattern show that the design spacing ratio of 100:93 was effectively attained. The asymmetry of trace "1 + 3", on the contrary, shows a departure from the ratio 100:59 and a study of the asymmetry of the ghost pattern affords a basis for the quantitative determination of the departure. Traces "1 + 2 + 3" and "0 + 1 + 2 + 3" indicate that effective monochromatism has been attained. The improvement in the ghost system arising out of the departure of $l_3/l_1$ from exactly 0.5900 came about in the first instance by accident. The reproduction of Fig. 1 is defective, especially in that it loses certain peaks near order zero and order fourteen of the fifth line ("1 + 2") and incompletely reproduces certain other material. Line "1 + 2" is practically symmetric, left to right, and every line has a peak of approximately the same size in order zero.

is usually a sufficiently good approximation for surfaces with defects other than spherical. Currently the best available plates are flat, except near the edges, to about $^1/_{100}$ of a wavelength of green light, which imposes the limitation $N \leqslant N_D \sim 50$.

The use of inferior plates can seriously reduce the over-all quality of a polyetalon spectrometer. First, on account of the broadening of the passband caused by the transmission of different wavelengths by different regions of the plates, obviously the resolution, ghost rejection, and filtrage are degraded. Secondly, even with a single etalon, the luminosity is reduced by an *automasking* effect that results in a reduction of the effective aperture when $N_D < N_R$; for if a pair of plates with reflective finesse $N_R$ has a region with spacing $l_0$ such that $\lambda_0$ is peaked, i.e., the Airy curve has a maximum at $\lambda_0$, then $\lambda_0$ is transmitted strongly only over a region for which the deviation $\delta l$ about $l_0$ is such that $|\delta l| < \lambda_0/2N_R$, which, since $N_R > N_D$, must be less than the full aperture. Thirdly, in a polyetalon system peaked at $\lambda_0$, the effective aperture is only that which is common to the projected effective apertures of the individual etalons. As a consequence, even with rather good plates, a polyetalon instrument is subject to a *mutual masking* or compounded loss of luminosity. If care is taken to orient the etalons favorably in azimuth with respect to one another the loss may be minimized.

In its automasking effect, an error in adjusting the plates of an individual etalon for parallelism is equivalent to a defect in the flatness of the plates. Consequently, even higher standards of care and precision must be applied to the adjustment of etalons for polyetalon than for single-etalon spectroscopy.

It is to be emphasized that the reduction of effective aperture is forced upon the system by the automasking effect of imperfect flats so that, at least in principle, it is possible to narrow the passband by masking the beam geometrically without further loss of luminosity.

## D. Practical Choice of Spacings

For the initial run of the pilot model, it was decided to aim at an $\mathcal{R}_t$ value of about $5 \times 10^5$ in the yellow. Accordingly, with $N \sim 30$, a spacing $l$ of 0.3 cm was chosen for the first (and widest) etalon. By itself, this etalon would have a resolving limit [cf. Eqs. (2b), (3a)] of about 55 mK [where 1 K (1 kayser) $\equiv$ 1 cm$^{-1}$]. The computed gain factor (cf. Sec. IIC, resolution of a polyetalon) of 1.65 for the three-etalon train selected would reduce the computed resolving limit to 34 mK; the actual gain factor was found to be somewhat over 1.5.

Figure 1, which illustrates our first actual laboratory experience with a PEPSIOS spectrometer, gives evidence that the experience was altogether satisfactory. The spacer ratios 100:93:~59 were chosen as described at the end of Sec. II. The several rows in Fig. 1 show the behavior of individual elements and combinations, and finally of the complete assembly consisting of the interference filter and the train of all three etalons.

With all three etalons but no interference filter in the train (row "1 + 2 + 3") and with exactly the nominal ratios, the intensities of the serious ghosts would have had the following flux values relative to that of the main peak: order number 44 (3%), 56 (3%), and 100 of the widest etalon (100%). The free spectral range of the widest etalon being 1.67 K required that if the instrument be used on a continuum or a rich spectrum, the interference filter have a low relative transmittance at $(44/100) \times 167$ K = 73 K and a much lower one at 167 K from the main peak. The interference filter transmittances actually observed (row "0") were $3.5 \times 10^{-2}$ at 73 K and $7 \times 10^{-3}$ at 167 K.

## E. Bias and Required Accuracy in Spacing Ratios

The effect of deliberate bias or of error in a spacing ratio is to alter the ghost intensities; hence, the criterion for determining whether the ratios are acceptable is whether the integral of the ghost strengths weighted by the transmittance of the interference filter is below the maximum tolerable level.

As an example, in the pilot model, where the computed peaks from all three etalons coincide at order 100 of $E_1$, consider the case of the strong ghosts at orders 44 and 56. Integral orders of $E_2$ and $E_3$ are missed [Eq. (14)] by 0.08 and 0.04 orders, respectively. A slight bias to reduce order 100 will affect orders 44 and 56 antisymmetrically. In view of the role of the interference filter, it is best to introduce such a bias, increasing order 56 and reducing orders 44 and 100. The system is most sensitive to the ratio showing the closest match, namely $l_3/l_1$. Figure 1 row "1 + 2 + 3" shows that with the actual spacing ratios, orders 44, 56, and 100 show heights roughly inversely as the corresponding ordinate values of row "0", leading to a lower average ordinate, row "0 + 1 + 2 + 3", than if we had adhered exactly to the computed commensurable ratios. A better solution in principle, but probably not in practice, could have been found by introducing $l_2/l_1$ as another adjustable parameter.

Although the theory and practice are not sufficiently developed to let one know in every case how important it is to attain high accuracy in making the spacers, our experience with the pilot model indicates that the tolerance in ratio is of the same order as the bias that has already been discussed, namely, $N^{-2}$. Thus, in the pilot model, the tolerance is of the order of a near ultraviolet wavelength. We believe the demands to be considerably less stringent here than in photographic polyetalon work, which calls for one spacing to be precisely an integral multiple of another in order to allow the photographing of the components of a line in several orders.

## F. Auxiliary Filtering

Although in describing the polyetalon spectrometer it is convenient to avoid counting the interference filter as an etalon, distinguishing between the etalons on the one hand and the interference filter on the other as is done elsewhere in this account, the filter is really a very narrow-spaced etalon (with a solid, rather than a scannable gas, spacer) and as such affects the ghost intensity in qualitatively the same manner as any other etalon. If the filter finesse were not high enough, the sum of the strengths of the ghosts near the designed peak, the nearest of which in the pilot model are distant from the peak by 44, 56, and 100 orders of the widest-spaced etalon, would be greater than tolerable. The reflective finesse of the interference filter can ordinarily be made sufficiently high, but the over-all finesse in the present state of the manufacturing art is ordinarily limited by nonuniformity in the deposition of the spacer layer, giving rise to a shift, of the same order of magnitude as the half-intensity width, between the extreme values of the peak wavelength transmitted by the several area elements of the filter.

The luminosity of the instrument is reduced by the interference filter, as by an etalon, through absorption in the layers and through automasking due to variations in spacer layer thickness beyond that allowed by the reflectance of the reflecting layers sandwiching the spacer layer. The other filters, particularly those used to eliminate light to the red of that under study, further reduce the luminosity. The still further reduction of luminosity by reflection losses at the several glass-air interfaces in the beam could be mitigated by antireflection coating, but the reflection losses in the surfaces between etalons have an important function in reducing the loss in contrast occasioned by multiple reflections between etalons, as discussed in the next paragraph.

## G. Reflections between Etalons

The case of a polyetalon is complicated beyond that of a single etalon because of reflections between the etalons. If, in agreement with Eq. (15a), the transmittance of one etalon is written:

$$T_j(\sigma) = [1 - A/(1 - R)]^2 \mathcal{A}_j(\sigma) \qquad j = 1,2,3 \tag{15b}$$

the transmittance $T_{123}(\sigma)$ of a three-etalon system without consideration of reflection between etalons would be:

$$T_{123}(\sigma) = T_1(\sigma)T_2(\sigma)T_3(\sigma)t^2 = T_1T_2T_3t^2, \tag{16a}$$

where $t$ is the transmittance of the medium between two adjacent etalons and $\mathcal{A}_j(\sigma)$ is the Airy function given by Eq. (1).

Considering all multiple reflections between parallel etalons used at normal incidence in a three-etalon system with coatings of reflectance $R$, one obtains

$$T'(\sigma) = \frac{T_1T_2T_3t^2}{(1 - R_1R_2t^2)(1 - R_2R_3t^2) - R_1R_3T_2^2t^4}, \tag{16b}$$

where

$$R_j(\sigma) = (1 - A)(1 - \mathcal{A}) + A^2\mathcal{A}R/(1 - R)^2. \qquad j = 1,2,3$$

The calculation shows that when $t = 1$, the filtrage is lower by a factor of about 3 or 4 than in the case described by Eq. (16a), but when $t \sim 0.85$, as in the case of four uncoated air-glass interfaces between etalons, the filtrage is again almost as high as given by Eq. (16a).

By slightly tilting the etalons with respect to one another it is possible to throw the reflected beams outside the aperture, eliminating the multiple reflections completely. Calculation shows that by slightly tilting only the second etalon of the three, one obtains a filtrage which is only inappreciably lower than in the case of no reflection. In the case where only the intermediate etalon is tilted one obtains

$$T''(\sigma) = \frac{T_1T_2T_3t^2}{1 - R_1R_3T_2^2t^4}. \tag{16c}$$

In practice, leaving the glass-air surfaces uncoated, we have attained adequate values of the filtrage without resorting to tilting of the etalons.

## H. Phase Shift on Reflection

When light is reflected from a dielectric reflecting multilayer, it undergoes a phase shift which depends upon the wavenumber of the incident light. It is easily shown that in this case the nominal free spectral range of an etalon is $Q = 1/\{2\,[l + (2\pi)^{-1}\partial\phi/\partial\sigma|_0]\}$, where $\phi$ is the phase shift on reflection and the subscript zero implies a value taken at the wavenumber of the incident light. If $\phi(\sigma)$ is linear in $\sigma$, which is approximately true over the useful range of a reflecting surface consisting only of quarter-wavelength dielectric layers, the only effect is a slight change in the effective spacing, which can be compensated for, if necessary, in the final precise grinding of the spacers. For a seven-layer ZnS–$Na_3AlF_6$ multilayer peaked at $\sigma$ = 20,000 K, $\partial\phi/\partial\sigma = 1.6\ \mu$. Thus the effective spacing is changed by about 0.26 $\mu$. The value of $\partial\phi/\partial\sigma$ at the reflectance peak of the coatings depends upon the value of $\sigma$ at which the peak occurs. Our calculations show that for coatings peaked in the visible, $\partial\phi/\partial\sigma < 2.2\ \mu$, corresponding to a change of less than 0.35 $\mu$ in the effective spacing. As shown above, this difference is tolerable for the pilot model.

For broad-band reflecting layers such as those described by Baumeister,[30] $\partial\phi/\partial\sigma$ is not even approximately linear over the useful range of the layer and goes to a maximum of about 32.5 $\mu$, which gives a change in effective spacing of 5.2 $\mu$. This limits the usefulness of broad-band reflection layers in this instrument.

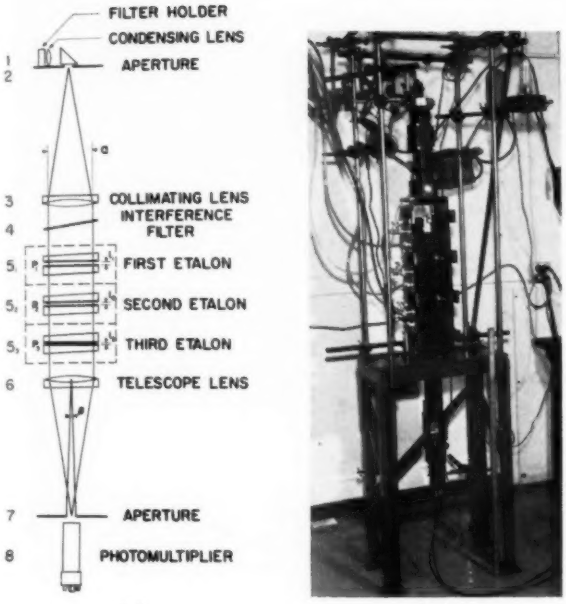

(a) (b)

Fig. 2. The PEPSIOS spectrometer pilot model. (a) Schematic drawing. The parts are numbered as in Secs. IV and V. (b) Photograph. Notice the meter stick at the near right. Ordinarily three etalon chambers are used. When the picture was taken there were four chambers in the train; the top one is shown open with an etalon installed, and the botton one empty.

## IV. Elements of the PEPSIOS Spectrometer

The PEPSIOS spectrometer is a series arrangement (in the pilot model vertical, with light traveling downward) as shown in Fig. 2, consisting essentially of:

(1) A rotatable table with a 45° reflecting prism for convenience in admitting light horizontally;
(2) A circular aperture in the focal plane;
(3) A collimating lens;
(4) An interference filter, arranged to rotate about an axis normal to that of the spectrometer;
(5) Several (in the pilot model, three) etalon assemblies, each in a pressure chamber, valved so that as the pressure $p_m$ of the gas (in the pilot model, air) in one chamber, which may be called the *master* chamber, is varied arbitrarily, that in each of the others (the *slave* chambers) can be first adjusted to a desired value $P_j = P_m + \Delta_j P$ and then locked to maintain a constant $\Delta_j P$;
(6) A telescope lens;
(7) A second aperture, in the focal plane of the telescope lens;
(8) A photomultiplier and recording system.

The instrument allows one to do spectrometry at any predetermined resolution between a low value and somewhat over $10^6$. The relative range of a single sweep is limited by the refractive index of the gas (in the pilot model to about $10^{-3}$), but the instrument can easily be reset to any region within the compass of the reflection coatings, the interference filter, the optical media, and the detecting system.

The over-all size of the pilot model is 22 cm × 22 cm × 150 cm, not counting a control rack and pressure, vacuum, and electric facilities.

## V. The Optical System

Items in this section are numbered in agreement with Sec. IV.

(1) The table, fitted with a filter holder, may be used as a simple optical bench. It can be rotated about the vertical axis to accept a beam from any horizontal direction, with detents at intervals of 30°.

(2, 7) The apertures are conjugate to one another and only one diaphragm would be necessary if it were not for scattering, fluorescence, and asymmetric reflections originating between the two. For a selected resolution $\mathcal{R}$ and a collimating or telescope lens with focal length $f$, the diameter $b$ of the aperture is $f\beta$, where the field angle $\beta$ equals approximately $2(2/\mathcal{R})^{1/2}$ [Eq. (7)]. In practice, focusing is accomplished by screw adjustment of a table designed to hold the limiting aperture. The first aperture may be viewed from the top, and either one may be viewed from the direction of the etalon through a side opening in the lens tube. Provision is made for the lateral adjustment of the second aperture (as well as the telescope lens—see next paragraph) for optimizing the illumination of the photomultiplier.

(3, 6) The collimator and telescope lenses may be identical, corrected only for on-axis aberrations. (In the pilot model, they are nominally identical glass achromats with focal length $f = 305$ mm and diameter somewhat greater than the 54-mm clear aperture of the etalons. In a prospective model, they are quartz-fluorite achromats with about the same dimensions.) The telescope lens, but not the collimator lens, is mounted in a frame subject to lateral adjustment by means of two thumb screws that slide it on a plane normal to the axis. Interrupting the cylindrical tube of each lens near the focus is a rectangular segment, opening on two opposite sides and arranged for the convenient insertion, at 45°, of a mirror or a diffuse white scattering sheet.

(4) A calibrated tiltable holder allows for the insertion or retraction of the interference filter. (In the pilot model, the filter is 60-mm diam or 50 mm square and the holder allows it to tilt up to 15° from the normal.)

(5) Each chamber is a nearly cubical aluminum alloy casting, large enough to hold an etalon assembly with extra space to allow the manual adjustment of the etalon screws or the insertion of a 45° mirror as high as

the beam diameter, with a solid aluminum alloy door and two axial window holes. Successive chambers are locked together by flanged window assemblies, of which the lower ring in each chamber has a point-line-plane for mounting an etalon. The windows themselves (in the pilot model, optical glass, plane parallel to 0.5 $\mu$; in a prospective model, fused silica) are canted 0.01 rad from the normal to cast window-reflected beams outside the aperture. All joints are sealed by O-rings.

The etalon assemblies need not be described in detail here, as they follow the main tradition for the design of such assemblies. Except for the plates and for three springs each, they are made entirely of Invar, with over-all dimensions 98 mm diam by about 88 mm long at mid-range adjustment. The plates themselves are 60 mm in diameter with wedges of 0.01 rad that put the beams reflected from the backs of the plates outside the aperture for designs with $\mathcal{R}_t > 2 \times 10^4$.

The liability to mutual masking (Sec. IIIC) increases the seriousness of nonflatness in a polyetalon system. The flatness specification for the plates used in the pilot model was: the difference between maximum and minimum spacing between the plates shall be not more than 1/100 wavelength of green light. As flatter plates become available they can be expected to improve the performance of the PEPSIOS instrument since the luminosity-resolution product is still limited by flatness.

(6) The telescope lens. See paragraph 3 above.

(7) The second aperture stop. See paragraph 2 above.

(8) Since the PEPSIOS spectrometer presents no special problem for a photomultiplier-recorder system, the system used need not be discussed further.

### *Alignment and Tuning Procedure*

While any of several optical adjustment programs is feasible, the one below has appeared up to now to be the best.

The alignment is begun by shining a bright continuous source upon the entrance aperture. The tilt of $E_1$ is adjusted by autocollimation. A mirror is inserted in the upper part of chamber 3, to let one look through $E_2$ and $E_1$ at the entrance aperture. With the chemical absorbing filters removed, there is enough light transmitted by the side bands of the interference filter to let the tilt of $E_2$ be adjusted by centering the images formed from the light repeatedly reflected between etalons. This procedure is repeated for the rest of the etalons in the train; in the case of the last etalon, the alignment mirror is inserted in the side opening of the telescope tube. Finally, the telescope lens is adjusted laterally to pass the beam through the exit aperture; if there is not enough light to see the focused spot, a bright line source may be used before the last etalon in the series and its ring system centered on the exit aperture by the lateral motion of the telescope lens.

The tuning of the instrument is accomplished by illuminating the entrance aperture with a bright source having a line at or near the wavelength to be studied. Starting with the interference filter, with the help of an auxiliary mirror inserted successively behind each element to be tuned the element is tuned visually for highest transmission—in the case of the interference filter by tilting and in case of an etalon by adjustment of the chamber pressure, $P_j$. A final tuning may be achieved by fine adjustment of the filter tilt and chamber pressures to maximize the photomultiplier output. A modification to permit the tuning of a faint line with the aid of an auxiliary photomultiplier is under construction.

A scheme can be devised for shifting from an available line to an arbitrary point in the spectrum without exceeding the scanning range of the instrument.

## VI. The Scanning System

From the electromagnetic theory of the polarizability of an amorphous substance[31] it can be shown that the refractive index $n$ of an ideal gas is given by the Lorentz–Lorenz law as

$$(n^2 - 1)/(n^2 + 2) = \text{constant} \times P/T$$
$$= [2(\epsilon - \epsilon^2/6 + \ldots)]/3, \quad (17)$$

where $P$ is the pressure relative to the standard atmosphere, $T$ is the temperature, and $\epsilon \equiv n - 1$. The constant is proportional to the molecular refractivity; in the case of a mixture, the effective refractivity is the sum of the refractivities of the components weighted by their molar concentrations. The term in $\epsilon^2$ can be neglected for our purposes. For a gas at laboratory temperature the index can be written

$$n = 1 + \epsilon_1 P, \quad (18)$$

where $\epsilon_1$ is the value of $\epsilon$ at 1 atm and the pressure $P$ is expressed in atmospheres. The vacuum wavelength transmitted by an etalon with spacing $l$ in order $m$ [Eq. (1)] is

$$\lambda_{\text{vac}} = 2nl/m = 2l(1 + \epsilon_1 P)/m. \quad (19)$$

Therefore, changes in $\lambda_{\text{vac}}$ are proportional to the pressure and it follows that a pressure scan is linear in wavelength. To keep two etalons transmitting the same vacuum wavelength in an ideal gas, a constant pressure difference must be maintained between the corresponding chambers.

### A. Accuracy of Pressure Control

In order to estimate the accuracy required by a pressure scanning system, consider a monochromatic line of wavenumber $\sigma_0$ falling normally on an etalon of finesse $N$ and nominal free spectral range $Q$, filled with

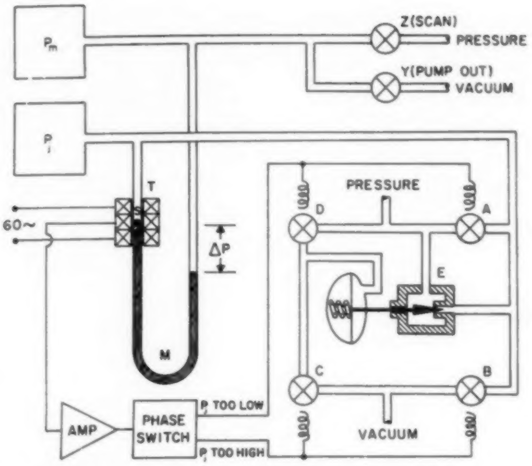

Fig. 3. The constant pressure difference control, simplified schematic drawing. A train of $M$ pressure-scanned etalons requires $M - 1$ such systems.

gas of index $(n_0 + \delta n)$ such that $\sigma_0$ falls at an Airy peak when $n = n_0$. (Notice the universal practice, that any reference to wavenumber is always to vacuum wavenumber.) The ratio of the transmittance of the etalon to the peak transmittance is the Airy function, here modified to use the experimentally determined finesse, $N$, cf. Eqs. (1) through (3b):

$$\mathcal{A} = \{1 + 4N^2\pi^{-2}\sin^2[\pi\sigma_0(n_0 + \delta n)/Q]\}^{-1} = 1 - \eta, \quad (20)$$

where $\eta$ is the fractional change in the transmittance produced by a pressure misalignment corresponding to $\delta n$. Suppose that the etalon is peaked at $\sigma_0$ (i.e., for $\delta n = 0$) and hence $\sin(\pi\sigma_0 n_0/Q) = 0$. Noting that $N\sigma_0/Q$ is the resolution $\mathcal{R}$ and that $\delta n = \epsilon_1 \delta P$ and neglecting terms in $(\pi\sigma\delta n/Q)^4$, one finds the solution of Eq. (20) to be $\eta = 4\mathcal{R}^2\epsilon_1^2(\delta P)^2$. Thus, for a certain $\mathcal{R}$, the value of $\delta P$ that can be tolerated without exceeding a certain $\eta$ is inversely proportional to $\mathcal{R}$, and for air with $\epsilon_1 = 3 \times 10^{-4}$, if $\mathcal{R} = 10^6$ and one allows $\eta = 0.01$, the required accuracy in pressure control is $\delta P = 1.7 \times 10^{-4}$ atm or 0.13 torr.

Thus the aim of the pressure control system is to produce an increase in pressure $P_m$ in the master chamber that is linear with the time, while simultaneously increasing the pressure $P_j$ in a slave chamber so as to maintain a constant pressure difference $\Delta_j P = P_j - P_m$ between chambers. The linear increase is readily obtained by a needle valve Z (Fig. 3) and a reservoir with pressure high enough so that the change of $P_m$ does not make a significant change in the flow rate through the valve. In practice a gauge pressure of 4 atm is a sufficient supply, as long as $P_m$ and $P_j$ do not exceed 2 atm; it has been pointed out[32] that the supersonic flow through the orifice of the valve which occurs in this case produces a much more nearly linear flow than one is led to expect from the more usual assumption of laminar flow.

## B. Means of Pressure Control

Although ideally, the slave chamber could be caused to follow the main chamber simply by using a valve identical with Z and starting with the pressure difference to be maintained, in practice some form of servomechanism is required to obtain the requisite accuracy in $\Delta P$. The system employed uses a mercury manometer M in which a ferrite sphere is floated to measure $\Delta P$ directly. The position of the sphere is determined by a differential transformer T, whose output is amplified and sent to a *phase switch*, which has the property of sending out power on one of two channels, depending on the phase and the amplitude of the input. Since the phase of the differential transformer output depends upon the sign of the error in $\Delta P$, the over-all function of the electronics is to send out signal on the "$P_j$ too high" channel when $P_j$ is greater than $P_m + \Delta_j P$ by a preset value, say 0.1 torr, and similarly on the "$P_j$ too low" channel when $P_j$ is less than $P_m + \Delta_j P$.

The pressure-activated "dome" valve can be automatically positioned to match valve Z, as follows: Suppose that a sweep has been begun and the rate determined by E is too fast. The pressure in the slave chamber will build up in time and the phase switch will send out signal on the "$P_j$ too high" channel opening valves B and C, at which time the excess pressure will be vented to the vacuum line through B until the error is reduced enough to stop the signal. But since valve C will be open during the correction process, valve E will be found to have closed somewhat so that the rate will be slower on the slave chamber after the correction cycle. After a few such cycles the dome valve finds its proper position and the solenoid valves operate only to correct random errors.

The system as actually used is further complicated by throttling valves in series with A, B, C, D, several other solenoid and manually operated valves, and a meter measuring the error signal for setting the position of the differential transformer. The additional solenoid valves make it possible to pump out the chambers (valve Y) while leaving the pressure in the dome valve at its previous setting so that the slave rate is approximately correct when a new sweep is begun. The other valves are for the manual adjustment of the chamber pressures during the initial tuning of the etalons.

Of course, two complete pressure-control systems are required for a three-etalon PEPSIOS spectrometer.

## VII. Representative PEPSIOGRAMS

Figure 4 is a trace of the mercury green line, made with the PEPSIOS pilot model for the purpose of testing its behavior. The source was a commercial 4-W germicidal lamp. The interference filter was tuned from its normal peak wavelength of 5470 Å; it had a resolution of only about 50 and could hardly have

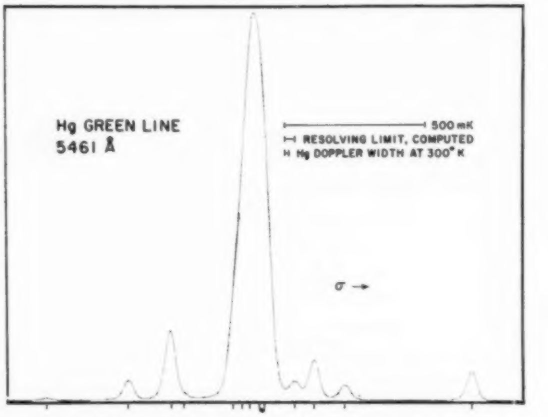

Fig. 4. Emission Pepsiogram of the mercury green line, 5461Å, taken with the same spacings as Fig. 2, i.e., with a design resolution not quite sufficient to resolve the third and fourth components counting from the red end. The computed components are shown by marks below the zero-intensity line.

been used on a rich line spectrum or a continuum. The etalon plates had seven-layer ZnS–$Na_3AlF_6$ coatings, peaked at 5700 Å to accommodate the green line and the sodium resonance lines. Three 60-mm etalons were used with spacings $l_1 = 3.000$ mm, $l_2 = 2.790$ mm, $l_3 = 1.769$ mm. $\beta$ was set equal to $3.3 \times 10^{-3}$, a value somewhat smaller than that dictated by the expected resolution, $\mathcal{R}$. $\mathcal{R}$, as seen from Fig. 4, is at least $4.5 \times 10^5$, which is the approximate resolution planned for the pilot model.

Figure 5 is an example of the possibility of using the PEPSIOS spectrometer with a continuous spectrum. The instrumental conditions were the same as for Fig. 4 except that the interference filter was tuned from its normal peak of 5930 Å and had a resolution of $5 \times 10^2$. The residual of only 4% at the bottom of the completely blocked sodium resonance lines appears to us as very satisfactory.

The instrument was also tested in the blue and violet region with another set of appropriately coated etalon plates and auxiliary filters. The behavior of the instrument was comparable to that in the yellow and green. At 4700 Å the width of the pass band isolated by the PEPSIOS spectrometer from a continuous source was measured by scanning a fourth, widely spaced etalon placed at the end of the series. The result indicated a resolution somewhat in excess of $4 \times 10^5$, in reasonable agreement with the designed value.

This work could not have been done as it was without the help of many others, only a few of whom we can name. O. S. Duffendack's advice, and particularly his help in the procurement of high-quality flat plates, has been invaluable. W. L. Fadner supervised and contributed much to the development and construction of the pressure control system. D. J. Schroeder has made available his experience and his computations of the properties of dielectric reflecting multilayers. Important help has come from R. H. Barber, F. Barmore, G. Batz, H. G. Berry, Katherine Carroll, Mark Daehler, J. P. Fox, S. S. Lee, J. R. Moore, and E. L. Zimmermann, and the departmental shop staff.

Some future papers in this series may be submitted to the *Journal of the Optical Society of America*.

## References

1. C. Dufour and R. Picca, Rev. opt. **24,** 19 (1945).
2. P. Jacquinot and C. Dufour, J. Rech. Centre Natl. Rech. Sci. Lab. Bellevue (Paris) **No. 6,** 91 (1948).
3. R. Chabbal, J. Rech. Centre Natl. Rech. Sci. Lab. Bellevue (Paris) **No. 24,** 138 (1953). English translation by R. B. Jacobi, UKAEA Research Group, Harwell 1958/JMR HX 4128.
4. P. Jacquinot, J. Opt. Soc. Am. **44,** 761 (1954).
5. R. Chabbal, J. Rech. Centre Natl. Rech. Sci. Lab. Bellevue (Paris) **No. 39,** 77 (1957).
6. R. Chabbal, theses, Paris, 1957; Rev. opt. **37,** 49 (1958).
7. H. Chantrel, J. Rech. Centre Natl. Rech. Sci. Lab. Bellevue (Paris) **No. 46,** 17 (1957).
8. P. Jacquinot, Rept. Progr. Phys. **23,** 267 (1960).
9. R. Chabbal and P. Jacquinot, Rev. opt. **40,** 157 (1961).

**References** *continued on facing page*

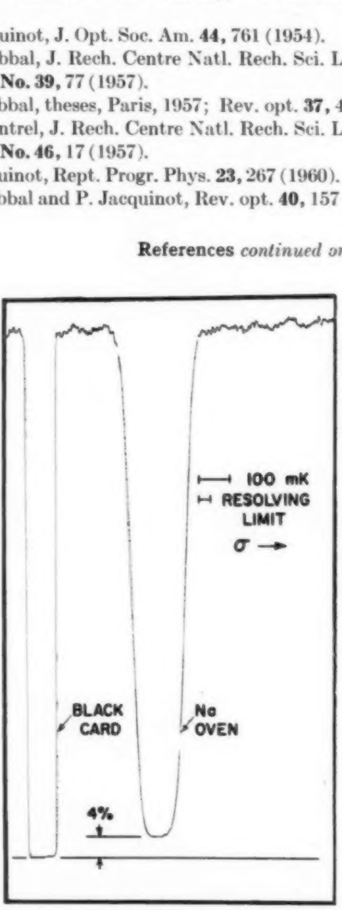

Fig. 5. Absorption of NaI $3s^2S_{1/2} - 3p^2P_{3/2}$, 5890Å, from the continuum by a sodium vapor cell 20 cm thick at about 180°C. The parasitic light of all wavelengths outside the absorbed region yields an amplitude only 4% as great as that from the continuum. Of the two slave chambers used in producing Figs. 4 and 5, only one was automatically controlled as described in Sec. VI; for the other, $\Delta P$ was kept constant by a manually controlled valve system following cathetometer observation.

10. *Colloque International sur les Progrès Recents in Spectroscopie Interferentielle*, September 9–13 1957. Fifty-one papers in J. Phys. Radium **19,** 185–436 (1958).
11. H. Fizeau, Ann. chim. phys. (3) **66,** 429 (1862).
12. A. Michelson, Am. J. Science **39,** 115 (1890); Phil. Mag. **34,** 280 (1892).
13. H. Rubens and R. W. Wood, Phil. Mag. **21,** 249 (1911).
14. P. Fellgett, J. Phys. Radium **19,** 187 (1958); **19,** 237 (1958).
15. R. Greenler, J. Opt. Soc. Am. **45,** 788 (1955); **47,** 642 (1957).
16. E. Gehrcke and O. von Baeyer, Ann. Physik (4) **20,** 269 (1906).
17. W. V. Houston, Phys. Rev. **29,** 478 (1927).
18. E. Gehrcke and E. Lau, Z. Tech. Physik **8,** 157 (1927).
19. G. W. Series, Proc. Roy. Soc. (London) **A226,** 377 (1954).
20. K. W. Meissner, private communication ca. 1940. We have not found any published account of Meissner's early work in this field.
21. C. Fabry and A. Perot, Compt. rend. **126,** 34 (1898); Ann. chim. phys. (7) **16,** 115 (1899).
22. O. Lummer, Verhandel Deut. Physikal. Ges. **3,** 85 (1901); O. Lummer and E. Gehrcke, Ann. Physik (4) **10,** 457 (1903).
23. F. L. Roesler, PhD thesis, Wisconsin, 1962.
24. H. C. Burger and P. H. van Cittert, Physica **2,** 87 (1935).
25. C. F. Bruce and R. M. Hill, Australian J. Phys. **14,** 64 (1961).
26. W. R. Bennett, Jr., and P. J. Kindlmann, Rev. Sci. Instr. **33,** 601 (1962).
27. D. A. Jackson and H. Kuhn, Proc. Roy. Soc. (London) **A167,** 205 (1938).
28. J. G. Hirschberg and R. Kadesch, J. Opt. Soc. Am. **48,** 177 (1958).
29. P. Connes, J. Phys. Radium **19,** 262 (1958).
30. P. Baumeister, J. Opt. Soc. Am. **48,** 955 (1958).
31. J. H. Van Vleck, *The Theory of Electric and Magnetic Susceptibilities* (Oxford Press, New York, 1932), p. 15.
32. D. H. Rank and J. N. Shearer, J. Opt. Soc. Am. **46,** 463 (1956).

# Applied Optics BOOKS

*Books for review should be submitted to the Managing Editor, APPLIED OPTICS, 1155 16th St., N.W., Washington 6, D.C.*

**Diffuse X-Ray Reflections from Crystals.** By W. A. Wooster. Clarendon Press, Oxford, 1962. 200 pp. $5.60.

Although all real crystals at normal temperatures fall short in some way of the precise and infinite repetition of the unit-cell contents required by the ideal crystal of theory, the x-ray diffraction patterns of many single crystals consist of relatively sharp spots on a clear, or at least uniform, background. Sometimes, however, some or all of the spots are diffuse, or diffuse regions of scattering may occur in the background between the sharp spots. The occurrence of any diffuse scattering indicates the presence of some kind of imperfection of considerable magnitude. Dr. Wooster's book is concerned with the relationships between the diffuse scattering and the particular imperfection from which it arises.

The book begins with a general survey of the theoretical basis of the relationship first introduced by means of optical diffraction patterns. Two-dimensional masks of holes, representing atomic sites, produce diffraction patterns with visible light that are closely related to the x-ray photographs of the corresponding materials. These optical photographs are used to give a visual introduction to the various classes of phenomena to be discussed and are a valuable feature of the book. The introduction is followed by an analytical treatment which is fairly conventional, although there is greater emphasis on the basic physics than on the mathematics. In view of this emphasis, of the use of Fourier transform ideas in the latter parts of the book, and of the optical introduction, it is perhaps a little surprising that the analytical treatment is not given in terms of the transform concept.

The experimental aspects of the subject are treated comprehensively. The various procedures for recording diffuse reflections photographically are described, and the apparatus and techniques for densitometric studies of the resulting photographs are discussed. There is also an account of the alternative technique for recording diffuse reflections using geiger or scintillation counters. A counter diffractometer for systematically exploring diffuse regions, controlled by punched paper tape, is described, and the relative value of the photographic and counter methods is considered. Various geometrical and other corrections arise in both methods; the author gives details of various methods of making them, including the design of suitable charts.

The remainder of the book is divided into four sections, each covering the interpretation of a particular class of diffuse scattering. The determination of the elastic constants of a crystal is considered first. The elastic waves generated by thermal vibrations within the crystal give rise to diffuse scattering in regions near to the normal sharp spots. Although, as the author says, the diffuse reflection method is not an easy method of determining elastic constants, it may be the only one available if the crystals are particularly small or soft or if the measurements are to be made at unusual temperatures. The theory of the method and examples of its application by both the photographic and the counter technique are given. In the second section, the determination of the spectra of the elastic vibrations in a crystal—the distribution of the energy of vibration as a function of frequency—is discussed theoretically and specifically. The third section deals with diffuse reflection arising from structural imperfections and includes stacking faults in layer structures, the diamond structure, order-disorder phenomena, and age-hardening in alloys. Finally, there is a chapter on molecular crystals, including some discussion of the possibility of using diffuse reflections as an aid in structure determination.

The author has introduced one or two special verbal contractions that, on the whole, are acceptable; for example, he uses "relp" for reciprocal-lattice point. Some confusion may arise from one of them, however: "rekha" turns out to be not a contraction but a word of Indian origin; unfortunately, it is neither included in the index nor clearly defined in the text.

The book is, of course, designed for specialists and covers a relatively narrow field. It has been written especially with the needs of young research workers in mind and fulfills a valuable dual function: it provides an introduction which concentrates on the physical basis of the subject and gives a useful survey of the possibilities of a field that is undoubtedly growing in importance.

C. A. Taylor

**Annotated Bibliography on Soft X-Ray Spectroscopy.** By H. Yakowitz and J. R. Cuthill. National Bureau of Standards Monograph 52. U.S. Government Printing Office, Washington, D.C., 1962. 108 pp. $1.00.

In this monograph the authors list and abstract over 500 papers in which soft x-ray spectroscopy is used to study the electronic structure of the valence bands of solids. The abstracts are clear, concise statements of the work covered in each paper and are a useful source of information as well as a valuable guide to the original work. The bibliography lists the papers by year and alphabetically by author within each year. Cross indices provide listings by element and author, so that any abstract may be quickly found. The bibliography claims to be a complete coverage of the soft x-ray literature that appeared between 1950 and 1960 and to include some of the more comprehensive earlier papers. The claim to completeness is not valid and should not be relied upon; in spite of this the work is a valuable guide for anyone interested in this subject.

M. Parker Givens

**Optics of Flames.** By F. J. Weinberg. Butterworths, London, 1963. 261 pp. $10.95.

Combustion and flame phenomena are complex. An essential complexity resides in the extreme conditions that prevail in the combustion wave or "flame front". Chemical transformation occurs with great rapidity within a narrow zone; there are high gradients of temperature, velocity, and concentrations under conditions of high temperature; and superimposed on these are the complex processes of transport of heat and mass within the wave. In the past, many studies have been made on flames for the purpose of learning something about this structure. Often, these have introduced into the wave an object like a thermocouple or a sampling probe, which have distorted actual conditions in the wave. The use of noninterfering methods of refractive-index measurements is particularly attractive for the study of structure. Another purpose for which optical methods are used in combustion research is in the visualization of flames and associated flow phenomena. Fairly simple optical systems may be used for this purpose. For accurate quantitative measurements on the geometry of optical surfaces within the flame zone, refinements of such qualitative visualization require more complex systems.

There is need for monographs that emphasize and elaborate particular areas of the rather broad field of combustion. The present monograph describes optical methods and their application to the study of combustion; in some instances, they provide information not obtainable in any other way. Dr. Weinberg is particularly successful in his presentation; in the introduction he provides a strong case for the use of optical methods. The first chapter contains an excellent short exposition of the elements of optics, modified where needed for the case of media with refractive index close to unity. The second chapter is concerned with the dependence of refractive index on the gas parameters in the flame, i.e., variation of temperature and composition. The third chapter, constituting about one-third of the book, is reserved for a discussion of various flame processes and their optical properties in flames of premixed gases, diffusion flames, and high-intensity combustion. The second half of the book describes optical methods useful in combustion research, namely, Schlieren, shadow, interferometry, and deflection mapping.

The author has performed a valuable service in examining the usefulness of optical systems for combustion research and in demonstrating how optical methods can help unravel some of the complexities, sometimes in a very simple way. Much of this monograph is original, the treatment having formed the basis of postgraduate lectures at the Imperial College of Science and Technology, London, where Dr. Weinberg is Senior Lecturer in Combustion. The monograph is lucidly written, for which the author deserves special commendation. It is highly recommended for inclusion in the libraries of researchers in combustion, aerodynamics, and other allied fields.

Bernard Lewis

**Electroluminescence.** By H. K. Henisch. Pergamon Press, Oxford, 1962. 368 pp. $12.50.

Henisch's book deals with a new and interesting field of solid-state physics—the direct transformation of electric energy into visible light in solid-state materials. This phenomenon, discovered by G. Destriau in 1936 is known today as "electroluminescence." Since that time, a great effert has been made by many physicists and chemists to find out the mechanism of this conversion of energy, and engineers have looked for possible applications. It seems that until the present time we have neither model nor theory able to explain all experimental observations. There exist a number of theories with contradictory basic assumptions, which compete with each other in an attempt to range the facts. Realizing this state of our knowledge, it might be thought difficult to write a clearly organized survey of this topic. Nevertheless, Henisch, who is well known for his authorship of other books in the field of solid-state physics, has succeeded in giving a helpful introduction to this borderland between insulators and orthodox semiconductors.

The book first introduces in a general survey a short description of the basic observations of electroluminescence and of some of the effects of electrophotoluminescence. The first chapter provides an empirical and descriptive account of electroluminescence in the multiplicity of forms in which this kind of generation of light has been observed on different materials: a certain amount of the early history of electroluminescence is quoted, including the proof that electroluminescence is a primary effect and not a hidden discharge phenomenon. The next chapter discusses the process that can, in principle, lead to light emission from nonincandescent solids under the influence of an electric field. The basic semiconductor phenomena, as far as they are involved in electroluminescence, are discussed in a well-balanced manner: carrier injection and accumulation, impact ionization, space-charge phenomena, electric breakdown, and dielectric properties of phosphors. Intrinsic luminescence processes, such as recombination, trapping, and structure of centers, are dealt with briefly. For this topic, the book refers the reader to special publications. The main experimental section is divided into three chapters: experiments on single-crystal phosphors (ZnS : CdS), electroluminescence at crystal boundaries, and experiments on microcrystalline phosphors. This organization of the great number of experimental observations prevents the reader from getting lost among the experimental facts. On the other hand, this organization seems to be somewhat arbitrary from the point of view of the mechanism involved in the different effects. The last part of the book deals with electroluminescent devices: The reader finds not only a clear description of the construction of electroluminescent cells and panels but also a discussion of problems in the application of electroluminescence as a light source. The chapter concerning the applications of electroluminescent panels is especially stimulating. An extensive bibliography, organized chronologically, is included.

In conclusion, I recommend this book to those who have a general background in solid-state physics and are about to study the phenomena of direct conversion of electric energy into light in solid-state materials. Engineers and technologists will find the book a useful and clearly written "status report."

H.-E. Gumlich

**Books** *continued on page 908*

# Infrared Transmission of the Atmosphere to Solar Radiation

David M. Gates and Walter J. Harrop

Infrared solar spectrum observations taken on 12 January 1955, in Denver, Colorado, with a double-pass NaCl prism spectrometer have been analyzed for transmission coefficients for the "selective" absorption and for the "continuum" extinction. The analysis was performed over the range 1.0–12.5 $\mu$. The goodness of fit for the average transmission for a random band model and for a regular band model is given for each of 203 data points distributed throughout the spectrum.

## Introduction

The transparency of the earth's atmosphere at infrared wavelengths is of interest in studies of the heat balance of the earth's surface involving the transmission of solar radiation to the surface, the radiation of the surface to space, and the absorption and re-emission of the atmosphere. The present paper reports measurements of atmospheric absorption coefficients obtained from solar observations with a prism instrument. The atmospheric attenuation for infrared solar radiation wavelengths passing through a clear sky is of two types: (a) Selective absorption by the polyatomic gaseous constituents of the atmosphere; and (b) continuum attenuation due to scattering and absorption by particulate matter and water droplets suspended in the atmosphere, and the integrated absorption effect of the wings of the multitude of absorption lines which are distributed throughout the spectrum. The selective absorption is characterized by many thousands of absorption lines forming the absorption bands due to the various molecules. With a very high-resolution spectrometer it is possible to observe these individual lines and to deduce the frequency dependence of the atmospheric absorption coefficients with a detail commensurate with the observed line structure. For many applications, such detail is unnecessarily complex and it is sufficient to obtain absorption coefficients for the gross band structure as deduced from data obtained by means of lower resolution prism spectrometers. In this case it is necessary that the bandpass of the spectrometer be large compared with the width and spacing of single rotation lines and small compared to the width of an entire absorption band. Gates[1] described the technique and instrumentation as used here when applied to the near infrared atmospheric spectrum. The present paper is an extension of the earlier one to cover the atmospheric infrared spectrum throughout the wavelength range 1.0 to 12.5 $\mu$.

## Observations

The solar spectrum observations were made on a clear cold day, 12 January 1955, from the University of Denver campus in Denver, Colorado, at 1615 m above sea level. The invasion of the region by a very cold mass of arctic air the night before the day of observation caused a considerable amount of moisture to be condensed out of the air in the form of snow. As a result, 12 January 1955 was an unusually clear day. A Perkin-Elmer double-pass infrared spectrometer, Model 112, was used for the observations. A siderostat located outside of the laboratory window directed sunlight to a parabolic mirror which formed an image of the sun of 8.8-mm diam on the spectrometer entrance slit. In order to eliminate edge effects in the mirror system, the solar beam was limited in diameter by an aperture. The spectrometer contained an NaCl prism and a thermocouple detector. The solar spectrum was scanned from 1.0 to 12.5 $\mu$ in approximately 15 min; a total of 10 complete scans were made during the day and a couple of extra scans were also made for certain wavelength regions. The observed solar spectrum is shown in Fig. 1 where the four major transmission intervals between 1.0 and 12.5 $\mu$ are defined. The four regions were separated by the major absorption bands located at 2.7, 4.3, and 6.0 $\mu$. Due to the intensity of these absorption bands, very little energy is transmitted through the entire atmosphere at the center of these bands and hence observations could not be made within

---

The authors are at the U. S. National Bureau of Standards, Boulder, Colorado.

Received 6 February 1963.

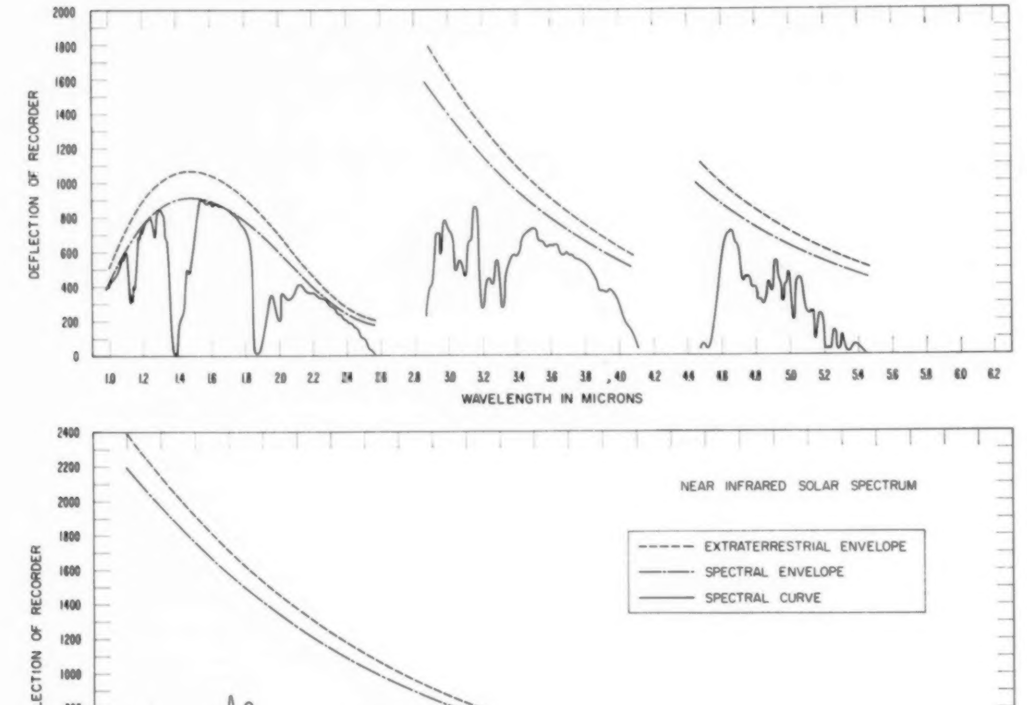

Fig. 1. Direct recording of the infrared solar spectrum with the atmospheric absorption bands as recorded with a prism spectrometer. The extraterrestrial envelope represents the response of the spectrometer to the solar radiation outside of the earth's atmosphere. The spectrum envelope curve represents the separation between the continuum and the selective absorption.

them. The physical slit-width was changed at these separating positions and kept constant throughout each of the transmission intervals. Table I gives the actual physical slit-width and the corresponding spectral slit-widths used for each of the transmission regions to be reported in this paper. The spectral slit-width is taken to be the total spectral interval passed by the exit slit and was taken directly from the Perkin-Elmer manual for the double monochromator.

## Data Reduction

In order to reduce the spectral curves to numerical form, the analysis was performed at numerous discrete wavelength positions. The number of these positions within each spectral region is given in Table I. These positions were closely spaced in order to permit accurate interpolation of the absorption coefficient between the measured values. In order to obtain the wavelength distribution of the response of the spectrometer to the extraterrestrial solar energy flux, the value of the observed deflection at each of the selected wavelength positions was plotted as the logarithm of the deflection vs the air mass. The air mass is defined as the ratio of the slant path length for the solar rays through the atmosphere to the path length if the sun were in the zenith. This ratio is usually equal to the secant of the solar zenith angle, except for large angles when atmospheric refraction and earth curvature need to be taken into account The basic air-mass relationship for all solar angles has been computed by Bemporad[2] and his curve was used for computing the air-mass values. For each of the wavelength positions a least-squares straight line was fitted to the logarithm of the deflection to the base $e$ vs air-mass data by means of a computer program. Not all of the points were used for the computation of the equations of the lines, but only the points which appeared subjectively to represent the "best" values. These points are shown heavier than the others in Fig. 2, which is a plot of the logarithm of the recorder deflection vs the air mass. The same

**Table I. Wavelength Regions Scanned, Spectral Slit-Widths, and Number of Data Points for Data Reduction**

| Wavelength region ($\mu$) | 1.0–2.5 | 2.9–4.0 | 4.5–5.4 | 7.4–13.0 |
|---|---|---|---|---|
| Physical slit-width ($\mu$) | 20 | 150 | 300 | 1700 |
| Spectral slit-width in $cm^{-1}$ | 26.2–27.2 | 96.2–52.0 | 68.8–37.1 | 71.5–18.6 |
| Number of wavelength data points | 51 | 32 | 29 | 91 |

points used to determine these lines were used throughout the entire analysis. However, the point at the largest air mass was lost for the region from 4.5 to 13.0 $\mu$ when the sun set during the recording of the last spectrum. It will be noticed that the other points, particularly those observations toward noon, tend to depart strongly from a straight line fit. This phenomenon has been noted by nearly all observers of atmospheric transmission and appears to be one of increasing turbulence toward noon which brings more dust and water vapor into the tropospheric air near the ground. This is evident from Fig. 3, which shows the change in zenith water-vapor amount throughout the day. For this reason it is necessary to determine from the data the most probable "best" straight line along which all the points would fall if there were not any transient disturbances in the lower atmosphere. The points chosen seem to represent this position best. The arrows in Fig. 3 indicate the regions of that curve corresponding to the points used in the analysis.

The intercept of the straight line with the zero air-mass position gave the deflection corresponding to the extraterrestrial solar energy at each wavelength. A smooth curve was then fitted to these points which represents the approximate extraterrestrial deflection envelope the spectrometer would record if it were receiving solar energy outside of the earth's atmosphere. In the window regions, where the absorption is small, the extrapolation to the extraterrestrial deflection is of high accuracy. Nearby and within the absorption bands the extrapolation to the extraterrestrial deflection is poor. The extrapolation is particularly poor within the limits of the large absorption bands which separate the major wavelength regions. Since it is desirable that the extraterrestrial deflection at the extension of the long wavelength terminus of one region be consistent with the extraterrestrial deflection at the beginning of the next region, with the proper allowance for slit-width change, it is necessary to consider the energy response characteristics of the spectrometer. The energy received by the thermocouple detector through the spectrometer exit slit is given by the following relationship:

$$e_\lambda = N_\lambda s l \frac{A}{f^2} \Delta\lambda T_\lambda,$$

where $N_\lambda$ = monochromatic radiance of the sun in cal/(cm² sr sec $\mu$), $s$ = slit-width in cm (entrance and exit slit are equal), $l$ = slit length in cm, $A$ = effective area of the prism projected normal to the light path in cm², $f$ = focal length of the spectrometer collimating mirror in cm, $\Delta\lambda$ = spectral bandpass of the spectrometer in microns, $T_\lambda$ = monochromatic transmission coefficient of the spectrometer including reflectivity losses by mirrors and absorption loss in the prism. The spectral bandpass of the spectrometer, $\Delta\lambda$, was computed as a function of the wavelength. Hence, it was first necessary to obtain the monochromatic radiance of the sun, $N_\lambda$, as a function of the wavelength

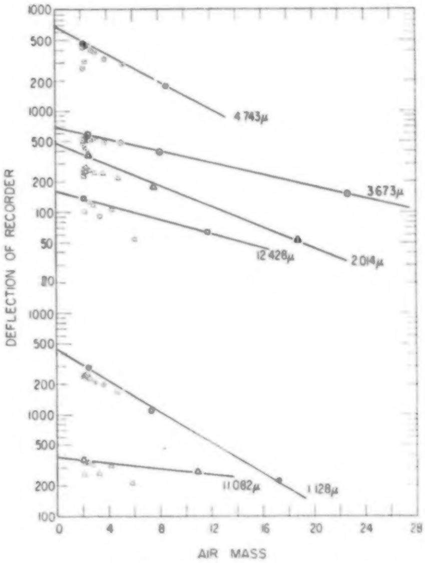

Fig. 2. Logarithm of deflection of recorder vs air mass as used to obtain values of deflection on the extraterrestrial solar radiation curve at zero mass. The heavier points were those used for computing the equation of each line.

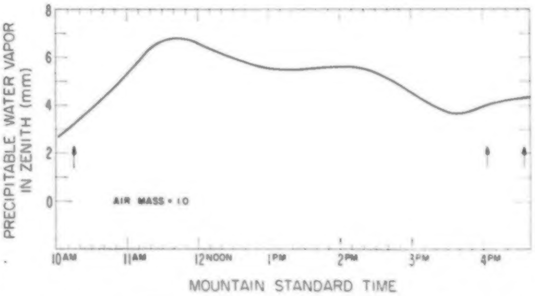

Fig. 3. The amount of precipitable water vapor in mm in a vertical column of the atmosphere as a function of the time of day over Denver, Colorado, on 12 January 1955.

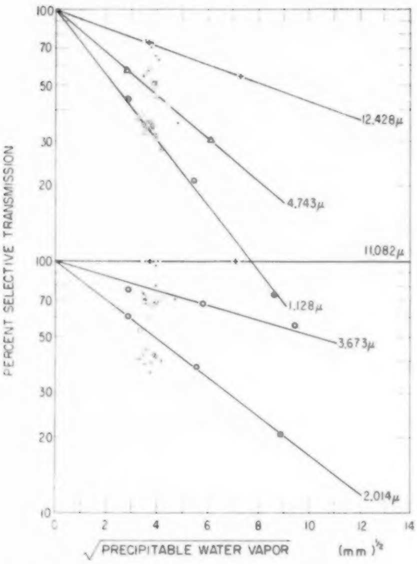

Fig. 4. Selective absorption on a log $\bar{T}$ vs square root of precipitable water vapor in mm for selected wavelengths throughout the infrared spectrum. The heavier points were those used for computing the slope of each line.

over the range 1.0 to 13.0 μ. Use was made of the data by Peyturaux[3] for the near infrared from 1.0 to 2.4 μ, the determination by Saiedy and Goody[4] at 11.10 μ, and the compilation by Kuiper[5] to determine the shape of $N_\lambda$ as a function of the wavelength. In between data points, across a sizable gap from 2.4 to 11.1 μ, a curve was plotted which represented a smooth transition in the apparent blackbody temperature from 5880°K at 2.4 μ to 5036°K at 11.1 μ, which was consistent with the observations referred to above.

The deflection of the recorder is proportional to the energy passing through the exit slit, hence

$$D_\lambda = K_\lambda e_\lambda = K_\lambda N_\lambda s \Delta\lambda \frac{lA}{f^2} T_\lambda = N_\lambda s \Delta_\lambda \tau_\lambda,$$

where $K_\lambda$ is the proportionality constant and $\tau_\lambda = K_\lambda(lA/f^2)T_\lambda$. From the plot of $N_\lambda$, the known values of $s$ and $\Delta\lambda$, and the approximate extraterrestrial deflection envelope which was determined as described above, a continuous $\tau_\lambda$ was then smoothed so that it was a continuous function of the wavelength, unperturbed by the effect of any of the large absorption bands. From these smoothed values of $\tau_\lambda$, the supposed extraterrestrial deflection $D_\lambda$ at every wavelength position was then determined. This then tied together, as a consistent envelope, the extraterrestrial deflections within each of the wavelength regions, despite the fact that the physical slit-width was changed considerably at each boundary between wavelength regions. This permitted a careful determination of the extraterrestrial deflections within the broad absorption bands where otherwise they would be unavailable. The extraterrestrial deflection envelope is shown in Fig. 1.

The problem of deciding a "correct" location for the spectrum envelope is a difficult one and somewhat arbitrary. In fact, there is probably no strictly unique location for the spectrum envelope. It represents essentially the separation between the "selective" absorption and the "continuum" depletion. The monochromatic "continuum" depletion represents the ratio of the deflection on the spectrum envelope to the deflection on the extraterrestrial curve at a given wavelength position.

The means used for the determination of the spectrum envelope in the present work was to select the best "windows" throughout the spectrum, namely at 1.542 and 11.082 μ, and to normalize the spectrum envelope to touch the spectrum curve at these wavelength positions. Actually, the continuum was determined at these window positions for air mass 1.0, and since the value of the continuum depletion was nearly the same at 11.082 μ as at 1.542 μ, a straight line continuum was taken over the entire wavelength span. This zenith continuum function was then applied to each spectrum and a different spectral envelope was adjusted to each spectrum, since the continuum depletion is a function of the air mass. This perforce throws the responsibility for attenuation more strongly into the "selective" absorption term rather than letting the "continuum" depletion vary drastically with the wavelength. Although this is not a completely correct procedure, there is really no unique way to distinguish the line of demarcation between the "continuum" and the "selective" depletion processes from this type of observational data. The departure from the "true" continuum curve will only be significant within the strong absorption bands. Deirmendjian[6] has discussed the shape of the continuum curve with wavelength, as calculated using scattering theory including absorption. It might be possible to normalize Diermendjian's position on our continuum curve and to then assume that the continuum follows the shape of his curve throughout the spectrum. Although this might be a somewhat better approach to reality, there is no assurance that this actually represents the observed continuum behavior with wavelength. For this reason, in the present analysis, only a monotonically smooth continuum was derived. Once the spectrum envelope was fixed, then the selective absorption could be derived.

In order to analyze the "selective" absorption an analysis must first be made concerning the nature of the absorption. Because of the complexity of the vibration–rotation absorption bands for polyatomic molecules and the enormous difficulty of describing the detailed behavior of the absorption as a function of the wavelength, it has been convenient for workers to make use of transmission functions which describe

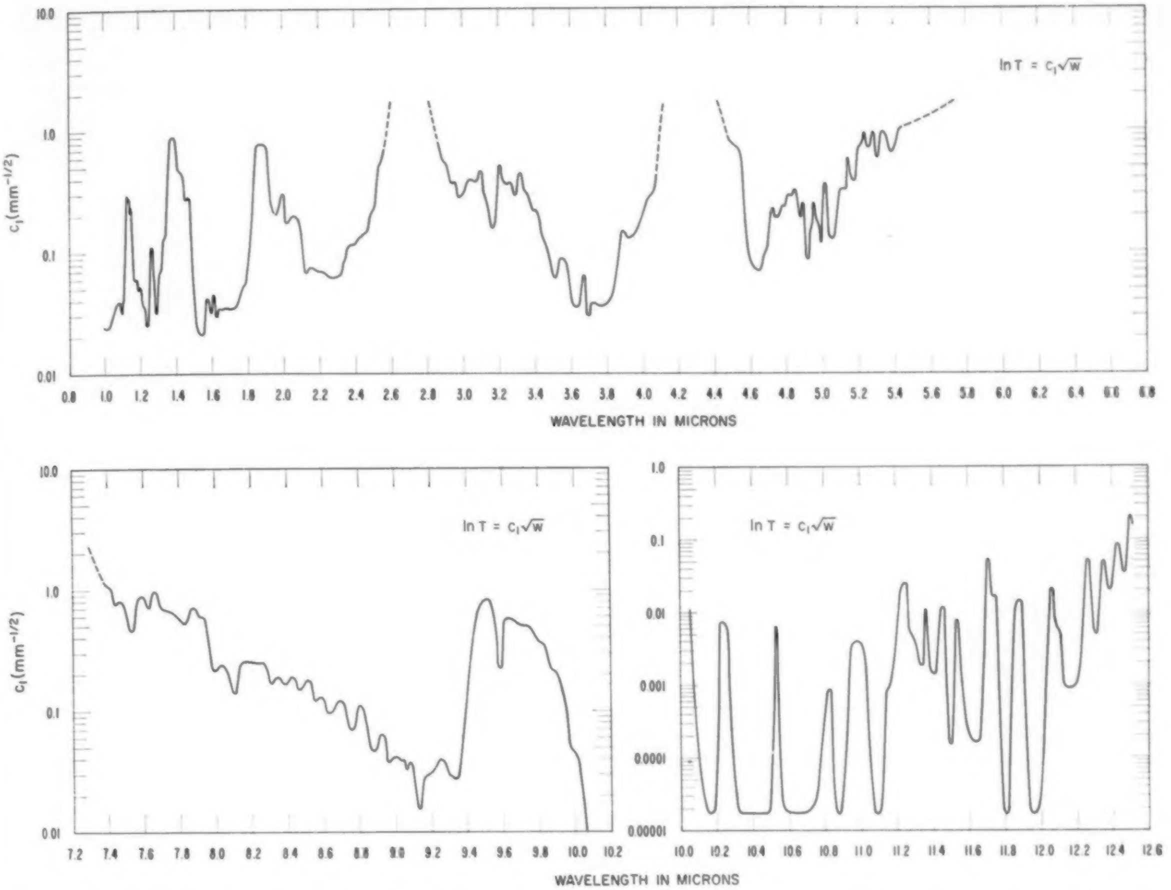

Fig. 5. The extinction coefficient, $c_1$, defined by the strong random band model, ln $\bar{T}$ vs square root water vapor, given as a function of the wavelength for a slant path through the entire atmosphere.

the gross behavior of the transmission over a given wavelength interval to a reasonable degree of approximation. Since the infrared absorption by atmospheric gases is primarily due to water vapor, carbon dioxide, and ozone, it is then necessary to consider the transmission functions for these gases. For water vapor a random model derived by Goody[7] has matched very closely the disordered distribution of the numerous absorption lines within the bands. The mean transmission over a large number of lines is given by the following relationship:

$$\bar{T}(\alpha,w) = \exp\left[-\frac{kw}{2\pi\delta\left(1+\dfrac{kw}{\pi\alpha}\right)^{1/2}}\right],$$

where $w$ = quantity of water vapor along the path, $k$ = average line intensity in the spectral interval, $\alpha$ = mean half-width of the lines, and $\delta$ = mean spacing of the lines.

This expression can be approximated in the following fashion:

If $kw/\pi\alpha \gg 1$

$$\ln \bar{T} \cong \left(\frac{-k\alpha}{4\pi\delta^2}\right)^{1/2} w^{1/2} = -c_1 w^{1/2};$$

If $kw/\pi\alpha = 1$

$$\ln \bar{T} \cong \frac{-k}{(2\delta)^{1/2}}\, w = -c_2 w;$$

If $kw/\pi\alpha \ll 1$

$$\ln \bar{T} \cong \frac{-kw}{\delta}\left(1 - \frac{1}{2}\frac{kw}{\pi\alpha}\right) = -\,(c_3 w - c_4 w^2).$$

The square-root law approximation will be expected to hold true throughout the main body of the absorption band and, depending upon the optical depth of the path length, may hold true out into the wings of the absorption band where the lines are weak. The lower approximation in the form of a quadratic should apply in the wings of bands and for small optical depth. The strictly linear approximation law should hold for intermediate situations. Clearly $c_4$ will be very much

**Table II. Values of the Atmospheric Extinction Coefficients for Various Infrared Wavelengths and the Identification of the Absorbing Constituents**[a]

| $\lambda$ ($\mu$) | $-c_1$ mm$^{-1/2}$ | $\Sigma(\Delta y)^2c_1$ | $-c_2$ mm$^{-1}$ | $\Sigma(\Delta y)^2c_3$ | $c_5$ $m^{-1}$ | $\Sigma(\Delta y)^2c_5$ | Atmospheric absorbers |
|---|---|---|---|---|---|---|---|
| 1.018 | $2.39 \times 10^{-2}$ | $6.33 \times 10^{-4}$ | $3.05 \times 10^{-3}$ | $3.94 \times 10^{-3}$ | $4.90 \times 10^{-2}$ | $4.59 \times 10^{-4}$ | $H_2O$ |
| 1.082 | 3.97 | $3.66 \times 10^{-3}$ | 5.30 | 1.53 | 7.57 | $3.39 \times 10^{-3}$ | $H_2O$ |
| 1.094 | 3.36 | 1.31 | 4.43 | 1.73 | 6.60 | 1.42 | $H_2O$ |
| 1.098 | 3.19 | 2.83 | 4.27 | $5.58 \times 10^{-4}$ | 6.26 | 2.95 | $H_2O$ |
| 1.101 | 3.82 | 2.09 | 5.04 | $2.03 \times 10^{-3}$ | 7.35 | 1.98 | $H_2O$ |
| 1.128 | $3.00 \times 10^{-1}$ | $6.45 \times 10^{-4}$ | $3.86 \times 10^{-2}$ | $9.31 \times 10^{-2}$ | $2.80 \times 10^{-1}$ | $4.89 \times 10^{-2}$ | $H_2O$ |
| 1.131 | 2.72 | $2.19 \times 10^{-3}$ | 3.52 | 7.34 | 2.69 | 3.13 | $H_2O$ |
| 1.137 | 2.83 | $1.29 \times 10^{-4}$ | 3.63 | 9.89 | 2.76 | 4.74 | $H_2O$ |
| 1.144 | 2.15 | $2.53 \times 10^{-3}$ | 2.79 | 5.64 | 2.44 | 1.27 | $H_2O$ |
| 1.147 | 2.34 | 1.58 | 3.05 | 6.90 | 2.56 | 2.22 | $H_2O$ |
| 1.178 | $6.05 \times 10^{-2}$ | 4.66 | $7.99 \times 10^{-3}$ | $3.83 \times 10^{-3}$ | 1.08 | $3.87 \times 10^{-3}$ | $H_2O$ |
| 1.189 | 4.90 | 6.70 | 6.56 | 1.04 | $9.00 \times 10^{-2}$ | 6.42 | $H_2O$ |
| 1.193 | 5.32 | 5.25 | 7.06 | 2.32 | 9.66 | 4.87 | $H_2O$ |
| 1.222 | 3.54 | 4.06 | 4.65 | 1.12 | 6.81 | 4.37 | $CO_2$, $H_2O$ |
| 1.236 | 2.53 | 4.20 | 3.36 | 1.10 | 5.04 | 4.76 | $H_2O$ |
| 1.264 | $1.13 \times 10^{-1}$ | 7.22 | $1.45 \times 10^{-2}$ | $1.43 \times 10^{-2}$ | $1.68 \times 10^{-1}$ | 2.19 | $O_2$ |
| 1.276 | $6.56 \times 10^{-2}$ | 4.66 | $8.50 \times 10^{-3}$ | $5.68 \times 10^{-3}$ | 1.14 | 3.53 | $O_2$, $H_2O$ |
| 1.288 | 3.17 | 5.70 | 4.20 | 1.35 | $6.15 \times 10^{-2}$ | 6.24 | $H_2O$, $O_2$ |
| 1.314 | 7.09 | $1.01 \times 10^{-2}$ | 9.24 | 4.79 | $1.20 \times 10^{-1}$ | 8.28 | $H_2O$ |
| 1.335 | $1.32 \times 10^{-1}$ | $4.60 \times 10^{-3}$ | $1.68 \times 10^{-2}$ | $3.03 \times 10^{-2}$ | 1.87 | 4.72 | $H_2O$ |
| 1.384 | 9.00 | 4.92 | $1.03 \times 10^{-1}$ | $1.83 \times 10^{-1}$ | 3.37 | $3.72 \times 10^{-1}$ | $H_2O$ |
| 1.432 | 4.26 | 2.06 | $5.24 \times 10^{-2}$ | 1.73 | 3.09 | 1.61 | $H_2O$, $CO_2$ |
| 1.457 | 2.72 | 6.06 | 3.47 | $5.90 \times 10^{-2}$ | 2.64 | $2.73 \times 10^{-2}$ | $H_2O$ |
| 1.472 | 2.89 | $4.74 \times 10^{-3}$ | 3.69 | $6.69 \times 10^{-2}$ | 2.70 | 3.51 | $H_2O$ |
| 1.542 | $2.12 \times 10^{-2}$ | 3.36 | $2.84 \times 10^{-3}$ | $4.32 \times 10^{-4}$ | $4.28 \times 10^{-2}$ | $3.82 \times 10^{-3}$ | $H_2O$, $CO_2$ |
| 1.572 | 4.08 | 3.92 | 5.31 | $2.40 \times 10^{-3}$ | 7.73 | 4.20 | $CO_2$ |
| 1.599 | 3.18 | 3.92 | 4.16 | 1.75 | 6.20 | 4.44 | $CO_2$ |
| 1.608 | 4.26 | 4.31 | 5.54 | 2.76 | 8.02 | 4.59 | $CO_2$ |
| 1.626 | 2.95 | 5.34 | 3.93 | $7.95 \times 10^{-4}$ | 5.77 | 5.84 | $CH_4$ |
| 1.644 | 3.46 | 4 83 | 4.57 | 8.40 | 6.67 | 5.16 | $CO_2$, $CH_4$ |
| 1.650 | 3.43 | 4.95 | 4.52 | $1.29 \times 10^{-3}$ | 6.62 | 5.39 | $CO_2$, $CH_4$ |
| 1.676 | 3.49 | 5.42 | 4.60 | 1.34 | 6.71 | 5.86 | $H_2O$, $CH_4$ |
| 1.732 | 3.50 | 4.23 | 4.57 | 2.37 | 6.76 | 4.76 | $H_2O$, $CH_4$ |
| 1.782 | 5.43 | 5.43 | 6.93 | 4.44 | 9.76 | 5.08 | $H_2O$, $CH_4$ |
| 1.862 | $7.80 \times 10^{-1}$ | 9.29 | $8.94 \times 10^{-2}$ | $2.26 \times 10^{-1}$ | $3.30 \times 10^{-1}$ | $3.81 \times 10^{-1}$ | $H_2O$ |
| 1.955 | 2.05 | $4.74 \times 10^{-4}$ | 2.53 | 9 54 $\times 10^{-2}$ | 2.38 | $3.05 \times 10^{-2}$ | $H_2O$, $CO_2$ |
| 2.008 | 3.05 | $8.73 \times 10^{-3}$ | 3.68 | $1.96 \times 10^{-1}$ | 2.82 | $1.22 \times 10^{-1}$ | $CO_2$, $H_2O$ |
| 2.014 | 1.77 | $8.57 \times 10^{-5}$ | 2.19 | $6.97 \times 10^{-2}$ | 2.21 | $1.52 \times 10^{-2}$ | $CO_2$, $H_2O$ |
| 2.057 | 1.99 | $4.13 \times 10^{-4}$ | 2.48 | 7.12 | 2.33 | 1.88 | $CO_2$, $H_2O$ |
| 2.124 | $6.79 \times 10^{-2}$ | $1.32 \times 10^{-3}$ | $8.52 \times 10^{-3}$ | 1.22 | 1.18 | $1.03 \times 10^{-3}$ | $H_2O$, $N_2O$ |
| 2.156 | 7.50 | $5.59 \times 10^{-4}$ | 9.37 | 1.70 | 1.28 | $4.00 \times 10^{-4}$ | $H_2O$, $CH_4$ |
| 2.201 | 7.00 | $5.31 \times 10^{-3}$ | 8.90 | $6.64 \times 10^{-3}$ | 1.19 | $3.88 \times 10^{-3}$ | $CH_4$, $H_2O$ |
| 2.266 | 6.21 | $2.14 \times 10^{-2}$ | 8.23 | $3.01 \times 10^{-4}$ | 1.06 | $1.71 \times 10^{-2}$ | $CH_4$, $N_2O$, $H_2O$ |
| 2.320 | 6.60 | 1.39 | 8.61 | 4.81 | 1.12 | 1.03 | $CH_4$, $H_2O$ |
| 2.338 | 8.55 | 2.03 | $1.11 \times 10^{-2}$ | $1.67 \times 10^{-3}$ | 1.35 | 1.33 | $CH_4$, $H_2O$ |
| 2.356 | $1.10 \times 10^{-1}$ | 1.87 | 1.42 | 4.32 | 1.62 | $8.05 \times 10^{-3}$ | $CH_4$, $H_2O$ |
| 2.388 | 1.14 | $8.76 \times 10^{-3}$ | 1.45 | $1.31 \times 10^{-2}$ | 1.68 | 3.05 | $H_2O$, $CH_4$ |
| 2.415 | 1.30 | $1.02 \times 10^{-2}$ | 1.66 | 1.43 | 1.81 | 1.58 | $H_2O$, $CH_4$ |
| 2.453 | 1.41 | $6.84 \times 10^{-3}$ | 1.80 | 2.29 | 1.91 | $5.38 \times 10^{-4}$ | $H_2O$ |
| 2.494 | 2.14 | $1.75 \times 10^{-2}$ | 2.51 | $1.78 \times 10^{-1}$ | 2.48 | $8.87 \times 10^{-2}$ | $H_2O$ |
| 2.537 | 5.33 | $3.05 \times 10^{-3}$ | 6.43 | 1.93 | 3.16 | $2.37 \times 10^{-1}$ | $H_2O$ |
| 2.900 | $5.49 \times 10^{-1}$ | $2.58 \times 10^{-3}$ | $6.60 \times 10^{-2}$ | $1.11 \times 10^{-1}$ | $2.99 \times 10^{-1}$ | $1.88 \times 10^{-1}$ | $H_2O$, $N_2O$ |
| 2.941 | 3.75 | $1.82 \times 10^{-2}$ | 4.62 | $5.02 \times 10^{-2}$ | 2.73 | $6.25 \times 10^{-2}$ | $H_2O$ |
| 2.954 | 3.82 | $4.34 \times 10^{-3}$ | 4.64 | 8.96 | 2.80 | 9.54 | $H_2O$, $N_2O$ |
| 2.973 | 2 82 | $1.07 \times 10^{-2}$ | 3.46 | 5.18 | 2.54 | 3.24 | $H_2O$ |
| 3.005 | 2.97 | $9.55 \times 10^{-3}$ | 3.65 | $5.76 \times 10^{-2}$ | 2.59 | 3.98 | $H_2O$ |
| 3.045 | 3.98 | 2.79 | 4.84 | 9.94 | 2.82 | $1.07 \times 10^{-1}$ | $H_2O$ |
| 3.056 | 3.81 | 7.89 | 4.58 | 7.80 | 2.72 | $9.28 \times 10^{-2}$ | $H_2O$ |
| 3.097 | 4.62 | 8.57 | 5.58 | 8.16 | 2.81 | $1.31 \times 10^{-1}$ | $H_2O$ |
| 3.132 | 2.81 | 9.37 | 3.40 | 5.77 | 2.49 | $3.92 \times 10^{-2}$ | $H_2O$, $CH_4$ |

*continued*

| λ ($\mu$) | $-c_1$ mm$^{-1/2}$ | $\Sigma(\Delta y)^2 c_1$ | $-c_2$ mm$^{-1}$ | $\Sigma(\Delta y)^2 c_3$ | $c_5$ $m^{-1}$ | $\Sigma(\Delta y)^2 c_5$ | Atmospheric absorbers |
|---|---|---|---|---|---|---|---|
| 3.156 | 1.57 | $1.10 \times 10^{-2}$ | 1.91 | 2.43 | 1.94 | $1.52 \times 10^{-3}$ | $H_2O$, $CH_4$ |
| 3.204 | 5.20 | $2.91 \times 10^{-4}$ | 6.19 | $1.38 \times 10^{-1}$ | 2.92 | $2.11 \times 10^{-1}$ | $H_2O$, $CH_4$ |
| 3.214 | 4.10 | $1.43 \times 10^{-3}$ | 4.91 | 1.19 | 2.78 | 1.35 | $H_2O$, $CH_4$ |
| 3.245 | 3.66 | 5.09 | 4.42 | $9.06 \times 10^{-2}$ | 2.69 | $9.04 \times 10^{-2}$ | $H_2O$, $CH_4$ |
| 3.260 | 3.76 | 1.74 | 4.49 | $1.09 \times 10^{-1}$ | 2.74 | $1.12 \times 10^{-1}$ | $H_2O$, $CH_4$ |
| 3.285 | 2.97 | $1.69 \times 10^{-2}$ | 3.63 | $5.14 \times 10^{-2}$ | 2.49 | $3.27 \times 10^{-2}$ | $CH_4$ |
| 3.317 | 4.51 | $7.66 \times 10^{-4}$ | 5.37 | $1.47 \times 10^{-1}$ | 2.85 | $1.78 \times 10^{-1}$ | $CH_4$, $H_2O$ |
| 3.344 | 3.17 | $1.37 \times 10^{-2}$ | 3.87 | $5.72 \times 10^{-2}$ | 2.55 | $4.46 \times 10^{-2}$ | $H_2O$, $CH_4$ |
| 3.403 | $2.22 \times 10^{-1}$ | 1.54 | $2.72 \times 10^{-2}$ | 3.92 | $2.26 \times 10^{-1}$ | $9.99 \times 10^{-3}$ | $CH_4$, $H_2O$ |
| 3.450 | 1.24 | 1.78 | 1.53 | 1.42 | 1.68 | 1.27 | $CH_4$, $H_2O$ |
| 3.507 | $6.14 \times 10^{-2}$ | $4.86 \times 10^{-3}$ | $7.44 \times 10^{-3}$ | 1.01 | 1.06 | 1.66 | $CH_4$, HDO |
| 3.538 | 8.87 | 2.68 | $1.06 \times 10^{-2}$ | 2.24 | 1.40 | $5.14 \times 10^{-4}$ | $CH_4$, HDO, $H_2O$ |
| 3.573 | 8.09 | $3.10 \times 10^{-2}$ | 1.00 | 3.01 | 1.27 | $1.89 \times 10^{-2}$ | HDO, $CH_4$, $N_2O$ |
| 3.633 | 3.54 | $8.72 \times 10^{-3}$ | $3.82 \times 10^{-3}$ | $3.20 \times 10^{-2}$ | $6.85 \times 10^{-2}$ | 1.01 | $CH_4$, HDO |
| 3.673 | 6.48 | 3.93 | 7.33 | 4.13 | $1.12 \times 10^{-1}$ | $7.70 \times 10^{-3}$ | HDO, $CH_4$ |
| 3.696 | 3.00 | $1.67 \times 10^{-2}$ | 3.09 | 4.09 | $5.93 \times 10^{-2}$ | $1.80 \times 10^{-2}$ | HDO, $CH_4$ |
| 3.712 | 3.80 | 1.36 | 4.02 | 4.38 | 7.28 | 1.63 | $CH_4$, HDO |
| 3.765 | 3.63 | 1.45 | 3.82 | 4.40 | 7.00 | 1.72 | HDO, $CH_4$ |
| 3.812 | 4.01 | 1.47 | 4.26 | 4.72 | 7.64 | 1.76 | $H_2DO$, $CH_4$ |
| 3.888 | $1.50 \times 10^{-1}$ | $2.94 \times 10^{-3}$ | $1.73 \times 10^{-2}$ | 8.52 | $1.93 \times 10^{-1}$ | 2.50 | NO |
| 3.923 | 1.30 | 5.97 | 1.49 | 8.89 | 1.80 | 2.53 | $N_2O$,$CH_4$ |
| 3.948 | 1.37 | $3.60 \times 10^{-4}$ | 1.59 | 6.07 | 1.83 | 1.37 | $N_2O$, $CH_4$ |
| 4.045 | 2.90 | $5.75 \times 10^{-2}$ | 3.49 | $1.80 \times 10^{-1}$ | 2.42 | $1.08 \times 10^{-1}$ | $N_2O$ |
| 4.494 | $7.87 \times 10^{-1}$ | $1.36 \times 10^{-3}$ | $1.36 \times 10^{-1}$ | $6.64 \times 10^{-2}$ | $4.39 \times 10^{-1}$ | $1.21 \times 10^{-1}$ | $N_2O$, $CO_2$ |
| 4.515 | 7.58 | 4.92 | 1.28 | 9.34 | 4.41 | 1.38 | $N_2O$, CO |
| 4.656 | $6.99 \times 10^{-2}$ | 2.41 | $1.25 \times 10^{-2}$ | $1.47 \times 10^{-3}$ | 1.27 | $2.60 \times 10^{-3}$ | $N_2O$, $H_2O$, CO |
| 4.681 | 9.86 | 1.64 | 1.74 | 5.61 | 1.68 | 1.19 | $N_2O$, $H_2O$, CO, $O_3$ |
| 4.727 | $2.29 \times 10^{-1}$ | $7.27 \times 10^{-4}$ | 4.00 | $3.03 \times 10^{-2}$ | 2.92 | 2.05 | $CO_2$, $O_3$, $H_2O$, CO |
| 4.743 | 1.94 | 1.45 | 3.38 | 2.98 | 2.68 | 1.54 | $CO_2$, $O_3$, CO, $H_2O$ |
| 4.783 | 2.41 | 4.99 | 4.22 | 3.40 | 3.01 | 3.29 | $O_3$, $H_2O$, $CO_2$, CO |
| 4.812 | $2.96 \times 10^{-1}$ | 1.29 | $5.16 \times 10^{-2}$ | 4.61 | $3.33 \times 10^{-1}$ | $1.03 \times 10^{-2}$ | $CO_2$, $O_3$, $H_2O$, CO |
| 4.846 | 3.23 | 3.65 | 5.64 | 4.54 | 3.44 | 1.22 | $CO_2$, $H_2O$, CO, $O_3$ |
| 4.879 | 1.95 | $2.52 \times 10^{-3}$ | 3.44 | $1.78 \times 10^{-2}$ | 2.66 | $8.61 \times 10^{-6}$ | $CO_2$, $H_2O$, CO |
| 4.893 | 2.51 | 2.23 | 4.42 | 2.62 | 3.05 | $1.56 \times 10^{-3}$ | $CO_2$, $H_2O$, CO |
| 4.918 | $8.70 \times 10^{-2}$ | 1.97 | 1.54 | $3.61 \times 10^{-3}$ | 1.52 | 1.77 | $CO_2$, $H_2O$, CO |
| 4.955 | $2.54 \times 10^{-1}$ | $4.05 \times 10^{-5}$ | 4.40 | $4.83 \times 10^{-2}$ | 3.12 | 8.59 | $H_2O$, $CO_2$ |
| 4.979 | 1.75 | $2.32 \times 10^{-3}$ | 3.08 | 1.53 | 2.49 | $4.43 \times 10^{-5}$ | $H_2O$, $CO_2$ |
| 4.991 | 1.19 | 3.47 | 2.11 | $5.39 \times 10^{-3}$ | 1.92 | $2.00 \times 10^{-3}$ | $H_2O$, $CO_2$ |
| 5.019 | 3.74 | $1.80 \times 10^{-4}$ | 6.46 | $6.59 \times 10^{-2}$ | 3.67 | $2.96 \times 10^{-2}$ | $H_2O$ |
| 5.055 | 1.27 | $3.69 \times 10^{-3}$ | 2.22 | $6.42 \times 10^{-3}$ | 2.01 | $1.74 \times 10^{-3}$ | $H_2O$, $CO_2$ |
| 5.113 | 3.36 | 1.12 | 5.79 | $4.17 \times 10^{-2}$ | 3.46 | $1.18 \times 10^{-2}$ | $H_2O$, $CO_2$ |
| 5.131 | 3.35 | 3.44 | 5.82 | 3.15 | 3.43 | $7.19 \times 10^{-3}$ | $H_2O$, $CO_2$ |
| 5.142 | 5.94 | $2.01 \times 10^{-4}$ | $1.01 \times 10^{-1}$ | 6.98 | 4.11 | $7.95 \times 10^{-2}$ | $H_2O$, $CO_2$ |
| 5.183 | 3.78 | $1.19 \times 10^{-2}$ | $6.63 \times 10^{-2}$ | 1.70 | 3.51 | $4.02 \times 10^{-3}$ | $H_2O$, $CO_2$ |
| 5.208 | 7.48 | $2.27 \times 10^{-3}$ | $1.25 \times 10^{-1}$ | 8.14 | 4.31 | $1.31 \times 10^{-1}$ | $H_2O$, $CO_2$ |
| 5.236 | 9.53 | $1.21 \times 10^{-4}$ | 1.64 | 3.21 | 4.32 | 1.23 | $CO_2$, $H_2O$ |
| 5.257 | 7.21 | $2.59 \times 10^{-2}$ | 1.28 | $3.16 \times 10^{-3}$ | 3.98 | $2.80 \times 10^{-2}$ | $H_2O$, $CO_2$ |
| 5.282 | 9.57 | $5.93 \times 10^{-6}$ | 1.64 | $3.56 \times 10^{-2}$ | 4.34 | $1.29 \times 10^{-1}$ | $H_2O$, $CO_2$ |
| 5.304 | 5.94 | $5.03 \times 10^{-3}$ | 1.04 | 2.82 | 4.00 | $4.28 \times 10^{-2}$ | $H_2O$, $CO_2$ |
| 5.335 | 9.74 | $1.90 \times 10^{-4}$ | 1.65 | $4.13 \times 10^{-2}$ | 4.37 | $1.43 \times 10^{-1}$ | $H_2O$ |
| 5.382 | 6.63 | 1.34 | 1.13 | 6.32 | 4.19 | $9.38 \times 10^{-2}$ | $H_2O$ |
| 5.436 | $1.02 \times 10^{0}$ | $1.12 \times 10^{-3}$ | 1.68 | 5.00 | 4.41 | $1.62 \times 10^{-1}$ | $H_2O$ |
| 7.407 | $1.07 \times 10^{0}$ | $5.69 \times 10^{-5}$ | $1.75 \times 10^{-1}$ | $4.26 \times 10^{-3}$ | $4.18 \times 10^{-1}$ | $2.18 \times 10^{-1}$ | $CH_4$, $H_2O$, HDO |
| 7.442 | $7.59 \times 10^{-1}$ | $1.53 \times 10^{-2}$ | 1.28 | $1.16 \times 10^{-4}$ | 3.97 | 1.06 | $H_2O$, $CH_4$ |
| 7.468 | 8.06 | $6.18 \times 10^{-3}$ | 1.35 | $8.58 \times 10^{-4}$ | 4.04 | 1.40 | $H_2O$, $CH_4$ |
| 7.535 | 4.57 | $4.35 \times 10^{-2}$ | $7.77 \times 10^{-2}$ | $2.11 \times 10^{-3}$ | 3.61 | $2.18 \times 10^{-2}$ | $H_2O$, $CH_4$ |
| 7.593 | 8.82 | $7.01 \times 10^{-3}$ | $1.48 \times 10^{-1}$ | $1.03 \times 10^{-4}$ | 4.05 | $1.45 \times 10^{-1}$ | $H_2O$, $CH_4$, $N_2O$ |
| 7.628 | 7.17 | 8.53 | 1.20 | 9.94 | 3.99 | 1.19 | $N_2O$, $H_2O$, $CH_4$ |
| 7.663 | 9.70 | 5.24 | 1.63 | $6.23 \times 10^{-5}$ | 4.08 | 1.60 | $CH_4$, $N_2O$, $H_2O$ |
| 7.710 | 6.87 | $2.56 \times 10^{-2}$ | 1.17 | $1.22 \times 10^{-3}$ | 3.89 | $7.64 \times 10^{-2}$ | $CH_4$, $N_2O$, $H_2O$ |
| 7.784 | 5.99 | 3.18 | 1.02 | 1.41 | 3.81 | 5.50 | $CH_4$, $N_2O$, $H_2O$ |
| 7.829 | 5.32 | 2.63 | $9.00 \times 10^{-2}$ | $7.19 \times 10^{-5}$ | 3.76 | 5.05 | $N_2O$, $CH_4$, $H_2O$ |
| 7.874 | 7.08 | $5.24 \times 10^{-3}$ | $1.18 \times 10^{-1}$ | $3.02 \times 10^{-3}$ | 4.01 | $1.31 \times 10^{-1}$ | $N_2O$, $CH_4$, $H_2O$ |

*continued*

| $\lambda$ ($\mu$) | $-c_1$ $mm^{-1/2}$ | $\Sigma(\Delta y)^2c_1$ | $-c_2$ $mm^{-1}$ | $\Sigma(\Delta y)^2c_3$ | $c_5$ $m^{-1}$ | $\Sigma(\Delta y)^2c_5$ | Atmospheric absorbers |
|---|---|---|---|---|---|---|---|
| 7.924 | 5.89 | 4.44 | $9.76 \times 10^{-2}$ | 7.16 | 3.94 | 1.12 | $CH_4$, $N_2O$, $H_2O$ |
| 7.994 | 2.14 | $1.68 \times 10^{-2}$ | 3.58 | 1.18 | 2.84 | $2.80 \times 10^{-3}$ | $CH_4$, $N_2O$, $H_2O$ |
| 8.037 | 2.42 | $9.95 \times 10^{-3}$ | 4.03 | 5.23 | 3.03 | $1.12 \times 10^{-2}$ | $CH_4$, $N_2O$, $H_2O$ |
| 8.108 | 1.40 | $1.22 \times 10^{-4}$ | 2.25 | $2.30 \times 10^{-2}$ | 2.28 | 1.57 | $CH_4$, $N_2O$, $H_2O$ |
| 8.163 | 2.56 | $1.11 \times 10^{-4}$ | 4.12 | $3.72 \times 10^{-2}$ | 3.18 | 5.05 | $CH_4$, $H_2O$, HDO |
| 8.221 | 2.48 | 1.75 | 3.99 | 3.78 | 3.14 | 4.89 | $CH_4$, $H_2O$, HDO |
| 8.258 | 2.52 | $1.46 \times 10^{-3}$ | 3.95 | 5.18 | 3.15 | 6.33 | $H_2O$, $CH_4$, $N_2O$ |
| 8.307 | 1.71 | 9.76 | 2.63 | 7.00 | 2.60 | 5.88 | $N_2O$, $CH_4$, $H_2O$ |
| 8.347 | 1.87 | 7.73 | 2.88 | 6.78 | 2.73 | 6.04 | $N_2O$, $CH_4$, $H_2O$ |
| 8.390 | 1.67 | 7.52 | 2.57 | 6.23 | 2.55 | 5.13 | $N_2O$, $CH_4$, $H_2O$ |
| 8.426 | 1.90 | 3.87 | 2.95 | 5.49 | 2.74 | 4.95 | $N_2O$, $CH_4$, $H_2O$ |
| 8.467 | 1.51 | 4.41 | 2.34 | 4.86 | 2.40 | 3.64 | $N_2O$, $CH_4$, $H_2O$ |
| 8.518 | $1.80 \times 10^{-1}$ | 2.29 | $2.82 \times 10^{-2}$ | 4.66 | $2.66 \times 10^{-1}$ | $3.95 \times 10^{-2}$ | $N_2O$, $H_2O$, $CH_4$ |
| 8.556 | 1.23 | 5.47 | 1.90 | 4.42 | 2.10 | 2.99 | $N_2O$, $H_2O$, $CH_4$, O |
| 8.584 | 1.29 | 3.32 | 2.00 | 3.90 | 2.17 | 2.62 | $N_2O$, $H_2O$, $O_3$ |
| 8.629 | $9.72 \times 10^{-2}$ | 4.84 | 1.50 | 3.44 | 1.77 | 2.10 | $N_2O$, $O_3$ |
| 8.693 | $1.22 \times 10^{-1}$ | 1.07 | 1.91 | 2.79 | 2.08 | 1.70 | $N_2O$, $O_3$, $H_2O$ |
| 8.755 | $7.05 \times 10^{-2}$ | 5.16 | 1.08 | 2.64 | 1.38 | 1.53 | $N_2O$, $O_3$, $H_2O$ |
| 8.803 | $1.11 \times 10^{-1}$ | 1.56 | 1.73 | 2.74 | 1.95 | 1.61 | $N_2O$, $O_3$, $H_2O$ |
| 8.878 | $4.67 \times 10^{-2}$ | 7.21 | $6.94 \times 10^{-3}$ | 2.22 | $9.67 \times 10^{-2}$ | 1.37 | $O_3$, $N_2O$, $H_2O$ |
| 8.921 | 6.39 | 3.70 | 9.78 | 2.09 | $1.27 \times 10^{-1}$ | 1.15 | $O_3$, $H_2O$ |
| 8.960 | 3.79 | 4.62 | 5.66 | 1.47 | $8.05 \times 10^{-2}$ | $8.72 \times 10^{-3}$ | $O_3$, $H_2O$ |
| 9.014 | 4.10 | 2.94 | 6.23 | 1.24 | 8.68 | 6.74 | $O_3$, $H_2O$ |
| 9.039 | 3.92 | 2.58 | 5.95 | 1.12 | 8.34 | 5.97 | $O_3$, $H_2O$ |
| 9.060 | 3.28 | $1.75 \times 10^{-3}$ | 4.98 | $7.84 \times 10^{-3}$ | 7.09 | 4.02 | $O_3$, $H_2O$ |
| 9.080 | 3.75 | $4.61 \times 10^{-4}$ | 5.84 | 5.55 | 8.05 | 2.18 | $O_3$, $H_2O$ |
| 9.128 | 1.56 | $2.12 \times 10^{-3}$ | 2.25 | 4.76 | 3.48 | 3.09 | $O_3$, $H_2O$ |
| 9.166 | 2.85 | $2.22 \times 10^{-4}$ | 4.38 | 3.27 | 6.28 | 1.11 | $O_3$, $CO_2$, $H_2O$ |
| 9.256 | 3.96 | $2.52 \times 10^{-5}$ | 6.21 | 2.69 | 8.48 | $4.71 \times 10^{-4}$ | $O_3$, $CO_2$, $H_2O$ |
| 9.308 | 2.91 | $6.54 \times 10^{-3}$ | 4.14 | $1.52 \times 10^{-2}$ | 6.27 | $9.92 \times 10^{-3}$ | $O_3$, $CO_2$, $H_2O$ |
| 9.330 | 2.77 | 7.52 | 3.89 | 1.61 | 5.97 | $1.09 \times 10^{-2}$ | $O_3$, $CO_2$, $H_2O$ |
| 9.518 | $8.31 \times 10^{-1}$ | 4.54 | $1.34 \times 10^{-1}$ | $2.36 \times 10^{-3}$ | $3.97 \times 10^{-1}$ | $1.60 \times 10^{-1}$ | $O_3$, $CO_2$, $H_2O$ |
| 9.585 | 2.24 | $2.90 \times 10^{-4}$ | $3.51 \times 10^{-2}$ | $2.79 \times 10^{-2}$ | 2.94 | $3.03 \times 10^{-2}$ | $O_3$, $CO_2$, $H_2O$ |
| 9.628 | 5.76 | 4.98 | 9.08 | 2.27 | 3.89 | $1.44 \times 10^{-1}$ | $O_3$, $CO_2$, $H_2O$ |
| 9.718 | 5.01 | $8.04 \times 10^{-3}$ | 8.05 | $7.94 \times 10^{-3}$ | 3.74 | $8.26 \times 10^{-2}$ | $O_3$, $H_2O$, $CO_2$ |
| 9.816 | $3.60 \times 10^{-1}$ | $2.14 \times 10^{-4}$ | $5.66 \times 10^{-2}$ | $3.45 \times 10^{-2}$ | $3.53 \times 10^{-1}$ | $7.91 \times 10^{-2}$ | $O_3$, $H_2O$ |
| 9.882 | 2.13 | $2.21 \times 10^{-2}$ | 3.15 | $1.16 \times 10^{-1}$ | 2.91 | $1.09 \times 10^{-1}$ | $O_3$, $H_2O$ |
| 9.984 | $4.75 \times 10^{-2}$ | $3.36 \times 10^{-4}$ | $7.38 \times 10^{-3}$ | $2.46 \times 10^{-3}$ | $9.90 \times 10^{-2}$ | $2.18 \times 10^{-4}$ | $O_3$, $H_2O$ |
| 10.058 | 1.13 | 1.35 | 1.68 | $8.75 \times 10^{-4}$ | 2.61 | 3.38 | $O_3$, $H_2O$ |
| 10.163 | $1.72 \times 10^{-5}$ | $1.73 \times 10^{-9}$ | $2.47 \times 10^{-6}$ | $4.80 \times 10^{-9}$ | $4.06 \times 10^{-5}$ | $2.61 \times 10^{-9}$ | $O_3$, $C_2O$, $H_2O$ |
| 10.232 | $7.48 \times 10^{-3}$ | $8.36 \times 10^{-5}$ | $1.19 \times 10^{-3}$ | $9.97 \times 10^{-6}$ | $1.78 \times 10^{-2}$ | $2.27 \times 10^{-5}$ | $CO_2$, $H_2O$, $O_3$ |
| 10.334 | $1.72 \times 10^{-5}$ | $1.73 \times 10^{-9}$ | $2.47 \times 10^{-6}$ | $4.80 \times 10^{-9}$ | $4.06 \times 10^{-5}$ | $2.61 \times 10^{-9}$ | $CO_2$, $H_2O$ |
| 10.367 | 1.72 | $1.73 \times 10^{-9}$ | 2.47 | $4.80 \times 10^{-9}$ | 4.06 | 2.61 | $CO_2$, $H_2O$ |
| 10.470 | 1.72 | 1.73 | 2.47 | 4.80 | 4.06 | 2.61 | $CO_2$, $H_2O$ |
| 10.533 | $6.57 \times 10^{-3}$ | $3.68 \times 10^{-5}$ | $9.82 \times 10^{-4}$ | $2.77 \times 10^{-4}$ | $1.54 \times 10^{-2}$ | $9.73 \times 10^{-5}$ | $CO_2$, $H_2O$ |
| 10.622 | $1.72 \times 10^{-5}$ | $1.73 \times 10^{-9}$ | $2.47 \times 10^{-6}$ | $4.80 \times 10^{-9}$ | $4.06 \times 10^{-5}$ | $2.61 \times 10^{-9}$ | $CO_2$, $H_2O$ |
| 10.831 | $8.67 \times 10^{-4}$ | $1.66 \times 10^{-4}$ | $7.71 \times 10^{-5}$ | $1.97 \times 10^{-4}$ | $1.80 \times 10^{-3}$ | $1.78 \times 10^{-4}$ | $CO_2$, $H_2O$ |
| 10.872 | $1.70 \times 10^{-5}$ | $1.80 \times 10^{-9}$ | $2.39 \times 10^{-6}$ | $4.93 \times 10^{-9}$ | $4.00 \times 10^{-5}$ | $2.68 \times 10^{-9}$ | $CO_2$, $H_2O$ |
| 10.985 | $3.90 \times 10^{-3}$ | $7.71 \times 10^{-4}$ | $4.71 \times 10^{-4}$ | $1.13 \times 10^{-3}$ | $8.68 \times 10^{-3}$ | $8.94 \times 10^{-4}$ | $H_2O$, $CO_2$ |
| 11.082 | $1.70 \times 10^{-5}$ | $1.80 \times 10^{-9}$ | $2.39 \times 10^{-6}$ | $4.95 \times 10^{-9}$ | $4.00 \times 10^{-5}$ | $2.68 \times 10^{-9}$ | $H_2O$ |
| 11.152 | $9.02 \times 10^{-4}$ | $1.80 \times 10^{-4}$ | $8.00 \times 10^{-5}$ | $2.14 \times 10^{-4}$ | $1.87 \times 10^{-3}$ | $1.93 \times 10^{-4}$ | $H_2O$ |
| 11.254 | $2.50 \times 10^{-2}$ | 2.30 | $3.70 \times 10^{-3}$ | $2.93 \times 10^{-3}$ | $5.54 \times 10^{-2}$ | 9.62 | $H_2O$ |
| 11.275 | $5.29 \times 10^{-3}$ | $2.22 \times 10^{-3}$ | $5.95 \times 10^{-4}$ | 3.01 | 1.14 | $2.50 \times 10^{-3}$ | $H_2O$ |
| 11.297 | 5.01 | $4.11 \times 10^{-4}$ | 8.43 | $1.33 \times 10^{-4}$ | 1.22 | $3.02 \times 10^{-4}$ | $H_2O$ |
| 11.335 | 1.84 | 7.46 | 1.62 | 8.86 | $3.78 \times 10^{-3}$ | 7.99 | $H_2O$ |
| 11.366 | $1.11 \times 10^{-2}$ | $1.34 \times 10^{-3}$ | $1.51 \times 10^{-3}$ | $2.93 \times 10^{-3}$ | $2.51 \times 10^{-2}$ | $1.86 \times 10^{-3}$ | $H_2O$ |
| 11.408 | $1.42 \times 10^{-3}$ | $4.45 \times 10^{-4}$ | $1.25 \times 10^{-4}$ | $5.28 \times 10^{-4}$ | $2.92 \times 10^{-3}$ | $4.76 \times 10^{-4}$ | $H_2O$ |
| 11.457 | $1.19 \times 10^{-2}$ | $1.16 \times 10^{-3}$ | $1.61 \times 10^{-3}$ | $2.82 \times 10^{-3}$ | $2.67 \times 10^{-2}$ | $1.68 \times 10^{-3}$ | $H_2O$ |
| 11.498 | $1.52 \times 10^{-4}$ | $4.69 \times 10^{-6}$ | $1.38 \times 10^{-5}$ | $5.65 \times 10^{-6}$ | $3.22 \times 10^{-4}$ | $5.04 \times 10^{-6}$ | $H_2O$ |
| 11.538 | $7.82 \times 10^{-3}$ | $3.06 \times 10^{-4}$ | $1.09 \times 10^{-3}$ | $9.20 \times 10^{-4}$ | $1.80 \times 10^{-2}$ | $4.84 \times 10^{-4}$ | $H_2O$ |
| 11.582 | $3.32 \times 10^{-4}$ | $2.46 \times 10^{-5}$ | $2.90 \times 10^{-5}$ | $2.93 \times 10^{-5}$ | $6.94 \times 10^{-4}$ | $2.63 \times 10^{-5}$ | $H_2O$ |
| 11.627 | 1.66 | $5.70 \times 10^{-6}$ | 1.50 | $6.86 \times 10^{-6}$ | 3.52 | $6.11 \times 10^{-6}$ | $H_2O$ |
| 11.712 | $5.37 \times 10^{-2}$ | $8.94 \times 10^{-4}$ | $8.12 \times 10^{-3}$ | $2.36 \times 10^{-3}$ | $1.09 \times 10^{-1}$ | $7.13 \times 10^{-5}$ | $H_2O$ |

*continued*

| $\lambda$ ($\mu$) | $-c_1$ $\text{mm}^{-1/2}$ | $\Sigma(\Delta y)^2c_1$ | $-c_2$ $\text{mm}^{-1}$ | $\Sigma(\Delta y)^2c_3$ | $c_5$ $m^{-1}$ | $\Sigma(\Delta y)^2c_5$ | Atmospheric absorbers |
|---|---|---|---|---|---|---|---|
| 11.731 | 1.71 | 1.88 | 2.48 | 1.73 | $3.88 \times 10^{-2}$ | $5.81 \times 10^{-4}$ | $H_2O$ |
| 11.751 | 1.68 | 1.94 | 2.43 | 1.70 | 3.80 | 5.80 | $H_2O$ |
| 11.805 | $1.68 \times 10^{-5}$ | $1.89 \times 10^{-9}$ | $2.31 \times 10^{-6}$ | $5.09 \times 10^{-9}$ | $3.95 \times 10^{-5}$ | $2.75 \times 10^{-9}$ | $H_2O$ |
| 11.886 | $1.45 \times 10^{-2}$ | $5.94 \times 10^{-4}$ | $2.05 \times 10^{-3}$ | $2.30 \times 10^{-3}$ | $3.29 \times 10^{-2}$ | $1.09 \times 10^{-3}$ | $H_2O$ |
| 11.951 | $1.68 \times 10^{-5}$ | $1.89 \times 10^{-9}$ | $2.31 \times 10^{-6}$ | $5.09 \times 10^{-9}$ | $3.95 \times 10^{-5}$ | $2.75 \times 10^{-9}$ | $H_2O$ |
| 12.063 | $2.11 \times 10^{-2}$ | $2.98 \times 10^{-5}$ | $3.11 \times 10^{-3}$ | $1.56 \times 10^{-3}$ | $4.74 \times 10^{-2}$ | $3.45 \times 10^{-4}$ | $H_2O$, $CO_2$ |
| 12.084 | $7.55 \times 10^{-3}$ | $7.45 \times 10^{-4}$ | $9.89 \times 10^{-4}$ | 1.58 | 1.72 | 9.97 | $H_2O$ |
| 12.106 | 5.53 | $2.56 \times 10^{-3}$ | 5.98 | 3.48 | 1.20 | $2.87 \times 10^{-3}$ | $H_2O$ |
| 12.142 | $9.08 \times 10^{-4}$ | $2.04 \times 10^{-4}$ | $7.52 \times 10^{-5}$ | $2.42 \times 10^{-4}$ | $1.88 \times 10^{-3}$ | $2.18 \times 10^{-4}$ | $H_2O$, $CO_2$ |
| 12.261 | $5.04 \times 10^{-2}$ | $5.69 \times 10^{-5}$ | $7.32 \times 10^{-3}$ | $7.00 \times 10^{-3}$ | $1.03 \times 10^{-1}$ | $1.86 \times 10^{-3}$ | $H_2O$ |
| 12.307 | $4.90 \times 10^{-3}$ | $5.05 \times 10^{-3}$ | $4.20 \times 10^{-4}$ | 6.05 | $9.94 \times 10^{-3}$ | 5.42 | $CO_2$ |
| 12.353 | $5.03 \times 10^{-2}$ | $6.11 \times 10^{-6}$ | $7.36 \times 10^{-3}$ | 5.40 | $1.03 \times 10^{-1}$ | 1.09 | $H_2O$, $CO_2$ |
| 12.384 | 2.02 | $1.52 \times 10^{-3}$ | 2.77 | 5.16 | $4.49 \times 10^{-2}$ | 2.64 | $CO_2$ |
| 12.428 | 8.40 | $4.52 \times 10^{-6}$ | $1.22 \times 10^{-2}$ | $1.37 \times 10^{-2}$ | $1.56 \times 10^{-1}$ | 4.59 | $H_2O$, $CO_2$ |
| 12.465 | 3.45 | $8.16 \times 10^{-4}$ | $4.90 \times 10^{-3}$ | $6.89 \times 10^{-3}$ | $7.40 \times 10^{-2}$ | 2.64 | $H_2O$, $CO_2$ |
| 12.502 | $2.06 \times 10^{-1}$ | $7.91 \times 10^{-3}$ | $3.09 \times 10^{-2}$ | $1.10 \times 10^{-2}$ | $2.68 \times 10^{-1}$ | 9.61 | $H_2O$, $CO_2$ |
| 12.542 | 1.82 | 9.11 | 2.73 | $7.68 \times 10^{-3}$ | 2.52 | 4.61 | $H_2O$, $CO_2$ |

[a] The extinction coefficients are defined for the following absorption laws: strong random band model $\ln \bar{T} = -c_1w^{1/2}$, weak random band model $\ln \bar{T} = -(c_3w - c_4w^2)$, and strong regular band model $\bar{T} = 1 - c_5m^{1/2}$. The goodness of fit of the various models is given in terms of the sum of the squares of the deviation of the transmission from the straight line fit, $\Sigma(\Delta y)^2$. $w$ is precipitable water vapor along the path in mm; $m$, which is dimensionless, is proportional to the quantity of absorbing material and is defined in the text.

smaller than $c_3$ and can usually be neglected. This would make $c_3$ essentially indistinguishable from $c_2$.

Although for solar radiation traversing the entire atmosphere it is likely that most of the transmission will follow the square-root law, it is nevertheless possible there will be regions in the "windows" where the transmission will follow the linear law to a good approximation. For this reason the monochromatic "selective" transmission data were plotted both as $\ln \bar{T}$ vs square-root water vapor and $\ln T$ vs water vapor. The term "water vapor" as used here refers to the amount of water vapor contained in the path and condensed into a liquid film of thickness in mm. The monochromatic "selective" transmission is defined as the ratio of the deflection on the spectrum curve to the deflection on the spectrum envelope at a given wavelength. Although the square-root law was obeyed by most of the data there are wavelength regions where the linear law appears to be a better fit. These exceptions will be discussed later. The slope of the $\ln \bar{T}$ vs square-root water vapor plot represents the coefficient $c_3$. In Fig. 4 are shown examples of the square-root water vapor plots to which least-squares straight lines were fitted. These computations were made using an IBM 7090 computer. All computations were based on the logarithm to the base $e$ and not to the base 10.

The determination of the amount of water vapor in the solar radiation path was by the method of Fowle[8] using the calibration curve established by Gates[9] for selective absorption in the $\Phi$ band at 1.1 $\mu$. The specific wavelength used was 1.13 $\mu$ and by virtue of using this wavelength position for the water-vapor calibration all of these points fall precisely on a straight line of $\log T$ vs square-root water vapor.

There are regions of the infrared spectrum where the role of water-vapor absorption is negligible but where other molecular species in the atmosphere influence the transmission. The most important of these species is carbon dioxide. The absorption lines comprising an absorption band of carbon dioxide are regularly distributed throughout the band rather than having the appearance of a random-like distribution as for water vapor. Again it is convenient to derive a transmission function for the mean transmission across a portion or all of a band which is comprised of regularly spaced lines. Elsasser[10] derived the following transmission function for a regular band model.

$$T = \int_{-1/2}^{+1/2} \exp\left[-\frac{mk}{\delta}\,\frac{\sinh 2\pi\,\alpha/\delta}{\cosh 2\pi\alpha/\delta - \cos\nu/\delta}\right]\frac{d\nu}{\delta}.$$

This expression leads to the following approximations: When $mk/2\pi\alpha \gg 1$ then

$$\bar{T} \cong 1 - \operatorname{erf}\left[\pi\frac{\alpha}{\delta}\left(\frac{mk}{\pi\alpha}\right)^{1/2}\right]$$

$$\cong 1 - \frac{2(\alpha mk)^{1/2}}{\delta} = 1 - c_5m^{1/2}.$$

## Results

At each of the wavelength positions throughout the spectrum from 1.0 to 12.5 $\mu$ the coefficient $c_1$ was determined by the computer by means of a least-squares straight line fit to the points used for an $\ln \bar{T}$ vs square-root water vapor relationship. The straight line was also forced to pass through $\ln \bar{T} = 0.0$ for zero water

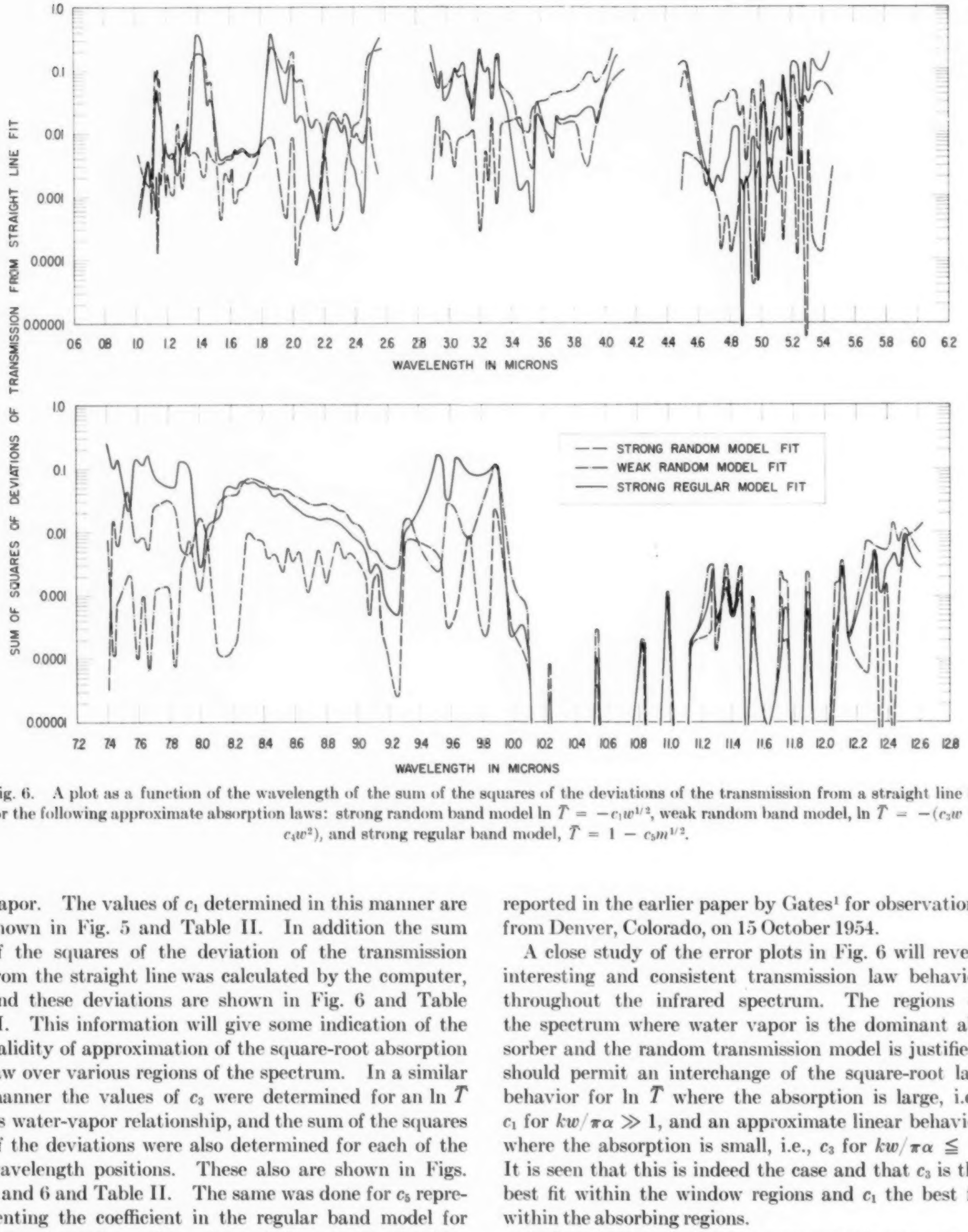

Fig. 6. A plot as a function of the wavelength of the sum of the squares of the deviations of the transmission from a straight line fit for the following approximate absorption laws: strong random band model ln $\bar{T} = -c_1 w^{1/2}$, weak random band model, ln $\bar{T} = -(c_3 w - c_4 w^2)$, and strong regular band model, $\bar{T} = 1 - c_5 m^{1/2}$.

vapor. The values of $c_1$ determined in this manner are shown in Fig. 5 and Table II. In addition the sum of the squares of the deviation of the transmission from the straight line was calculated by the computer, and these deviations are shown in Fig. 6 and Table II. This information will give some indication of the validity of approximation of the square-root absorption law over various regions of the spectrum. In a similar manner the values of $c_3$ were determined for an ln $\bar{T}$ vs water-vapor relationship, and the sum of the squares of the deviations were also determined for each of the wavelength positions. These also are shown in Figs. 5 and 6 and Table II. The same was done for $c_5$ representing the coefficient in the regular band model for large absorption values when $mk/2\pi\alpha \gg 1$ and where the fit $1 - \bar{T}$ was tested as a function of the square root of the air mass.

The values of the coefficient $c_1$ obtained for the first wavelength region agree very closely with the values reported in the earlier paper by Gates[1] for observations from Denver, Colorado, on 15 October 1954.

A close study of the error plots in Fig. 6 will reveal interesting and consistent transmission law behavior throughout the infrared spectrum. The regions of the spectrum where water vapor is the dominant absorber and the random transmission model is justified, should permit an interchange of the square-root law behavior for ln $\bar{T}$ where the absorption is large, i.e., $c_1$ for $kw/\pi\alpha \gg 1$, and an approximate linear behavior where the absorption is small, i.e., $c_3$ for $kw/\pi\alpha \leq 1$. It is seen that this is indeed the case and that $c_3$ is the best fit within the window regions and $c_1$ the best fit within the absorbing regions.

A plot of transmission vs square-root air mass represents an approximate behavior for the regular band model in a region where the lines are regularly spaced and of nearly equal intensity and for relatively large amounts of absorbing matter. The constant $c_5$

represents the best fit for many narrow regions where the lines distributed through the spectrum with even spacing. This should be true in regions where $CO_2$, $CH_4$, and $N_2O$ act singly. When the absorption lines of these gases are intermixed, either together or with $H_2O$ lines, a random appearance may result. This actually would appear to be the situation as shown in Fig. 6. The ozone lines are also distributed more in random fashion and random model should fit best where ozone dominates the spectrum.

A few comments will be made concerning the behavior of the error plots as a function of the wavelength, shown in Fig. 6. In the near infrared, the first wavelength region from 1.0 to 2.5 $\mu$, the situation is very well defined. Considering the water-vapor transmission functions only, the strong random model is by far the best fit in the water bands and the weak random model is generally the best fit in the window regions. At 1.28 $\mu$ the regular band model is the best fit, and this is a narrow region where $O_2$ in the atmosphere is the primary absorbing constituent. At 2.16 and 2.45 $\mu$ the strong regular model is the best fit. These two regions have absorption dominated by $CO_2$.

In the second wavelength region, from 2.9 to 4.0 $\mu$, the behavior in general is consistent. The strong random model fits very well from 2.90 to 3.39 $\mu$ where water vapor dominates the absorption. The entire region from 3.39 to 3.6 $\mu$ is one of strong $CH_4$ influence and relatively minor $H_2O$ influence throughout. It is strikingly clear that this region is one of regular band absorption. Comparison with the line distribution shown in the Migeotte *et al.*[11] atlas shows this to be true. The strong random band model fits best from 3.6 to 4.0 $\mu$; however, over a limited region the regular band model fits nearly as well. Although the wavelength region around 3.95 $\mu$ is dominated by $N_2O$, whose absorption is regular, the spectral slit-width used was sufficiently broad so as to include extraneous lines which interrupted the regularity of the absorption.

The third wavelength region, from 4.5 to 5.4 $\mu$, contains a number of interesting features. To begin with, from 4.5 to 4.73 $\mu$, the strong random model is the best fit, probably because of the very wide spectral slit-width used which caused the spectrometer to observe several absorbing constituents simultaneously. From 4.73 to 4.86 $\mu$ the strong random model dominates and this is because of the numerous $O_3$ lines and some $H_2O$ lines which enter into this region. Then the regular band model is the best fit at 4.88, 4.98, 5.06, and 5.19 $\mu$. An inspection of the Migeotte *et al.* atlas shows the absorption lines to be rather evenly distributed across an interval commensurate with the spectral slit-width centered on each of these wavelengths. The strong random model is the best fit at 4.96, 5.02, 5.28, and 5.38 $\mu$. These are generally regions where there are strong water-vapor lines and where the distribution of lines in the spectrum is very uneven. The really interesting feature is the apparent ability of the spectrometer, with finite slit-width, to distinguish between the strong random line distribution and the regular line distribution over closely spaced intervals. It is not that the response of the instrument uniquely identifies the absorbing constituent by this means, but it does rather uniquely classify the region passed by the slit-width as consisting of randomly spaced lines or regularly spaced lines. There are, of course, transition regions in between where neither situation is unique.

The fourth spectral region, from 7.4 to 12.6 $\mu$ is unusual in that throughout this region are located many excellent "windows". The weak random model fits best from 7.4 to 7.9 $\mu$. Although a few water lines exist throughout this region, it is mainly comprised of $N_2O$ and $CH_4$ absorption. However, the absorption lines are badly mixed and the end result is one of a very irregular type of distribution. The irregularity appears to even out somewhat from 7.9 to 8.04 $\mu$. The strong random model fits best from 8.04 to 9.3 $\mu$, a region which has many regularly spaced $CH_4$ lines or $N_2O$ lines, which also has numerous strong $H_2O$ lines and $O_3$ lines entering in a random fashion. Apparently the weak random fit takes over in a region from 9.40 to 9.54 $\mu$, but the strong random model fits best in the 9.6 to 9.9 $\mu$ region. This is as it should be since $O_3$ dominates the absorption throughout this region. Beyond this, from 10.0 to 12.1 $\mu$ all models are nearly equally good fits. This is because the absorption is very weak, the "windows" are extremely good and nearly any law will be a good representation. Beyond 12.15 $\mu$ the strong random model is the best fit since the spectral slit-width was sufficiently large so as to always include a substantial number of water lines.

Table II lists for each of the wavelength positions throughout the spectrum the values of $c_1$, $c_3$, and $c_5$ as defined by the equations and also the sum of the squares of the deviations of the transmission values from these slopes. A table is particularly useful when one needs to look up a specific value for computational use and although the plot of this data gives a good overall graphic view, when specific numbers are needed a table is easier to use. It should be noted that $c_1$ and $c_3$ are coefficients depending upon the quantity of precipitable water vapor in the atmospheric path in millimeters. The coefficient $c_5$ relates the transmission to the quantity of absorbing material in the path, which depends upon the geometrical air mass factor including atmospheric refraction, earth curvature, and a pressure factor which is the ratio of the pressure at Denver (1610 m above mean sea level) to the mean sea-level pressure. The absorbing constituent is assumed to be in constant mixing ratio throughout the atmosphere. The $m$ in the formula defining $c_5$ is dimensionless since it only includes the air mass and pressure factors.

Although Fig. 5, which is a plot of $c_1$ vs wavelength, is the only coefficient plotted, it is clear from the discussion of the accuracy of fit that no single coefficient is valid throughout the spectrum. In fact, to make a proper calculation of the transmission as a function of the wavelength, one must use $c_1$, $c_3$, or $c_5$, depending upon which one represents the best fit of the data at a particular wavelength position. This means there will be many wavelength positions which fall in transition zones between one model or another. The transmission can always be estimated easily for these transition zones if the transmission is calculated for wavelengths to either side where a specific model represents a more precise approximation.

The continuum coefficient, which is slowly varying with the wavelength and which has been forced to change linearly with the wavelength, has the value $1.210 \times 10^{-2}$ mm$^{-1}$ at 1.542 $\mu$ and $1.075 \times 10^{-2}$ mm$^{-1}$ at 11.082 $\mu$ representing the slope of the straight line fit ln $\bar{T}_c$ vs water vapor. $\bar{T}_c$ is the transmission due to the continuum only. A very much more accurate fit is given for the continuum by a straight line on the ln $\bar{T}_c$ vs quantity of absorbing material. For this the value of the continuum coefficient is $6.195 \times 10^{-2}$ at 1.542 $\mu$ and $5.989 \times 10^{-2}$ at 11.082 $\mu$.

## References

1. D. M. Gates, J. Opt. Soc. Am. **50,** 1299 (1960).
2. A. Bemporad, Met. Z. **24,** 309 (1907).
3. R. Peyturaux, Ann. Astrophys. **15,** 302 (1952).
4. F. Saiedy and R. M. Goody, Monthly Notices Roy. Astron. Soc. **119,** 213 (1959).
5. G. P. Kuiper, *The Sun* (Univ. of Chicago Press, Chicago, 1954).
6. D. Deirmendjian, Quart. J. Roy. Met. Soc. **86,** 371 (1960).
7. R. M. Goody, *The Physics of the Stratosphere* (Cambridge Univ. Press, New York, 1958).
8. F. E. Fowle, Astrophys. J. **35,** 149 (1912); **37,** 359 (1913); **42,** 394 (1915).
9. D. M. Gates, J. Meteorol. **13,** 369 (1956).
10. W. M. Elsasser, Harvard Meteorological Studies, No. 6 (1942).
11. M. Migeotte, L. Neven, and J. Swenson, "The Solar Spectrum from 2.8 to 23.7 $\mu$," Parts I and II, Geophysics Research Directorate, Air Force Cambridge Research Center, Bedford, Mass., 1957.

# The Publications of W. W. Coblentz on Infrared Spectroscopy

The principal work of the late W. W. Coblentz on infrared spectroscopy originally appeared in three Publications of the Carnegie Institution of Washington. Publication No. 35, issued in 1905, dealt with his investigations at Cornell University of the infrared absorption spectra of some 135 organic compounds, with shorter supplementary sections on transmission and reflection spectra. Publication No. 65 (1906) and Publication No. 97 (1908) are concerned with later work on the transmission and reflection spectra of minerals and other inorganic compounds carried out at the U.S. Bureau of Standards.

These classical investigations form the basis of most modern work on analytical infrared spectroscopy. The journals have long been out of print, but, with the kind permission of the Carnegie Institution, they have recently been reprinted in a single volume under the joint sponsorship of the Coblentz Society and the Perkin-Elmer Corporation.

All concerned with modern applications of infrared spectroscopy to problems of chemical structure and analysis should be conversant with this early work, which provides the basis for much of the modern technique. To maintain a properly balanced outlook on the subject, this volume should accompany the standard modern texts on the library shelf of the spectroscopy laboratory.

A limited number of copies of the first reprinting are still available at $3.50 per copy on application to Dr. H. B. Kessler, The Secretary, c/o The Perkin-Elmer Corporation, Norwalk, Connecticut.

*photos D. L. MacAdam*

D. E. Williamson *Cordis* (left) *Applied Optics* Patents Panelist and Deane B. Judd *NBS* retiring editor of *J. Opt. Soc. Am.*

R. E. Stephens *NBS* and I. C. Gardner, a past president of the Optical Society of America.

# Microspectrophotometry

J. J. Wolken and G. K. Strother

Microspectrophotometers, manual and recording, have been constructed with cadmium selenide (CdSe) photoconductive cells and are in use in our laboratory as a spectroscopic tool in the study of the pigment chemistry of photoreceptors in living cells. The basic design and operation of these microspectrophotometers for obtaining absorption spectra are described. The absorption spectrum from the ultraviolet, visible, and near infrared can be obtained in a single sweep for specimen areas as small as 2 $\mu^2$. Examples of absorption spectra of the chloroplast of plant cells, the retinal rods of the visual cells of the eye, and the red blood cell are illustrated. The applications of microspectrophotometry to a variety of biological, biochemical, and chemical problems are indicated.

## Introduction

The use of sensitive, high-speed spectrophotometry for the investigation of the chemistry of plant and animal cells is just in its beginnings. Living cells contain cellular organelles, for example, nucleus, mitochondria, chromatophores, and other structures, whose precise composition is difficult to determine and whose functional chemistry is even more complicated to unravel. Therefore, the development of microanalytical instrumentation to attack this kind of biological problem is necessary. One such method which can be applied to the quantitative study of the chemistry of tissue cells and their organelles is microspectrophotometry.

This was recognized in the late 1930's by Caspersson in Sweden where he initiated the development of microspectrophotometric instrumentation and techniques for the study of the chemistry of the cell and the nucleic acids of the cell nucleus by ultraviolet absorption spectroscopy. The instrumentation in microspectrophotometry and its application to the chemistry of biological tissue cells has been continuously pursued.[1−3] Developments in microspectrophotometry have also been discussed in several texts of cytochemical methods and in recent published symposia.[4−8] Microspectrophotometers for obtaining absorption spectra of living cells have recently been constructed in many laboratories. Descriptions of the designs of some of these instruments and their application to biological studies will be briefly examined.

The microspectrophotometers presently in use are laboratory-built instruments. The essential elements of all of these microspectrophotometers are a monochromatic light source, a microscope, a light chopper, a sensitive photocell (usually a photomultiplier tube), an amplifier, and an output device, usually a recorder. By means of reflecting and quartz optics, a spectral range from the ultraviolet through the visible can be obtained. Living as well as fixed and stained tissue cells have been studied by measuring the absorption spectrum of specimen areas as small as 0.5 $\mu$. Information on cellular constituents can be obtained by scanning specimen areas at fixed wavelengths when their specific absorption peaks are known, for example, nucleic acids, porphyrins, cytochromes, etc.

However, most instruments except, for example, the simplified microspectrophotometer constructed by Denton[9] for the study of the pigments of the retinal rods of the frog eye are generally elaborate ones employing either split or dual-beam optical systems with mechanical beam chopping devices, voltage-regulated photomultiplier tubes with feedback mechanisms, and automatic-recording outputs.[3,10] Quantitative measurements of the optical density of a given specimen, with an instrumental error of less than 5%, can be obtained. The response times of the instruments may be of the order of milliseconds, and measurements from the ultraviolet through the visible are recorded in a few minutes.

---

The authors are at the Biophysical Research Laboratory, Eye and Ear Hospital, University of Pittsburgh School of Medicine, Pittsburgh 13, Pennsylvania.

Received 16 February 1963.

This work was aided in part by the U.S. Public Health Service Institute of Neurological Diseases and Blindness and the National Aeronautics and Space Administration.

Part of this work was completed while Professor Strother was a visiting Stoner Fellow in the Biophysical Research Laboratory. Present address: Department of Physics, Pennsylvania State University, University Park, Pennsylvania.

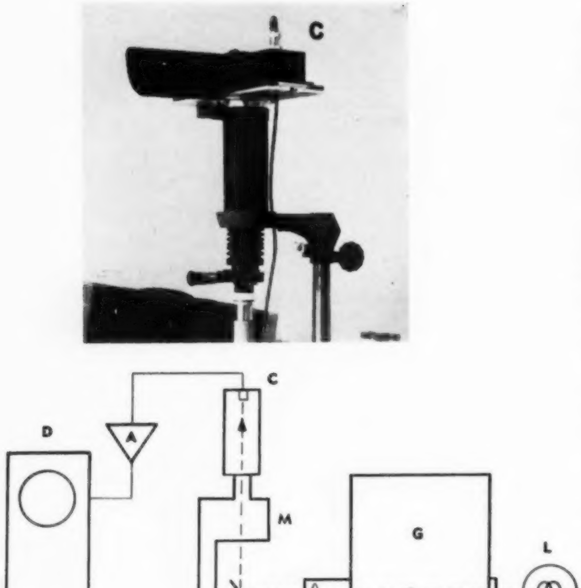

Fig. 1. Diagram of simplified microspectrophotometer (M-1). L, light source; G, monochromator; M, microscope with reflecting optics; C, photoconductive cell; A, dc amplifier; D, oscilloscope. (In place of A and D, a dc voltmeter, Hewlett-Packard type 412 A, is used.) The line drawing shows housing for photocell, viewer, and mounting on sliding track.

## Instrumentation: Design and Construction

### Simplified Microspectrophotometer

In our laboratory we have designed and constructed a simplified microspectrophotometer (M-1) using a CdSe photoconductive cell as the light sensitive element.[11]

Photoconductive CdSe cells have been used for spectral measurements in the infrared region and for x-ray spectroscopy.[12] In our instrument we have applied these cells to visible and ultraviolet microspectrophotometry. Figure 1 is a diagram of the basic design of the instrument, indicating that the light from source L enters a grating monochromator G and that the exit slit of the monochromator is focused by a quartz lens on the condenser of the microscope M. The light passes through the specimen to the photoconductive cell C, which is accurately positioned relative to the image 25 cm above the eyepiece of the microscope. The electrical signal from the photocell is either amplified by the dc amplifier A and displayed on an oscilloscope D or read from a high-impedance dc voltmeter (Hewlett-Packard Type 412 A).

The microspectrophotometer uses either a xenon arc or a tungsten ribbon filament light source and a Bausch & Lomb 250-mm grating monochromator. The microscope is equipped with reflecting objectives (50× with numerical aperture of 0.5, American Optical Company). With these components, the instrument is usable over the wavelength range from 200 to 990 mμ in a single sweep. Using a tungsten ribbon light source the useful range is from 370 to 900 mμ for specimen areas of the order of $2\mu^2$ or larger.

In the construction of this instrument, we have adapted a light-tight rubber bellows which fits over the eyepiece of the microscope and into a light-tight tube. At the other end of the tube, either the ground-glass viewer or the photocell holder may be placed by operating it on a sliding track. (This is shown in Fig. 1.) The entire assembly is swung into place by means of a vertical bar arrangement mounted on a base plate. The height of the photocell can be adjusted by telescoping the tube supporting it. The specimen can be viewed at all times through the telescope inserted between the eyepiece and the bellows.

The photoconductive cells being used at present are special purpose cells (manufactured by the Clairex Corporation of New York) with a photosensitive surface of 0.5 by 1 mm and a radiation sensitivity per unit area roughly equivalent to a photomultiplier tube. They do not require high voltages. The spectral response of the cadmium selenide cells extends from the far ultraviolet to the near infrared, with a rather sharp cutoff at about 1 μ. The peak response is in the visible region of the spectrum at 720 mμ. At high light intensity the time constant of the cell is of the order of milliseconds. At extremely low light levels, the time constant is of the order of seconds.

The maximum magnification employed is 500×. At this magnification, spectra from areas of 2 $\mu^2$ ($1 \times 2$ μ in the object plane) are easily obtained. No limiting apertures are used in this instrument, since the entire photosensitive surface is used for measurements. Optical alignment is not critical, and no light chopping is necessary. A 67.5-V bias supply is used, and at each wavelength setting the dc photocell current is measured by means of the dc voltage drop across a 2-MΩ load resistor. The noise level as determined by photocell current fluctuations is about $2 \times 10^{-3}$ optical density units. Since the entire photosurface of the cell is exposed to the light beam, no effects due to variation in the sensitivity of the photosurface are observed.

The procedure for obtaining an absorption spectrum with the apparatus is relatively simple. The area of interest in the specimen is located on a marked ground-glass screen at the top of the apparatus. The photocell is then put into position, and the dark current is balanced out with a separate bias voltage. At each desired wavelength setting, one reading is taken over the specimen and another over a reference area by moving the cell assembly from one area to the other.

Before another reading, the dark current level is checked and set to zero. The time required to determine a spectral curve depends upon the number of wavelength settings desired and the time constant of the photocell; for a 10-m$\mu$ interval over the range from 400 to 700 m$\mu$, the time required is about 20 minutes. The absorption spectra in Figs. 4 and 6 were obtained with this simplified microspectrophotometer.

## Recording Microspectrophotometer

Recorded data and faster time responses than those available with the simplified microspectrophotometer are desirable, especially for the spectroscopy of photosensitive pigments. As a result, a single-beam recording microspectrophotometer, a modification of our simplified microspectrophotometer, which also uses a photoconductive photocell, has recently been developed in our laboratory.[13] A diagram of the automated instrument (M-2) is shown in Fig. 2. Light from the monochromator is passed through a 100 cps chopper to the substage mirror (front surface) of a microscope equipped with reflecting substage condenser and objective lenses. The light is chopped to allow the use of an ac amplifier tuned to 100 cps. The sample image is focused on a plate having two holes of the same size (holes of approximately 1-mm diam and a magnification of 500 × are used, but these can be varied depending on the sample size). The image of the specimen is adjusted over one hole by moving the slide; the other hole is used for the reference area.

Above the blocking plate a second chopper in the form of a half disk, rotating at 10 cps, alternately exposes the sample and reference holes and allows the light to fall on a converging lens which is focused on the detecting photocell. A mechanical adjustment for the phasing network is necessary to allow the electronic switching circuit to be synchronized with the above 10 cps chopper. The outside edge of this chopping disk is black for 180° and silvered for the other 180°. A Clairex CL 3 photocell and lamp are used as a phasing network and mounted so that light reflected from the silvered edge of the chopping disk will operate the synchronous relay.

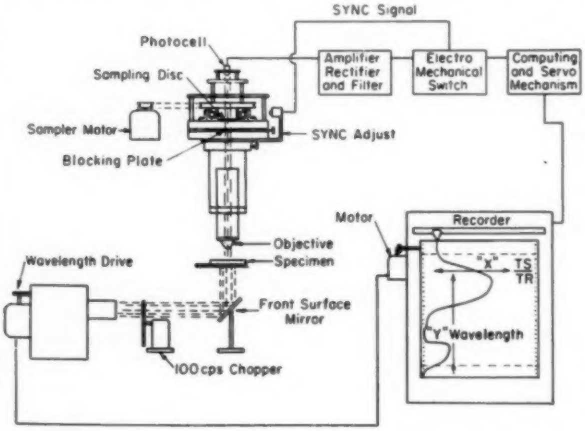

Fig. 2. Diagram of recording microspectrophotometer (M-2) showing mounting of photocell and rotating sampling disk.

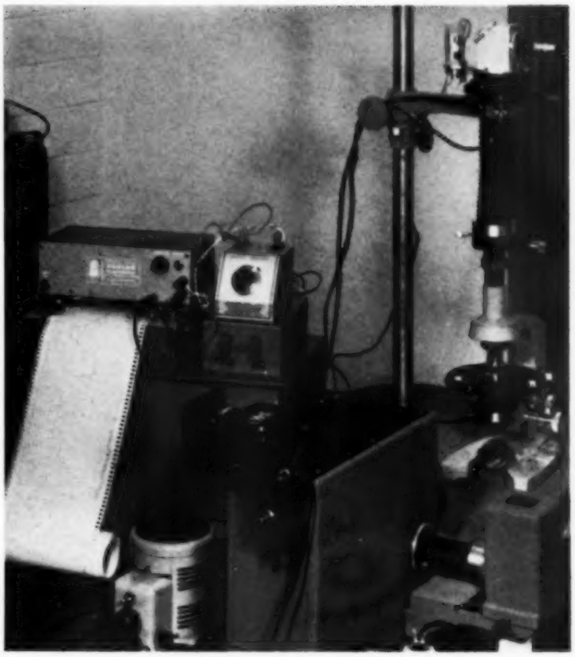

Fig. 3. Recording microspectrophotometer (M-3) adapted from M-2; light chopper incorporated in sampling disk.

The output of the detecting photocell supplied by a 135-V battery and developed across a 2-M$\Omega$ resistor is coupled to the ac tuned amplifier. A 6V6 tube and plate transformer are used in a conventional manner as a power amplifier. The output of this stage is rectified by the 1N 2069 diode. This half-wave rectified signal is separated by the synchronous relay into sample and reference signals. After filtering, the signals are compared by a conventional null balance servo amplifier. To obtain a recording, a second 1000-$\Omega$ transmitting potentiometer supplied by an adjustable voltage source is operated with the balancing potentiometer, and its output is measured on a dc recorder. For example, a recorded *Euglena* cell absorption spectrum is illustrated in Fig. 5. This is a laboratory instrument to test certain phases of this basic design for its operation. Modifications are being incorporated into the instrument (M-3) for improved imaging, greater sensitivity, and better specimen handling.[32] This instrument, which is presently in use, is shown in Fig. 3.* A recorded absorption spectrum obtained for a frog red blood cell (4-$\mu$ diam) is shown in Fig. 7.

---

* A complete report of the instrumental design, operation, and application will be published.[32]

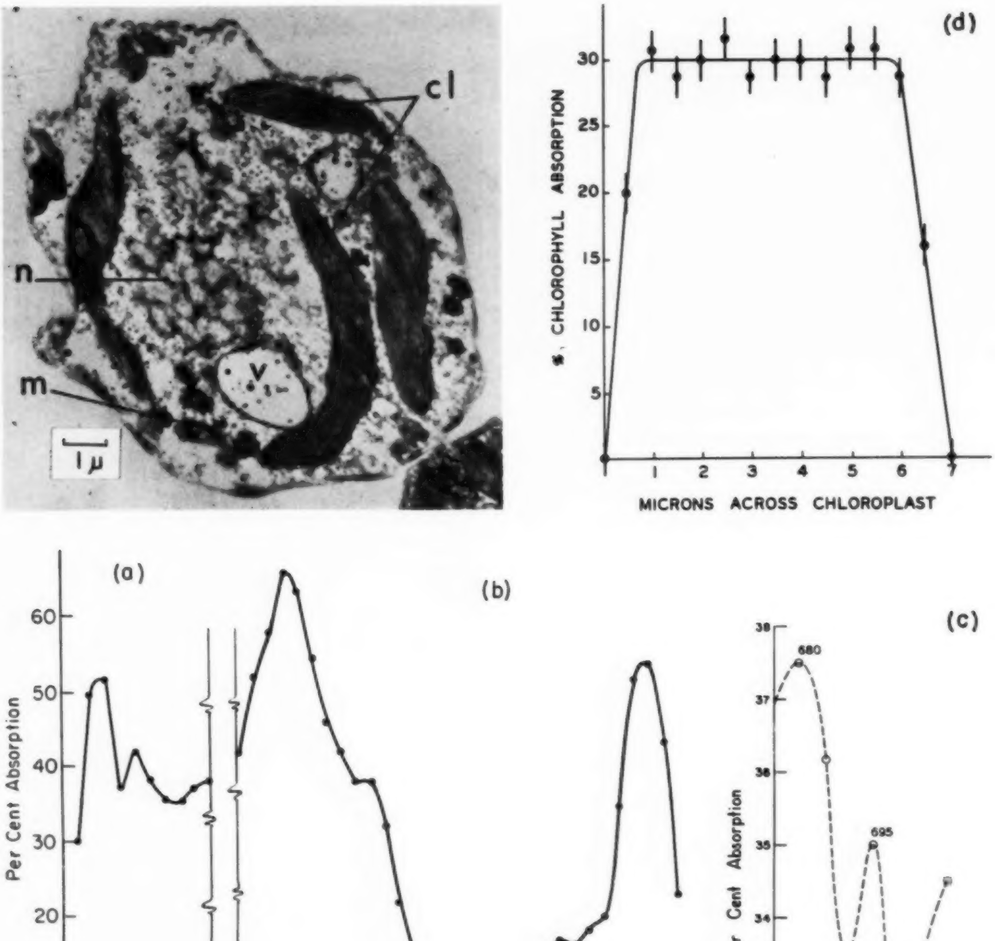

Fig. 4. Section of *Euglena gracilis*, electron micrograph (fixed in 1% osmium tetroxide); note size of chloroplasts (cl) and other cellular organelles, e.g., mitochondria (m), nucleus (n). Curve (*a*)—chloroplast absorption spectrum in the uv. Curve (*b*)—chloroplast absorption spectrum in the visible. Curve (*c*)—chloroplast absorption spectrum of young culture at low light levels from 675 to 710 mμ. Curve (*d*)—scan across chloroplast (0.5-μ intervals) at a chlorophyll major absorption peak, 675 mμ. (Figure 4 is taken from refs. 16, 17, and 19.)

The design of both the simplified and recording microspectrophotometers is such that it permits the operator to choose the sample and the reference areas within the tissue cell (or use the surrounding medium as a reference). The living cells can be viewed at all times during the spectral analysis. For kinetic studies, a temperature-controlled specimen chamber with thermoelectric elements has been constructed and adapted to the microscope stage; temperatures from −20° to +100°C are easily obtained in the specimen chamber.* The cells can be grown in this tissue cell temperature chamber and scanned at periodic intervals. The kinetics, for example, the bleaching of pigments vs temperature in photoreceptors can also be followed. The instrument is ideally suited for scanning single cells at fixed wavelengths to geometrically locate cell constituents which have characteristic absorption

---

[*] J. J. Wolken, in Ninth Annual Report of the Biophysical Research Laboratory, University of Pittsburgh School of Medicine, 1962–1963.

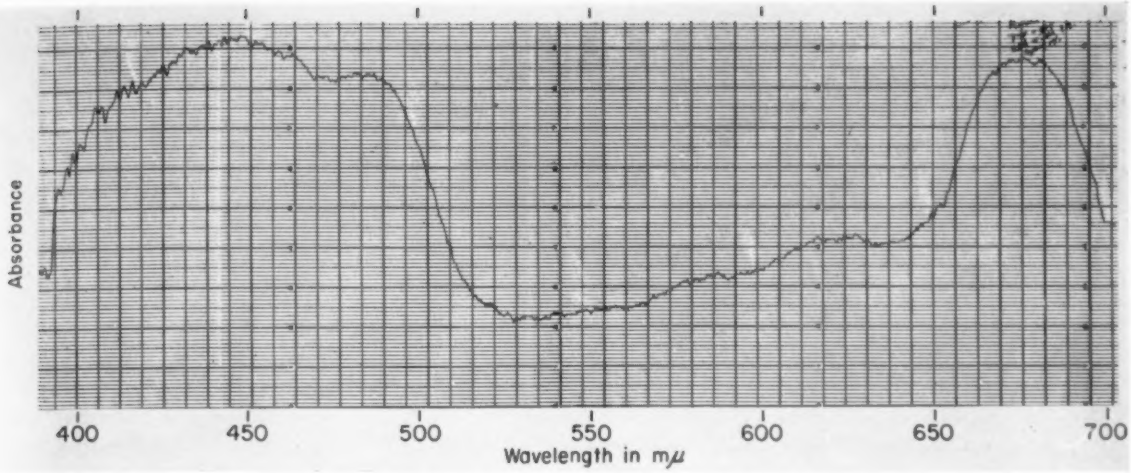

Fig. 5. *Euglena* chloroplast absorption spectrum obtained with recording microspectrophotometer (M-2). Peak positions and peak heights compare very closely with chlorophyll *a*. Entering half-bandwidth, 6 mμ; time of scan, 4 min.

peaks. It can also be used for spectral analysis of fixed and stained cells. High resolving power can be achieved at low magnification, and data from the ultraviolet, visible, and near infrared regions of the spectrum can be easily obtained without changing the photocell.

## Absorption Spectra of Photoreceptors

Microspectrophotometry is then an ideal microanalytical method for the study of pigments within photoreceptor cells. The photoreceptors are cellular organelles containing photosensitive pigment complexes for light absorption in the initiation of such physiological processes as phototropisms, photosynthesis, and vision. The photoreceptors of plant cells are the chromatophores, plastids, and chloroplasts for photosynthesis; in animals they are the retinal cells the retinal rods and cones of vertebrate eyes for vision. The photoreceptors are therefore the receptors for light and function as energy storage and transfer devices. The elucidation of these processes are the major concern of our laboratory.[14,15]

## Chloroplast Pigments

In the study of plant cells we are interested in the pigments of the chloroplast, for example, the chlorophylls and the carotenoids, their biosynthesis, synthesis, and chemistry. For these studies we have chosen the organism *Euglena gracilis*, which is a large, single cell protozoan (it can be as large as 100 μ in length and 30 μ in diameter). This organism has been intensely studied in our laboratory.[16] It has two photoreceptors, the *eyespot* which is attached to the base of the flagellum by which it moves in response to the intensity and wavelengths of light, and the *chloroplast* which absorbs light for photosynthesis. When grown in the dark, the organism loses its ability to carry on photosynthesis, but when it is restored to light the process is reversible. In mutant forms (produced by temperature, drugs, etc.), the process is irreversible and the behavior of the organism is that of an animal cell.

A cross section of a *Euglena* cell showing the chloroplasts *in situ* is shown in Fig. 4. It will be noted that the *Euglena* chloroplasts are elongated cylinders from 5 to 10 μ in length and from 0.5 to 2 μ in diameter. Absorption spectra obtained on individual *in vivo* chloroplasts are shown in Fig. 4 (curves *a*, *b*, *c*, *d*) and in Fig. 5. At a magnification of 250×, a chloroplast area of 8 $\mu^2$ is viewed with an entering half-bandwidth of 2.6 mμ. The reference area is the clear region in the cytoplasm adjacent to the chloroplast. Figure 4 (curve *a*) shows an ultraviolet spectrum taken over the range from 250 to 340 mμ at 10-mμ intervals. Spectral peaks at 265, 290, and 340 mμ are indicative of the proteins and lipids of the chloroplast. Figure 4 (curve *b*) is an absorption spectrum of a single chloroplast showing maximum absorption at 430, 485, 585, 620, and 680 mμ. The 485-mμ peak is due to carotenoids; the other peaks are due to chlorophylls *a* and *b* (mostly chlorophyll *a*). To obtain more detail from the chloroplast spectrum, data were taken at 5-mμ intervals (at a spectral half-bandwidth of 2.0 mμ). The major peaks of Fig. 4 (curve *b*) have considerable *fine structure* when investigated in this manner[17]. Comparison with other spectral studies indicates that this may be due to various forms of *in vivo* chlorophyll. Investigations of the long wavelength (red) chlorophyll peak in *Chlorella* (a green alga), by the use of cell suspensions, indicate *in vivo* absorption maxima

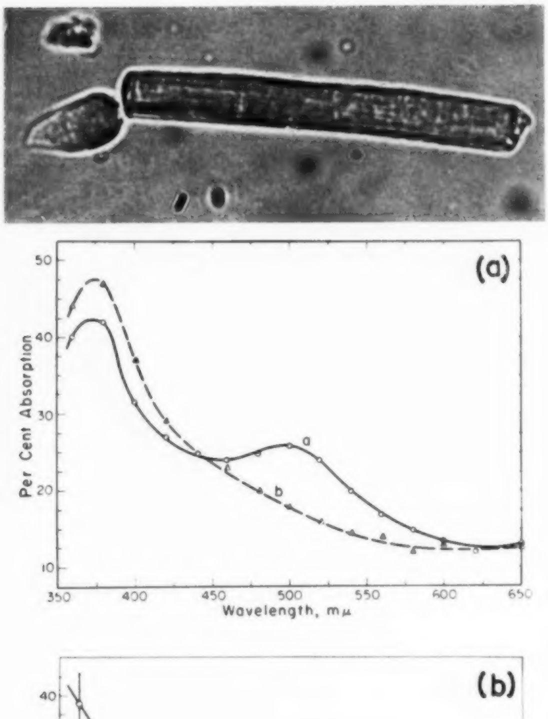

Fig. 6. Frog retinal rod, freshly isolated and photographed in red light. (a) Absorption spectrum of frog retinal rod (curve *a*), compared to bleached rod, in light and $NH_2OH$ (curve *b*). (b) Composite absorption spectrum (curve *a*) of frog rods, in which only one wavelength was used for each rod, total average of 100 retinal rods. Curve *b*, frog rhodopsin (extract of rods in 2% aqueous digitonin). (c) Absorption at 500 mμ for scan across (0.5-μ intervals) length and diameter of frog retinal rod. (Figure 6 is taken from refs. 15 and 20.)

at 673, 684, and 695 mμ for young cultures. *Euglena* grown at low light levels (Fig. 4, curve *c*) also shows absorption peaks at 680, 695, and possibly at 710 mμ.

Information on the chloroplast structure can also be obtained by scanning across it mechanically at fixed wavelengths. Figure 4 (curve *d*) shows absorption at 675 mμ (a major chlorophyll absorption peak) across a single chloroplast of *Euglena* at 0.5-μ intervals, indicating that chlorophyll is equally distributed throughout the chloroplast. The height of the spectral peaks (optical density) can be used to estimate the chlorophyll concentration in a single chloroplast. Using such data, the number of chlorophyll molecules was calculated to be $1.3 \times 10^9$ which is of the order of magnitude obtained by pigment extraction of a variety of plant cells.[16–19]

Figure 5 of the *Euglena* chloroplast is similar in peak positions and height to the spectrum of chlorophyll *a* (for a monolayer at a water–air or water–oil interface), which accounts for 80–90% of the *Euglena* chlorophylls.

[Using the recording microspectrophotometer (M-3), an absorption spectrum from 400 to 700 mμ can be obtained in 2 minutes.]

## Retinal Pigments

Studies of the retinal cells and their photoreceptors, the retinal rods and cones of the eye, indicate that microspectrophotometry is also useful for the analysis of the visual pigment complex (i.e., the photochemistry of the visual process during light<. . .>dark reactions).

The principal component of the retinal rod is the photosensitive visual pigment-complex, rhodopsin. It accounts for about 40% of the dry weight of the frog retinal rod outer segment and 14% of the dry weight in cattle rods.[15,20] Spectrophotometric data obtained from extracts of retinal rods and measurements of the spectral sensitivity of the eye have led to the conclusion that rhodopsin (absorption maximum near 500 mμ) is the light absorbing pigment and is responsible for the "primary event" in visual excitation.

From the retinas of dark-adapted frogs (*Rana pipiens*), the retinal rods (approximately 6 μ in diameter and 60 μ in length) were isolated and suspended in frog Ringer's solution. A drop of the suspension of rods was placed on a microscope slide with a cover glass and sealed with petrolatum. All operations, including the preparation, focus, and location of the rod, were carried out within 10 minutes after dissection in dim red light (see isolated rod, Fig. 6, in red light). Absorption spectra of these rods were obtained from areas as small as $2\ \mu^2$ to $16\ \mu^2$ at an entering half-bandwidth of 2.6 mμ, at a temperature of 22°C.[15]

A typical spectrum from 360 to 650 mμ is illustrated in Fig. 6(a) (curve *a*) showing peaks near 380 mμ (retinene) and 500 mμ (rhodopsin). The ultraviolet spectrum (not shown here) shows peaks at 280, 340, and 355 mμ, indicative of the protein and lipid absorption of the retinal rod.[15] A bleached spectrum, Fig. 6(a) (curve *b*), shows the increase of absorption at 380 mμ and the loss of the rhodopsin 500-mμ peak (a more complete discussion of the photochemistry can be found in refs. 15, 20, 21). Since the rods are photosensitive, their exposure during the process of taking the absorption spectrum results in some bleaching. Therefore, readings were taken at only one wavelength for each rod which was exposed for less than 10 seconds. Measurements of more than 100 individual rods were necessary to construct the spectrum Fig. 6(b) (curve *a*). This is compared to the absorption of extracted frog rhodopsin Fig. 6(b) (curve *b*).

The results of a sweep at 500 mμ along the length and width of the rod at intervals of 0.5 μ [Fig. 6(c)] indicate that rhodopsin is evenly distributed throughout the whole outer segment of the rod as visualized in our retinal rod model.[14] The volume of the retinal rod, its absorption maximum at 500 mμ, and the molar extinction coefficient being known, the number of rhodopsin molecules per retinal rod was estimated to be $3 \times 10^9$. This is in agreement with calculations for extracted frog rhodopsin (based on the number of retinal rods and the optical density).

The cones are more difficult to study. They are fewer in number and smaller in size and much more photosensitive than the retinal rods. Knowledge of their pigments is extremely important to our understanding of color vision. An average absorption curve for the frog retinal cone shows absorption peaks near or at 420, 470, 540, 570, 610, 660, and 690 mμ, with a considerable scattering of the absorption peaks.[20] Some of these peaks may be products of bleaching, since the cones appear to disintegrate more rapidly than the rods. The curve obtained for the carp cone by Hanaoka and Fujimoto[22] shows absorption peaks in the regions of 420 to 430, 490 to 500, 520 to 540, 560 to 580, 620 to 640, and 670 to 680 mμ. The goldfish cone absorption peaks were also recently reported to be at 460 ± 15, 535 ± 10, and 610 ± 5 mμ by Marks and MacNichol.[23]

Pigmented retinal oil globules are also associated with the retinal cones of amphibians, reptiles, and birds. What function they have in the visual process is still unknown. In the chicken retinas, the globules (3 to 5 μ in diameter) occur between the inner and outer segments of the retinal cones. The predominant colors observed in a freshly excised chicken retina are red, green, and yellow. Absorption spectra for individual colored globules indicate that each globule contains a mixture of carotenoids.[24] Further studies of the pigeon, turkey, and turtle retinal oil globules confirm that these globules act as color filters, since each color globule has a characteristic cutoff wavelength, below which 85% of the incoming light is absorbed.[25]

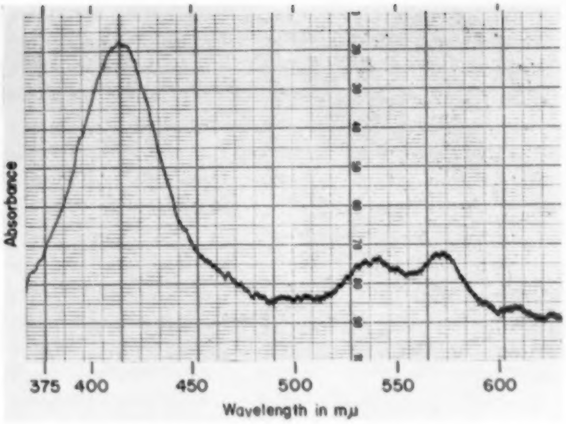

Fig. 7. Frog red blood cell, 4 μ diam, entering half-bandwidth, 5 mμ; time of scan, 2 min.

## Related Photoreceptor Pigments

Absorption spectra of photosynthetic bacteria, for example, *Rhodospirillum rubrum*, show that there are major peaks at 880 and 590 mμ which are due to bacteriochlorophyll and other peaks in the region near 500 to 550 mμ which are due to the bacterial carotenoids.[11]

The eyespot of *Euglena*, an orange-red structure (about 2 × 3 μ) located close to the flagellum, is believed to be the photoreceptor for phototactic (swimming) responses.[16] In other algae, for example, *Chlamydomonas* and *Volvox*, the eyespot is intimately associated with the chloroplast and photosynthesis. The *Euglena* eyespot absorption spectrum has absorption peaks at 430, 480 to 490, 510, 530, and 630 mμ; the region 400–500 mμ is indicative of carotenoids, which have not been completely identified.[16,17]

Photosynthetic cells also contain haem-proteins, cytochrome-*c* types, which have specific reduced and oxidized peaks in the visible spectrum. This enzyme system is associated with the chloroplast in photosynthesis, but whether it is directly involved in light reception is not exactly known.[26]

The chemistry of the chlorophylls (magnesium porphyrins) and the cytochromes (iron porphyrins) has led us to studies of the red blood cell (hemins). For example, see Fig. 7 of a frog red blood cell. Iron storage in the human body is in the form of ferritin and hemosiderin, which are usually characterized by their histological properties. The composition of hemosiderin is unknown; however, absorption spectra were obtained which indicate that these granules contain porphyrins with similarities to protoporphyrin.[27]

## Other Instrumentation Developments

Microspectrophotometric instrumentation of various designs is being developed in other laboratories.

However, the basic design of microspectrophoto-

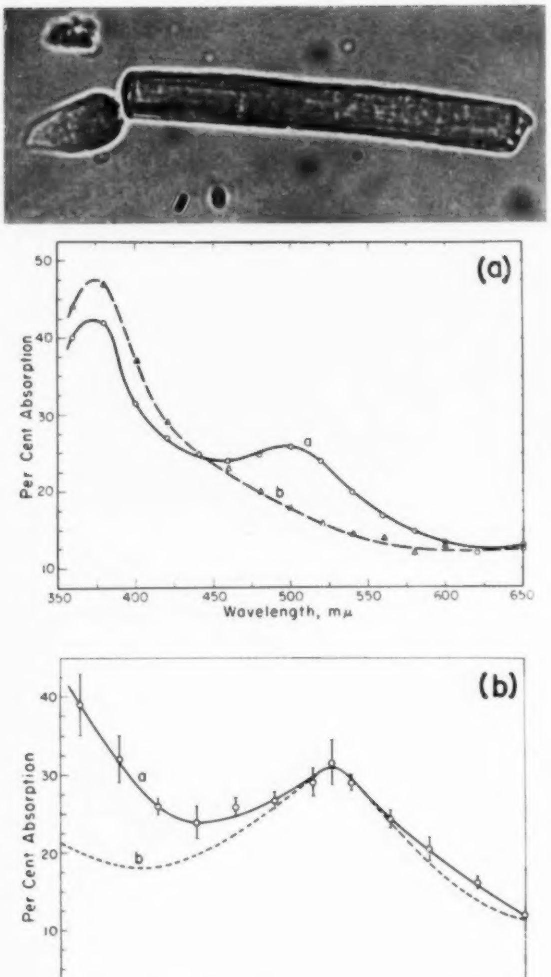

Fig. 6. Frog retinal rod, freshly isolated and photographed in red light. (a) Absorption spectrum of frog retinal rod (curve *a*), compared to bleached rod, in light and $NH_2OH$ (curve *b*). (b) Composite absorption spectrum (curve *a*) of frog rods, in which only one wavelength was used for each rod, total average of 100 retinal rods. Curve *b*, frog rhodopsin (extract of rods in 2% aqueous digitonin). (c) Absorption at 500 mμ for scan across (0.5-μ intervals) length and diameter of frog retinal rod. (Figure 6 is taken from refs. 15 and 20.)

at 673, 684, and 695 mμ for young cultures. *Euglena* grown at low light levels (Fig. 4, curve *c*) also shows absorption peaks at 680, 695, and possibly at 710 mμ.

Information on the chloroplast structure can also be obtained by scanning across it mechanically at fixed wavelengths. Figure 4 (curve *d*) shows absorption at 675 mμ (a major chlorophyll absorption peak) across a single chloroplast of *Euglena* at 0.5-μ intervals, indicating that chlorophyll is equally distributed throughout the chloroplast. The height of the spectral peaks (optical density) can be used to estimate the chlorophyll concentration in a single chloroplast. Using such data, the number of chlorophyll molecules was calculated to be $1.3 \times 10^9$ which is of the order of magnitude obtained by pigment extraction of a variety of plant cells.[16-19]

Figure 5 of the *Euglena* chloroplast is similar in peak positions and height to the spectrum of chlorophyll *a* (for a monolayer at a water–air or water–oil interface), which accounts for 80–90% of the *Euglena* chlorophylls.

[Using the recording microspectrophotometer (M-3), an absorption spectrum from 400 to 700 mμ can be obtained in 2 minutes.]

## Retinal Pigments

Studies of the retinal cells and their photoreceptors, the retinal rods and cones of the eye, indicate that microspectrophotometry is also useful for the analysis of the visual pigment complex (i.e., the photochemistry of the visual process during light<. . .>dark reactions).

The principal component of the retinal rod is the photosensitive visual pigment-complex, rhodopsin. It accounts for about 40% of the dry weight of the frog retinal rod outer segment and 14% of the dry weight in cattle rods.[15,20] Spectrophotometric data obtained from extracts of retinal rods and measurements of the spectral sensitivity of the eye have led to the conclusion that rhodopsin (absorption maximum near 500 mμ) is the light absorbing pigment and is responsible for the "primary event" in visual excitation.

From the retinas of dark-adapted frogs (*Rana pipiens*), the retinal rods (approximately 6 μ in diameter and 60 μ in length) were isolated and suspended in frog Ringer's solution. A drop of the suspension of rods was placed on a microscope slide with a cover glass and sealed with petrolatum. All operations, including the preparation, focus, and location of the rod, were carried out within 10 minutes after dissection in dim red light (see isolated rod, Fig. 6, in red light). Absorption spectra of these rods were obtained from areas as small as 2 $\mu^2$ to 16 $\mu^2$ at an entering half-bandwidth of 2.6 mμ, at a temperature of 22°C.[15]

A typical spectrum from 360 to 650 mμ is illustrated in Fig. 6(a) (curve *a*) showing peaks near 380 mμ (retinene) and 500 mμ (rhodopsin). The ultraviolet spectrum (not shown here) shows peaks at 280, 340, and 355 mμ, indicative of the protein and lipid absorption of the retinal rod.[15] A bleached spectrum, Fig. 6(a) (curve *b*), shows the increase of absorption at 380 mμ and the loss of the rhodopsin 500-mμ peak (a more complete discussion of the photochemistry can be found in refs. 15, 20, 21). Since the rods are photosensitive, their exposure during the process of taking the absorption spectrum results in some bleaching. Therefore, readings were taken at only one wavelength for each rod which was exposed for less than 10 seconds. Measurements of more than 100 individual rods were necessary to construct the spectrum Fig. 6(b) (curve *a*). This is compared to the absorption of extracted frog rhodopsin Fig. 6(b) (curve *b*).

The results of a sweep at 500 mμ along the length and width of the rod at intervals of 0.5 μ [Fig. 6(c)] indicate that rhodopsin is evenly distributed throughout the whole outer segment of the rod as visualized in our retinal rod model.[14] The volume of the retinal rod, its absorption maximum at 500 mμ, and the molar extinction coefficient being known, the number of rhodopsin molecules per retinal rod was estimated to be $3 \times 10^9$. This is in agreement with calculations for extracted frog rhodopsin (based on the number of retinal rods and the optical density).

The cones are more difficult to study. They are fewer in number and smaller in size and much more photosensitive than the retinal rods. Knowledge of their pigments is extremely important to our understanding of color vision. An average absorption curve for the frog retinal cone shows absorption peaks near or at 420, 470, 540, 570, 610, 660, and 690 mμ, with a considerable scattering of the absorption peaks.[20] Some of these peaks may be products of bleaching, since the cones appear to disintegrate more rapidly than the rods. The curve obtained for the carp cone by Hanaoka and Fujimoto[22] shows absorption peaks in the regions of 420 to 430, 490 to 500, 520 to 540, 560 to 580, 620 to 640, and 670 to 680 mμ. The goldfish cone absorption peaks were also recently reported to be at 460 ± 15, 535 ± 10, and 610 ± 5 mμ by Marks and MacNichol.[23]

Pigmented retinal oil globules are also associated with the retinal cones of amphibians, reptiles, and birds. What function they have in the visual process is still unknown. In the chicken retinas, the globules (3 to 5 μ in diameter) occur between the inner and outer segments of the retinal cones. The predominant colors observed in a freshly excised chicken retina are red, green, and yellow. Absorption spectra for individual colored globules indicate that each globule contains a mixture of carotenoids.[24] Further studies of the pigeon, turkey, and turtle retinal oil globules confirm that these globules act as color filters, since each color globule has a characteristic cutoff wavelength, below which 85% of the incoming light is absorbed.[25]

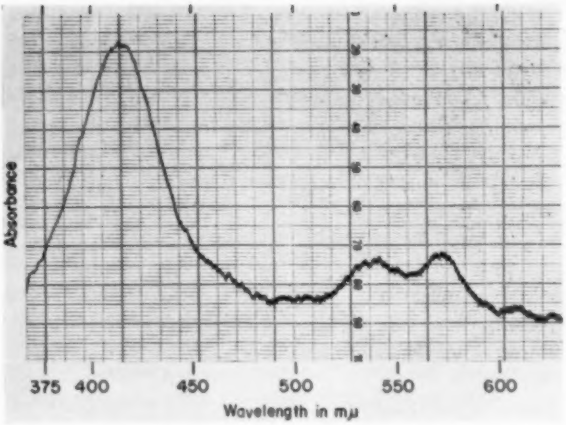

Fig. 7. Frog red blood cell, 4 μ diam, entering half-bandwidth, 5 mμ; time of scan, 2 min.

## Related Photoreceptor Pigments

Absorption spectra of photosynthetic bacteria, for example, *Rhodospirillum rubrum*, show that there are major peaks at 880 and 590 mμ which are due to bacteriochlorophyll and other peaks in the region near 500 to 550 mμ which are due to the bacterial carotenoids.[11]

The eyespot of *Euglena*, an orange-red structure (about 2 × 3 μ) located close to the flagellum, is believed to be the photoreceptor for phototactic (swimming) responses.[16] In other algae, for example, *Chlamydomonas* and *Volvox*, the eyespot is intimately associated with the chloroplast and photosynthesis. The *Euglena* eyespot absorption spectrum has absorption peaks at 430, 480 to 490, 510, 530, and 630 mμ; the region 400–500 mμ is indicative of carotenoids, which have not been completely identified.[16,17]

Photosynthetic cells also contain haem-proteins, cytochrome-*c* types, which have specific reduced and oxidized peaks in the visible spectrum. This enzyme system is associated with the chloroplast in photosynthesis, but whether it is directly involved in light reception is not exactly known.[26]

The chemistry of the chlorophylls (magnesium porphyrins) and the cytochromes (iron porphyrins) has led us to studies of the red blood cell (hemins). For example, see Fig. 7 of a frog red blood cell. Iron storage in the human body is in the form of ferritin and hemosiderin, which are usually characterized by their histological properties. The composition of hemosiderin is unknown; however, absorption spectra were obtained which indicate that these granules contain porphyrins with similarities to protoporphyrin.[27]

## Other Instrumentation Developments

Microspectrophotometric instrumentation of various designs is being developed in other laboratories.

However, the basic design of microspectrophotometers is so similar to that of commercial recording spectrophotometers (manufactured by Beckman Instruments, Inc., Cary, and others) that Brown,[28] at Harvard University, converted a Cary Model 14 dual-beam recording spectrophotometer into a microspectrophotometer by replacing the sample cell compartment with a microscope for the sample light beam and equivalent optics for the reference beam. This instrument can be used for solution spectroscopy or for microspectrophotometry by simply interchanging components. Absorption measurements can be made over the range 350–650 mμ for fields 4 μ in diameter. For sample areas of 0.1 to 1 mm in diameter, the usable wavelength range is 300–700 mμ. Additional provisions include increasing the sensitivity of the recorder from 0–1 optical density units to 0–0.1 optical density units full scale and the addition of a monochromator light source for locating the specimen and selective bleaching of visual pigments. The limiting aperture (4 μ) is obtained by masking the image at the entrance to the phototube housing with a small hole in metal foil. This modified Cary Model 14 microspectrophotometer can sweep the visible spectrum in about 2 minutes and has been used with considerable success to obtain recorded absorption spectra of frog retinas and isolated individual retinal rods with a peak-to-peak noise level of about $10^{-2}$ optical density units. A few disadvantages of this system are that the reference beam does not pass through the microscope slide chamber containing the experimental specimen and the absorption of other cellular constituents surrounding the area under investigation must be subtracted unless a pure solution is used for the suspending medium.

Britton Chance at the Johnson Research Foundation, University of Pennsylvania, has been pioneering in the development of rapid microspectrophotometric methods to investigate the respiratory enzymes (the cytochrome system) in living cells. A single-beam recording instrument has been built by Chance *et al.*,[10] in which sample areas 1.5 μ in diameter can be studied over a spectral range from 240 to 600 mμ, with a noise level of the order of $10^{-4}$ optical density units, to detect concentrations of $10^{-18}$ mole at a signal-to-noise ratio of 50 to 1. This instrument is being applied to numerous biological problems.

A modified version of this microspectrophotometer has recently been adapted by Liebman[29] to investigate absorption and dichroism in isolated single frog retinal rods, indicating a pigment (rhodopsin) concentration of 2.5 mM ± 20%. The maximum optical density change recorded here was about 0.09 at a rod thickness of 5 μ or 0.9 per 50 μ, indicating that the frog retinal rods absorb nearly 90% of the axially incident light. In these studies, the microscope was fitted with Zeiss ultrafluar optics (320×), and was illuminated by a Bausch & Lomb 250-mm grating monochromator with 1200 lines per mm. To fill the condenser back aperture (N.A. = 0.4) the monochromator exit slit-width was set at 1.8 mm for a spectral bandwidth of 5 μ. A beam splitter above the ocular permits viewing of the specimen and provides a light path for the signal, which is imaged in the plane of a pair of circular apertures (6.5 μ in the object plane). A mechanical shutter alternately selects the object or the reference area at 60 cycles per second for illumination of the photomultiplier. The output of the photomultiplier is controlled by a dynode feedback circuit. Integrating of the measure-reference signal is performed by an R-C network, and the output is recorded on a Varian dc recorder in per cent absorption, proportional within 10% to an optical density of 0.1 or less. A time constant of 2 sec and a noise level of about $4 \times 10^{-4}$ optical density units peak-to-peak are possible with this instrument.

Because of the need of microanalytical tools, there are now two commercial models available, one from the Carl Zeiss Company, Inc.,[30] and the other from the Canal Industrial Corporation.[31] The recording microspectrophotometer manufactured by Carl Zeiss is claimed usable for study of the spectral range from 240 to 700 mμ. It is a dual-beam system with separate optics for each light path. Quartz optics are used throughout, and the light source is a high-pressure xenon arc with a continuous output in the ultraviolet and in the visible. Neither the Zeiss nor the Canal Corporation instrument provides for an automatic, direct comparison between the sample and an adjacent reference area in a biological cell. The Canal Corporation instrument is also similar to the Zeiss, in that it uses a beam-splitter before the microscope to provide for a reference beam.

## Concluding Remarks

We have emphasized here our own instrumentation developments in microspectrophotometry and have selected only a few examples of our biological investigations, all of which are still in progress. The illustrated spectra described are only to indicate our application to the study of pigment systems in photoreceptor structures. Microspectrophotometry is, then, a vital tool to explore the chemistry of living cells. It can also be applied to the search for organic molecules and their identification in oceanic sediments, fossils, meteorites, and extraterrestrial debris.

## References

1. T. Caspersson, *Cell Growth and Cell Function* (Norton, New York, 1950).
2. T. Caspersson, G. Lomakka, G. Svensson, and R. Säfström, Exp. Cell Res. Suppl. **3**, 40 (1955).
3. T. Caspersson, Fed. Proc. **20**, 858 (1961).
4. A. W. Pollister and L. Ornstein, in *Analytical Cytology*, 2nd ed., R. C. Mellors, ed. (McGraw-Hill, New York, 1959), p. 431.

5. P. M. M. Wallace, in *General Cytochemical Methods*, J. F. Danielli, ed. (Academic Press, New York, 1958), Vol. 1, p. 163.
6. H. Swift and E. Rasch, in *Physical Techniques in Biological Research*, G. Oster and A. W. Pollister, eds. (Academic Press, New York, 1956), Vol. III, p. 353.
7. Cytochemical Methods With Quantitative Aims, Exp. Cell Res. Suppl. 4 (1957).
8. Scanning Techniques in Biology and Medicine, Ann. N.Y. Acad. Sci. **97**, 331 (1962).
9. E. J. Denton, Proc. Roy. Soc. B, **150**, 78 (1959).
10. B. Chance, R. Perry, L. Akerman, and B. Thorell, Rev. Sci. Instr. **30**, 735 (1959).
11. G. K. Strother and J. J. Wolken, Science, **130**, 1084 (1959).
12. B. Henry, and H. Cole, Rev. Sci. Instr. **30**, 90 (1959).
13. J. J. Wolken, V. Jackman, R. Kerr, and G. Ludwig, (unpublished research).
14. J. J. Wolken, J. Theoret. Biol. **3**, 192 (1962).
15. J. J. Wolken, J. Opt. Soc. Am. **53**, 1 (1963).
16. J. J. Wolken, *Euglena: An Experimental Organism for Biochemical and Biophysical Studies* (Rutgers University Press, New Brunswick, New Jersey, 1961).
17. G. K. Strother and J. J. Wolken, J. Protozool. **8**, 261 (1961).
18. J. J. Wolken and F. A. Schwertz, J. Gen. Physiol. **37**, 111 (1953).
19. J. J. Wolken, in *Macromolecular Complexes*, M. V. Edds, Jr., ed. (Ronald Press, New York, 1961), p. 85.
20. J. J. Wolken, Inves. Ophth. **1**, 327 (1962).
21. H. J. A. Dartnall, in *The Visual Pigments* (Wiley, New York, 1957).
22. T. Hanaoka and K. Fujimoto, Jap. J. Physiol. **7**, 276 (1957).
23. W. B. Marks and E. F. MacNichol, Abstracts of the Sixth Biophysical Society Meeting, TE-2, Washington, D.C. and W. B. Marks, "Difference Spectra of Visual Pigments in Single Goldfish Cones", Thesis, Johns Hopkins Univ., Baltimore, Md., 1963.
24. G. K. Strother and J. J. Wolken, Exp. Cell Res. **21**, 504 (1960).
25. G. K. Strother, Exp. Cell Res. **29**, 349 (1963).
26. J. J. Wolken and J. A. Gross, J. Protozool. (in press, 1963).
27. C. L. Wells and J. J. Wolken, *Nature* **193**, 977 (1962).
28. P. K. Brown, J. Opt. Soc. Am. **51**, 1000 (1961).
29. P. A. Liebman, Biophys. J. **2**, 161 (1962).
30. Carl Zeiss, Inc., 485 Fifth Avenue, New York, N.Y.
31. Canal Industrial Corporation, Bethesda, Maryland.
32. J. J. D. van der Gon and J. J. Wolken (unpublished research) and 9th Annual Report Biophysical Research Lab., Univ. of Pittsburgh School of Medicine, 1962–1963.

---

### International Commission for Optics

## CONFERENCE ON PHOTOGRAPHIC AND SPECTROSCOPIC OPTICS

### Tokyo and Kyoto 1–8 September 1964

### arranged by

### SCIENCE COUNCIL OF JAPAN and JAPANESE SOCIETY OF APPLIED PHYSICS

A Conference on Photographic and Spectroscopic Optics, arranged on an international level by the Science Council of Japan and the Japanese Society of Applied Physics under the auspices of the International Commission for Optics, will be held in Tokyo and Kyoto, Japan, 1–8 September 1964. The Conference will be composed of some 10 sessions, and each session will include one or two invited papers (30–40 min presentation time) and some contributed papers (15 min each). The subjects to be dealt with at the Conference will be:

**Design and Evaluation of Photographic and Spectroscopic Optical Systems**
**Recent Instrumentation in the Far Infrared and the Extreme Ultraviolet**
**Optical Materials for Use in Photographic and Spectroscopic Optics**

Offers of papers should be made no later than 31 January 1964, by sending an abstract to the Organizing Committee. This abstract must be adequate for the Committee to decide on the suitability of the paper: the scope of the paper should be indicated, and principal new results included. The working languages of the Conference will be English, French, and German. However, in view of the fact that English will be the only language comprehensible to the majority of participants, speakers are strongly recommended to read their papers in English.

Visits to research institutes, universities, and optical companies are being planned. More detailed information will be circulated in due course.

**All inquiries concerning the Conference should be addressed to: Prof. H. Kubota, Secretary, Organizing Committee, ICO-Tokyo & Kyoto, Science Council of Japan, Ueno Park, Tokyo. For planning purposes the Japanese Committee is very eager to estimate the number of people who will attend; If you are interested in this meeting please write immediately to Prof. Kubota for further information.**

**Books** *continued from page 886*

*Elsevier's* **Dictionary of General Physics.** In six languages (English/American, French, Spanish, Italian, Dutch, and German). W. E. Clason. Elsevier Publishing Co., Amsterdam-New York, 1962. 859 pp. $22.50.

The author of this dictionary, who has also compiled six books in other fields of physics and technology, is the former head of the Translation Department of Philips, Eindhoven. The present book is restricted to the essential terminology of the various branches of physics, omitting the more specialized terms that have been covered in his earlier books. Each of the 3397 numbered words is given first in English, with differentiation of American usage, spelling, and preference. An English definition of the term follows and then its equivalent in each of the other languages given in the title. These words in other languages are also listed separately and alphabetically in thumb-indexed sections, with the numbered key to the basic table. The typography is clear, and the book is agreeable to use.

Such a limited space for the whole domain of physics can permit only a selection of terms; in this case, it has followed the principle indicated above. The reviewer cannot do better than turn over the leaves and see what he reacts to and then choose certain words and study them more carefully. The definitions are, on an average, four lines of column width type. When possible, the author has given a mathematical relation to other physical quantities; often, however, the definition is given literally but with physical rigor. When this was too difficult, a vaguer description is given such as the following: for *dielectric constant, permittivity:* "A measure of that property of a medium by virtue of which it modifies the mutual interaction of electrified bodies immersed in it or separated by it." In this definition as well as in the one for *permeability,* some indication of their relationship to the Maxwell equations could be in order; *acoustic impedance* is well treated. Keeping to waves, the term *phase slowness* is misunderstood; it is not equivalent to *retard de phase* or *Phasenverzögerung,* but has the dimension inverted velocity: here, it should be substituted by *phase delay, phase lag.* Viscosity should have been more rigorously treated, particularly in regard to why *kinematic viscosity* is used in other connections.

Optics has a comparatively large place in this dictionary and is, on the whole, well treated. Distinction is made between *optic axis* and *optical axis. Ronchi test* and other relatively modern terms are incorporated; however, *transfer function* is not. As one of the German equivalents to response, *Frequenzgang* is given, which means *response function* (of frequency). This important and multivalid term response could have been clarified. More stringent definitions of *dispersive power, dispersitivity,* and *refractive dispersitivity* would have been valuable, the *Abbe number* being a specific number. Your reviewer thinks that *plane of polarization* as historically given should be abandoned (as does Condon in *Handbook of Physics*) and the perpendicular *transmission plane* or *plane of vibration* (all three given here) extensively used.

Sometimes terms are criticized, as is *photoelasticity.* National terms are often misleading and may cause confusion. In a dictionary such as this, one is reminded of the favorable fact that most terms in physics are international. Such monsters as the German *Gummilinse* for *zoom lens* (here called *Zoomar lens,* although *zoom* is more common) are the exception. In physics, composite words sometimes cause difficulties, particularly in French. The author might have felt the need for main headings and subheadings, but this would have necessitated a different typographic design and a modification of his system.

This reviewer considers the book an excellent survey of physical terms in these six languages, which are the most common in physical literature. It seems that a Russian supplement is in preparation; it would have been well justified to have induced the Russian terms in this main volume. The dictionary is recommended for every physicist's bookshelf.

Erik Ingelstam

---

**Atlas of Optical Phenomena.** By Michel Cagnet, Maurice Francon, and Jean Claude Thrierr. Springer-Verlag, Berlin, Göttingen, Heidelberg. Prentice-Hall, Englewood Cliffs, N.J., 1962. 45 pp. $24.00.

The *Atlas of Optical Phenomena* is a collection of 45 outstanding photographs of different fundamental optical phenomena. Each photograph is accompanied by a brief explanation describing the experiment, and an abbreviated sketch is included indicating the relative positions of the more important optical elements. The photographs are divided into six groups: geometrical aberrations, interferences, diffraction at infinity, diffraction at a finite distance, polarization, and phase contrast and interference contrast. In the group on geometrical aberrations are photographs of images of a point at different distances from the focal plane in the presence of such third-order aberrations as spherical aberration, coma, astigmatism, and distortion. Knife-edge methods are also utilized to investigate the effects of these aberrations on the image. In the group on interferences are photographs of fringes that are loci of constant path differences and fringes that are loci of constant angular differences. Optical qualities of elements of both poor and high quality are investigated with these interference techniques. Thus, we find photographs of interference fringes in glass plates, interference fringes between flat and curved surfaces (Newton's rings), interference fringes between two plane-parallel plates (Fabry-Perot type) showing fine structure of spectral lines, and optical polish of surfaces of high optical quality. Both Michelson and Twyman-Green interferometers are used to obtain many interesting interference patterns of various optical phenomena and of lenses and mirrors possessing different amounts of third-order aberrations. Interference methods are also utilized in obtaining some interesting photographs of the surface contours of liquids supporting small insects and of crystal growth. The photographs of various diffraction phenomena occupy several pages in the book. The photographs are of both the Fraunhofer and the Fresnel type and utilize square, rectangular, round, and triangular apertures and opaque objects. Multiple apertures are also utilized with both coherent and incoherent light. The diffraction patterns of lenses both in and out of the focal plane in the presence of various third-order aberrations provide many striking photographs. The effects of diffraction on the evolution of the image provided by a lens of increasing numerical aperture also yields a striking photograph. The photographs in polarized light are devoted primarily to birefringence in crystals and other optical materials subjected to stress. Some phase-contrast photographs are also of considerable interest and are described in a simple, straightforward way.

The chief interest in this book lies in its high-quality photographs of these various optical phenomena. These pictures will be excellent for teaching or illustration purposes. Also, enough detail is given to reproduce these phenomena in the laboratory, but the results obtained will usually be different because experimental details have been largely avoided in the book, and the optical elements utilized also will usually be different from those of the authors. The book also will be interesting in that it will, to be sure, stimulate similar work by others.

A. I. Mahan

# Spectrographie Infrarouge à Haute Résolution: Application à l'Étude de Quelques Molécules Simples

Ph. Arcas, C. Haeusler, C. Joffrin, C. Meyer, Nguyen van Thanh, et P. Barchewitz

Two high-resolution spectrographs, running between 1.2 μ and 3 μ, are described. At 6000 cm$^{-1}$ the resolving power attained is 0.09 cm$^{-1}$ for the Czerny type and 0.06 cm$^{-1}$ for the Fastie–Ebert type. These spectrographs are fitted with a calibration device which makes it possible to record simultaneously the studied absorption spectrum and the calibration interference peaks. The latter are produced by a Perot–Fabry etalon, the fringes of which, at infinity, are projected on the entrance slit of the spectrograph. They allow localization of the absorption lines relative to standard lines. A few results obtained with gaseous HI, NO, and $N_2O$ are listed.

## Introduction

Le Laboratoire d'Infrarouge dispose de deux spectrographes à haut pouvoir de résolution, réservés à l'analyse des bandes de vibration-rotation. Ces deux appareils diffèrent par leur montage optique; l'un appartient au type Czerny et permet d'atteindre un pouvoir séparateur de 0,09 cm$^{-1}$ à 6000 cm$^{-1}$; quant à l'autre, du type Fastie–Ebert, à double passage sur le réseau, il permet de résoudre 0,06 cm$^{-1}$ pour la même valeur du nombre d'onde. Ils fonctionnent actuellement l'un et l'autre entre 1,2 μ et 3 μ. Le dispositif de détection du rayonnement infrarouge est identique pour les deux montages, ainsi d'ailleurs que le dispositif d'étalonnage.

Dans ce qui va suivre nous nous proposons, dans une première partie, de décrire ces deux spectrographes et de comparer leurs performances; dans une seconde partie nous fournirons des résultats obtenus sur des molécules simples diatomiques et triatomiques.

## I. Instrumentation

### A. Description des Spectrographes

*1°/ Montage Czerny*[1,2]

Ce montage (Fig. 1) comporte deux miroirs aluminités $M_1$ et $M_2$ de 150 cm de distance focale, un réseau échelette R à 600 traits/mm de dimensions 200 × 130 mm. Ces éléments ainsi que les fentes $F_1$ et $F_2$ sont fixés sur une platine rigide située à l'intérieur d'un cylindre métallique étanche. La rotation du réseau est obtenue par un moteur synchrone qui entraîne une vis micrométrique; un écrou intégrateur guidé agit sur un levier solidaire de l'axe du réseau.

Le pouvoir de résolution théorique du réseau est $\mathcal{R} = kn$ (où $k$ est l'ordre et $n$ le nombre total de traits du réseau) égal à 120 000.

*2°/ Montage Fastie–Ebert*

L'intérêt de ce montage est de pouvoir réaliser un double passage du faisceau infrarouge sur le monochromateur, ce qui permet de doubler la résolution théorique du système.[3]

Le schéma optique de cet appareil est celui de la Fig. 2. Un miroir concave M est placé de sorte que son axe définisse l'axe $XX'$ de symétrie du spectrographe; son rayon de courbure est de 360 cm. Les fentes $F_1$ (fente d'entrée) et $F_2$ (fente de sortie) doivent être placées de manière aussi précise que possible dans le plan focal de ce miroir (le réseau sera alors éclairé en lumière parallèle). Ces fentes sont courbes et placées sur un cercle comme l'indique la Fig. 2. Le rayon de ce cercle, qui est donc aussi le rayon de courbure des fentes, est calculé en fonction des autres données de l'appareil comme l'indique Fastie.[4]

Pour permettre un second passage du faisceau infrarouge sur le réseau, les fentes $F_1$ et $F_2$ sont décalées de 20 mm en hauteur par rapport au plan horizontal contenant l'axe du spectrographe. La première image de la fente d'entrée se forme donc en $F'_1$ (elle est virtuelle). Un système de miroirs m et m′ placés à 45° de l'axe la renvoie en $F''_1$ qui est également

---

The authors are with the Laboratoire d'Infrarouge, Chimie-Physique, Faculté des Sciences, Orsay (Seine-et-Oise) France.

Received 16 February 1963.

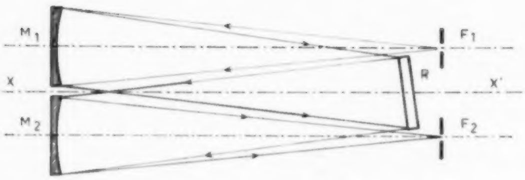

Fig. 1. Montage du spectrographe de type Czerny.

virtuelle mais jouera le rôle de deuxième fente objet. Une image intermédiaire se forme évidemment en H.

Il est important que les traits du réseau soient parallèles à l'axe $ZZ'$ du spectrographe pour que dans sa rotation le monochromateur fasse défiler les différentes images toujours à la même hauteur devant la fente de sortie. Ceci nécessite également que l'axe de rotation du réseau soit bien parallèle à $ZZ'$.

Cet appareil est actuellement équipé d'un réseau échelette à 600 traits/mm, ce qui correspond à un pouvoir de résolution théorique.[3]

$$\mathcal{R} = P\,k\,n$$

soit 240 000 dans le premier ordre. Dans cette formule $P$ est le nombre de passages de la lumière sur le réseau, $n$ le nombre total de traits, et $k$ l'ordre.

Les éléments du montage sont fixés comme dans le montage Czerny sur une platine rigide, disposée dans un cylindre étanche. Le système d'entraînement du réseau est identique à celui décrit dans le paragraphe précédent.

## B. Dispositif d'Etalonnage[2,5,6]

Le principe de la méthode consiste à enregistrer simultanément la bande d'absorption et des repères équidistants en nombre d'onde. Ceux-ci permettent d'étalonner les raies d'absorption par rapport à des raies d'émission référence. Les repères équidistants sont obtenus par un étalon Perot–Fabry.

Le montage a été réalisé pratiquement de la façon suivante (Fig. 3): Un étalon Perot–Fabry dont l'axe est placé perpendiculairement à l'axe du spectrographe est éclairé par la lumière blanche émise par une lampe à arc au zirconium S, située au foyer de la lentille $L_1$. Les anneaux d'interférences à l'infini donnés par l'étalon sont projetés sur l'une des extrémités de la fente d'entrée $F_1$ du spectrographe (sur le bas de la fente pour le montage du type Czerny, sur le haut de la fente pour le montage du type Fastie) par l'intermédiaire d'une lentille $L_2$ et d'un miroir de petites dimensions $M_3$. Seul l'anneau central est conservé, grâce à l'utilisation d'un diaphragme. Le faisceau lumineux, après dispersion sur le réseau du spectrographe, se trouve concentré sur le haut de la fente de sortie $F_2$. Un petit miroir $M_4$ et une lentille $L_3$ permettent de focaliser l'énergie lumineuse sur la cathode d'un photomultiplicateur D.

L'étalon Perot–Fabry est situé dans une enceinte vide d'air. Une seconde enceinte permet de maintenir la température constante. L'échauffement par rayonnement est évité en interposant sur le trajet lumineux des verres antithermiques. Les cales d'épaisseur de l'étalon ont été réalisées en invar; leurs épaisseurs sont respectivement de 3 mm pour le montage Czerny et de 6 mm pour le montage Fastie–Ebert.

Les sources d'émission utilisées comme référence de nombre d'onde sont, soit un tube sans électrodes contenant du $Hg_{198}$, alimenté par un générateur haute fréquence, soit un tube avec électrodes contenant du

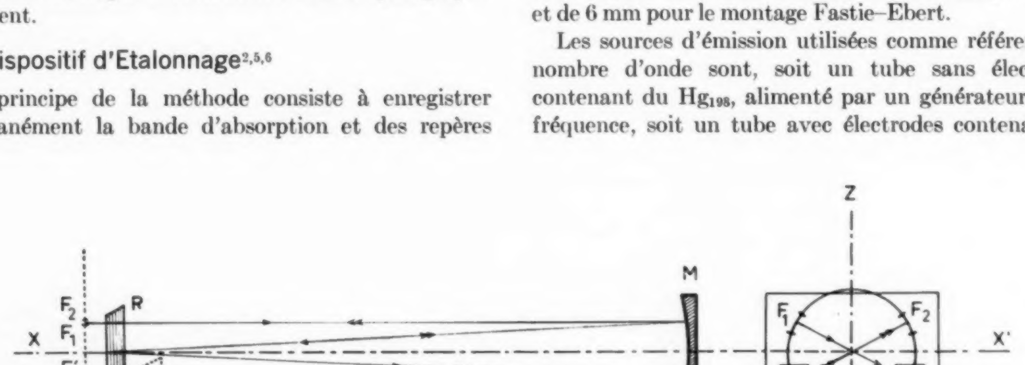

Fig. 2. Montage du spectrographe de type Fastie–Ebert.

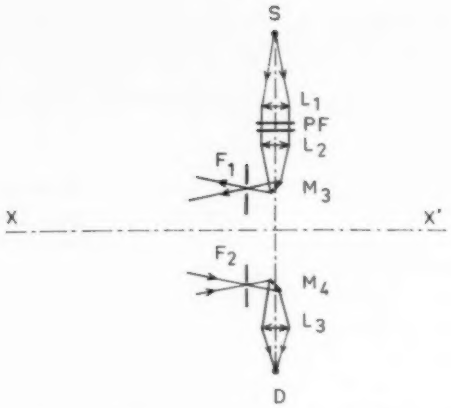

Fig. 3. Dispositif d'étalonnage des spectrographes de types Czerny et Fastie–Ebert.

Ne sous une faible pression. Le rayonnement émis par ces sources étalon est détecté par un photomultiplicateur.

La précision absolue des mesures peut atteindre 0,01 $cm^{-1}$ lorsque les raies étudiées sont bien séparées et symétriques. La précision relative est supérieure; elle atteint 0,005 $cm^{-1}$ et parfois dépasse cette valeur pour le montage Fastie–Ebert.

## C. Détection

Le rayonnement infrarouge est détecté par une cellule au PbS, refroidie à la température de la neige carbonique. Le flux lumineux reçu par cette dernière est modulée à 125 hertz. Le signal électrique est amplifié par un amplificateur linéaire à détection de phase et la tension obtenue redressée. Celle-ci est appliquée sur un millivoltmètre enregistreur à double entrée et double plume. Sur l'autre entrée, on applique une tension proportionnelle au courant anodique du photomultiplicateur servant à détecter le système de franges produit par l'étalon Perot–Fabry. Nous pouvons ainsi enregistrer simultanément le spectre infrarouge et les franges repères.

Un inverseur permet d'appliquer sur l'entrée habituellement réservée au signal infrarouge, une tension, proportionnelle au courant anodique du photomultiplicateur utilisé pour détecter les raies d'émission étalon. Nous avons donc la possibilité d'enregistrer simultanément le spectre d'émission et les franges repères. Par comparaison de ces deux enregistrements, on en déduit les nombres d'onde des raies de vibration-rotation à étudier.

## D. Performances

Si nous utilisons comme définition du pouvoir de résolution pratique d'un spectrographe l'expression:

$$\mathcal{R}_p = \frac{\nu}{d\nu},$$

où $\nu$ représente le nombre d'onde et $d\nu$ le pouvoir séparateur mesuré, nous obtenons pour le spectrographe du type Czerny:

$$\mathcal{R}_{p_1} = (6300/0{,}09) = 70.000$$

soit 60% du pouvoir de résolution théorique. Quant au spectrographe du type Fastie–Ebert, nous obtenons:

$$\mathcal{R}_{p_2} = (6300/0{,}06) = 105.000$$

soit 45% du pouvoir de résolution théorique. Le pouvoir séparateur expérimental $d\nu$ a été déterminé au moyen des raies $Q_8$ et $Q_7$ de la branche $Q$ du méthane à 6000 $cm^{-1}$ en utilisant le critère de résolution et les résultats expérimentaux de Rank.[7,8]

Ce pouvoir séparateur est confirmé par la largeur des raies du spectre cannelé donné par l'étalon Perot–Fabry (Fig. 3 bis).

Cette différence importante entre le pouvoir de résolution théorique et le pouvoir de résolution pratique a plusieurs causes. Les principales sont les suivantes:

Les réseaux utilisés sont signalés comme ayant par leur fabrication, un pouvoir de résolution réel notablement inférieur au pouvoir de résolution théorique.

Les fentes des spectrographes ont une largeur appréciable, de l'ordre de quelques centièmes de millimètres. Pour des valeurs inférieures, nous sommes limités par le bruit du détecteur infrarouge dont le rapport signal sur bruit devient trop faible.

En ce qui concerne le montage du type Fastie–Ebert, nous constatons une diminution du pouvoir de résolution théorique plus importante que dans le montage du type Czerny. Ceci nous semble dû principalement à une perte d'énergie lumineuse plus grande par réflexions, ce qui limite inférieurement la largeur des fentes que nous pouvons utiliser.

La Fig. 4 reproduit partiellement deux spectres de vibration-rotation de l'oxyde azoteux au voisinage

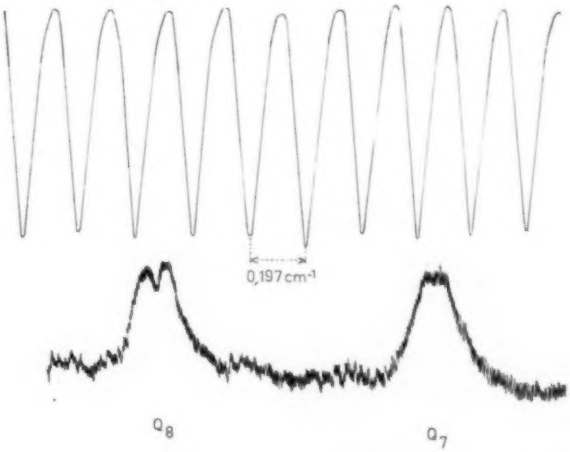

Fig. 3 bis. Branche $Q$ de la composante $F_2$ de 2 $\nu_3$ du méthane à 6000 $cm^{-1}$.

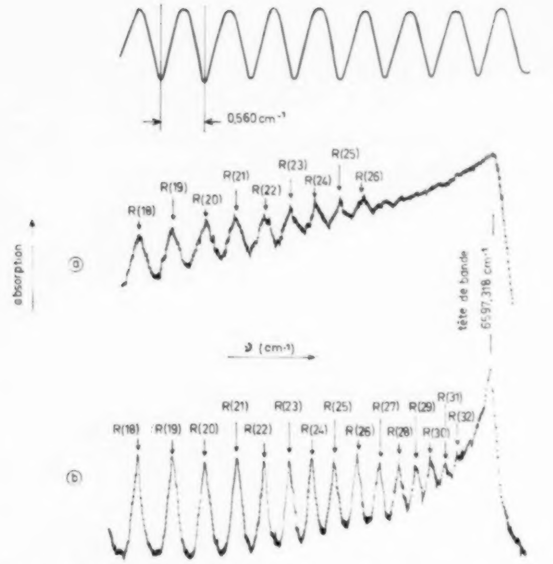

Fig. 4. Fin de la branche $R$ de la bande $3\nu_3$ de l'oxyde nitreux à 1,5 $\mu$. a—spectrographe du type Czerny. b—spectrographe du type Fastie-Ebert.

de la tête de bande, obtenus respectivement avec les spectrographes du type Czerny (a) et du type Fastie–Ebert (b). On remarquera une amélioration très nette dans la structure fine malgré l'augmentation relativement faible du pouvoir de résolution pratique.

## II. Résultats

Nous avons entrepris, ou poursuivi, sur les spectrographes que nous venons de décrire et de comparer, une série d'études sur les molécules très simples: molécules diatomiques telles que HI et NO, molécules triatomiques telles que $N_2O$.

### A. Spectre de Vibration-Rotation de l'Acide Iodhydrique Gazeux. Etude de la Bande $3\nu$.

#### *1°/Introduction*

L'iode n'ayant pas d'isotope naturel, il ne se produit pas de superposition des diverses variétés isotopiques comme dans le cas de l'acide bromhydrique et de l'acide chlorhydrique. Les bandes, fondamentale $\nu$ et première harmonique $2\nu$, ont été étudiées en 1935 par Nielsen et Nielsen.[9] Plus récemment, en 1950, Naudé et Verleger[10] ont réussi à analyser la bande $4\nu$, mais son intensité très faible ne leur a pas permis d'examiner plus de sept raies. En 1952, Boyd et Thompson[11] ont réétudié la bande fondamentale. Dans le domaine spectral de l'infrarouge lointain, Palik,[12] en 1955, a observé plusieurs raies de rotation et a pu ainsi déterminer les constantes rotationnelles $B_0$ et $D_0$, que nous pourrons comparer utilement aux valeurs obtenues dans l'infrarouge proche. La bande $3\nu$ fait l'objet de la présente étude. Nous avons pu déterminer quelques nouvelles constantes de vibration-rotation et avons observé en fin de branche $R$ un retournement de raies, que laisse prévoir la théorie.

#### *2°/Préparation de HI gazeux**

L'acide iodhydrique a été obtenu par hydrolyse de l'iodure d'aluminium. Nous avons préparé l'iodure d'aluminium par action de l'iode sur des copeaux d'aluminium très pur, portés à une température de 500°C environ. L'hydrolyse du produit recueilli a été faite avec une solution concentrée d'acide iodhydrique p.p.a. du commerce. Pour éliminer toutes traces d'eau et d'iode, on faisait passer l'acide iodhydrique dans une colonne desséchante contenant de l'iodure de calcium et dans un piège contenant un mélange glace-sel. Ensuite, l'acide iodhydrique était distillé. Toutes les opérations précédentes se faisaient sous vide. L'acide obtenu était ensuite introduit dans une cuve d'absorption en verre d'un mètre de longueur terminée par deux fenêtres également en verre (fenêtres soudées). Les pressions utilisées pour l'enregistrement du spectre infrarouge étaient comprises entre 40 et 76 cm de mercure.

Une des difficultés rencontrées au cours de ce travail consiste en la décomposition lente de l'acide iodhydrique exposé à la lumière. Après chaque manipulation, un faible dépôt (cristaux d'iode) observé dans la cuve révélait une décomposition partielle du produit (durée de chaque manipulation 30 à 40 heures). La préparation était refaite à chaque manipulation. Des travaux récents,[13–15] en particulier sur l'acide chlorhydrique, montrent que la position des raies d'absorption dépend de la pression du gaz et qu'elle peut être modifiée par la présence d'un gaz étranger. Cet effet est généralement très faible. En tenant compte de ce résultat nous estimons que la précision absolue de nos mesures n'a pas atteint 0,01 cm⁻¹, mais pourrait être de l'ordre de 0,02 cm⁻¹ (la précision relative étant meilleure).

#### *3°/Résultats des mesures; calcul des constantes de rotation*

Les raies de vibration-rotation relatives à une molécule diatomique ont des nombres d'onde définis par la relation:

$$\nu = \nu_{v''-v'} + (B_{v'} + B_{v''})m + (B_{v'} - B_{v''} - D_{v'} + D_{v''})m^2 - 2(D_{v'} + D_{v''})m^3 - (D_{v'} - D_{v''})m^4 \quad (1)$$

avec $m = 1, 2, 3 \ldots$ pour les raies de la branche $R$, $m = -1, -2, -3\ldots$ pours les raies de la branche $P$, $v''$, nombre quantique de vibration du niveau de départ, $v'$, nombre quantique de vibration du niveau d'arrivée.

---

* La méthode de préparation nous a été indiquée par Monsieur le Professeur Chrétien auquel nous adressons nos remerciements.

**Tableau I. Bande 3$\nu$ de HI Gazeux[a]**

| $m$ | $\nu_{\text{observé}}$ (cm$^{-1}$) | $\nu_{\text{calculé}}$ (cm$^{-1}$) | $\nu_{\text{obs}} - \nu_{\text{cal}}$ (cm$^{-1}$) | |
|---|---|---|---|---|
| −9 | 6 295,675 | 6 295,673 | +0,002 | |
| −8 | 6 316,638 | 6 316,630 | +0,008 | |
| −7 | 6 336,597 | 6 336,593 | +0,004 | |
| −6 | 6 355,559 | 6 355,557 | +0,002 | |
| −5 | 6 373,520 | 6 373,516 | +0,004 | |
| −4 | 6 390,459 | 6 390,464 | −0,005 | |
| −3 | 6 406,388 | 6 406,396 | −0,008 | |
| −2 | 6 421,297 | 6 421,306 | −0,009 | |
| −1 | 6 435,174 | 6 435,190 | −0,016 | |
| 1 | 6 459,860 | 6 459,858 | +0,002 | |
| 2 | 6 470,629 | 6 470,631 | −0,002 | |
| 3 | 6 480,359 | 6 480,359 | 0,000 | |
| 4 | 6 489,040 | 6 489,035 | +0,005 | |
| 5 | 6 496,659 | 6 496,656 | +0,003 | |
| 6 | 6 503,220 | 6 503,216 | +0,004 | |
| 7 | 6 508,714 | 6 508,713 | +0,001 | |
| 8 | 6 513,144 | 6 513,141 | +0,003 | |
| 9 | 6 516,505 | 6 516,497 | +0,008 | |
| 10 | 6 518,778 | 6 518,777 | +0,001 | |
| 11 | 6 519,99 | 6 519,977 | | |
| 12 | | 6 520,094 | | retournement des raies |
| 13 | 6 519,08 | 6 519,123 | | |
| 14 | 6 517,00 | 6 517,061 | | |

[a] Les nombres d'onde sont rapportés au vide.

Les constantes rotationnelles $B_v$ et $D_v$ varient en fonction de $V$ et sont définies par les relations:

$$B_v = B_e - \alpha_e(v + {}^1/_2) + \ldots, \qquad (2)$$
$$D_v = D_e + \beta_e(v + {}^1/_2) + \ldots.$$

Les constantes de rotation $B_{v'}$, $B_{v''}$, $D_{v'}$, $D_{v''}$ et le terme $\nu_{v'' \to v'}$ peuvent être déterminés très simplement en utilisant des relations de combinaisons.[16]

Les résultats des mesures sont consignés dans le tableau I. Nous remarquerons que les constantes $B_0$ et $D_0$, figurant dans le tableau II, sont en bon accord avec celles de Palik, obtenues dans le domaine de l'infrarouge lointain. L'accord est médiocre avec les constantes déterminées par Naudé et Verleger, excellent avec celles déterminées par Boyd et Thompson.

**Tableau II. Constantes Rotationnelles de HI Gazeux[a]**

| | Nos résultats (cm$^{-1}$) | Naudé et Verleger[10] (cm$^{-1}$) | Boyd et Thompson[11] (cm$^{-1}$) | Palik[12] (cm$^{-1}$) |
|---|---|---|---|---|
| $B_e$ | 6,512 8 | 6,551 | 6,512 | |
| $B_0$ | 6,426 4 | 6,460 | 6,426 | 6,427 5 |
| $B_3$ | 5,908 0 | (5,911)[b] | | |
| $\alpha_e$ | 0,172 80 | 0,183 | (0,171 5)[b] | |
| $D_e$ | 0,000 209 | 0,000 213 | | |
| $D_0$ | 0,000 208 | 0,000 212 | 0,000 20 | 0,000 205 |
| $D_3$ | 0,000 203 | (0,000 203)[b] | | |
| $\beta_e$ | −0,000 002 | −0,000 003 | | |
| 3$\nu$ | 6 448,043 | | | |

[a] Les nombres d'onde sont rapportés au vide.

[b] Ces valeurs sont calculées d'après les constantes rotationnelles données par les auteurs cités en référence.

Les constantes étant connues, la relation (1) nous permet de calculer les nombres d'onde $\nu$ des raies, qui figurent également dans le tableau I. Nous constatons que, jusqu'à la raie $m = 10$, les valeurs mesurées et calculées sont en bon accord.

Nous avons pu observer distinctement le retournement dans la position des raies de la branche $R$. Sur la Fig. 5 nous pouvons constater que la raie $m = 11$ est anormalement large; le tableau des résultats révèle par ailleurs que les raies $m = 11$ et $m = 12$ ont des nombres d'onde très voisins. On peut donc penser que la raie large, notée $m = 11$, est en fait la superposition des raies $m = 11$ et $m = 12$, ce qui explique le mauvais accord entre la valeur calculée et la valeur mesurée pour $m = 11$. Ces deux raies non résolues se situent au voisinage de la tête de bande (nous n'avons pu réduire suffisamment la pression afin de résoudre cette tête de bande). On distingue une raie $m = 13$ dans le pied de la raie $m = 10$ et une raie $m = 14$ dans celui de la raie $m = 9$. Ces deux raies dues au retournement n'ont pu être pointées correctement, ce qui pourrait expliquer la différence entre les valeurs calculées et observées.

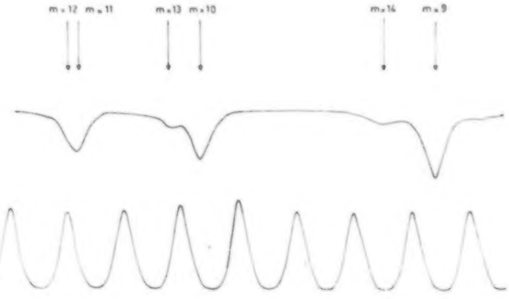

Fig. 5. Fin de la branche $R$ de la bande 3$\nu$ de l'acide iodhydrique gazeux à 6520 cm$^{-1}$.

## B. Spectre de Vibration-Rotation 3$\nu$ de l'Oxyde Nitrique NO

### *1°/Introduction*

L'oxyde nitrique est une des rares molécules dont l'état de base électronique ne soit pas un état $\Sigma$. Le moment éléctronique angulaire $\Lambda$ est égal à 1 et le moment de spin $\Sigma$ égal à $\pm\ {}^1/_2$.

Le moment électronique total $\Omega = \Lambda + \Sigma$ prend deux valeurs $\Omega = {}^1/_2$ et $\Omega = {}^3/_2$. Donc, à l'état de base, la molécule possède deux niveaux électroniques désignés par ${}^2\Pi_{1/2}$ et ${}^2\Pi_{3/2}$. La théorie qui rend compte de l'état d'une telle molécule s'apparente à la théorie des bandes électroniques. Nous en rappelons les principales conséquences pour l'interprétation des spectres de vibration-rotation.

**Tableau III. Bande $3\nu$ de NO**[a]

| $J + {}^1/_2$ | Nos valeurs (cm$^{-1}$) | Valeurs calculées (cm$^{-1}$) | Ecarts $\nu_{obs} - \nu_{cal}$ (cm$^{-1}$) |
|---|---|---|---|
| | $R_1(J + {}^1/_2)$ | | |
| 1 | 5 548,878 | 5 548,872 | +0,006 |
| 2 | 5 551,939 | 5 551,959 | −0,020 |
| 3 | 5 554,921 | 5 554,944 | −0,023 |
| 4 | 5 557,818 | 5 557,825 | −0,007 |
| 5 | 5 560,599 | 5 560,604 | −0,005 |
| 6 | 5 563,284 | 5 563,279 | +0,005 |
| 7 | 5 565,812 | 5 565.851 | −0,039 |
| 8 | 5 568,294 | 5 568,320 | −0,026 |
| 9 | 5 570,672 | 5 570,686 | −0,014 |
| 10 | 5 572,917 | 5 572,942 | −0,025 |
| 11 | 5 575,073 | 5 575,104 | −0,031 |
| 12 | 5 577,151 | 5 577,157 | −0,006 |
| 13 | 5 579,120 | 5 579,106 | +0,014 |
| 14 | 5 580,947 | 5 580,950 | −0,003 |
| 15 | 5 582,701 | 5 582,690 | +0,011 |
| 16 | 5 584,328 | 5 584,323 | +0,005 |
| 17 | 5 585,860 | 5 585,852 | +0,008 |
| 18 | 5 587,267 | 5 587,275 | −0,008 |
| 19 | 5 588,586 | 5 588,591 | −0,005 |
| 20 | 5 589,788 | 5 589,801 | −0,013 |
| 21 | 5 590,889 | | |
| | $R_2(J + {}^1/_2)$ | | |
| 1 | — | — | — |
| 2 | 5 551,545 | 5 551,515 | +0,030 |
| 3 | 5 554,578 | 5 554,574 | +0,004 |
| 4 | 5 557,537 | 5 557,524 | +0,013 |
| 5 | 5 560,376 | 5 560,365 | +0,011 |
| 6 | 5 563,112 | 5 563,097 | +0,015 |
| 7 | 5 565,716 | 5 565,720 | −0,004 |
| 8 | (5 568,294)[b] | 5 568,233 | +0,061 |
| 9 | (5 570,672) | 5 570,636 | +0,036 |
| 10 | (5 572,917) | 5 572,930 | −0,013 |
| 11 | (5 575,073) | 5 575,114 | −0,041 |
| 12 | (5 577,151) | 5 577,188 | −0,037 |
| 13 | (5 579,120) | 5 579,153 | −0,033 |
| 14 | (5 580,947) | 5 581,008 | −0,061 |
| 15 | (5 582,701) | 5 582,753 | −0,054 |
| 16 | (5 584,328) | 5 584,388 | −0,060 |
| 17 | (5 585,860) | 5 585,914 | −0,054 |
| 18 | (5 587,267) | 5 587,329 | −0,062 |
| 19 | (5 588,586) | 5 588,636 | −0,050 |
| 20 | (5 589,788) | 5 589,833 | −0,045 |
| 21 | (5 590,889) | | |
| | $P_1(J + {}^1/_2)$ | | |
| 1 | — | — | — |
| 2 | 5 538,993 | 5 538,994 | −0,001 |
| 3 | 5 535,498 | 5 535,496 | +0,002 |
| 4 | 5 531,884 | 5 531,896 | −0,012 |
| 5 | 5 528,199 | 5 528,192 | +0,007 |
| 6 | 5 524,389 | 5 524,386 | +0,003 |
| 7 | 5 520,467 | 5 520,478 | −0,011 |
| 8 | 5 516,467 | 5 516,466 | +0,001 |
| 9 | 5 512,374 | 5 512,352 | +0,022 |
| 10 | 5 508,137 | 5 508,135 | +0,002 |
| 11 | 5 503,808 | 5 503,814 | −0,006 |
| 12 | 5 499,398 | 5 499,392 | +0,006 |
| 13 | 5 494,861 | 5 494,863 | −0,002 |
| 14 | 5 490,234 | 5 490,232 | +0,002 |
| 15 | 5 485,491 | 5 485,498 | −0,007 |
| 16 | 5 480,668 | 5 480,659 | +0,009 |
| 17 | | 5 475,726 | |
| 18 | 5 470,652 | 5 470,669 | −0,017 |
| 19 | 5 465,519 | 5 465,518 | +0,001 |
| 20 | 5 460,254 | 5 460,261 | −0,007 |
| 21 | 5 454,897 | 5 454,899 | −0,002 |
| | $P_2(J + {}^1/_2)$ | | |
| 1 | — | — | — |
| 2 | — | — | — |
| 3 | 5 534,589 | 5 534,592 | −0,003 |
| 4 | 5 530,879 | 5 530,884 | −0,005 |
| 5 | 5 527,060 | 5 527,068 | −0,008 |
| 6 | 5 523,131 | 5 523,145 | −0,014 |
| 7 | 5 519,119 | 5 519,115 | +0,004 |
| 8 | 5 514,971 | 5 514,979 | −0,008 |
| 9 | 5 510,734 | 5 510,737 | −0,003 |
| 10 | 5 506,372 | 5 506,390 | −0,018 |
| 11 | 5 501,932 | 5 501,937 | −0,005 |
| 12 | | 5 497,379 | |
| 13 | 5 492,737 | 5 492,716 | +0,021 |
| 14 | 5 487,930 | 5 487,950 | −0,020 |
| 15 | 5 483,059 | 5 483,080 | −0,021 |
| 16 | 5 478,073 | 5 478,106 | −0,033 |
| 17 | 5 472,987 | 5 473,030 | −0,043 |
| 18 | | 5 467 782 | |
| 19 | 5 462,499 | 5 462,492 | +0,007 |
| 20 | 5 451,095 | 5 457,091 | +0,004 |
| 21 | 5 457,622 | 5 451,610 | +0,012 |
| | $Q_1(J + {}^1/_2)$ | | |
| 1 | 5 544,002 | 5 544,011 | −0,009 |
| 2 | | | |
| 3 | | | |
| 4 | | | |
| 5 | | | |
| 6 | | | |
| 7 | | | |
| 8 | | | |
| | $Q_2(J + {}^1/_2)$ | | |
| 1 | — | — | — |
| 2 | 5 543,199 | 5 543,190 | +0,009 |
| 3 | 5 542,911 | 5 542,919 | −0,008 |
| 4 | 5 542,547 | 5 542,540 | +0.007 |
| 5 | 5 542,064 | 5 542,053 | +0,011 |
| 6 | 5 541,454 | 5 541,458 | −0,004 |
| 7 | 5 540,748 | 5 540,754 | −0,006 |
| 8 | 5 539,942 | 5 539,942 | 0.000 |

[a] Les nombres d'onde sont rapportés au vide.

[b] Pour $J > {}^{13}/_2$ nous avons pris la même valeur mesurée dans la branche $R$ des deux sous-états puisque nous ne pouvons plus les séparer.

L'interaction entre le moment électronique et la rotation de la molécule entraîne la règle de sélection supplémentaire $\Delta J = 0$, expliquant l'existence d'une branche $Q$, en plus des branches $P$ et $R(\Delta J = \pm 1)$. L'existence des deux sous-niveaux ${}^2\Pi_{1/2}$ et ${}^2\Pi_{3/2}$ et la règle de sélection $\Delta\Sigma = 0$ entraîne un dédoublement des branches $P, Q, R$.

Pour désigner chaque raie, nous prendrons la notation $R$, $P$, $Q$, suivie de 1 pour le sous-état ${}^2\Pi_{1/2}$ ou de 2 pour le sous-état ${}^2\Pi_{3/2}$, et nous caractériserons le niveau de départ par la valeur de l'expression $J + {}^1/_2$ correspondante.

Pour déterminer les niveaux d'énergie de la molécule, il faut faire intervenir une énergie de couplage du spin avec le moment électronique angulaire. On montre que pour NO les termes spectraux sont:

$$
{}^2\Pi_{1/2}T_1 = G_1 + F_1 = G_1(v) - \frac{A}{2} + \frac{B_{v_1}}{4} + B_{v_1}J(J+1) - D_{v_1}J^2(J+1)^2,
$$

$$
{}^2\Pi_{3/2}T_2 = G_2 + F_2 = G_2(v) + \frac{A}{2} - \frac{7B_{v_2}}{4} + B_{v_2}J(J+1) - D_{v_2}J^2(J+1)^2.
$$

Les constantes $B_{v_i}$ et $D_{v_i}$ sont des constantes effectives qui sont reliées aux constantes classiques $B_v$ et $D_v$ par les relations suivantes:

$$
B_{v_i} = B_v\left[1 + (-1)^i\left(\frac{B_v}{A} - \frac{2B^2{}_v}{A^2}\right)\right],
$$

$$
D_{v_i} = D_v - (-1)^i\,\frac{B^4{}_v}{A^3}.
$$

Ces équations montrent que chaque sous-état peut être considéré séparément, et pour le calcul des constantes effectives, nous pourrons utiliser les relations de combinaison habituelles.

### 2°/*Partie expérimentale*

L'oxyde nitrique, fourni par la "Matheson Gas Company", avait un état de pureté de 99% et fut employé sans purification préalable. Le gaz était introduit dans une cuve à réflexions multiples. Nous avons choisi une pression de 21 cm de mercure et un parcours de 32 mètres. Les résultats obtenus ne sont pas définitifs.

Le tableau III donne les nombres d'onde rapportés au vide des raies dans chacune des branches $P, Q, R$.

Nous estimons la précision de nos mesures absolues à 0,03 cm$^{-1}$. Cette erreur relativement grande est due à la présence de raies de l'eau assez intenses dans le domaine spectral où nous travaillons. A partir de $J = {}^{13}/_2$ les raies des deux branches $R$ ne sont plus séparables. Les valeurs calculées, données dans le tableau IV, montrent que la distance des deux raies est inférieure au pouvoir séparateur du spectrographe. La raie pointée est donc un doublet non séparé, ce qui ajoute une incertitude sur le nombre d'onde exact de chaque raie.

**Tableau IV. Constantes Vibrationnelles et Rotationnelles de NO**[a]

| Constantes moléculaires | Nos valeurs | Autres valeurs |
|---|---|---|
| $B_{01}$ | 1,671 99 cm$^{-1}$ | 1,671 98[26] cm$^{-1}$ |
| $B_{02}$ | 1,719 58 | 1,722 4[21] |
| $B_0$ | 1,695 78 | 1,696 5 |
| $B_{31}$ | 1,620 65 | 1,615 0 |
| $B_{32}$ | 1,665 28 | 1,666 5 |
| $B_3$ | 1,642 96 | 1,640 8 |
| $B_e$ | 1,704 82 | 1,706 0 |
| $D_e$ | $(5{,}46.10^{-6})^b$ | $(5{,}46.10^{-6})^b$[21] |
| $D_{01}$ | $1{,}77.10^{-6}$ | $(1{,}67.10^{-6})^b$[21] |
| $D_{02}$ | $(9{,}77.10^{-6})^b$ | — |
| $D_{31}$ | $1{,}14.10^{-6}$ | $(1{,}16.10^{-6})^b$[21] |
| $D_{32}$ | $(9{,}26.10^{-6})^b$ | — |
| $\nu_{0\to 3,1}$ | 5 544,061 | $(5\ 544{,}21)^b$[19] |
| $\nu_{0\to 3,2}$ | 5 543,299 | $(5\ 543{,}35)^b$[19] |
| $\alpha_e$ | 0,017 57 | 0,0178 |
| $I_e$ | 1,6404 $10^{-39}$ gcm$^2$ | 1,6404 $10^{-39}$ gcm$^2$ |
| $r_e$ | 1,150 7 Å | 1,150 3 Å |

[a] Les nombres d'onde sont rapportés au vide.

[b] Ces valeurs sont calculées d'après les constantes rotationnelles ou vibrationnelles données par les auteurs cités en référence.

Il est intéressant de noter que les branches $P$ et $R$ correspondant au sous-état ${}^2\Pi_{1/2}$ sont les plus intenses. Dans la branche $Q$ (Fig. 6), le phénomène inverse se produit: le sous-état ${}^2\Pi_{3/2}$ donne une branche $Q$ intense, alors que l'autre sous-état donne une branche $Q$ très faible.

### 3°/*Constantes moléculaires*

(*a*) *Constantes rotationnelles.* Pour les calculer, nous avons employé les relations de combinaison[16] habituelles. Nous avons tracé la droite:

$$
\frac{\Delta_2F(J)}{J + {}^1/_2} = f\,[(J + {}^1/_2)^2]
$$

pour le sous-état ${}^2\Pi_{1/2}$. Pour le second sous-état, nous

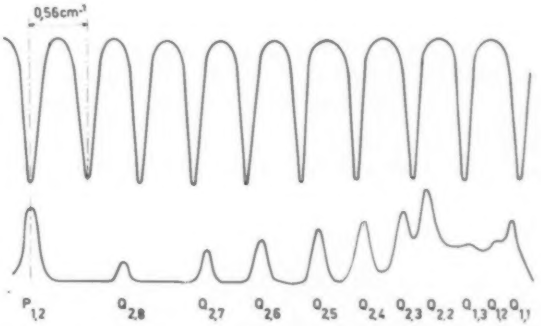

Fig. 6. Deux branches $Q$ de la bande $3\nu$ de l'oxyde nitrique à 5544 cm$^{-1}$.

Tableau V. Bande $3\nu_3$ de $N_2O$[a]

| $J$ | $\nu_{\text{observé}}$ (cm$^{-1}$) $P(J)$ | $\nu_{\text{calculé}}$ (cm$^{-1}$) $P(J)$ | $\nu_{\text{cal}} - \nu_{\text{obs}}$ (cm$^{-1}$) $\Delta P(J)$ | $\nu_{\text{observé}}$ (cm$^{-1}$) $R(J)$ | $\nu_{\text{calculé}}$ (cm$^{-1}$) $R(J)$ | $\nu_{\text{cal}} - \nu_{\text{obs}}$ (cm$^{-1}$) $\Delta R(J)$ |
|---|---|---|---|---|---|---|
| 0 | | | | | 6 581,619 | |
| 1 | | 6 579,964 | | | 6 582,415 | |
| 2 | | 6 579,105 | | 6 583,196 | 6 583,192 | −0,004 |
| 3 | 6 578,231 | 6 578.226 | −0,005 | 6 583,953 | 6 583,947 | −0,006 |
| 4 | 6 577,337 | 6 577,326 | −0,011 | 6 584,680 | 6 584,681 | +0,001 |
| 5 | 6 576,403 | 6 576,405 | +0,002 | 6 585,399 | 6 585,395 | −0,004 |
| 6 | 6 575,459 | 6 575,463 | +0,004 | 6 586,097 | 6 586,088 | −0,009 |
| 7 | 6 574,502 | 6 574,501 | −0,001 | 6 586,767 | 6 586,761 | −0,006 |
| 8 | 6 573,515 | 6 573,518 | +0,003 | 6 587,421 | 6 587,412 | −0,009 |
| 9 | 6 572,515 | 6 572.515 | 0,000 | 6 588,054 | 6 588,043 | −0,011 |
| 10 | 6 571,502 | 6 571,490 | −0,012 | 6 588,665 | 6 588,654 | −0,011 |
| 11 | 6 570,439 | 6 570,445 | +0,006 | 6 589,247 | 6 589,243 | −0,004 |
| 12 | 6 569,379 | 6 569,380 | +0,001 | 6 589,810 | 6 589,812 | +0,002 |
| 13 | 6 568,295 | 6 568,293 | −0,002 | 6 590,366 | 6 590,360 | −0,006 |
| 14 | 6 567,209 | 6 567.186 | −0,023 | 6 590,888 | 6 590,888 | 0,000 |
| 15 | 6 566,060 | 6 566,058 | −0,002 | 6 591,396 | 6 591,395 | −0,001 |
| 16 | 6 564,905 | 6 564,910 | +0,005 | 6 591,886 | 6 591,881 | −0,005 |
| 17 | 6 563,740 | 6 563,740 | 0,000 | 6 592,340 | 6 592,346 | +0,006 |
| 18 | 6 562,556 | 6 562,550 | −0,006 | 6 592,761 | 6 592,791 | +0,030 |
| 19 | 6 561.344 | 6 561,340 | −0,004 | 6 593,199 | 6 693,215 | +0,016 |
| 20 | 6 560,109 | 6 560,109 | 0,000 | 6 593,611 | 6 593,618 | +0,007 |
| 21 | 6 558,869 | 6 558,864 | −0,005 | 6 593,980 | 6 593,994 | +0,014 |
| 22 | 6 557,590 | 6 557,592 | +0,002 | 6 594,334 | 6 594,355 | +0,021 |
| 23 | 6 556,295 | 6 556,299 | +0,004 | 6 594,688 | 6 594,695 | +0,007 |
| 24 | 6 554,973 | 6 554,986 | +0,013 | | | |
| 25 | 6 553,643 | 6 553,652 | +0,009 | | | |
| 26 | 6 552,312 | 6 552,298 | −0,014 | | | |
| 27 | 6 550,926 | 6 550,924 | −0,002 | | | |
| 28 | 6 549,530 | 6 549,529 | −0,001 | | | |
| 29 | 6 548,108 | 6 548,112 | +0,004 | | | |
| 30 | 6 546,668 | 6 546,676 | +0,008 | | | |
| 31 | 6 545,244 | 6 545,219 | −0,025 | | | |
| 32 | 6 543,743 | 6 543,741 | −0,002 | | | |

[a] Les nombres d'onde sont rapportés au vide.

avons pris une valeur moyenne, car les nombres d'onde sont trop imprécis pour des grandes valeurs de $J$ dans la branche $R$.

$$4B_{v_2} = \frac{\Delta_2 F(J)}{J + {}^1/_2} + 8D_{v_2}(J + {}^1/_2)^2.$$

Pour $D_{v_2}$, nous avons pris la valeur théorique donnée dans le tableau IV.

(*b*) *Constantes vibrationnelles.* Pour déterminer $\nu_{0\to3,1}$ c'est-à-dire le centre de la bande, relatif au sous-état ${}^2\Pi_{1/2}$, nous avons employé la relation de combinaison suivante:

$$R(J-1) + P(J) - 2(B_{v'} - B_{v''})J^2 + 2(D_{v'} - D_{v''})J^4 = 2\left(\nu_{0\to3,1} + \frac{B_{31} - B_{01}}{4}\right).$$

Pour le second sous-état ${}^2\Pi_{3/2}$, nous avons préféré utiliser la branche $Q_2\,(J + {}^1/_2)$ dont les raies sont bien pointables. Nous avons reporté $Q_2\,(J + {}^1/_2)$ en fonction de $J(J+1)$ selon la relation:

$$Q_2\,(J + {}^1/_2) = \left[\nu_{0-3,2} - \frac{7}{4}(B_{02} - B_{32})\right] + (B_{v'} - B_{v''})\,J(J+1).$$

Les valeurs trouvées sont données dans le tableau IV, ainsi que celles recalculées à partir des constantes vibrationnelles données par Gillette et Eyster.[17] Les écarts importants montrent qu'il est nécessaire de recalculer les constantes vibrationnelles de NO.

(*c*) *Constantes rotationnelles à l'équilibre.* Nous avons porté, en fonction de $(v + {}^1/_2)$, les valeurs des constantes rotationnelles $B_v$ selon la relation (2).

Pour compléter nos valeurs, nous avons pris $B_1$ dans les travaux de Shaw,[18] et de Gillette et Eyster sur la fondamentale de NO. Celles de $B_2$ proviennent de Nichols *et al.*[19] sur la bande $2\nu$ et celles de Schmid *et al.*[20] sur le système $\beta_{2\to2}$.

Les constantes, ainsi que le moment d'inertie et la distance des noyaux à l'équilibre, sont donnés par le tableau IV.

**Tableau VI. Constantes Vibrationnelles et Rotationnelles $N_2O$[a]**

| | Nos résultats | Plyler, Allen, et Tidwell[23] | Tidwell et Plyler[24] | Grenier-Besson[22] |
|---|---|---|---|---|
| $B_{00^00}$ | 0.419 01 cm$^{-1}$ | 0,419 011 cm$^{-1}$ | | |
| $B_{00^03}$ | 0,408 66 cm$^{-1}$ | | | |
| $\alpha_3$ | 0,003 450 cm$^{-1}$ | | 0,003 44 cm$^{-1}$ | 0,003 45 cm$^{-1}$ |
| $3\nu_3$ | 6 580,802 cm$^{-1}$ | 6 580,83 cm$^{-1}$ | | |
| $\omega_3{}^\circ$ | 2 238,825 cm$^{-1}$ | | | 2 238,85 cm$^{-1}$ |
| $x_{33}$ | −15,075 | | −15,02 | −15,10 |

[a] Les nombres d'onde sont rapportés au vide.

(*d*) *Distance séparant les deux sous-niveaux.* La valeur $A$ se déduisant facilement des constantes effectives, on trouve que:

$$A = \frac{2B^2{}_v}{B_{ve} - B_{vi}}\left[1 + 2\,\frac{B_v}{A}\right].$$

Nous avons deux façons de calculer $A$, soit avec les constantes du niveau 0, soit avec celles du niveau 3. Les deux résultats sont en bon accord:

pour le niveau 0 $\quad A = 124{,}147\ \text{cm}^{-1}$,

pour le niveau 3 $\quad A = 124{,}159\ \text{cm}^{-1}$.

Nous pourrons donc adopter la valeur moyenne:

$$A = 124{,}153\ \text{cm}^{-1}.$$

## C. Spectre de Vibration-Rotation de l'Oxyde Azoteux. Etude de la Bande $3\nu_3$.

### 1°/*Introduction*

Plusieurs auteurs ont étudié récemment le spectre infrarouge de la molécule d'oxyde azoteux avec des spectrographes à très haut pouvoir de résolution. Nous avons entrepris les mois écoulés l'étude de la bande $3\nu_3$ à 1,5 $\mu$, qui a déjà fait l'objet d'une communication.[21] Nous poursuivons actuellement une série de mesures sur l'oxyde azoteux dans le même domaine spectral. La communication[21] comporte une bibliographie détaillée sur les travaux récents qui ont été effectués sur cette molécule. Nous nous contenterons de citer ici les articles qui permettront une comparaison des différents résultats.[22–24]

Le but de cette étude a été de déterminer et de réajuster, s'il y a lieu, les constantes de vibration-rotation de la bande $3\nu_3$ et de confronter l'expérience et la théorie.

### 2°/*Etude experimentale*

Le gaz était introduit dans une cuve à réflexions multiples, sous une pression de 9 cm de mercure. Le trajet lumineux nécessaire n'a jamais excédé 32 mètres. Ces trajets et la pression de gaz ont été choisis de façon à permettre le repérage du centre de la bande avec la meilleure précision, en utilisant la structure fine de vibration-rotation.

Les résultats des mesures qui figurent dans le tableau V sont des nombres d'onde rapportés au vide.

### 3°/*Resultats des mesures*

(*a*) *Determination des constantes rotationnelles.*[16,22] La bande $3\nu_3$ est une bande parallèle qui correspond à une transition $\Sigma^+ \rightarrow \Sigma^+$. La relation (1), définie dans le cas d'une molécule diatomique, reste donc valable. Quant à la relation (2) qui explicite le terme $B_v$, nous l'écrirons sous la nouvelle forme:

$$B_{v_1v_2v_3} = B_e - \alpha_1(v_1 + {}^1/_2) - \alpha_2(v_2 + 1) - \alpha_3(v_3 + {}^1/_2). \tag{2'}$$

En utilisant des relations classiques obtenues à partir de la relation (1), nous avons pu obtenir les constantes rotationnelles qui figurent dans le tableau VI, ainsi que le terme $3\nu_3$ définissant le centre de la bande.

Nous n'avons pu fournir un résultat valable pour le terme de distorsion $D_v$.

Il est possible, connaissant les valeurs du centre de la bande et des constantes $B_{000_0}$, $B_{00_03}$ et $D_0$,[24] de calculer les nombres d'onde de chaque raie de rotation (tableau V).

(*b*) *Determination des constantes vibrationnelles.* Le nombre d'onde du centre de la bande de vibration-rotation correspondant à une transition du niveau (00$^0$0) au niveau ($v_1v_2{}^{l_2}v_3$) est donné par la relation:

$$\nu(00^00 \rightarrow v_1v_2{}^{l_2}v_3) = \omega_1{}^0v_1 + \omega_2{}^0v_2 + \omega_3{}^0v_3$$
$$+ x_{11}v_1{}^2 + x_{22}v_2{}^2 + x_{33}v_3{}^2 + x_{12}v_1v_2 + x_{13}v_1v_3 + x_{23}v_2v_3 + x_{l_2l_2}l_2{}^2.$$

La formule précédente permet de calculer les constantes $x_{33}$ et $\omega_3{}^\circ$. On a en effet:

$$\begin{cases} \nu(00^00 \rightarrow 00^01) = \omega_3{}^0 + x_{33}. \\ \nu(00^00 \rightarrow 00^03) = 3\omega_3{}^0 + 3^2x_{33} \end{cases}$$

et

$$x_{33} = \frac{\nu(00^00 \rightarrow 00^03) - 3\nu(00^00 \rightarrow 00^01)}{6}$$

avec les valeurs:

$$\nu(00^00 \rightarrow 00^01) = 2223,\ 75\ \text{cm}^{-1} \qquad \text{(ref. 25)}$$

$$\nu(00^00 \rightarrow 00^03) = 6580,\ 802 \pm 5.10^{-3}\ \text{cm}^{-1}$$

d'où les valeurs suivantes:

$$x_{33} = -15.075 \pm 5.10^{-3}\ \mathrm{cm}^{-1},$$

$$\omega_3^0 = 2238,825 \pm 5.10^{-3}\ \mathrm{cm}^{-1}.$$

Nous résumons dans le tableau VI les valeurs comparées des résultats que nous avons pu obtenir, et ceux obtenus par Grenier-Besson,[22] et ceux de Plyler *et al.*[23,24]

## Bibliographie

1. Y. Cornet, C. Haeusler, et P. Barchewitz, Compt. Rend. **248,** 3290 (1959).
2. C. Haeusler, Y. Cornet, et P. Barchewitz, J. Phys. Radium **12,** 809 (1960).
3. D. H. Rank, A. H. Guenther, C. R. Burnett, and T. A. Wiggins, J. Opt. Soc. Am. **47,** 631 (1957).
4. W. G. Fastie, J. Opt. Soc. Am. **43,** 1174 (1953).
5. A. E. Douglas and D. S. Sharma, J. Chem. Phys. **21,** 3 (1953).
6. E. K. Plyler, L. R. Blaine, and W. S. Connor, J. Opt. Soc. Am. **45,** 102 (1955).
7. D. H. Rank, J. M. Bennett, and T. A. Wiggins, J. Opt. Soc. Am. **43,** 707 (1953).
8. D. H. Rank, D. P. Eastman, G. Skorinko, and T. A. Wiggins, J. Mol. Spectry. **5,** 78 (1960).
9. A. H. Nielsen and H. H. Nielsen, Phys. Rev. **47,** 585 (1935).
10. S. M. Naudé and H. Verleger, Proc. Phys. Soc. (London) **A63,** 470 (1960).
11. D. R. J. Boyd and H. W. Thompson, Spectrochim. Acta **5,** 308 (1952).
12. E. D. Palik, J. Chem. Phys. **23,** 217 (1955).
13. S. Kimel, M. A. Hirshfeld, and J. H. Jaffe, J. Chem. Phys. **31,** 81 (1959).
14. D. H. Rank, W. B. Birtley, D. P. Eastman, and T. A. Wiggins, J. Chem. Phys. **32,** 296 (1960).
15. M. A. Hirshfeld, J. H. Jaffe, and S. Kimel, J. Chem. Phys. **32,** 297 (1960).
16. G. Herzberg, *Molecular Spectra and Molecular Structure* (Van Nostrand, Princeton, N. J., 1950), Vol. I.
17. R. H. Gillette and E. Eyster, Phys. Rev. **56,** 1113 (1939).
18. J. H. Shaw, J. Chem. Phys. **24,** 399 (1956).
19. N. L. Nichols, C. D. Hause, and R. H. Noble, J. Chem. Phys. **23,** 57 (1955).
20. R. Schmid, T. König, and D. Farkas, Z. Physik **64,** 84 (1930).
21. Nguyen Van Thanh, C. Haeusler, and P. Barchewitz, J. Phys. Radium **23,** 348 (1962).
22. M. L. Grenier-Besson, Cahiers Phys. **68,** 5 (1956); Cahiers Phys. **69,** 8 (1956).
23. E. K. Plyler, H. C. Allen, and E. D. Tidwell, J. Chem. Phys. **24,** 95 (1956).
24. E. D. Tidwell and E. K. Plyler, J. Opt. Soc. Am. **50,** 1243 (1960).
25. H. W. Thompson and R. L. Williams, Proc. Roy. Soc. (London), **Ser. A 220,** 435 (1953).
26. C. A. Burrus and W. Gordy, Phys. Rev. **92,** 1437 (1953).

---

## Information for Contributors

**Scope:** Papers are welcomed in the broad areas of applied optics, in disciplines related to optics and employing optical techniques. Papers should be sent to *The Editor, APPLIED OPTICS, 1155 Sixteenth St. N.W., Washington 6, D.C.* Manuscripts may be submitted in English, French, German, or Russian, and the presentation should be as succinct as comprehension will permit. In general, the metric system of units is preferred. One original and one carbon copy of the manuscript, with two sets of all illustrations, must be sent in. Manuscripts should be typed double or triple spaced on one side of 22 × 28 cm ($8^1/_2$ × 11 in.) paper, leaving a 3.8 cm ($1^1/_2$ in.) margin all around. Equations must be typed not hand written wherever possible. Papers on the more fundamental aspects of experimental and theoretical optics should be sent to *The Editor, JOURNAL OF THE OPTICAL SOCIETY OF AMERICA, National Bureau of Standards, Washington 25, D.C.*

An **abstract,** adequate as an index and a summary, of not more than 100 words should appear at the beginning of the paper after the *title, author's name, affiliation, and address.* In the case of papers in a non-English language, they must be accompanied by an abstract in English as well as an abstract in the language of the paper. It should be borne in mind that this abstract may be used in toto by the abstracting journals, therefore it should be self-contained.

**Figures** suitable for printer's use should be sent. Bear in mind that illustrations will normally be reduced to column width (8.4 cm—$3^5/_{16}$ in.—20 picas). *Halftones:* two sets of glossy prints are needed, which should be mailed flat, with any proportion or framing indicated on a working copy. *Line drawings* should be suitable for reproduction and be not larger than 22 × 28 cm ($8^1/_2$ × 11 in.). *Captions* should be listed on a separate sheet in addition to each caption appearing on each illustration.

**Tables** should be typed on separate sheets and the data therein be intelligible, by title, without reference to the text. Tables should include a minimum of vertical ruling.

**References** must be typed on a separate sheet, be numbered consecutively in the order of their appearance in the text, and follow this form:

1. F. C. Brown, Phys. Rev. **12,** 345 (1821).
2. J. Culpeper, *Space Optics* (Georgetown Institute of Technology Press, Washington, D.C., 1861), pp. 12, 345.

A list of abbreviations for the names of journals is published in *Chem. Abstr. List of Periodicals 1961.* To make for uniformity of presentation generally, the American Institute of Physics, *Style Manual,* second edition, should be used. In general, *APPLIED OPTICS* differs from the *Style Manual* only inasmuch as footnotes appear at the bottom of the page of text, while references are listed numerically at the end of the paper.

There will be no **page charge** for publishing in *APPLIED OPTICS* for the time being.

**Letters to the Editor** should follow the above suggestions, but no abstract is required.

# The Spectroscopy of Shock-Excited Powdered Solids

R. W. Nicholls, W. H. Parkinson, and E. M. Reeves

The shock tube is shown to be an excellent spectroscopic source for controlled thermal excitation of astrophysically interesting spectra. Spectroscopic studies of the luminosity from shock-excited powdered solids made in three laboratories during the past seven years are discussed in detail. A wide range of inorganic oxides, nitrides, hydrides, carbides, and sulfides and other compounds have been treated in addition to samples of meteorite. A few aromatic organic materials have also been studied. Time-resolved emission and absorption techniques have been used. Spectra of most inorganic materials change from molecular to atomic with increase in shock Mach number, and an over-all thermal excitation mechanism appears to be most probable. The situation with organic materials, which have lower melting points, appears to be more complex.

## I. Introduction

Spectroscopic methods have been used in various laboratories for about ten years to study light arising from the propagation of shock waves in gases. In much of this work the spectroscopic approach has been used to study nonequilibrium chemical processes taking place in the hot gases,[1] and in the measurement of gas temperatures. Shock tube spectroscopy has also been used in the determination of oscillator strengths.[2,3] There has been, however, little emphasis upon use of the shock tube as a source for excitation of spectra which are difficult to produce in other ways.

Impurity radiation from dust particles entrained in the shock wave is a common nuisance in the spectroscopic study of shock-excited gases. Nevertheless it does suggest a means by which material may be subjected to a controllable transient high temperature–high particle density environment which is very suitable for absorption or emission spectroscopy.[4,5]

Hydrogen- or helium-driven shock waves in argon are easily produced by fairly simple equipment.[1,6] They provide a convenient method for maintaining temperatures of 1000–20,000°K (in the incident or reflected shock waves) for periods of the order of milliseconds. Immersion of powdered solid particles about 50-$\mu$ diam in the transient slug of hot gas of the shock wave results in an immediate luminosity which presumably arises from surface ablation from the powder particles. It is the purpose of this paper to report on the spectroscopic studies which have been made during the past seven years at the University of Western Ontario, Imperial College, and Harvard College Observatory on the luminosity excited in the interaction between a wide variety of powdered solids and shock waves.

## II. Experimental

### A. The Shock Tube

A tube in copper 5 to 7.5 cm in diameter and 3.5 to 6 m long is a convenient spectroscopic tube [see Fig. 1(b)]. It is divided into high-pressure (1–2.5 m) and low-pressure (2.75–3.5 m) sections which are separated by a diaphragm of aluminum or mylar, the rupture of which initiates the incident shock wave in the low-pressure section or channel. A reflected shock wave of about twice the temperature of the incident wave develops when the incident wave reaches the window at the end of the test section. A low molecular weight (often He or $H_2$), high-pressure (10–20 atmospheres) gas is used in the high-pressure section, and a high molecular weight (often Ar), low-pressure (few millimeters Hg) gas is used in the low-pressure test section. The shock wave is the interface which develops between undisturbed Ar and the slug of compressed Ar driven by the contact surface between the He and Ar, after rupture of the diaphragm. The shock velocity and the temperature behind the incident or reflected shock wave is determined by the initial ratios of molecular weights, pressures, and temperatures on either side of the diaphragm. Thus the excitation environment of the powders can be predetermined by suitable selection of these ratios. Experimental determination of the

---

R. W. Nicholls is with the Department of Physics, University of Western Ontario, London, Canada. W. H. Parkinson and E. M. Reeves are from Harvard College Observatory, Cambridge, Massachusetts.

Received 28 February 1963.

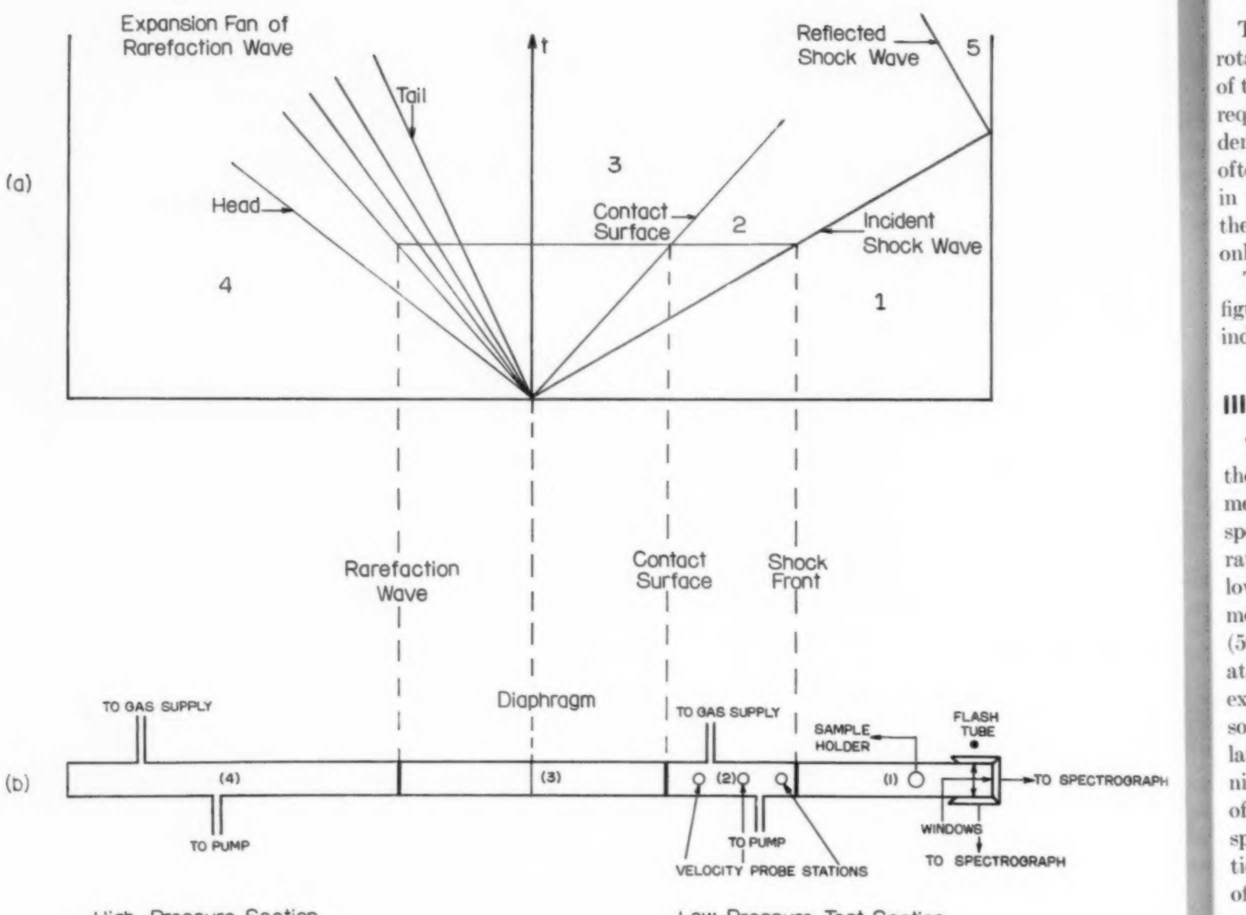
(a)
Expansion Fan of Rarefaction Wave
t
Tail
Head
3
4
Contact Surface
2
Reflected Shock Wave
5
Incident Shock Wave
1
Rarefaction Wave
Contact Surface
Shock Front
Diaphragm
(b)
TO GAS SUPPLY
(4)
TO PUMP
(3)
TO GAS SUPPLY
(2)
TO PUMP
VELOCITY PROBE STATIONS
SAMPLE HOLDER
(1)
FLASH TUBE
TO SPECTROGRAPH
WINDOWS
TO SPECTROGRAPH
High Pressure Section
Low Pressure Test Section

Fig. 1. (a) $x - t$ plot of shock tube operation. (b) Arrangement of shock tube and peripheral equipment.

incident shock velocity provides a good measure of temperature and other physical conditions in the tube for real gases, and thus the low-pressure section is often equipped with a number of thermal velocity probe stations.

The final 60 or 90 cm of the channel are often demountable and interchangeable sections in which a variety of window and sample holder configurations are incorporated.

A sample of 50–100 $\mu$ powder particles is axially located in the last 30 cm of the tube. The most convenient mounting technique has been to place the powder sample on a strip of cellulose tissue or plastic tape suspended from an easily demountable holder at the center of the tube so as to intercept the center of the shock wave. The shock-excited emission spectrum of the tissue or of the plastic (mylar) is merely a few of the common Na and Ca lines. This does not seriously modify the spectrum from the powdered sample. Neither does the support seriously attenuate the incident shock wave.

## B. Spectroscopy

A variety of straightforward emission and absorption spectroscopic techniques have been used to study the light arising from the interaction between the incident and/or reflected shock waves and the powder particles. The light from the 1 to 3 msec duration flash is sufficient to obtain a well-exposed emission spectrum in most cases on a Hilger, *f*/4 glass and quartz Raman spectrograph. The Bausch & Lomb 1.5 m grating, the Hilger Medium quartz, and Bausch & Lomb Large Littrow spectrographs have also been commonly used in various experiments in the conventional photographic quartz region (2000–10,000 Å) and photographic glass region (4000–10,000 Å). More recently a 1.0-m vacuum spectrograph has also been used over the wavelength range 1000–5000 Å.

Time-resolved studies in emission and absorption have been made in addition to time-integrated (over the whole flash) observations. These techniques are extremely powerful for the study of atomic and molecular species.

Time resolution in emission is easily obtained by rotating a sector (of Archimedes spiral profile) in front of the spectrograph slit. Time resolution in absorption requires controlled synchronization between the incidence of the shock wave and the absorbing flash. It often also requires a synchronized fast-moving shutter in front of the spectrograph slit. The shutter gates the spectrograph exposure time so that the slit is open only during the absorption flash.

The important parts of the shock tube and the configuration of peripheral equipment relative to it are indicated in Fig. 1(b).

## III. Excitation Environment of the Shock Wave

The temperature of the gas behind the incident and the reflected shock wave are very important experimental parameters which largely control the type of spectrum excited. As in stellar envelopes and laboratory furnaces, molecular spectra tend to appear at low temperatures (3000–6000°K), mixed atomic and molecular spectra to appear at medium temperatures (5000–8000°K), and entirely atomic spectra to appear at the higher attainable temperatures. One apparent exception to this is in the behavior of certain organic solids which evidently pyrolyze and which are discussed later. Thus although the detailed excitation mechanisms are far from clear, the shock wave may be thought of as a transient furnace which thermally excites spectra of vapor ablated from the surface of the particles. In most of the work reviewed below, excitation of molecular spectra has been the primary aim. Thus relatively low temperatures were employed. Such temperatures are readily obtained in incident and reflected shock waves in argon with a hydrogen or helium driver gas. The conditions necessary to obtain strong shock waves and a consequent high degree of ionization of atoms have been reviewed elsewhere.[7]

The propagation of the one-dimensional shock wave in a tube is represented by the familiar $x - t$ diagram [Fig. 1(a)]. The contact surface, the incident and reflected (at the end of the tube) wave, and the rarefaction wave which is propagated into the low-pressure section and reflected are also indicated. Five regions are conventionally recognized and labeled as follows:

(1) The undisturbed low-pressure channel gas between the end of the tube and the incident shock wave.

(2) A slug of compressed channel gas between the contact surface (boundary between high- and low-pressure gas) and undisturbed low-pressure gas.

(3) Expanding high-pressure gas between rarefaction wave and contact surface.

(4) Undisturbed high-pressure gas between end of high-pressure chamber and rarefaction wave.

(5) Hot channel gas between reflected shock wave and end of channel (only defined after incident shock wave has been reflected).

After rupture of diaphragm, the high-pressure gas of region 4 expands, at a flow velocity close to its sonic velocity, into the heavier low-pressure channel gas. Its sonic velocity is lower and thus it piles up into a slug of gas in region 2 ahead of the contact surface. The incident shock wave is the boundary between regions 1 and 2. The contact surface is the boundary between regions 2 and 3. The reflected shock wave is the boundary between regions 5 and 2.

Conventional one-dimensional shock wave theory applied to a perfect gas model[1] is admittedly an approximate representation both of the physical and of the aerodynamic behavior of shock wave propagation in real gases. It does nevertheless provide useful approximate predictions of the excitation environment to which the powder sample is exposed. The predicted temperatures $T_2$ and $T_5$ of Eqs. (5) and (6) below behind the respective incident and reflected shock waves arise from the well-known relations between initial pressure and temperature ratios ($P_4/P_1$, $T_4/T_1$) across the diaphragm, the shock Mach number $M_1$ [defined in Eq. (2)], and the parameters $\alpha$ and $\beta$ defined in Eq. (3) in terms of the adiabatic modulus $\gamma$.

The local sonic velocity $a$ is given by

$$a = (\gamma RT/\mu)^{1/2}, \tag{1}$$

where $\mu$ is the molecular weight and $R$ the gas constant. The shock Mach number $M_1$ is then defined by:

$$M_1 = v_1/a = v(\mu/\gamma RT)^{1/2}, \tag{2}$$

where $v_1$ is the shock velocity. $\alpha$ and $\beta$ are defined by

$$\alpha = \frac{\gamma + 1}{\gamma - 1}; \qquad \beta = (\gamma - 1)/2\gamma. \tag{3}$$

One-dimensional theory then leads to

$$\frac{P_4}{P_1} = \left[\frac{2\gamma_1}{\gamma_1 + 1} M^2_1 - \frac{\gamma_1 - 1}{\gamma_1 + 1}\right] \left[\frac{1}{1 - \frac{\gamma_4 - 1}{\gamma_1 + 1} \frac{a_1}{a_4}\left(M_1 - \frac{1}{M_1}\right)}\right]^{\frac{2\gamma_4}{(\gamma_4 - 1)}}, \tag{4}$$

$$\frac{T_2}{T_1} = \frac{1}{\alpha_1^2}\left[\frac{M_1^2}{\beta_1} - 1\right]\left[\frac{1}{\beta_1\gamma_1 M_1^2} + 1\right], \tag{5}$$

**Table I. Typical Operating Conditions of a Spectroscopic Shock Tube (Hydrogen or Helium Driven into Argon)**

| $P_4$ (atm) | $P_1$ (H$_2$ driver) (mm Hg) | $P_1$ (He driver) (mm Hg) | $M_1$ | $V_1$ mm/($\mu$sec) | $T_2$ (°K) | $T_5$ (°K) |
|---|---|---|---|---|---|---|
| 6.80 | 647 | 517 | 2 | 0.34 | 610 | 1,000 |
| 6.80 | 92.4 | 43 | 4 | 1.3 | 1723 | 3,660 |
| 6.80 | 20.7 | 5.2 | 6 | 1.9 | 3542 | 8,000 |
| 6.80 | 5.8 | 0.52 | 8 | 2.6 | 6138 | 14,200 |

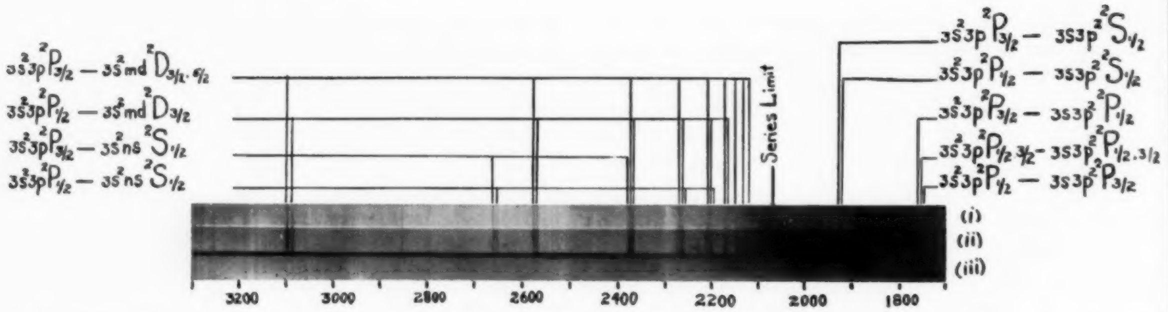

Fig. 2. Ultraviolet absorption spectrum of atomic line series in aluminum from shock-heated aluminum powder. (i) and (ii) show the effect of increased concentration and (iii) is the absorption spectrum through the shock tube section before the passage of shock wave.

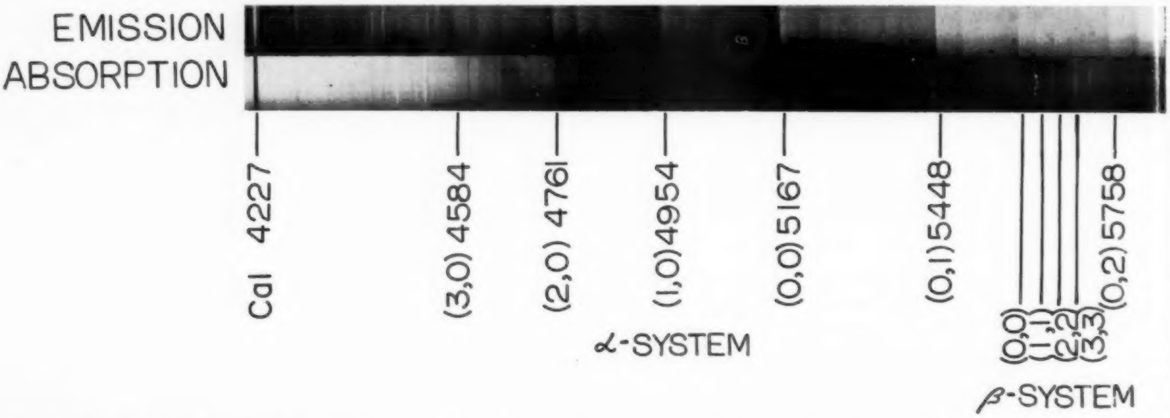

Fig. 3. Spectra of titanium oxide $\alpha$ and $\beta$ systems in emission and absorption. The spectra were obtained from shock heating of TiO$_2$

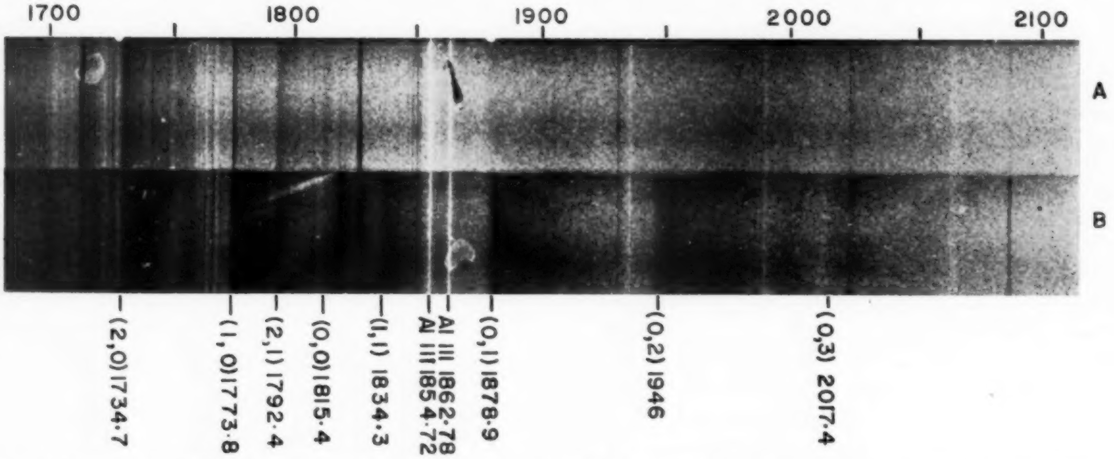

Fig. 4. Vacuum ultraviolet absorption spectrum of the BO $\gamma$ system $C^2\Pi - X^2\Sigma^+$ from shock heating of boron + 0.5% oxygen (A) and boric acid (B).

$$\frac{T_5}{T_1} = \frac{1}{\alpha_1{}^2M_1{}^2}\left[2(M_1{}^2 - 1) + \alpha_1M_1{}^2\right]\left[2(M_1{}^2 - 1) + \alpha_1\right]. \tag{6}$$

Real gas effects tend to reduce $T_2$ and $T_5$ below those predicted by Eqs. (5) and (6) by a few percent. Typical operating conditions for spectroscopic shock tubes are displayed in Table I.

## IV. Spectroscopic Results

Typical absorption and emission spectra of shock-excited powdered solids are displayed in Figs. 2–4.

**Table II. Spectra from Shock-Excited Inorganic Compounds**

| Element | Powdered material | Shock conditions | | Spectrum | | Remarks | References |
|---|---|---|---|---|---|---|---|
| | | $M_1$ | $H_2$ or He | Band systems | Lines | | |
| Al | $Al_2O_3$ | 5.2 | He | AlO ($A^2\Sigma-X^2\Sigma$) | | Very strong bands | (11) |
| | | 6.7 | He | AlO ($A^2\Sigma-X^2\Sigma$) | Al I: $3^2P^0-4^2S$ | Bands greatly weakened | |
| | | 7.5 | He | | Al I: $3^2P^0-4^2S$ | No bands | |
| | Al + H | 5.4 | He | AlH ($A^1\Pi-X^1\Sigma^+$)<br>AlO ($A^2\Sigma-X^2\Sigma$) | Al I: $3^2P^0-4^2S$, $3p^2\ ^4P$, $3^2D$<br>$4^2S-6^2P^0$ | Al pretreated by heating in flowing $H_2$ | (11, 17) |
| | Al | | He | AlH ($A^1\Pi-X^1\Sigma^+$)<br>AlO ($A^2\Sigma-X^2\Sigma$) | <br>Al I: $3^2P^0-4^2S$ | $H_2$ (15%) mixed with A<br>(0,0) and (1,1) bands only | (18) |
| | | | He | AlO ($A^2\Sigma-X^2\Sigma$) | Al I: $3^2P^0-4^2S$ | Band systems more strongly developed, lines strongly broadened and self-absorbed | |
| | | | He | AlO ($A^2\Sigma-X^2\Sigma$) | Al I: $3^2P^0-4^2S$ | AlH bands weak, AlO bands very pronounced | |
| | | 4.7 | $H_2$ | AlO ($A^2\Sigma-X^2\Sigma$)<br>AlH ($A^1\Pi-X^1\Sigma^+$) | Al I | Absorption of lines and bands. All lines of $^2D$ and $^2S$ series to the ionization limit, as well as several allowed and forbidden transitions beyond the limit (see Fig. 2) | (19) |
| | $LiAlH_4$ | 4.0 | He | AlH ($A^1\Pi-X^1\Sigma^+$)<br>AlO ($A^2\Sigma-X^2\Sigma$) | Li I: $2^2S-2^2P^0$; $2^2P^0-3^2D$, $4^2S$, $4^2D$<br>Al I: $3^2P^0-4^2S$ | Band and lines weak | (18) |
| | | 4.8 | He | AlO ($A^2\Sigma-X^2\Sigma$) | Al I: $3^2P^0-4^2S$ | AlO bands stronger, AlH bands remain weak. $O_2$ concentration less than 1 in $10^6$ | |
| | | 5.4 | He | AlO ($A^2\Sigma-X^2\Sigma$) and AlH($C^1\Sigma-A^1\Pi$) | Al I: $3^2P^0-4^2S$ | AlO bands weaker. Li lines strong and broadened | |
| | | 6.0 | He | None | Al I: $3^2P^0-4^2S$ | No bands, Li and Al lines very strong and not so broad | |
| B | B + 10% $N_2$ | 6.0 | $H_2$ | BH ($A^1\Pi-X^1\Sigma^+$)<br>BO$\beta$ ($B^2\Sigma-X^2\Sigma$) | B I | Absorption of bands and lines. Note BO$\alpha$ system outside observable wavelength range. Possible record of (1,0) and (0,0) of BN ($A^3\Pi-X^3\Pi$) | (19) |
| | B + 0.5% $O_2$<br>$H_3BO_3$ | 5.3 | $H_2$ | BO$\beta$($B^2\Sigma-X^2\Sigma$)<br>BO$\gamma$($C^2\Pi-X^2\Sigma$) | B I | Strong band absorption as well as well-developed line series (BO$\gamma$, see Fig. 4) | (19) |
| B | BN | 4 | He | $BO_2$ (fluctuation bands)<br>($B^2\Sigma_u^+-X^2\Pi_g$;<br>$A^2\Pi_u-X^2\Pi_g$) | | | (20) |
| | | 4.5 | He | $BO_2$ (fluctuation bands)<br>BO$\alpha$($A^2\Pi-X^2\Sigma^+$)<br>BH($b^3\Sigma-a^3\Pi$) | | A few lines of Na I, Ca I, II, Fe I, Cu I, Cr I, Sr I, Mg I, Pb I were present, evidently arising from impurities in the samples of BN | |
| | | 5.0 | He | CN($B^2\Sigma-X^2\Sigma$)<br>NH($A^3\Pi-X^3\Sigma$)<br>BO$\alpha$($A^2\Pi-X^2\Sigma^+$) | B I | CN(0,0) (11,11) and (12,12) observed<br>No BN spectra appeared in absorption or emission between $M_1 = 4$ and $M_1 = 6$ | |
| | | 5.5 | He | BH($B^1\Sigma-A^1\Pi$)<br>$B_2$($A^3\Sigma_u^--A^3\Sigma_g^-$)<br>NH($A^3\Pi-X^3\Sigma$) | B I | B I lines increase in intensity at higher Mach numbers | |
| | | 6.0 | He | NH($A^3\Pi-X^3\Sigma$), ($C^1\Pi-a^1\Delta$)<br>BH($B^1-A^1\Pi$)<br>$B_2$($A^3\Sigma_u^--A^3\Sigma_g^-$) | B I | Very weak BH($A^1\Pi-X^1\Sigma^+$) bands. $Q$ heads overlapped by strong BO$\alpha$ bands | |

*continued*

**Table II. Spectra from Shock-Excited Inorganic Compounds**

| | | Shock conditions | | Spectrum | | | |
|---|---|---|---|---|---|---|---|
| Element | Powdered material | $M_1$ | $H_2$ or He | Band systems | Lines | Remarks | References |
| | $H_3BO_3$ | 5 | He | $BO\alpha(A^2\Pi-X^2\Sigma)$ | | The $BO(B^2\Sigma-X^2\Sigma)$ beta bands were also probably present, but outside the range of the spectrograph used | (11) |
| | | 5.7 | He | $BO\beta(B^2\Sigma-A^2\Pi)$<br>$BO_2$ (fluctuation bands) | No B I lines observed | | |
| | | 7.5 | He | — | — | Band intensities decrease rapidly as $M_1$ increased | |
| Ba | BaO | 5.0 | He | $BaO(A^1\Sigma-X^1\Sigma)$ | Strongest lines of Ba I: $6^3P^0-6^3D$ and $5^3D-5d6p^3P^0$ multiplets | Bands also observed in absorption experiments | (11) |
| | | 5.5 | He | $BaO(A^1\Sigma-X^1\Sigma)$ | Ba I: $5^3D-4^3F^0$, $5d6p^3P^0$<br>$6^3P^0-6^3D$<br>$6^1S-6^1P^0$ | Bands weaken, lines intensify and become more copious | |
| Ba | BaO | 7.5 | He | None | Above Ba I multiplets and Ba II: $6^2P^0-6^2D, 7^2S$<br>$6^2S-6^2P^0$<br>$5^2D-6^2P^0$ | | |
| | | 3.8 | He | $BaO(A^1\Sigma-X^1\Sigma)$ | Ba I: $6^1S-6^1P_0$; $5^3D-4^3F_0$<br>Ba II: $6^2S-6^2P_0$, $6^2P^0-6^2D$ | Observed in absorption experiment | (11) |
| | $BaO_2$ | 4–6 | $H_2$ | $BaO(A^1\Sigma-X^1\Sigma)$<br>$BaO(B\rightarrow X^1\Sigma)$ | Ba I<br>Ba II | Absorption spectra studied<br>Atomic lines present during first 200 μsec | (12) |
| | | | | BaOH, $Ba_2O_2$ | Impurity lines of Ca I, Na I, Cu I, and Al I also present | Molecular bands appear after 200 μsec and reach maximum intensity at 1 msec | |
| | $BaCl_2$ | 5.0 | $H_2$ | — | Complete Ba I spectrum | Atomic absorption spectra studied. First example of "forced autoionization" in laboratory experiment | (21) |
| | | 4–6 | $H_2$ | $BaCl(D^2\Sigma-X^2\Sigma)$<br>$BaCl(E^2\Sigma-X^2\Sigma)$ | Ba I | | (12, 19) |
| | $Ba(OH)_2$ | 4–6 | $H_2$ | BaOH | | Unanalyzed vibrational bands | (12) |
| Be | BeO | 5 | He | $BeO(C^1\Sigma-X^1\Sigma)$ | | All strong Be I lines lie below 4000 Å and thus none were observed | (11) |
| | | | | $BeH(A^2\Pi-X^2\Sigma)$ | | Only the (0,0) BeH band | |
| | | 5.3 | | $BeO(C^1\Sigma-X^1\Sigma)$ | | Bands decrease in intensity with increase of $M_1$ | |
| C | AgCN | 6 | He | $CN(B^2\Sigma^+-X^2\Sigma^+)$<br>$C_2(A^3\Pi_g-X^3\Pi_u)$<br>Carbon particle continuum | Ag I lines | | (11) |
| | $K_3Fe(CN)_6$ | 6 | He | Carbon particle continuum | Fe I, K I lines | | |
| | $K_3Co(CN)_6$ | 6 | He | Carbon particle continuum | Co I, K I lines | | |
| | KCN | 6 | He | Carbon particle continuum | K I lines | | |
| | $NH_4Cl + KNO_2 + \frac{1}{20}C$ | 5.6 | He | $CN(B^2\Sigma^+-X^2\Sigma^+)$<br>$C_2(A^3\Pi_g-X^3\Pi_u)$ | K I lines | The CN violet system was most intense and negligible continuum was seen | (11,22) |
| | C | 5 | $H_2$ | $CN(B^2\Sigma^+-X^2\Sigma^+)$<br>$C_2(A^3\Pi_g-X^3\Pi_u)$ | | Both molecular systems in absorption | (19) |

*continued*

**Table II. Spectra from Shock-Excited Inorganic Compounds**

| Element | Powdered material | Shock conditions | | Spectrum | | Remarks | References |
|---|---|---|---|---|---|---|---|
| | | $M_1$ | $H_2$ or He | Band systems | Lines | | |
| Ca | CaO | 5 | He | CaOH ("CaO" orange and red systems) at 5550 Å and 6230 Å | Ca I resonance line at 4227 Å self-absorbed | The bands decrease in intensity and lines become stronger and more copious as $M_1$ increases. Ca I multiplets include $3^3D$–$5^3F^0$, $4^3F^0$, $3d4p\,^3P^0$, $3d4p\,^3D^0$, $4^1S$–$4^1P^0$; $4^3P^0$–$4p^2\ ^3P$, $4^3D$, $3^1D$–$5^1F^0$, $6^1P^0$, $4^1F^0$, $5^1P^0$, $4^1P^0$–$5^1D$, $4p^2\ ^1D$ | (11) |
| | | 5.7 | He | CaOH ("CaO" orange and red systems) at 5550 Å and 6230 Å | Ca I lines see remarks | Ca II multiplets $4^2S$–$4^2P$ | |
| | | 7.5 | He | CaOH ("CaO" orange and red systems) at 5550 Å and 6230 Å | Ca I lines see remarks | | |
| | $Ca(OH)_2$ | | $H_2$ | | | | (19) |
| | CaS | 4 | He | CaOH ("CaO" orange and red systems) at 5550 Å and 6230 Å<br>$CaF(B^2\Sigma$–$X^2\Sigma)$ | Ca I and Ca II multiplets listed in above entry | No CaS spectrum observed<br>Ca I and II lines appear in all spectra and increase in intensity with temperature | (20) |
| | | 4.5 | He | | | | |
| | | 5.0 | He | | | | |
| | | 5.5 | He | | | Bands are prominent at $M_1 = 4$–5 and decrease in intensity at higher temperatures. A few impurity lines of Na, Sr, Ba, Cu, Al were present | |
| | | 6.0 | He | | | | |
| | | 6.5 | He | | | | |
| | $CaF_2$ | 6.0 | $H_2$ | $CaF(C^2\Pi$–$X^2\Sigma^+)$<br>$CaF(D^2\Sigma$–$X^2\Sigma^+)$<br>$CaF(E^2\Sigma$–$X^2\Sigma^+)$<br>$CaF(F^2\Sigma$–$X^2\Sigma^+)$ | | All band systems observed in absorption. Several new systems of bands below λ 2500 Å were observed. These bands are probably due to CaF and have been observed in furnace absorption | (19)<br>(23) |
| Cr | $Cr_2O_3$ | 5.2 | He | $CrO(A$–$X)$ | | | (11) |
| | | 6.3 | He | $CrO(A$–$X)$ | Cr I lines of a $^5G$–$y^5H^0$, $Z^5G^0Z^5F^0$<br>$a^7S$–$Z^7P^0$; $a^5D$–$Z^5F^0$, $y^5P^0$, $Z^5P^0$, $Z^7F^0$ multiplets | | |
| | | 7.5 | He | No bands except (0,0) | Cr I lines of a $^5G$–$y^5H^0$, $Z^5G^0Z^5F^0$<br>$a^7S$–$Z^7P^c$; $a^5D$–$Z^5F^0$, $y^5P^0$, $Z^5P^0$, $Z^7F^0$ multiplets | | |
| Cu | CuO | 5 | He | $CuO(A^2\Sigma^+$–$X^2\Sigma^+)$ | | | (11) |
| | | 5.7 | | $CuO(A^2\Sigma^+$–$X^2\Sigma^+)$ | Cu I lines of $_04^2P^0$–$6^2S$, $4^2D$ $4^2S^2D$–$4^2P_0$ multiplets | | |
| | | 7.5 | He | No bands | Cu I lines of $_04^2P^0$–$6^2S$, $4^2D$ $4^2S\ ^2D$–$4^2P_0$ multiplets | | |
| | CuH | 5 | He | $CuH(A^1\Sigma^+$–$X^1\Sigma^+)$<br>$CuO(A^2\Sigma^+$–$X^2\Sigma^+)$ | Cu I lines of the $4s^2\ ^2D$–$4^2P^0$, $4^2P^0$–$4^2D$ multiplets | (0,0) band of CuO only | (11, 17) |
| | $Cu(OH)_2$ | 5 | $H_2$ | CuOH<br>$CuO(A^2\Sigma^+$–$X^2\Sigma^+)$ | | System of CuOH not analyzed | (12) |
| | Cu | 4.6 | $H_2$ | $CuH(A^1\Sigma^+$–$X^1\Sigma^+)$<br>$CuH(^1\Pi$–$X^1\Sigma\lambda 2239$ A) | Cu I | Absorption systems of bands and atomic lines. Cu I lines observed to below ionization limit | (19) |
| Fe | $Fe_2O_3$ | 5 | He | FeO(A) | | | (11) |
| | $Fe_3O_4$ | 5.52 | He | FeO(B) | Fe I lines of the following multiplets | Iron arc spectrum of Fe I lines. No bands | |
| | | 6.7 | | — | | | |

*continued*

**Table II. Spectra from Shock-Excited Inorganic Compounds**

| Element | Powdered material | Shock conditions | | Spectrum | | Remarks | References |
|---|---|---|---|---|---|---|---|
| | | $M_1$ | $H_2$ or He | Band systems | Lines | | |
| | $FeTiO_3$ | 5 | | TiO($C^3\Pi-X^3\Pi$)<br>TiO($c^1\phi-a^1\Delta$)<br>FeO(A)<br>FeO(B) | $a^5D-Z^7D^0, Z^7F_0, Z^5D^0$<br>$Z^5F^0, Z^5P^0, y^5D^0$<br>$a^5F-y^5D^0, y^5F^0, Z^3P^0, Z^5G^0$<br>$a^3H-Z^5G^0;\ a^3G-y^3F^0$<br>$Z^5P^0-e^5D$ | | |
| | FeS | 4–7 | He | No bands | Fe lines as in above entry | No FeS bands. Some solid powder continuum in red at lowest values of $M_1$ absorption | (20) |
| | $Fe(OH)_2$ | | $H_2$ | FeOH | Fe I lines | Emission | (12) |
| | $Fe(CO)_5$ | 4–8 | $H_2$ | No bands | Fe I lines | Absorption measurements of well-developed series and used for temperature determination | (19) |
| Ge | Ge metal | 5.0 | $H_2$ | GeO($A^1\Sigma^+-X^1\Sigma^+$) | Ge I series | Absorption | (19) |
| | Ge + 10% $H_2$ | 5.0 | $H_2$ | GeO($A^1\Sigma^+-X^1\Sigma^+$) | | | |
| | | | | GeH($^2\Delta(b)$ or $^2\Sigma-^2\Sigma(a)$ | Ge I | Absorption | (19) |
| Li | $Li_2O$ | 4–6 | He | No bands | Very broad Li lines | Blackbody continuum in red | (24) |
| | $Li_2O_2$ | 4–6 | He | | | | |
| Mg | MgO | 5 | He | MgO($B^1\Sigma-X^1\Sigma$) | | A band of 3860 Å probably due to the MgO ultraviolet system | (11, 1 |
| | | 6.3 | He | MgO($B^1\Sigma-X^1\Sigma$) | Mg lines of the $3^3P^0-3^3D$, $4^3S$, $3^1P^0-7^1S$, $5^1D$, $4^1D$ multiplets | | |
| | | 7.5 | He | — | Mg lines of the $3^3P^0-3^3D$, $4^3S$, $3^1P^0-7^1S$, $5^1D$, $4^1D$ multiplets | | |
| | $Mg(OH)_2$ | 4–6 | $H_2$ | MgOH, MgH, MgO | | | (12) |
| | Mg + H | | He | MgH($A^2\Pi-X^2\Sigma$) | | 15% H in argon | |
| | | | He | MgH($A^2\Pi-X^2\Sigma$) | Mg I lines of $3^3P^0-3^3D$, $4^3S$ $3^1S-3^3P^0$ multiplets | Bands stronger, lines weak | (18) |
| | | | He | MgH($A^2\Pi-X^2\Sigma$) | Mg I lines of $3^3P^0-3^3D$, $4^3S$ $3^1S-3^3P^0$ multiplets | Bands weak, lines weak | |
| | | | He | MgH($A^2\Pi-X^2\Sigma$) | Mg I lines of $3^3P^0-3^3D$, $4^3S$ $3^1S-3^3P^0$ multiplets | Bands very weak, lines weak | |
| Mn | Mn | 4–6 | $H_2$ | | Mn I | | (12) |
| | $Mn(OH)_2$ | 4–6 | $H_2$ | MnOH | Mn I | | (12) |
| Na | $Na_2O$ | 4–6 | He | | | | |
| | $Na_2O_2$ | 4–6 | He | No band systems | Very broad Na lines | Blackbody continuum in red | (24) |
| Pb | PbO | 5 | He | PbO($A-X^1\Sigma^+$)($B-X^1\Sigma^+$) | | | (11) |
| | $Pb_3O_4$ | 5.7 | He | No bands | Pb I lines of the $6p^3P-7s^3P$ and $6p^1P-7s^3P^0$ multiplets | | |
| | | 7.5 | He | — | Pb I lines of the $6p^3P-7s^3P$ and $6p^1P-7s^3P^0$ multiplets | | |
| Si | $SiO_2$ | 4–6 | He | SiO($A^1\Pi-X^1\Sigma^+$) | Si I series between 2300 and 3000 Å | Bands only appeared between 4.75 $M_1$ 5.00. Lines increase in strength with $M_1$ | (20) |
| | SiC | 4 | He | $C_2(A^3\Pi_g-X^3\Pi_u)$ | Na impurity line | | |
| | | 4.5 | He | CN($B^2\Sigma-X^2\Sigma$) | Na, Ti impurity lines | | |
| | | 5 | He | CaCl red and | Na, Ti, Ca impurity lines | | |
| | | 5.5 | He | orange (0,0) bands | Na, Ti, Ca, and Si lines | | |
| | | 6.8 | He | No bands | of the $3p^2\ ^1D-4s^3P^0$<br>CuCl impurity<br>$4s^1P^0-5p^1D$<br>$3d^3D^0-4f^3F$, $4f^3G$, $5f^3G$<br>$4p^3D-5d^3F^0$ multiplets | No SiC or $SiC_2$ bands | (20) |
| | Si + 10% $N_2$ | 6–7 | $H_2$ | SiO($A^1\Pi-X^1\Sigma^+$)<br>SiO($E-X^1\Sigma^+$)<br>SiN($B^2\Sigma^+-X^2\Sigma^+$) | Si I series | Absorption | (19) |

*continued*

**Table II. Spectra from Shock-Excited Inorganic Compounds**

| | | Shock conditions | | Spectrum | | | |
|---|---|---|---|---|---|---|---|
| Element | Powdered material | $M_1$ | $H_2$ or He | Band systems | Lines | Remarks | References |
| | Si + 10% $H_2$ | 7.0 | $H_2$ | $\mathrm{SiH}(^2\Delta-^2\Pi)$ | Si I | Absorption | (19) |
| | SiS | 4.5 | $H_2$ | $\mathrm{SiS}(D^1\Pi-X^1\Sigma^+)$ | Si I | Absorption | (19) |
| | $Si_3N_4$ | 6–7 | $H_2$ | $\mathrm{SiO}(A^1\Pi-X^1\Sigma^+)$<br>$\mathrm{SiO}(E-X^1\Sigma^+)$<br>$\mathrm{SiN}(B^2\Sigma^+-X^2\Sigma^+)$ | Si I | Absorption | (19) |
| Sr | SrO | 5 | He | SrO orange-red system (SrOH?) at 6000 Å | Self-absorbed Sr I resonance line at 4607 Å | | |
| | | 6. .3 | He | SrO orange-red system (SrOH?) at 6000 Å | Lines of the following Sr I multiplets<br>$5^3P^0-7^3S$, $5p^2\,^3P$, $5^3D$<br>$5^1S-5^1P^0, 4^1D-4^1P^0$<br>$4^3D-4d^5P^3D$ | Resonance line more strongly self-absorbed | (11) |
| | | 7.5 | He | No bands | Above lines and in addition lines of the following Sr II multiplets<br>$5^2S-5^2P^0$, $5^2P^0-6^2S$ | | |
| Ta | TaC | 4 | He | | Impurity Na line | | (20) |
| | | 4.5 | He | | Impurity lines of Na and Ca | | |
| | | 4.75 | He | | | | |
| | | 5 | He | $C_2(A^3\Pi_g-X^3\Pi_u)$ | | Bands appear over a very small temperature range | |
| | | 5.5 | He | $\mathrm{CN}(B^2\Sigma-X^2\Sigma)$ | | No bands of TaC | |
| | | 6 | He | No bands | Ta I lines of multiplets | | |
| | | 7 | He | | $a^4F-1^02^04^08^012^017^052^062^0$<br>$a^4P-10^0, 14^0$<br>$a^6D-23^028^032^0, 39^0, 53^0$<br>$3-24^0;\ 9-62^0$ | | |
| Ti | $TiO_2$ | 4.5– | He | $\mathrm{TiO}(C^3\Pi-X^3\Pi)$ | | Bands and lines observed in emission and in absorption (see Fig. 3) | (11, 19) |
| | | 5.5 | $H_2$ | $\mathrm{TiO}(c^1\phi-a^1\Delta)$<br>$\mathrm{TiO}(A^3\Sigma-X^3\Pi)$ | | | |
| | | 6.7 | He | Bands weaker | Ti I lines of the<br>$a^3F-y^3D^0, y^3F^0, Z^3F^0, Z^3G^0$<br>$a^5F-x^5D^0, w^3D^0, y^5F^0, y^5G^0$<br>$a^3G-v^3G^0$ multiplets appear | | |
| | | 7.5 | He | No bands | lines strengthen | | |
| | TiN | 4.5 | $H_2$ | New bands of TiN | Ti I | Absorption | (25) |
| | $TiCl_4$ | 5 | $H_2$ | $\mathrm{TiCl}(^4\Pi-^4\Sigma)$ | Ti I | Absorption | (19) |
| V | $V_2O_5$ | 5 | He | $\mathrm{VO}(^2\Delta-^2\Delta\ (?))$ | | Emission and absorption | (11, 19) |
| | | 7.5 | He | No bands | V I lines of $a^6D-y^6D$<br>$y^6F^0; a^4F-z^4F^0, Z^4G^0$<br>$a^4D-y^4D^0, y^4F^0, Z^4P^0$<br>multiplets appear | | |
| | | 5.0 | $H_2$ | $\mathrm{VO}(^2\Delta-^2\Delta\ (?))$ | V I | Absorption | (19) |
| W | $H_2W_4O_{13}$ | 5.5 | He | WO bands between 5851 and 3955 Å | | Bands have recently been fitted into a Deslandres array | (11) |
| | | 7.5 | He | No bands | Lines of the<br>$d^5s\,^7S-d^4sp\,^7D^0, d^4sp\,^7P^0$<br>$d^4s^2\,^5D-d^4sp\,^5P^0, d^4sp\,^7D^0$<br>multiplets of W I appear | | |
| Zn | ZnO | 4–6 | $H_2$ | Red degraded band at 3435Å | Zn I | Absorption | (12) |
| | Zn | 4–6 | $H_2$ | — | Zn I | Emission only | (12) |
| | $Zn(OH)_2$ | 4–6 | $H_2$ | $\mathrm{ZnH}(A^2\Pi-X^2\Sigma^+)$ | Zn I | Emission only | (12) |

*continued*

**Table II. Spectra from Shock-Excited Inorganic Compounds**

| Element | Powdered material | Shock conditions | | Spectrum | | Remarks | References |
|---|---|---|---|---|---|---|---|
| | | $M_1$ | $H_2$ or He | Band systems | Lines | | |
| Zr | ZrO | 5.3 | $H_2$ | ZrO$\gamma(A^3\phi-X^3\Delta)$<br>ZrO$\beta(B^3\Pi-X^3\Delta)$<br>ZrO$\alpha(C^3\Delta-X^3\Delta)$<br>ZrO$(b^1\Sigma-a^1\Sigma)$<br>ZrO 3507 Å system $[^3\Delta-^3\Pi(?)]$<br>ZrO 3060 Å system $[^3\Pi-^3(?)\Pi]$ | Zr I | All systems observed in absorption | (19) |
| | ZrO | 4-5.5 | He | ZrO$\gamma(A^3\phi-X^3\Delta)$<br>ZrO$\beta(B^3\Pi-X^3\Delta)$<br>ZrO$\alpha(C^3\Delta-X^3\Delta)$ | Many lines of Zr I, most predominant being the multiplets $a^3F-Z^3F^0$, $b^3F-w^3G^0$, $a^5F-y^5G^0$ | All systems in emission. 5% oxygen added to the low pressure section suppressed the lines, but not the bands. 10% oxygen suppressed both bands and lines | (26) |
| | | 6–8 | He | | Many lines of Zr I, most predominant being the multiplets $a^3F-Z^3F^0$, $b^3F-w^3G^0$, $a^5F-y^5G^0$ | | |

Figure 2 shows, in absorption, the ultraviolet line series of Al arising from shock excitation of powdered Al. Figure 3 exhibits, in emission and absorption, the visible band systems of TiO arising from shock-excited powdered $TiO_2$. Figure 4 shows, in absorption, the vacuum ultraviolet BO system arising from shock excitation of B in $O_2$ and of $H_3BO_3$.

Spectroscopic observations have been made on an extensive range of inorganic oxides (many of them are of astrophysical interest), sulfides, nitrides, carbides, hydrides, pure metals with adsorbed surface gases, and pure metals in Ar–H mixtures. Organic compounds which have been studied are discussed below. Emission and absorption techniques have been used. The results of this work are summarized in Table II.

Table II is arranged alphabetically by element, each compound of which has a separate entry as powdered material. The shock conditions are specified by $M_1$ and the driver gas ($H_2$ or He). The emission or absorption spectra are specified at each excitation condition by band systems and lines observed. For economy of space, no detailed list is made in the table of which bands of a system or which lines of a multiplet were observed. In general, the strongest features which might be expected from a thermal excitation standpoint appear. Bands on the primary Condon parabolae and strongest lines consistent with $T_2$ and $T_5$ of the quoted multiplets are observed. References cited in the table are mostly to the unpublished studies from which this table has been constructed. Some of the reports cited give detailed wavelength lists. Wavelengths are also available on request from the respective authors.

One further class of inorganic compounds which has been studied involves a number of powdered meteorite samples whose emission spectra were compared with those of meteors taken in flight.[8] This work has been published elsewhere.[9] There was excellent agreement, in shock-excited spectra of the meteorite specimens studied, with atomic features reported in meteor spectra. This agreement, though not unexpected, is interesting when it is recalled that meteor spectra (from *periodic* meteors) arise from ablation from small fragile porous solids and the upper atmospheres. On the other hand, our specimens of *sporadic* meteor were heavy and iron–nickel containing. Under none of the excitation conditions employed were molecular features observed.

In striking contrast to the results of shock excitation of inorganic solids are those obtained from the shock excitation of three aromatic organic compounds benzene, naphthalene, and anthracene.[10] The results of this are summarized in Table III, in which it is clear that even at the highest temperatures attainable in our shock tube, no atomic features (other than the familiar Na and Ca impurities) appeared. The major features were $C_2$, CN, and CH together with a carbon particle continuum.

## V. Discussion

The change from molecular to atomic spectra with increasing temperature or shock Mach of Table II suggests a general thermal excitation mechanism. This is consistent with the intensity distribution of each spectrum.

Details of specific mechanisms of excitation of the spectra resulting from the immersion of the powder particle in the hot gas behind the shock wave are not yet clear. It is not yet known, for example, whether the surface of the powder particle is evaporated as a molecular vapor which then dissociates into the species which radiate after thermal excitation by collisions with the heavy gas in the shock tube, or whether the evaporated material leaves the particle surface in atomic rather than molecular form and then, if the local environment is at low enough temperature, recombines into the thermally maintained radiating molecular species.

The only experimental information on this point is from time-resolved spectra in emission and absorption.[11,12] These always show atomic features for the first microsecond or so after passage of the shock wave. In the cooler gases, at lower values of $M_1$, the atomic features disappear after a few microseconds when molecular features appear. At higher values of $M_1$, in the hotter gases, the atomic features remain throughout the spectra which are either entirely atomic or mixed atomic and molecular. This is not considered to be conclusive evidence for an *atomic* ablation mechanism, although it is consistent with other physical changes which occur on the surfaces of the shock-excited powdered solids.[13] Ablation studies made on shock-excited particles are an aid in determining the heat transfer mechanisms at the surface of the particles which result in the evaporation of the vapor.[14] Research is now under way at the University of Western Ontario on the basic physical processes which occur in the shock-wave powder particle interaction.

There appears to be a striking difference between the effect of the shock wave upon inorganic solids which have high-temperature melting points and organic materials which have much lower melting points. It is doubtful if the same evaporation mechanism is operative in both cases. It seems more probable (in view of the much lower melting temperatures of organic compounds) that the shock treatment causes evaporation of a molecular vapor which is then pyrolyzed to carbon. Possibly by Porter's acetylene mechanism[15] confirmed by Greene *et al.*[16] for simple hydrocarbon vapors at higher temperatures, reactions between the carbon vapor and other gases (nitrogen and hydrogen) present in the tube following pyrolysis explain, qualitatively at least, the presence of CH and CN spectra. Spectra of atomic carbon lines were not observed because such lines do not lie within the spectral range of our instruments. Experiments are planned to look for C I lines in absorption in the vacuum ultraviolet.

Perhaps the most obvious conclusion which may be drawn from the results of this paper is that the shock tube is a remarkably simple, spectroscopic source for excitation of atomic and molecular spectra of astrophysical interest which are difficult to excite in more conventional ways. In particular the flash absorption technique when used with the shock tube is extremely powerful in elucidating the presence of active species and immediately suggests that the shock tube is an equally powerful tool for the measurement of oscillator strengths of important molecular bands and atomic lines.

**Table III. Spectra from Shock-Excited Organic Aromatic Compounds**

| | Benzene 4900–8440°K | | | Naphthalene 3890–13,000°K | | | Anthracene 3630–12,020°K | | |
|---|---|---|---|---|---|---|---|---|---|
| | Temp. of appearance | Temp. of maximum intensity | Comments | Temp. of appearance | Temp. of maximum intensity | Comments | Temp. of appearance | Temp. of maximum intensity | Comments |
| Atomic impurities (Na, Ca) | 4900° | 6990° | Present at lowest temp. Not present at 8440° | 3890° | 6,870° | Not present at 13,000° | — | — | — |
| C-particle continuum | — | — | Benzene not in powder form | 3890° | 4,800° | Reaches low value at 6900°, remains until 13,000° | — | — | Reaches low value at 6350° and remains constant to 12,020° |
| $C_2$ Swan bands | 4900° | 6990° | Weak at 8440° | 4800° | 10,250° | Constant to 13,000° | 5950° | 6350° | Weak at 12,020° |
| CN violet bands | 4900° (weak) | 6990° | Not present at 8440° | 6080° | ? | Gradual increase to 13,000° | 4970° | 5950° | Absent above 8600° |
| CH 4315 Å band | 6990° | ? | Present at 8440° | 6870° | ? | Gradual increase to 13,000° | 5950° | 6350° | Absent above 8600° |

We wish to thank A. T. McGregor, M. D. Watson, and D. C. Tyte, who have allowed us to mention results of their unpublished work in this paper, and also other colleagues at Imperial College and University of Western Ontario for many valuable discussions.

This work has been supported in part by research grants to the University of Western Ontario by the Air Force Office of Scientific Research, the National Research Council of Canada, and the Ontario Research Foundation and by contracts from the Department of Defence Production of Canada. It has also been supported in part by contracts with Harvard University from the National Aeronautics and Space Administration, the Office of Naval Research, and the National Science Foundation.

## References

1. J. N. Bradley, *Shock Waves in Chemistry and Physics* (Methuen, London, 1962).
2. M. Lapp, J. Quant. Spectry. & Radiative Transfer **1**, 30 (1961).
3. J. Keck, J. Camm, B. Kivel, and T. Wentink, Jr., Ann. Phys. **7**, 1 (1959).
4. R. W. Nicholls and W. H. Parkinson, J. Chem. Phys. **26**, 423 (1957).
5. R. S. Berry, C. W. Reimann, and G. N. Spokes, J. Chem. Phys. **37**, 2278 (1962).
6. J. K. Wright, *Shock Tubes* (Methuen, London, 1961).
7. A. C. Kolb and H. R. Griem, *Atomic and Molecular Processes*, ed. D. R. Bates (Academic Press, New York, 1962), Chap. 5.
8. A. F. Cook and P. M. Millman, Astrophys. J. **121**, 250 (1955).
9. R. W. Nicholls, M. D. Watson, and W. H. Parkinson, J. Roy. Astron. Soc. Can. **53**, 223 (1959).
10. R. W. Nicholls and M. D. Watson, Nature **188**, 568 (1960).
11. W. H. Parkinson and R. W. Nicholls, Shock Excitation of Powdered Solids, Scientific Report No. 1, Contract AF 19(604)-4560 (1959).
12. W. H. Parkinson, Proc. Phys. Soc. (London) **78**, 705 (1961).
13. R. W. Nicholls and W. H. Parkinson, Can. J. Phys. **26**, 423 (1957).
14. R. W. Nicholls, W. H. Parkinson, and H. Van der Laan, J. Appl. Phys. **30**, 797 (1959).
15. G. Porter, *Fourth International Symposium on Combustion* (Reinhold, New York, 1952), p. 248.
16. E. F. Greene, R. L. Taylor, and W. L. Patterson, Jr., J. Phys. Chem. **62**, 238 (1958).
17. W. H. Parkinson and R. W. Nicholls, Spectroscopic Temperature and Intensity Measurements in a Shock Tube, Scientific Report No. 3, Contract AF 19(604)-4560 (1959).
18. A. T. McGregor (unpublished work).
19. W. H. Parkinson and E. M. Reeves (unpublished work).
20. A. T. McGregor, M.Sc. Thesis, University of Western Ontario (1962).
21. W. R. S. Garton, W. H. Parkinson, and E. M. Reeves, Proc. Phys. Soc. (London) **80**, 860 (1962).
22. W. H. Parkinson and R. W. Nicholls, Can. J. Phys. **38**, 715 (1960).
23. E. M. Reeves and A. M. Bass (private communication).
24. G. R. Hébert, Ph.D. Thesis, University of Western Ontario (1960).
25. W. H. Parkinson and E. M. Reeves, Can. J. Phys. (in press, 1963).
26. A. T. McGregor and D. C. Tyte (unpublished work).

---

T. P. Vogel *Westinghouse* (left), C. Koester *American Optical*, and David S. Grey *Lincoln Laboratory* during an OSA Local Sections Meeting in Florida.

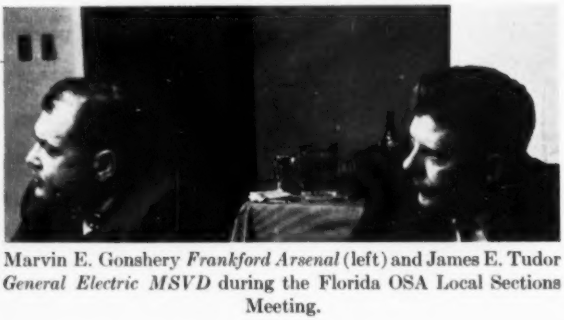

Marvin E. Gonshery *Frankford Arsenal* (left) and James E. Tudor *General Electric MSVD* during the Florida OSA Local Sections Meeting.

Geoffrey Harvey *Itek* (left) and Martin Rome, Secretary of the OSA Southwestern Conn. Section.

*photos D. L. MacAdam*

# An Atomic Absorption Spectrophotometer

Herbert L. Kahn and Walter Slavin

A double-beam, single-detector, time-sharing spectrophotometer has been designed with optimum parameters for the atomic absorption technique. The monochromator is a dual-grating, high-dispersion, Ebert–Fastie type. The major requirements of an atomic absorption spectrophotometer are stability, a wide range of slit-widths, and minimum sensitivity to emission from the flame. Many of the traditional requirements of an ultraviolet spectrophotometer can be relaxed. Ordinate scale expansion makes it possible to achieve lower detectability limits. With the present design, it has been possible to measure concentrations of less than 0.1 ppm of copper, cadmium, and chromium with coefficients of variation of less than 10%.

## Introduction

The principle of atomic absorption and its application to the analysis of metals was described in 1955 by Walsh[1] and by Alkemade and Milatz.[2] Since then, the subject has been extensively reviewed in the literature.[3–5] Briefly stated, a sample is converted into an atomic vapor, usually by a flame, and irradiated by the light from a source whose emission lines are those of the metal being sought. The absorption of the light by the vaporized sample is related to the concentration of the desired metal in it. While the principles of atomic absorption theroretically hold true for all elements, the application of the method to date has been limited mainly to metals whose resonance lines lie in the ultraviolet and visible regions of the spectrum.

The rather simple nature of the instrumentation required for basic work in atomic absorption has permitted the gathering of a great deal of data with accessories built onto equipment originally designed for other uses.[6,7] Suitable atomic absorption sources, such as hollow-cathode and discharge lamps, have long been available as wavelength references. A variety of monochromators exist, each of them adequate to the task for at least some metals. The photodetector and electronics can readily be assembled from available materials.

However, the steadily swelling number of applications has gradually made apparent a need for instrumentation that is more precise, more versatile, faster, and more convenient to use than the improvised apparatus utilized in the past. Moreover, in the early atomic absorption work the instability and noisiness of the flame were the limiting factors in the precision of the technique. Recent advances in the design of sampling flames[8] have now made these far quieter and more stable than was initially the case. As a result, the limitations of simple single-beam apparatus have become evident. In other words, a requirement has arisen for an instrument designed specifically for atomic absorption spectrophotometry.

This article describes such an instrument, designated Model 303, and the results obtained with it.

## General Requirements

The basic requirements for an instrument intended to achieve the best possible results in atomic absorption analysis can be defined as follows:

1. Stability is clearly one of the most important criteria, since one of the greatest benefits of atomic absorption is the precision of the results that can be obtained. Much can be done toward this end by very careful regulation of the electronics associated with the source, photodetector, and measuring system. However, most sources of potential instability can be eliminated by the extension to atomic absorption of the double-beam principle which is now standard in uv and ir spectroscopy. In such a system, the signal strength of the beam passing through the sampling flame is ratioed to the signal strength of a similar beam that bypasses the flame.

2. The resonance lines of many important metals, such as sodium, potassium, calcium, magnesium, and copper, lie well apart from other emission lines of the

---

The authors are with the Perkin-Elmer Corporation, Norwalk, Connecticut.

Received 4 February 1963.

Part of this material was presented at the Pittsburgh Conference on Analytical Chemistry, March 1963.

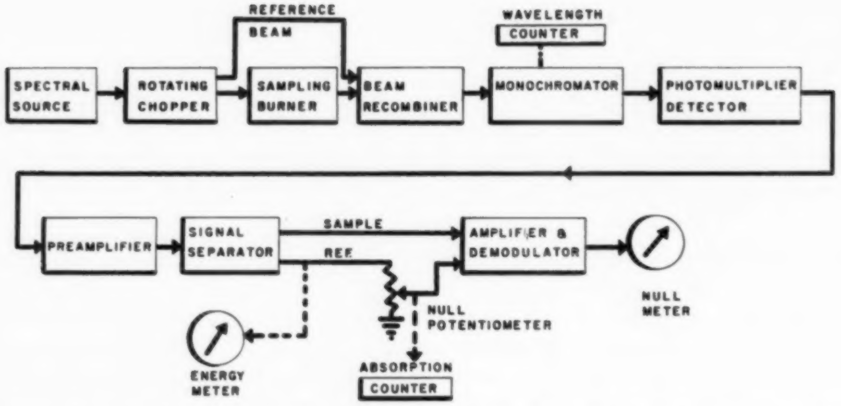
REFERENCE BEAM
WAVELENGTH COUNTER
SPECTRAL SOURCE
ROTATING CHOPPER
SAMPLING BURNER
BEAM RECOMBINER
MONOCHROMATOR
PHOTOMULTIPLIER DETECTOR
PREAMPLIFIER
SIGNAL SEPARATOR
SAMPLE
REF
AMPLIFIER & DEMODULATOR
NULL POTENTIOMETER
NULL METER
ENERGY METER
ABSORPTION COUNTER

Fig. 1. Block diagram of the instrument. Emission from the line source is split into sample and reference beams, then recombined and passed through monochromator. Signal from photodetector is amplified and fed into circuitry which produces a manual electronic null.

same metals. However, there is another group of metals, including iron and nickel, whose spectra are complex and whose resonance lines are closely surrounded by other spectral lines which must be excluded. The monochromator must therefore be a high-dispersion unit, in order to analyze for the latter group satisfactorily, but must have a capability of wide slits in order to take maximum advantage of the characteristics of the former group. With the ready availability of large, closely ruled diffraction grating replicas, these criteria are not difficult to satisfy.

3. Emission from the flame, both from the flame itself and from the excited atoms that may be within it, must not be allowed to affect the photometry. This is readily accomplished by chopping the light from the source, while leaving the flame light unchopped, and making the detector electronics insensitive to unchopped signals.

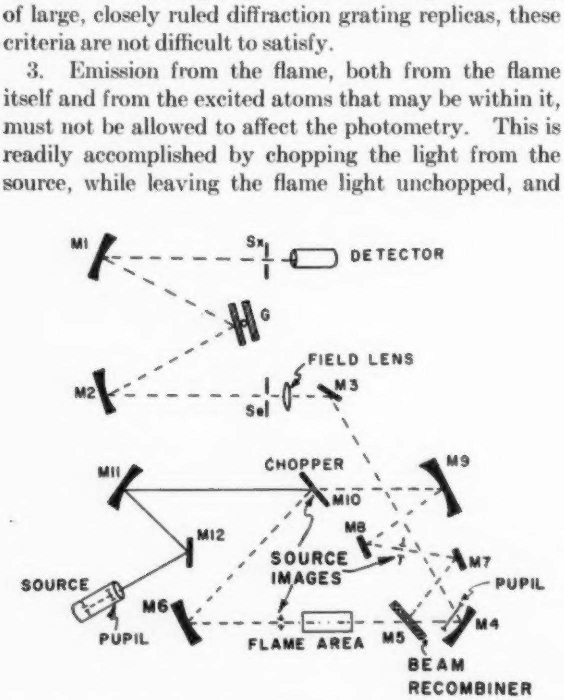
MI
Sx
DETECTOR
G
FIELD LENS
M2
Se
M3
MII
CHOPPER
M9
M10
M12
M8
SOURCE IMAGES
M7
SOURCE
PUPIL
M6
M4
PUPIL
FLAME AREA
M5
BEAM RECOMBINER

Fig. 2. Optical schematic. M10 is a rotating sector mirror. M5 is semitransparent beam recombiner. Monochromator is dual-grating Ebert-Fastie.

4. Many of the design requirements for conventional absorption spectrophotometry may be relaxed for atomic absorption. Since narrow spectral lines of the source are being measured, the presence in the monochromator of stray light is much less important. Since no 100% line must be drawn over a range of wavelengths, there is little need to equalize the path length of each beam. Because the resonance line for each metal can be "tuned in", there is not the need for wavelength accuracy that exists in the more elaborate spectrophotometers. All these normal criteria can therefore be traded for compactness, simplicity of operation, and reduced complexity.

5. Ordinate scale expansion is necessary in order to take advantage of the stability inherent in the technique. With its aid, the readability of the results can be improved, and the limits of detectability can be extended far beyond the limits established by the commonly used definition of sensitivity (concentration of sample producing 1% absorption).

## Instrument System

The instrument system is quite simple, as shown in the block diagram of Fig. 1 and schematically in Fig. 2. The emission from the source, which is usually a hollow-cathode lamp but can be a spectral discharge lamp, is split into two beams by a rotating sector mirror. One beam is directed through the sampling flame, while the other bypasses it. The two beams, after being recombined by a semitransparent mirror, pass through the monochromator to a photomultiplier detector. The detector output goes to a conventional preamplifier, after which the signal is separated into sample and reference channels by a vibrating-reed chopper.

The reference voltage is then attenuated by a slidewire and recombined with the sample voltage, in such a way that the difference is taken between them. This difference voltage is amplified, rectified, and fed to a microammeter. The operator turns the slidewire until the meter reads a null. A counter geared directly to the slidewire is made to read out in percent absorption. Alternatively, this nulling process can be accomplished automatically, by the use of a servomotor to drive the slidewire.

## Burner System

It is advantageous for the sampling flame to be long and narrow, in order to provide maximum path length. The flame for this instrument emerges from the burner[8] through a slit 10 cm long and about 1.6 mm wide. The liquid sample is aspirated into an atomizer, where it is mixed with the air required to support combustion. In the mixing chamber that follows, the air-sample mixture is mixed with the fuel, most often acetylene, and is then passed through a flow spoiler to render it turbulent before being forced into the burner head. There is provision for the admission of additional air into the mixing chamber, to stiffen the flame and provide greater stability.

While it is now possible to achieve excellent results for a large variety of metals using a flame as a sampling device, the flame nevertheless poses limitations in other ways. Since it uses oxygen, there is no possibility of purging the instrument in order to reach resonance lines in the far ultraviolet. Since most fuels contain carbon, it is difficult or impossible to analyze for this important element. As a result, a great deal of work is being done with the goal of eliminating the flame.[9–11]

## Photometer

The intent of the photometer design was to provide a large sampling space, in order to accommodate other sampling devices that might eventually become feasible. It proved possible to achieve a sampling space 23 cm long and 10 cm deep, while keeping the size of the optics within manageable dimensions.

Mirror M11 is a toroid which images the source onto M10, the rotating sector mirror. M10, shown in Fig. 3, rotates at a synchronous speed of 1800 rpm, giving a chopping frequency of 60 cps. The sample beam is reflected from the chopper. Toroid M6 reimages the source near the left end of the flame area. This image is about 30% smaller than the source itself, which is beneficial for two reasons. First, the best sensitivity is obtained by causing as much of the beam as possible to be intercepted by the maximum length of the flame. Second, for some metals such as calcium, a relatively small portion of the flame height is effective.

A narrow beam through the sample space can be achieved by placing a source image near one end and a pupil image near the other. In this design, the pupil is imaged on toroid M4.

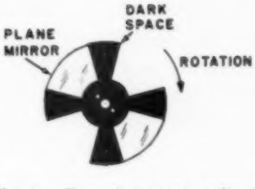

Fig. 3. Rotating sector mirror.

The reference beam is transmitted by the chopper and falls onto toroid M9, which is identical to M6. To conserve space, the reference beam is reflected from plane mirrors M8 and M7 before reaching the beam recombiner M5. M5 is a polka-dot mirror, with aluminum dots 1 mm in diameter evaporated on a thin fused-silica substrate to cover 50% of the surface. After recombination, the beam travels to toroid M4, which focuses it via plane mirror M3 onto the entrance slit of the monochromator. The magnification of M4 is such that the image on the slit is approximately equal in size to the source.

## Monochromator

For reasons previously given, the monochromator must have high dispersion over a wide wavelength region, and the possibility of wide slits. The commercial availability of very finely ruled replica gratings makes them an ideal choice for these requirements. The simplicity of the Ebert design, as described by Fastie[12] suggests its use.

The wavelength range extends from 8521 Å, the resonance wavelength of cesium, to the ultraviolet limit set by atmospheric absorption. It is covered by two Perkin-Elmer gratings, one of 1440 lines/mm blazed at 6000 Å, and the other of 2880 lines/mm blazed at 2100 Å. With a crossover at 4200 Å, the theoretical grating efficiency consistently exceeds 45%. The monochromator has a focal length of 400 mm, giving a reciprocal dispersion of 13 Å/mm in the visible range and 6.5 Å/mm in the ultraviolet. The *f* ratio is approximately 9.

With this monochromator, it is possible to use remarkably simple slit configurations. The slit-widths are variable between 0.03 and 10 mm. The slit height, dictated by the source dimensions, is 10 mm. The symmetry of the Ebert system compensates automatically for coma, leaving only astigmatic aberrations. In theory, the slits should be curved around the central axis of the monochromator, but with the relatively low slit height and the lack of need for the ultimate resolution, little is lost by using straight vertical slits.

The slits are moved by means of a simple rack-and-pinion arrangement. Each pair of jaws moves symmetrically about its centerline.

To provide maximum stability for the optics on a sheet metal base, the base is buttressed in a conventional "X" configuration. This system of ribs gives great stability per pound of metal. The height of the burner-atomizer combination and associated supports is approximately 30 cm above the table-top, automatically requiring a deep base which can be made very stable, and also providing space for the electronics underneath the optical system.

## Electronics

The electronics are readily divisible into three subsystems: detector and preamplifier, signal separator and readout, and power supplies. There is a general requirement of the electronics in spectrophotometers that also applies here: that the electronics place no limitation on the performance of the instrument. Since the sampling procedures and energy conditions are basically optical in nature, the electronics cannot actually enhance the photometric performance; properly designed, they can only refrain from degrading it. However, the requisite stability and versatility that this implies is not always easily achieved.

The detector is an eleven-stage end-window photomultiplier with an S10 cathode deposited on a window made of ultraviolet-transparent glass. This glass has transmission from the near infrared to about 1950 Å, where atmospheric oxygen begins to limit performance. When flameless sampling devices are developed, permitting purging of the optical path, this tube can be replaced with one that is identical except for having a fused silica window. S10 has good response in the far uv, while its output in the 7000 Å region is considerably better than that of the more common S11 cathode. The uniformity of cathode output that may be expected from this type of tube,[13] plus the fact that no wavelength scanning is required, make it possible to place the multiplier face directly at the exit slit of the monochromator.

## Preamplifier

A typical waveform from the photomultiplier is sketched in Fig. 4. The light is chopped at a 60-cps frequency, with dark spaces of 60 electrical degrees separating reference and sample beams. The dark spaces serve two functions: they establish a zero light level to which the beam intensities can be compared, and also furnish a neutral space during which the electronics that must separate the signals can function. The preamplifier must have a frequency response that does not degrade this waveform, but minimizes amplification of the high-frequency noise occurring in the detector. An amplifier which retains 70% of its gain at 0.5 and 700 cps is adequate. The photomultiplier load resistance is 1 MΩ, high enough to achieve the maximum signal-to-noise ratio of which the detector is capable, but not so high as to introduce pickup problems.

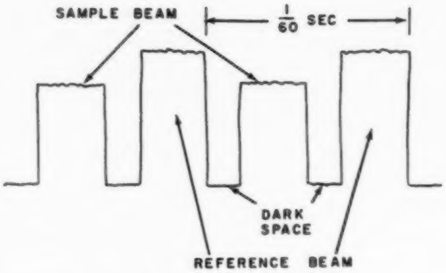

Fig. 4. Waveform of signal voltage. The same waveform appears at the detector output, preamplifier output, and at the input to first demodulator.

## Power Supplies

Power must be supplied to three separate functions: the electronics, the photomultiplier, and the hollow-cathode lamps. The electronics supply is regulated against line and load changes in a conventional manner. The hollow-cathode lamps require direct current, with starting voltages up to 350 V and running voltages of the order of 100 V. Different lamps have different current ratings, and individual lamps of the same metal may find their best operating points at currents differing substantially from each other. A supply is therefore required in which the current can be varied by an operator without the possibility of exceeding ratings. A simplified sketch of the circuit appears in Fig. 5. The lamp is plugged into the outlet giving its rated current at a maximum, while actual current is controlled by varying the bias on the tube in series with the output. The high resistor $R_B$ bypassing the tube ensures that the lamp will start regardless of the bias setting.

The photomultiplier requires a low-current negative voltage which varies between 300 and 1200 V depending on instrumental factors. The gain of the detector (volts out/lumens in) changes very greatly with changes in the detector supply voltage, so that the voltage control on the detector supply is the only gain control needed on the instrument. The supply must be well regulated against unwanted voltage changes. Power is provided by rectifying the output from a high-voltage oscillator operating at about 3 kc/sec. This has two advantages compared to a 60-cps supply: the filtering components are quite small, and any ripple does not affect the photometric accuracy, as it would if it had a 60- or 120-cps frequency.

## Signal Separator

The preamplifier output is the signal of Fig. 4, which must then be separated into reference and sample channels. The essential circuit and resultant waveforms are shown in Fig. 6. A vibrating-reed switch driven at line-frequency short circuits first one channel and then the other to ground. The reed is phased so that the switchover occurs during the dark portion of the signal. The output waveforms are shown in Fig. 6(b). The impedance of the capacitors at 60 cps is large compared to the impedance of the source, which minimizes cross-talk between the two channels. The outputs of the capacitors C1 and C2 go to separate cathode followers, amplifiers of unity gain which isolate the output from the input.

In order to maintain stability in the electronics of a doublebeam system, it is important to separate the channels for as short a path as possible, to undertake the very minimum of amplification when the beams are separated, and preferably not to attempt frequency conversion, such as a change from ac to dc. Any extraneous operation on the signals as they are separated adds to the likelihood that their relative intensities will change in unsought ways. This conservative philosophy unfortunately eliminates one attractive possibility, for if the two signals are converted separately to dc and then back to ac, it is far simpler to introduce long time constants to damp out noise, than it is to do the same thing after the signals have been recombined. However, in a manual-null system the difficulty is not insurmountable.

While the signals are separated, a nulling slidewire across the reference beam signal, with an attached digital counter, serves as the error-correcting device. For any absorption value, the nulling slidewire is turned to equalize the sample and reference signal outputs. The two signals are then immediately recombined, and look again like the waveform of Fig. 4.

Now, the nulling system must act on the 60-cps portion of this waveform. Stated another way, the interest now lies in the difference between the heights of the two flat-topped waves. If one proposes to measure per cent absorption to 0.1%, one must be able to see one part of 60-cps signal in the presence of 1000 parts of extraneous voltage. This extraneous voltage is made up of frequencies that are multiples of 60 cps, such as 120, 180, and 240 cps. It is best to eliminate these frequencies as early as possible. The signal is therefore fed to a synchronous rectifier, a type of demodulator whose output is a direct voltage, the magnitude and polarity of which are proportional only to the magnitude and phase of the 60-cps signal. In the output, the higher harmonic frequencies appear only as hash, with no dc contribution, and can easily be filtered out.

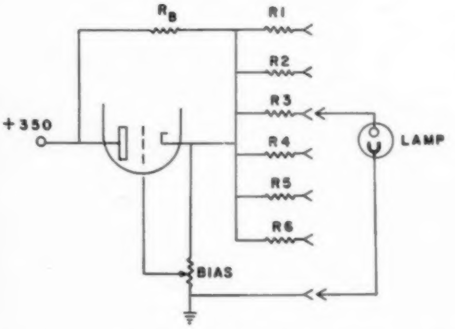

Fig. 5. Functional diagram of hollow-cathode lamp supply. This supplies continuously variable direct current to the lamp, up to its rating limit.

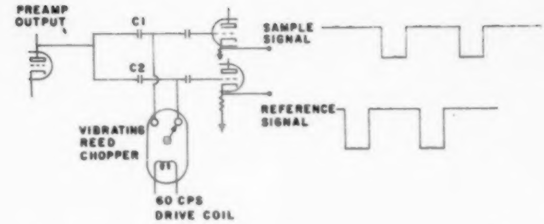

Fig. 6. Signal separator. Line-driven vibrating-reed switch shorts two channels alternately to ground, producing waveforms at right.

This direct voltage is filtered and then converted back to ac, amplified, again rectified synchronously, and measured with a microammeter. The operator turns the nulling slidewire until the meter reads zero.

## Scale Expansion and Response Control

With this nulling system, it is very easy to achieve scale expansion, and not difficult to produce increased time constants. In atomic absorption it is usually necessary to expand scale only at very low absorptions, to increase readability and therefore sensitivity. The simple circuit of Fig. 8 will accomplish ten times expansion. The nulling slidewire is made to travel over its full range to cover one-tenth the voltage that it would without expansion. In order to keep the gain constant, the gain of the amplifier following the first synchronous rectifier is increased correspondingly.

During a noisy analysis, it is often desirable to reduce noise even at the cost of some speed and convenience of operation. In a manual system, it is possible to achieve this by increasing the dc filtering capacitor C3 in Fig. 7 almost without limit. When the nulling slidewire is servo-driven, there are sharp limitations on the additional filtering possible, for the capacitor C3 is within the servo loop, and increasing the delay it causes would make the servo first overshoot and eventually even oscillate. However, the human operator represents a servomotor of almost infinitely variable gear ratio, who can adjust to any speed reduction required of him.

## Performance

The limiting sensitivity that is generally reported for the atomic absorption method[3-5] represents the con-

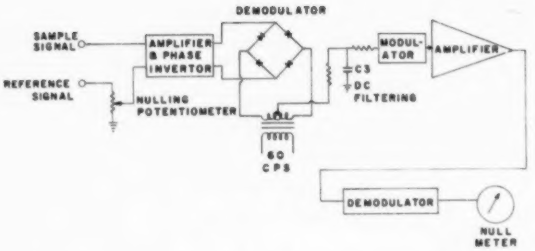

Fig. 7. Null balance circuit. Difference between sample and reference signals is amplified, demodulated, filtered, modulated, amplified, again demodulated and fed to a null meter. Operator adjusts nulling potentiometer until meter reads zero.

centration of a metal that will produce 1% absorption in the flame. The only virtue of this definition is that it is simple to measure and report. Analytically, a far more important quantity is the minimum concentration of metal that can be measured with useful precision, and this is dependent upon the signal-to-noise ratio for the particular analysis. For many metals this is so favorable that, with appropriate scale expansion, concentrations absorbing far less than 1% can be determined with considerable precision.

A number of experiments were performed on different elements, to determine instrumental precision. When the metal concentration was in an optimum analytical range, the coefficient of variation was generally of the order of 1%. With the use of 10 times scale expansion, solutions containing 0.05 ppm of copper, 0.1 ppm of cadmium, and 0.1 ppm of chromium yielded coefficients of variation between 5 and 10%. Figure 9 shows a small section of a recorder trace of 1 ppm of manganese, indicating that the noise level is not detectable when no scale expansion is used. The recorder trace was made by means of an accessory which will be described in detail in another paper. The sample and reference voltages are fed into an electronic circuit, where their ratio is taken without the requirement of a servo system. This ratio appears as an alternating voltage, which is rectified, filtered, and fed into any laboratory recorder.

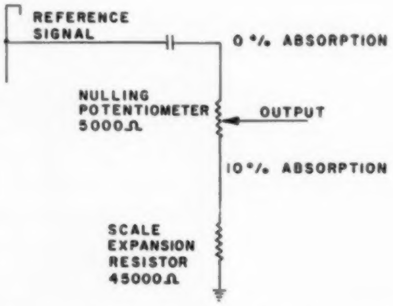

Fig. 8. Ten times scale expansion. Potentiometer covers its full range across one tenth of reference channel voltage.

The spectral range of Model 303 is sufficient to permit analysis of cesium at 8521 Å, and that of metals in the far ultraviolet, up to the point that absorption by atmospheric oxygen becomes the limitation. Cesium and zinc, whose resonance line is at 2138 Å, can be determined with a noise level of less than 0.1%. It is therefore now possible to measure the concentrations of such metals as copper, chromium, manganese, zinc, and cadmium at their natural levels in biological materials. Application of this instrument to this and other analytical problems will be reported in other journals.

The authors wish to express their thanks to J. Cohen for the ingenuity with which he produced the mechanical design. K. J. Miklus did much of the work on the optics and devised many clever adjustments and tests. Many good ideas were contributed by E. O'Neil, C. Chedester, J. Owen, and R. Meena, while D. C. Manning and S. Sprague performed the applications studies.

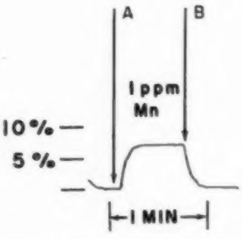

Fig. 9. Recorder trace of 1-ppm manganese without scale expansion. Sample was inserted at time *A*, removed at *B*.

## References

1. A. Walsh, Spectrochim. Acta **7**, 108 (1955).
2. C. T. J. Alkemade and J. M. W. Milatz, J. Opt. Soc. Am. **45**, 583 (1955).
3. A. Walsh, in *Advances in Spectroscopy*, H. W. Thompson, ed. (Interscience, New York, 1961), Vol. II.
4. J. B. Willis, in *Methods of Biochemical Analysis* (Interscience, New York, 1962), Vol. XI.
5. H. L. Kahn and W. Slavin, Intern. Sci. and Tech., November, 1962.
6. G. F. Box and A. Walsh, Spectrochim. Acta **16**, 255 (1960).
7. M. W. Leen and J. G. Atwood, Pittsburgh Conference, March 1961.
8. W. Slavin, Perkin-Elmer Atomic Absorption Newsletter No. 10, February, 1963.
9. B. V. L'vov, Spectrochim. Acta **17**, 761 (1961).
10. B. M. Gatehouse and A. Walsh, Spectrochim. Acta **16**, 602 (1960).
11. W. Slavin and D. C. Manning, Anal. Chem. **35**, 253 (1963).
12. W. Fastie, J. Opt. Soc. Am. **42**, 641 (1952).
13. H. L. Kahn, Paper presented at Eastern Photomultiplier Symposium, Boston, October 1962.

# Beer's Law and the Optimum Transmittance in Absorption Measurements

Harold K. Hughes

Beer's law is used widely in the determination of cross sections and of unknown solution concentrations in the form $\tau = 10^{-A}$, where $\tau$ is the transmittance and $A$ is the absorbance. By the criterion of minimum experimental error, the best value of the transmittance depends upon numerous parameters and varies between 2% and 90%. This paper considers the influence of the source, background, noise, counting time, and other parameters on the optimum transmittance.

## I. Introduction

### A. Beer's Law

When the absorption of a parallel beam of monoenergetic radiation or particles such as neutrons is proportional to the radiant power or flux (number of quanta or particles per unit area per unit time) and to the mass of homogeneous and isotropic matter intersected, Eq. (1) describes the transmittance. For convenience (1) is called "Beer's law" although we know[1] that Bouguer, Lambert, Bernard, Bunsen, and Roscoe also made contributions to its formulation.

$$\tau = P/P_0 = 10^{-A}, \tag{1}$$

where the absorbance $A$ is

$$A = A_w + b[a_1 + c_2(a_2 - a_1)], \tag{2}$$

and the other symbols are defined in Table I. The absorbance of the windows $A_w$ (when a cell is employed) includes as an equivalent absorbance the effect of reflection from the four surfaces. The magnitudes of these reflections depend upon the refractive indices of the windows and of the cell contents and are given by Fresnel's equations.

In nuclear physics, when dealing with the absorption of neutrons or other particles and with radiation, one generally sees Beer's law in the form

$$\tau = P/P_0 = e^{-\sigma nb}. \tag{3}$$

With x rays, still another form of Beer's law is in common use:

$$\tau = P/P_0 = e^{-\mu bc} = e^{-\mu'\rho bc} = 10^{-a'\rho bc}, \tag{4}$$

where the mass absorption coefficient $\mu'$ and the mass absorptivity $a'$ are related by (5):

$$\mu' = a' \ln 10 = 2.303\, a'. \tag{5}$$

### B. Analytical Precision and Reduction of Errors

The form of Beer's law in Eq. (1) is the easiest to remember and is, therefore, adopted for use throughout

**Table I. Definitions of Symbols**

| | |
|---|---|
| $a_1$ | Absorptivity of the solvent ($m^{-1}$) |
| $a_2$ | Absorptivity of the solid sample or of the component of interest in the solution ($m^{-1}$) |
| $a'$ | Mass absorptivity $= a/\rho$ ($m^2/kg$) |
| $1/ac$ | Free path (m) |
| $A$ | Absorbance; dimensionless |
| $A_w$ | Absorbance of the windows |
| $b$ | Breadth (thickness) of sample or cell interior (m) |
| $c_2$ | Mass fractional concentration of the component of interest in the solution; dimensionless |
| $e$ | Naperian base = 2.71828 . . . |
| $m$ | Relative background; see Sec. II-D-1 |
| $n$ | Number of absorbing or scattering centers per unit volume in $m^{-3}$; counts/sec with sample in the beam |
| $n_0$ | Counts/sec incident on sample |
| $N$ | Total count with sample in the beam |
| $N_0$ | Total count incident on the sample |
| $P$ | Radiant power transmitted by the sample or cell; W (or quanta/sec or particles/sec) per $m^2$ |
| $P_0$ | Radiant power incident on the sample or cell |
| $P_g$ | Radiant power of background |
| $t$ | Time of counting transmitted beam (sec) |
| $t_0$ | Time of counting incident beam |
| $T$ | Total time of counting |
| $\mu$ | Absorption coefficient ($m^{-1}$) |
| $\mu'$ | Mass absorption coefficient $= \mu/\rho$ ($m^2/kg$) |
| $\rho$ | Density ($kg/m^3$) |
| $\sigma$ | Cross section for absorption or scattering in $m^2$; standard deviation |
| $\tau$ | Transmittance; dimensionless |

---

The author is Chairman of the Department of Physics, Indiana State College, Terre Haute, Indiana.

Received 5 February 1963.

the remainder of this paper.[2] It has wide applications in nuclear cross-section measurements and analytical spectroscopy. Consequently, there is interest in the conditions under which the maximum precision in the unknown concentration or cross section may be achieved. It turns out that this precision can often be maximized by judicious choice of such experimental parameters as sample thickness, concentration, or gas pressure. The wavelength or energy is, of course, chosen at a prominent absorption peak whenever this is possible.

It is a purpose of this paper to examine the effects of zero error, 100% error, transmittance error, shot and Johnson noise, Poisson-source fluctuations, nonlinearity of the detector, and the concentration of the comparison solutions. It is also a purpose of this paper to determine the precision of absorbance measurements and the conditions under which the errors are minimized.

That the optimum analytical precision in absorption spectroscopy is often obtained with a transmittance of $1/e$ or 36.8% is well known.[3-10] Thus, it was a surprise several years ago to find that the best precision for the determination of sulfur[11,12] and tetraethyllead[13] in petroleum products by x-ray and $K$-capture absorption is at a transmittance of about 3%. This paper is a consequence of the investigation of this apparent anomaly, an investigation which has now been extended to cover several other cases of absorption measurements.

## C. Errors Not Considered

There are circumstances when Beer's law is not applicable, such as when the radiation source is bremsstrahlung. To limit the scope of this paper to manageable proportions, the following assumptions are made:

1. The geometry is "good"; that is, there is no rescattering into the detected beam and thus the absorptivities are independent of the sample thickness $b$ and the beam width. Equivalent statements of this requirement are: the mean free path for scattering is much greater than the sample thickness $b$; the absorption cross section is much greater than the scattering cross section. Spencer and Fano[14-16] at the National Bureau of Standards have studied the absorption of radiation in absorbers so thick that this assumption is not valid. Taylor and Whyte[17] have published a simple student experiment for measuring the amount of rescatter.
2. The temperature is constant or all partial derivatives with respect to the temperature are negligibly small.
3. Beer's law is valid at all concentrations[18]; that is, there are no intermolecular forces or other causes of association, the absorptivities are constant, and the absorbances of the various components are additive without cross-product (interaction) terms. Any absorber structure, such as that due to colloidal particles, is much smaller than the wavelength (does not apply to x rays).
4. The radiation is monoenergetic (monochromatic). Several workers have reported on finite slit-width errors.[19-22c]
5. The absorber is homogeneous, isotropic, and nonfluorescent; it is noncrystalline or, at least, there are no Bragg reflections such as Campbell[23] treats. Dichroism, in which the absorptivity depends upon the direction of polarization, is absent.[24]
6. Compton scattering or pair production, if present, does not invalidate Eq. (1).
7. The variation of solution refractive index with concentration is so small the $A_w$ may safely be assumed to be a constant in Eq. (1).
8. Multiple traverses of the cell[25] are absent. In practice this error may be present.[26]
9. When more than one cell is in use,[27] suitable means are employed to correct for the inherent differences in their path lengths, $b$, and window absorbances $A_w$.
10. There are no other systematic errors. Gibson,[28] Goldring *et al.*[26] and Caster[29] have surveyed all of the important chemical, instrumental, and technique errors in absorption spectrophotometry.

## II. Linear Detector

The optimum transmittance for least absorbance error depends upon the nature of the radiation source and the linearity of the detector. In this section we consider the conditions with a constant source and a linear detector. Subsequent sections describe the optimum conditions when the detector is subject to overload (nonlinear response) or to Johnson and shot noise, and when the source varies in time according to a Poisson distribution.

### A. Constant Source

In absorption measurements with a constant source, the quanta or particles arrive at such a high rate that the response of the detector does not depend upon their discrete nature. With a constant source it is proper to differentiate (1).

The spectrometer of Fig. 1 may be of the double-beam type or the various radiant powers may be read in time sequence with a single-beam instrument. Applying (1) and (2) to Fig. 1, we obtain

$$\tau = \left(\frac{P_{02}}{P_{01}}\right)\left[10^{-(A_{w2}-A_{w1})}\right]\left[10^{-a_1(b_2-b_1)}\right] \times \left[10^{-(a_2-a_1)(b_2c_2-b_1c_1)}\right] \qquad (6)$$

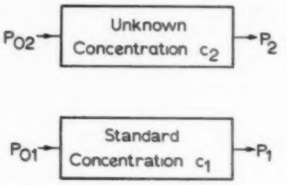

Fig. 1. Schematic spectrometer, defining four radiant powers.

### *1. Double-Beam Instrument, Solvent Comparison*

In a double-beam spectrometer with pure solvent in one beam, $c_1 = 0$, and the calibration procedure effectively sets the first three terms on the right of (6) equal to one. Then this equation reduces to

$$\tau = 10^{-(a_2 - a_1)bc_2}, \tag{7}$$

and the fractional error in $c_2$ is

$$\frac{\Delta c_2}{c_2} = \frac{0.4343\ \Delta\tau}{\tau \log \tau} \tag{8}$$

This error varies with sample thickness. Its value is a minimum when

$$\frac{\partial}{\partial b}\left(\frac{\Delta c_2}{c_2}\right) = 0 \tag{9}$$

or

$$(a_2 - a_1)bc_2 = 0.4343. \tag{10}$$

The optimum transmittance corresponding to this absorbance of 0.4343 is $1/e$ or 36.8%. From (8), the minimum error is

$$\Delta c_2/c_2 = -e(\Delta\tau) = -2.718(\Delta\tau). \tag{11}$$

Equation (11) is strictly true only when differentials replace the finite changes in $c_2$ and $\tau$. Although it appears to say that a 1% error in the transmittance causes a 2.7% error in the concentration, the actual error in $c_2$ may, in fact, be much larger when finite differences are taken. It is more reasonable to say[30] that a 0.1% error in $\tau$ produces a 0.27% error in $c_2$.

### *2. Adjustment for Minimum Error*

Beer's law is essentially symmetrical in cell length $b$ and concentration $c_2$, and the requirement in (10) can be met by an adjustment of either. When the sample is a gas, the pressure, and, therefore, the concentration, may be adjustable. The concentration is not always adjustable with liquids, however. It might seem that if $\tau$ is more than 36.8% one should add a known amount of solute to bring $\tau$ to the optimum value. This is never advantageous, for McBryde[31] has shown that the error is always increased by this procedure. In the determination of the concentration of trace constituents, the only recourse is to use a long cell.

As shown in Fig. 2, the plot of concentration or cross-section error as a function of transmittance is rather flat between 25% and 50%, so that careful adjustment to 36.8% is of little value.

It appears to be generally true for all of the experimental conditions considered in this paper that the error-vs-transmittance curve is rather flat, although the location of the minimum varies within wide limits.

### *3. Double-Beam Instrument, Standard Solution Comparison*

It is possible to reduce the error calculated in (11) by using a standard solution of concentration $c_1$ in the reference beam in place of pure solvent. This is known as the transmittance ratio method.[30, 32–41] Equation (8) then becomes

$$\frac{\Delta c_2}{c_2} = \frac{0.4343\ \Delta(P_2/P_1)}{(P_2/P_1)\log(P_2/P_0)}. \tag{12}$$

The minimum value of $\Delta c_2/c_2$ is at

$$P_2/P_1 = 10^{A_1}/e = 0.368\ (10^{A_1}) \tag{13}$$

or

$$P_2/P_0 = 1/e = 36.8\%. \tag{14}$$

Here $A_1$ is the absorbance of the standard solution. The minimum fractional error is

$$\Delta c_2/c_2 = -(e/10^{A_1})\ \Delta(P_2/P_1). \tag{15}$$

Equation (15) shows that it is advantageous to increase $A_1$ up to the limit at which $P_2 = P_1$ corresponding to $A_1 = 0.4343$. At this value of the absorbance of the standard solution, the error in $c_2$ is

$$\Delta c_2/c_2 = -\Delta(P_2/P_1), \tag{16}$$

which is lower by a factor of $e$ than when the comparison liquid is pure solvent. If, for some reason, $P_2/P_0$ cannot be adjusted to 36.8%, the best value for $P_1/P_0$ is $P_2/P_0$. Hiskey and Firestone[41] have extended this method to the analysis of multicomponent systems, particularly when absorption bands overlap.

Gridgeman's[30] Fig. 6 shows a family of error curves for various values of $A_1$ and $A_2$. Nowhere in the above analysis must the actual value of $c_1$ be used, although it may be. Its function is really to reduce the transmittance of the comparison beam to equal that of

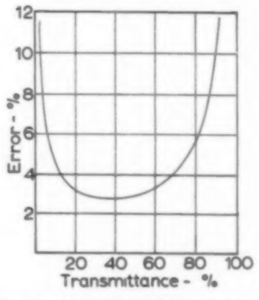

Fig. 2. Error in the absorbance as given by Eq. (8) for a 1% error in the transmittance.

the beam through the unknown. Thus one may use a graded series of variable-thickness solid absorbers just as well as a standard solution.

Reilley and Crawford[42] introduce an interesting variation of the transmittance ratio method. They adjust the "zero" and "100%" settings of the transmittance scale to a narrow range, just bracketing the unknown transmittance. The optimum value of the latter is at 36.8%.

### 4. *Double-Beam Instruments, Independent Errors*

In the differentiations of (6) above it is assumed that the error is in the transmittance $\tau$ without regard to its source in $\tau_2$ or $\tau_1$. This is equivalent to saying that $\Delta\tau_1 = 0$ and that $\Delta\tau_2$ is independent of $\tau_2$. The results apply, for example, to: (a) x-ray measurements on a series of unknowns when $P_0$ or $\tau_1$ is measured repeatedly but each $P_2$ or $\tau_2$ is measured with limited replication; and (b) chopped beams which are compared in a single detector. It may happen, however, that there are two uncorrelated sources of error. These are treated as follows, still assuming that the first three terms on the right of (6) are set equal to one in the calibration procedure.

$$P_2/P_1 = 10^{-(a_2-a_1)b(c_2-c_1)} = 10^{-(A_2-A_1)} \tag{17}$$

$$\Delta A_2 = 0.4343\left(\frac{\Delta P_1}{P_1} - \frac{\Delta P_2}{P_2}\right). \tag{18}$$

When $\Delta P_1$ and $\Delta P_2$ are not correlated, and each is a standard deviation, the standard deviation of $A_2$ is

$$\sigma_{A2} = 0.4343\left[\left(\frac{\sigma_{P1}}{P_1}\right)^2 + \left(\frac{\sigma_{P2}}{P_2}\right)^2\right]^{1/2}. \tag{19}$$

If

$$\sigma_{P1} = \sigma_{I2} = \sigma_P,$$

then

$$\sigma_{A2} = 0.4343\ \sigma_P\left(\frac{1}{P_1^2} + \frac{1}{P_2^2}\right)^{1/2}, \tag{20}$$

and the coefficient of variation is

$$\frac{\sigma_{A2}}{A_2} = \frac{0.4343\ \sigma_P}{A_2\ P_0}\left(10^{2A_1} + 10^{2A_2}\right)^{1/2} \tag{21}$$

$$\frac{\sigma_{A2}}{A_2} = \frac{0.4343\ \sigma_P}{A_2 P_1}\left[1 + 10^{2(A_2-A_1)}\right]^{1/2}. \tag{22}$$

The optimum transmittance is found from (21) by setting its derivative with respect to $A_2$ equal to zero. The result is

$$10^{-2(A_2-A_1)} + 1 = 2.303\ A_2. \tag{23}$$

There are two limiting cases to the solution of this transcendental equation.

(*a*) *No absorber in the comparison beam.* Cole[43] and Robinson and Cole[44] solve the case for which there is

**Table II. Optimum Absorbance and Transmittance to Use in Absorption Measurements**

| Conditions | Opt $A$ | Opt $\tau$ | Error |
|---|---|---|---|
| Sec. II. Linear Detector | | | |
| A. Constant source | | | |
| 1. 2-Beam, solvent comparison | 0.43 | 36.8% | 2.72 $\Delta\tau$ |
| 3. 2-Beam, standard solution | 0.43 | 36.8 | $\Delta\tau$ |
| 4. 2-Beam, independent error | | | |
| a. Pure solvent | 0.48 | 33.0 | 2.87 $\sigma_{P1}/P_0$ |
| b. Absorber | 0.87 | 13.5 | 0.707 $\sigma_{P1}/P_1$ |
| 5. 1-Beam, independent errors, 2 zeros | | | |
| a. Pure solvent | 0.54 | 28.7 | 3.11 $\sigma_{P0}/P_0$ |
| b. Absorber | 0.88 | 13.1 | $\sigma_{P0}/P_0$ |
| 6. 1-Beam, independent error, 1 zero | | | |
| a. Pure solvent | 0.52 | 30.5 | 3.01 $\sigma_{P0}/P_0$ |
| b. Absorber | 0.88 | 13.3 | 0.70 $\sigma_{P0}/P_1$ |
| 7. Penetrating background | See Eq. (46) | | |
| B. Noise | | | |
| 1. Johnson noise | 0.43 | 36.8 | |
| 2. Shot noise | 0.87 | 13.5 | |
| C. Poisson source | | | |
| 1. Fixed time, $t = t_0$ | 0.96 | 10.9 | 0.45 $(1/N_0 + 1/N)^{1/2}$ |
| 2. Fixed time, $t_0 = \infty$ | 0.87 | 13.5 | 0.50 $N^{-1/2}$ |
| 3. Absorber in comparison beam | Do not use | | |
| 4. Fixed total time | 1.11 | 7.8 | 1.79 $(n_0T)^{-1/2}$ |
| 5. Fixed count | 1.74 | 1.8 | 0.35 $N^{-1/2}$ |
| D. Poisson source with background | | | |
| 1. Fixed area | | $\tau$ = 7.8% to 31% depend on *bg* | |
| 2. Variable area | | $\tau$ = 22.8% to >90% depend on *bg* | |
| Sec. III. Limited Detector | | | |
| With respect solut. | 0.43 | 36.8 | |
| Absolute | | Much less, even as low as 2%. See discussion. | |

pure solvent in the comparison beam, that is for $A_1 = 0$, finding by trial and error

$$\begin{aligned} A_2 &= 0.4816, \\ \tau &= 32.99\%. \end{aligned} \tag{24}$$

Putting these values back into (21), we find that the minimum coefficient of variation in the unknown absorbance is

$$\sigma_{A2}/A_2 = 2.87\ \sigma_{P1}/P_0 \tag{25}$$

Thus, if the errors in the radiant powers transmitted through the absorbers in the two beams are $\sigma_{P1} = \sigma_{P2} = 0.1\%$ of $P_0$, the minimum error in the unknown absorbance is about 0.29%. This is likewise the minimum percentage error in the determination of a cross section, a mass absorption coefficient, or a solution concentration.

If $\sigma_{P1} = \sigma_{P2}$ is a constant independent of $P_0$, then the minimum error in $A_2$ is when $A_1 = 0$ and (24) still applies.

Using a "range-of-errors" criterion instead of the coefficient of variation, Cole[43] deduces that the optimum transmittance is 27.84%. This criterion is of questionable validity and is not recommended.[29]

(*b*) *Absorber in the comparison beam.* If $\sigma_{P1} = \sigma_{P2}$ is a fixed fraction of $P_1$, Eq. (22) shows that the best value of $A_1$ is $A_2$. The solution of (23) is then

$$\begin{aligned} A_2 &= 0.8686, \\ \tau_2 &= 13.5\%. \end{aligned} \tag{26}$$

Putting these values back into (22) produces

$$\sigma_{A2}/A_2 = 0.707\ \sigma_{P1}/P_1. \tag{27}$$

Thus, by adjusting the length of the beam through the unknown so that $\tau_2 = 13.5\%$ and by placing an absorber into the comparison beam so that its transmittance is likewise 13.5%, the error in the unknown absorbance is reduced to only 25% of the error when the comparison path is 100% transparent.

If $\sigma_{P1} = \sigma_{P2}$ is a fixed fraction of $P_0$, Eq. (21) shows that the best value of $A_1$ is zero, and the optima are given by (24). That is, there should be no absorber in the comparison beam.

### 5. *Single-Beam Instrument, Independent Errors*

For a single beam of radiant energy or particles, the second and third terms on the right of (6) are equal to one. Allowing for errors in $P_1$, $P_2$, $P_{01}$, and $P_{02}$, we find on differentiating that the standard deviation of $A_2$ is

$$\sigma_{A2} = 0.4343 \left[\left(\frac{\sigma_{P1}}{P_1}\right)^2 + \left(\frac{\sigma_{P2}}{P_2}\right)^2 + \left(\frac{\sigma_{P01}}{P_{01}}\right)^2 + \left(\frac{\sigma_{P02}}{P_{02}}\right)^2\right]^{1/2}. \tag{28}$$

A sufficient condition for the method of combination in (28) is for the independent random errors to be Gaussian-distributed. It may not be a necessary condition. This writer is not aware of any data on the distribution of absorption measurement errors. Indeed, published spectroscopic error distributions of any kind are rare. Lempicki *et al.*[45] found the plot of energy from a spectrograph slit vs wavelength to be closer to a Gaussian than to a Lorentzian distribution.

To simplify the remainder of the analysis, we assume that all four standard deviations on the right of (28) are equal to $\sigma_{P0}$ and that $P_{01} = P_{02} = P_0$.

$$\frac{\sigma_{A2}}{A_2} = \frac{0.4343\ \sigma_{P0}}{A_2P_0}\left[10^{2A_1} + 10^{2A_2} + 2\right]^{1/2}. \tag{29}$$

Setting the derivative of (29) equal to zero to find the minimum error, as usual, it follows that

$$A_2 = 0.4343\left[1 + 10^{-2A_2}\left(2 + 10^{2A_1}\right)\right]. \tag{30}$$

There are two limiting cases to the solution of this transcendental equation.

(*a*) *No absorber in the comparison beam.* Cole[43] and Robinson and Cole[44] solve the case when the comparison beam passes through pure solvent, that is, for $A_1 = 0$, finding

$$\begin{aligned} A_2 &= 0.5417, \\ \tau_2 &= 28.73\%. \end{aligned} \tag{31}$$

Putting these values back into (29) we find

$$\sigma_{A2}/A_2 = 3.11\ \sigma_{P0}/P_0. \tag{32}$$

Thus, for 0.1% coefficient of variation in $P_0$, there is a coefficient of variation in $A_2$ of about 0.31%.

If $\sigma_{P0}$ is a fixed fraction of $P_0$, Eq. (29) shows that the best values of $A_1$ is zero and there should be no absorber in the comparison beam.

Using what he names the "range-of-error" criterion instead of the coefficient of variation, Cole deduces that the optimum transmittance is 20.12%. This criterion is of questionable validity and is not recommended.[29]

(*b*) *Absorber in the comparison beam.* Rewriting (29) in the form

$$\frac{\sigma_{A2}}{A_2} = \frac{0.4343\ \sigma_{P0}}{A_2P_1}\left[1 + 10^{-2A_1}\left(10^{2A_2} + 2\right)\right]^{1/2}, \tag{33}$$

we see that if $\sigma_{P0}$ is a fixed fraction of $P_1$, the best value of $A_1$ is $A_2$. Equation (30) then becomes

$$1.151\ A_2 = 1 + 10^{-2A_2}, \tag{34}$$

whose solution is

$$\begin{aligned} A_2 &= 0.882, \\ \tau_2 &= 13.1\%. \end{aligned} \tag{35}$$

Inserting (35) into (33) we find that the coefficient of variation of $A_2$ is equal to $\sigma_{P0}/P_1$.

### 6. *Single Beam, Independent Errors, Only One Zero Reading*

In Eq. (28) it is assumed that there are two independent measurements of $P_0$, one each associated with $P_1$ and $P_2$. If, instead, the order of measurement is $P_1$,

$P_0$, $P_2$, or $P_2$, $P_0$, $P_1$, with only one reading of the incident radiant power $P_0$, then (30) becomes

$$A_2 = 0.4343\left[1 + 10^{-2A_2}\left(1 + 10^{2A_1}\right)\right]. \tag{36}$$

There are two limiting solutions to this transcendental equation.

(*a*) *No absorber in the comparison beam.* When $A_1 = 0$, Eq. (36) becomes

$$A_2 = 0.4343\left[1 + 2\,(10)^{-2A_2}\right], \tag{37}$$

whose solution is

$$\begin{aligned} A_2 &= 0.516, \\ \tau_2 &= 30.5\%. \end{aligned} \tag{38}$$

Putting these values back into (29) and remembering that the third term under the radical is one instead of two,

$$\sigma_{A2}/A_2 = 3.01\ \sigma_{P0}/P_0. \tag{39}$$

(*b*) *Absorber in the comparison beam.* If $\sigma_{P0}$ is a fixed fraction of $P_0$, Eq. (29) shows that there is no advantage in using a value of $A_1$ different from zero; that is, do not use an absorber in the comparison beam.

If $\sigma_{P0}$ is a fixed fraction of $P_1$, we modify (33) to

$$\frac{\sigma_{A2}}{A_2} = \frac{0.4343\ \sigma_{P0}}{A_2P_1}\left[1 + 10^{-2A_1}\left(10^{2A_2} + 1\right)\right]^{1/2}, \tag{40}$$

and find that the best value of $A_1$ is $A_2$. Inserting $A_1 = A_2$ into (36) there results

$$A_2 = 0.4343\ (2 + 10^{-2A_2}), \tag{41}$$

whose solution is

$$\begin{aligned} A_2 &= 0.877, \\ \tau_2 &= 13.3\%, \\ \sigma_{A2}/A_2 &= 0.703\ \sigma_{P0}/P_1. \end{aligned} \tag{42}$$

### 7. *Effect of Background*

It may happen that stray light, unwanted particles or radiation[46] are also present at energies so far removed from an absorption peak that their effect on the detector is approximately independent of $b$ or $c$. Let the radiant power of this background be $P_g$ and consider first the case where it can be measured readily. Assuming no window or cell errors and $c_1 = 0$, Beer's law (6) becomes

$$(P_2 - P_g) = (P_0 - P_g)10^{-(a_2-a_1)bc_2}. \tag{43}$$

Equation (43) is a statement of the well-known "base line" method.[47-50]

The coefficient of variation of the absorbance is

$$\frac{\sigma_{A2}}{A_2} = \frac{0.4343\ \sigma_{P2}}{(P_2 - P_g)bc_2(a_2 - a_1)}, \tag{44}$$

which is a minimum when

$$\frac{P_2 - P_g}{P_0 - P_g} = 1/e = 36.8\%. \tag{45}$$

It may not be easy to separate out the background when, for example, beta rays contaminate a gamma-ray source or an x-ray monochromator reflects harmonics. From (45) the optimum transmittance, uncorrected for background, is

$$P_2/P_0 = 0.368\ (1 + 1.718\ P_g/P_0), \tag{46}$$

which increases from a minimum of 36.8% as the penetrating background increases.

### 8. *Indirect Spectrophotometry*

In a method of spectrophotometry which he calls "indirect" Lothe[51] titrates a colored solution until it is colorless. He reports that the coefficient of variation of the absorbance decreases monotonically with increase of transmittance and recommends, therefore, the use of a very low absorbance.

## B. Johnson and Shot Noise

Equation (19) leads to different results, depending upon whether Johnson[52] or shot[53] noise predominates in the detector circuit of a double-beam spectrometer. Johnson noise is characteristic of thermal detectors and shot noise is characteristic of photoemissive detectors. Neglecting other errors, the optimum condition for Johnson noise is

$$\begin{aligned} A &= 0.4343, \\ \tau &= 36.8\% \end{aligned} \tag{47}$$

and for shot noise is

$$\begin{aligned} A &= 0.8686 \\ \tau &= 1/e^2 = 13.5\%. \end{aligned} \tag{48}$$

Wybourne[53] observes that, because Johnson noise error varies inversely with the square of the slit-width, and resolution decreases directly as the slit-width, it is advantageous to use a large slit. In contrast, shot noise is approximately independent of slit-width.

## C. Poisson Source, without Background

Because x rays and particles cannot be reflected without large losses, it is usual to employ only a single beam with such radiation, measuring the incident and transmitted radiant powers sequentially. If the detector is a Geiger counter, it responds to individual quanta or particles, and it is convenient to measure the radiant power in counts/sec $n$. If we assume that the cross section of the beam is constant and we use $N$ for the total count, then Beer's law is

$$N/t = n = n_0 10^{-A} = (N_0/t_0)10^{-A}. \tag{49}$$

The error in the absorbance $A$ is

$$\Delta A = 0.4343\left(\frac{\Delta n_0}{n_0} - \frac{\Delta n}{n}\right) = 0.4343\left(\frac{\Delta N_0}{N_0} - \frac{\Delta N}{N}\right). \tag{50}$$

The standard deviation of a Poisson distribution is $N^{1/2}$. If we use this standard deviation as the measure of the errors $\Delta n_0$ and $\Delta n$, and assume that these errors are independent and that there is no error in the time measurements $t$ and $t_0$, then the standard deviation of the absorbance is

$$\sigma_A = 0.4343 \left(\frac{1}{N_0} + \frac{1}{N}\right)^{1/2}. \qquad (51)$$

As usual, we find the optimum transmittance by setting the derivative of the coefficient of variation equal to zero, which leads to

$$A = 0.8686 \; [1 + (t/t_0)10^{-A}] = 0.8686 \; (1 + N/N_0). \qquad (52)$$

*1. Counting for Fixed Time and $t = t_0$*

The solution of (52) when $t = t_0$ is

$$\begin{aligned} A &= 0.9631, \\ \tau &= 10.9\%. \end{aligned} \qquad (53)$$

Taking 2-$\sigma$ or 3-$\sigma$ limits on the Poisson error does not change the location of the optimum transmittance.

The minimum coefficient of variation of the absorbance is

$$\frac{\sigma_A}{A} = 0.451 \left(\frac{1}{N_0} + \frac{1}{N}\right)^{1/2}. \qquad (54)$$

*2. Counting for Fixed Time and $t_0 = \infty$*

When the source is an isotope with long half-life or for some other reason the source is so steady that $n_0$ is known with substantially no error, the solution of (52) is

$$\begin{aligned} A &= 0.8686, \\ \tau &= 13.5\%. \end{aligned} \qquad (55)$$

The minimum coefficient of variation of the absorbance is

$$\sigma_A/A = 0.500/N^{1/2}. \qquad (56)$$

*3. Absorber in the Comparison Beam*

With a Poisson source, Eq. (28) becomes

$$\frac{\sigma_{A2}}{A_2} = \frac{0.4343}{A_2}\left[\frac{1}{N_1} + \frac{1}{N_2} + \frac{1}{N_{01}} + \frac{1}{N_{02}}\right]^{1/2}. \qquad (57)$$

Obviously, $N_1$ should be as large as possible and the transmittance ratio method should not be used.

*4. Counting for Fixed Total Time*

Let the time of counting without sample be $t_0$, the time of counting with the sample in the beam be $t$, and let $t_0 + t = T$ be a constant. Then from (51)

$$\frac{\sigma_A}{A} = \frac{0.4343}{A}\left[\frac{1}{n_0 t_0} + \frac{1}{n(T - t_0)}\right]^{1/2}. \qquad (58)$$

The optimum distribution of time between $t$ and $t_0$ results from setting

$$\frac{\partial}{\partial t_0}\left(\frac{\sigma_A}{A}\right) = 0, \qquad (59)$$

which leads to

$$\left(\frac{t_0}{t}\right)^2 = \frac{n}{n_0} = 10^{-A}. \qquad (60)$$

The optimum absorbance results from setting

$$\frac{\partial}{\partial A}\left(\frac{\sigma_A}{A}\right) = 0, \qquad (61)$$

which leads to

$$A = 0.8686 \left(1 + \frac{nt}{n_0 t_0}\right). \qquad (62)$$

Combining (60) and (62), we find for the best combination of absorbance and distribution of counting time

$$A = 0.8686(1 + 10^{-A/2}). \qquad (63)$$

The solution[54] of (63) is

$$\begin{aligned} A &= 1.110, \\ \tau &= 7.8\%. \end{aligned} \qquad (64)$$

Putting these values into (58) we obtain

$$\sigma_A/A = 1.79(n_0 T)^{-1/2}, \qquad (65)$$

where $n_0$ is the rate without sample, in counts/sec, and $T$ is the total counting time in seconds.

The optimum counting times are

$$\begin{aligned} t_0/t &= 10^{-0.555} = 0.278, \\ t_0 &= 0.219\ T, \\ t &= 0.781\ T. \end{aligned} \qquad (66)$$

According to Birks and Brown,[55] for equal precision, the total time for fixed-time counts is generally less than for fixed counts.

*5. Timing for Fixed Count*

The standard deviation of a count rate with a Poisson source is[56]

$$\sigma_n = (n/t)^{1/2}. \qquad (67)$$

Using this equation for $\Delta n$ and $\Delta n_0$ in (50), the error in $A$ is again given (51) and the optimum absorbance by (52). If $N = N_0$ then

$$\begin{aligned} A &= 1.736, \\ \tau &= 1/e^4 = 1.8\%. \end{aligned} \qquad (68)$$

With these values in (51) the coefficient of variation of the absorbance is

$$\sigma_A/A = 0.354\ N^{-1/2}. \qquad (69)$$

## D. Poisson Source with Background

With a Poisson source in the presence of unwanted background radiation or particles, Eq. (43) becomes

$$\frac{n}{n_0} = \frac{n_2 - n_g}{n_1 - n_g} = 10^{-A}, \qquad (70)$$

where $n_g$ is the background count rate, $n_1$ is the count rate (including background) without the sample in the beam, and $n_2$ is the count rate (including background) with the sample in the beam. The optimum transmittance depends upon whether the cross section of the beam is fixed or variable.

### 1. *Fixed Beam Area*

Assuming that the errors in the three count rates are independent, which is usually the case, and using (67),

$$\frac{\sigma_A}{A} = \frac{0.4343}{n_0 A}\left[\frac{n_1}{t_1} + \frac{n_g}{t_g} + 10^{2A}\left(\frac{n_2}{t_2} + \frac{n_g}{t_v}\right)\right]^{1/2}. \qquad (71)$$

Rose and Shapiro[57] minimize (71) as a function of the relative background $m = n_g/n_0$, presenting curves for the optimum transmittance and the distribution of the three counting times, all as functions of $m$. The optimum $\tau$ increases from 7.8% for no background as shown in (64) above, to 20% for $m = 0.1$, and to about 31% when $m \gg 10$. This result is true whether one counts for fixed time or times for fixed count.

The optimum fractional time $(t_1/T)$ devoted to counting the incident beam decreases slowly from 0.28 to about 0.13 as the relative background $m$ increases from zero to ten or more. The optimum fractional time $(t_2/T)$ devoted to counting the transmitted beam decreases from 0.72 to about 0.43 as $m$ increases from zero to ten or more. The optimum fractional time $(t_g/T)$ devoted to counting the background increases from zero to about 0.44 as $m$ increases from zero to ten or more.

### 2. *Variable Beam Area*

In this case we suppose that only a small volume of sample is available but that one can use any combination of thickness and cross section, provided that the volume remains constant. The total number of absorbing centers remains constant, each one always being in the beam. Rose and Shapiro[57] solve this case, finding that the optimum transmittance increases from 22.8% where there is no background to over 90% at high background counting rates.

The optimum fractional time $(t_1/T)$ decreases only slightly from 0.32 to 0.29; the optimum of $(t_2/T)$ decreases from 0.68 to 0.29, and the optimum of $(t_g/T)$ increases from zero to 0.42 as the background counting rate $n_g$ increases from zero to many multiples of $n_0$.

## III. Limited Detector

All of the results of Sec. II are circumscribed by the assumption that the response of the detector is always proportional to the radiant power or the number of particles per second incident upon it. This assumption is by no means universally justified. For example, a Geiger counter fails to detect some of the particles entering it when its recovery time is comparable to the average time between the arriving particles or quanta.

When the available radiant power may make the detector response nonlinear, there are at least three courses of action to follow. In the first course, the nonlinear response is calibrated[58–67] and the corrected response used as before in the equations of Sec. II. In the second course of action, the radiant power is reduced by any appropriate means, such as by narrowing the collimator slits. The third course is to increase the sample thickness until the transmitted radiant power no longer overloads the detector. A comparison of the second and third courses shows that it is the third which is preferable. This is shown as follows[68]:

Let $P_{\max}$ be the maximum radiant power at which the detector can operate and still remain linear and let this be the transmitted power when the concentration is zero or its smallest expected value. Then (1) becomes

$$P = P_{\max} 10^{-bc(a_2 - a_1)}. \qquad (72)$$

Since $P_{\max}$ is a constant, Eq. (72) is optimized for concentration sensitivity when

$$bc(a_2 - a_1) = 0.4343. \qquad (73)$$

The optimum transmittance with respect to the solvent or to the solution with minimum expected concentration is 36.8%, but the absolute transmittance is very much less than this value. In the determination of sulfur in distillate fuels by x-ray or *K*-capture absorption,[11,12] the optimum transmittance may be 2% or even lower, depending upon the strength of the source. In the routine determination of tetraethyl-lead concentration in gasoline, at a level of about 2 to 4 ml of TEL per gallon, using molybdenum *K*-$\alpha$ radiation, Hughes and Hochgesang[13] found the optimum transmittance to be about 4%.

The effect on the analytical sensitivity of variations in the initial radiant power is seen easily from (1). There is no optimum sample thickness. Rather, as $P_0$ increases, $b$ should also be increased while keeping the radiant power transmitted through the reference solution or solvent just below $P_{\max}$.

To summarize: with a very strong source, increase the sample thickness until the largest expected transmitted radiant power is slightly less than $P_{\max}$. Do not read the incident radiant power directly. For the monitoring or comparison beam use the incident beam with a metal insert thick enough to reduce the radiant power to $P_{\max}$. This procedure applies to both single-beam and double-beam spectrometers.

## IV. Summary

This paper is concerned with the experimental conditions under which the best precision is obtained in measurements of cross section or concentration using

Beer's law. The optimum transmittance depends upon the nature of the source, the presence or absence of interfering background (including stray light, and Johnson or shot noise), whether the spectrometer is of the single-beam or double-beam type, the nature of the material in the comparison beam, the counting scheme and other parameters. This optimum transmittance varies within wide limits. It may be as low as 2% or higher than 90%.

Table II summarizes the optimum conditions in abbreviated form. Fairly large departures from these optima produce only small losses in sensitivity.

## References

1. D. R. Malinin and J. H. Yoe, J. Chem. Educ. **38,** 129 (1961).
2. Report No. 6 of the Joint Comm. on Nomenclature in Applied Spectroscopy, H. K. Hughes (chairman) *et al.*, Anal. Chem. **24,** 1349 (1952).
3. F. Twyman and G. F. Lothian, Proc. Phys. Soc. (London) **45,** 643 (1933).
4. F. Twyman and C. B. Allsopp, *Practice of Absorption Spectrophotometry* (Hilger, London, 1934), 2nd ed.
5. T. R. Hogness, F. P. Zscheile, Jr., and A. E. Sidwell, Jr., J. Phys. Chem. **41,** 379 (1937).
6. R. B. Barnes, U. Liddel, and V. Z. Williams, Anal. Chem. **15,** 659 (1943).
7. R. B. Barnes, R. C. Gore, U. Liddel, and V. Z. Williams, *Infrared Spectroscopy* (Reinhold, New York, 1944), p. 29.
8. J. M. Vandenbelt, J. Forsyth, and A. Garrett, Anal. Chem. **17,** 235 (1945).
9. G. H. Ayres, Anal. Chem. **21,** 652 (1949).
10. M. G. Mellon, *Analytical Absorption Spectroscopy* (Wiley, New York, 1950), p. 113.
11. H. K. Hughes and J. W. Wilczewski, Proc. Am. Petrol. Inst. **30M,** 11 (1950).
12. H. K. Hughes and J. W. Wilczewski, Anal. Chem. **26,** 1889 (1954).
13. H. K. Hughes and F. P. Hochgesang, Anal. Chem. **22,** 1248 (1950).
14. L. V. Spencer and U. Fano, J. Res. Natl. Bur. Std. **46,** 446 (1951).
15. L. V. Spencer, Phys. Rev. **88,** 793 (1952).
16. U. Fano, J. Res. Natl. Bur. Std. **51,** 95 (1953); Nucleonics **11,** 8 (Aug. 1953); **11,** 55 (Sept. 1953).
17. H. W. Taylor and G. N. Whyte, Am. J. Phys. **29,** 315 (1961).
18. A. C. Hardy and F. M. Young, J. Opt. Soc. Am. **38,** 854 (1948).
19. G. L. Buc and E. I. Stearns, J. Opt. Soc. Am. **35,** 458 (1945).
20. A. C. Hardy and F. M. Young, J. Opt. Soc. Am. **39,** 265 (1949).
21. A. R. Philpotts, W. Thain, and P. G. Smith, Anal. Chem. **23,** 268 (1951).

22a. H. K. Hammond, III, and I. Nimeroff, J. Opt. Soc. Am. **42,** 367 (1952).

22b. S. Brodersen, J. Opt. Soc. Am. **43,** 877 (1933); **44,** 22 (1954).

22c. V. J. Coates and H. Hausdorff, J. Opt. Soc. Am. **45,** 425 (1955).

23. H. N. Campbell, J. Appl. Phys. **22,** 1139 (1951).
24. G. F. Lothian, *Absorption Spectrophotometry* (Macmillan, New York, 1958), p. 23*ff.*
25. T. H. Edwards, J. Opt. Soc. Am. **51,** 98 (1951).
26. L. S. Goldring, R. C. Hawes, G. H. Hare, A. O. Beckman, and M. E. Stickney, Anal. Chem. **25,** 869 (1953).
27. D. Z. Robinson, Anal. Chem. **24,** 619 (1952).
28. K. S. Gibson, "Spectrophotometry," Natl. Bur. Std. Circ. 484 (1949).
29. W. O. Caster, Anal. Chem. **23,** 1229 (1951).
30. N. T. Gridgeman, Anal. Chem. **24,** 445 (1952).
31. W. A. E. McBryde, Anal. Chem. **24,** 1639 (1952).
32. G. Körtum, Angew. Chem. **50,** 193 (1937).
33. A. Z. Ringbom, Anal. Chem. **11,** 332 (1939).
34. R. Bastian, Anal. Chem. **21,** 972 (1949).
35. C. F. Hiskey, Anal. Chem. **21,** 1440 (1949); Trans. N. Y. Acad. Sci. **11,** 223 (1949).
36. R. Bastian, R. Weberling, and F. Palilla, Anal. Chem. **22,** 160 (1950).
37. J. A. Perry, R. G. Sutherland, and N. Hadden, Anal. Chem. **22,** 1122 (1950).
38. C. F. Hiskey, J. Rabinowitz, and I. G. Young, Anal. Chem. **22,** 1464 (1950); **23,** 343 (1951).
39. C. F. Hiskey and I. G. Young, Anal. Chem. **23,** 1196 (1951).
40. H. J. Jones, G. R. Clark, and L. S. Harrow, J. Assoc. Offic. Agr. Chemists **34,** 135 (1951).
41. C. F. Hiskey and D. Firestone, Anal. Chem. **24,** 342 (1952).
42. C. N. Reilley and C. M. Crawford, Anal. Chem. **27,** 716 (1955).
43. R. Cole, J. Opt. Soc. Am. **41,** 38 (1951).
44. D. Z. Robinson and R. J. Cole, J. Opt. Soc. Am. **41,** 560 (1951).
45. A. Lempicki, H. Samelson, and A. Brown, J. Opt. Soc. Am **51,** 35 (1961).
46. "Stray Light Number," Photoelectric Spectrometry Group Bulletin **3,** 39 (1950).
47. M. N. States and J. C. Anderson, J. Opt. Soc. Am. **32,** 659 (1942).
48. R. R. Brattain, R. R. Rasmussen, and A. M. Cravath, J. Appl. Phys. **14,** 418 (1943).
49. A. Rouy, *A New Approach to Problems Encountered in Colorimetric Absorption Analysis* (Leitz, New York, 1949).
50. D. Z. Robinson, Anal. Chem. **23,** 273 (1951).
51. J. J. Lothe, Anal. Chem. **27,** 1546 (1955).
52. S. Brodersen, J. Opt. Soc. Am. **43,** 877 (1953).
53. B. G. Wybourne, J. Opt. Soc. Am. **50,** 84 (1960).
54. J. Rainwater and W. W. Havens, Phys. Rev. **70,** 146 (1946).
55. L. S. Birks and D. M. Brown, Anal. Chem. **34,** 240 (1962).
56. A. A. Jarrett, "Statistical Methods Used in the Measurement of Radioactivity with Some Useful Graphs and Nomographs" (OTS, Dept. Commerce, Washington, D. C., 1946).
57. M. E. Rose and M. M. Shapiro, Phys. Rev. **74,** 1853 (1948).
58. L. I. Schiff, Phys. Rev. **50,** 88 (1936).
59. L. I. Schiff and R. D. Evans, Rev. Sci. Instr. **7,** 456 (1936).
60. L. Alaoglu and N. M. Smith, Phys. Rev. **53,** 832 (1938).
61. H. Lifschutz and O. S. Duffendack, Phys. Rev. **54,** 714 (1938).
62. L. J. Rainwater and C. S. Wu, Nucleonics **3,** 1 (Oct. 1947).
63. C. E. Clark, Rev. Sci. Instr. **20,** 51 (1949).
64. L. Alexander, E. Kummer, and H. P. Klug, J. Appl. Phys. **20,** 735 (1949).
65. W. C. Elmore, Nucleonics **6,** 26 (Jan. 1950).
66. C. G. Cannon and I. S. C. Butterworth, Anal. Chem. **25,** 168 (1953).
67. F. K. du Pré, Philips Res. Rept. **8,** 411 (1953).
68. The author presented this result in part at the Second Pittsburgh Conference on Analytical Chemistry and Applied Spectroscopy, 7 March 1951.

# From the Editor

Perhaps this month we should take note of some recent events concerning the adoption of the metric system. In the *Transactions of the American Geophysical Union* **43,** 337 (1962) there appeared a short report of the AGU Committee for the Study of the Metric System in the United States, in which it was stated:

> The next important move regarding the use of the metric system in the United States could very well be an exhaustive study by the National Bureau of Standards. H. R. 2049, introduced by Representative George P. Miller and referred to the Committee on Science and Astronautics, provides for NBS to conduct a study to determine the practicability of the adoption of the metric system. This bill is now on the Consent Calendar. Since Representative Miller is now Chairman of the Science and Astronautics Committee, there appears to be a fair chance of favorable action by the present Congress.

The bill evidently did not pass, but the present 88th Congress now has before it an identical bill, H. R. 18, "to provide that the National Bureau of Standards shall conduct a program of investigation, research, and survey to determine the practicability of the adoption by the United States of the metric system of weights and measures". One should note that this is not a bill to adopt the system, but merely to study the advantages and disadvantages of adoption. The various government departments were asked for their views on this bill. Most of them have concurred in the making of the study. One department commented: "If the United States makes the change, the British Commonwealth nations would be under heavy pressure to follow suit. It would be highly undesirable for the United States to make the change without consultation with the British Commonwealth".

This opinion is somewhat different from some recent debate of one of the committees of the British Standards Institution also considering the change to the metric system. One of the committee observed that if the support of the U.S. were forthcoming on this subject, the change would be easier. In this connection another member referred to U.S. opposition to any change, particularly mentioning the engineering industry while the chairman reported that he had been informed of strong opposition from the U.S. photographic industry. In the view of another member, however, the U.K. should be the first to move in this matter and should not try to secure U.S. support first; he thought the U.S. views were likely to be "isolationist".

This feeling that neither the U.S. nor the U.K. should change before the other one does has been a convenient stall for many years. It is somewhat like being the last two dodos in captivity: hope springs eternal that perhaps they will mate.

What is new and different is the present British interest to adapt to the European Common Market: Britain may very well accept the metric system while we continue to search for compelling reasons not to do so; and the U.S.—that great champion of science and progress—will then be the last bastion of the English system after even the English have abandoned it.

On 22 January 1963 the ASTM issued a statement on the metric system:

> In a far-reaching policy decision requiring the inclusion of metric equivalents throughout its publications, the American Society for Testing and Materials, the major source for the thousands of standards used by industry for all its basic materials, has taken a position of leadership in expanding the American position in foreign trade by publishing its specifications in a form suitable for worldwide use. Implicit in this action was the realization that U.S. industry faces increasingly stiff competition for markets in countries using the metric system and so must have its specifications also include metric terms. While the Society believes it desirable and necessary that industry be prepared for wider use of the metric system it does not now advocate or recommend any change in presently established values or tolerances, but rather advocates publishing both the present units and their precise metric equivalents. In developing new standards, however, the Society recommends selection of quantities and/or tolerances which will convert to convenient, reasonable metric values.
>
> Adoption of this policy is actually a broadening of a long-time trend toward the inclusion of the metric system in more than sixty years of ASTM standardization activities. Standards established by chemical analysis committees have long been written in metric terms. During recent years metric usage has increased and other committees have adopted formal policies for including metric equivalents. This action by ASTM establishes a society-wide metric policy, but committees are permitted latitude in determining whether metric units alone are to be used, or whether they shall precede or follow the terms now used. Committees writing new standards, where units have not been firmly established, and where minor variations in controlling units are not critical, should be encouraged to select quantities and/or tolerances on these units which will convert to convenient, reasonable metric values. It is desirable that this practice become as completely effective as possible with the publication of the ASTM standards in 1964.

This sounds encouraging: we are told that the paint industry specifies the thickness of a coat of paint in grams per square foot. This specification should provide a genuine challenge to one of the 1964 committees.

John N. Howard

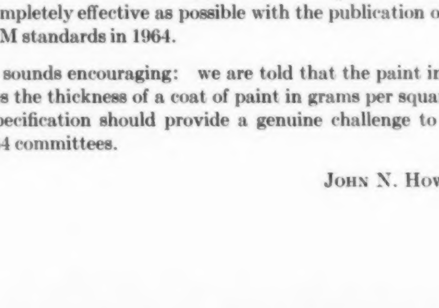

Two OSA editors—John N. Howard *Applied Optics* (left) and Deane B. Judd *Journal of the Optical Society of America*.

**December 1966 features OSA Half-Century!**

# Absorption Coefficients of Krypton in the 600 to 886 Å Wavelength Region

R. E. Huffman, Y. Tanaka, and J. C. Larrabee

The total absorption coefficients, or cross sections, of krypton have been measured with a photoelectric technique in the 600 to 886 Å wavelength region. In contrast to most earlier measurements, a helium continuum was used as background rather than a line source, and it was therefore possible to study all wavelengths within the range 600 to 1100 Å with a resolution of 0.5 Å. With this resolution, it was possible to measure the absorption coefficients of the autoionized lines which belong to the two series $p^6\,{}^1S_0 - p^5({}^2P_{1/2})ns'$ and $p^6\,{}^1S_0 - p^5({}^2P_{1/2})nd'$ and which occur between the two ionization limits, $4p^5\,{}^2P_{3/2}$ at 886 Å and $4p^5\,{}^2P_{1/2}$ at 845 Å. At wavelengths below the ionization threshold at 845 Å, the ionization continuum was found to be almost constant in intensity, but it showed a slight decrease below 725 Å. At the edge of the continuum (845 Å), the absorption coefficient was 1370 $\text{cm}^{-1} \pm 10\%$.

## Introduction

Cuthbertson[1] discovered strong absorption by the rare gases at wavelengths below 1000 Å. Beutler[2] obtained absorption spectra for argon, krypton, and xenon in this region. He not only made an analysis of the observed lines but also observed unusually strong and diffuse features in some of the member lines of the two Rydberg series which converge to the ${}^2P_{1/2}$ states of the respective ions, namely, $3p^5\,{}^2P_{1/2}$ ($\text{Ar}^+$), $4p^5\,{}^2P_{1/2}(\text{Kr}^+)$, and $5p^5\,{}^2P_{1/2}(\text{Xe}^+)$. The diffuseness of the lines is attributed by him to the effect of autoionization. More recently, krypton has been studied by Pery-Thorne and Garton.[3] They calculated the $f$ values of the autoionized lines from absorption data obtained photographically using the helium continuum as background. Also, absorption coefficients of the ionization continua were obtained at a number of wavelengths using photoelectric detection combined with continuum radiation from a flashtube.

We have recently developed a photoelectric scanning technique for measuring absorption coefficients of gases in the vacuum ultraviolet. This method is based on an intense, stabilized Hopfield helium continuum light source which is usable in the wavelength range 580 to 1100 Å. Using this technique we have measured the absorption coefficients of the autoionized lines of krypton and calculated their $f$ values. Also, we have measured the absorption coefficients of the ionization continua of krypton.

## Experimental

### Apparatus

A schematic diagram of the equipment used is shown in Fig. 1. Helium continuum radiation from the source is dispersed by the vacuum monochromator and passes through the absorption cell located behind the exit slit. At the end of the cell, the relative intensity is measured with a sodium salicylate-photomultiplier detector. This relative intensity is recorded as a function of wavelength first with an empty cell then with a known density of sample gas in the cell. From these measurements the absorption coefficients are calculated. A description of the apparatus used and procedures followed is given below.

The light source is a mildly condensed discharge through helium operated at a pressure of about 40 mm Hg as shown in Fig. 1. It produces the Hopfield continuum[4] in the wavelength region 580 to 1100 Å with sufficient intensity for photoelectric measurement at a resolution of 0.5 Å (100-μ slits). The π-shaped quartz discharge tube is triggered with an air-blown spark gap irradiated with a quartz mercury lamp. The pulse repetition frequency is about 4.5 kc/sec. Recorder traces of the intensity have 3–4% noise and a slow drift of about 3% in the main intensity level over a 5-hr period, after suitable warmup. The scattered light intensity is small over most of the wavelength region.

---

The authors are with the Air Force Cambridge Research Laboratories, Bedford, Massachusetts.

Received 29 January 1963.

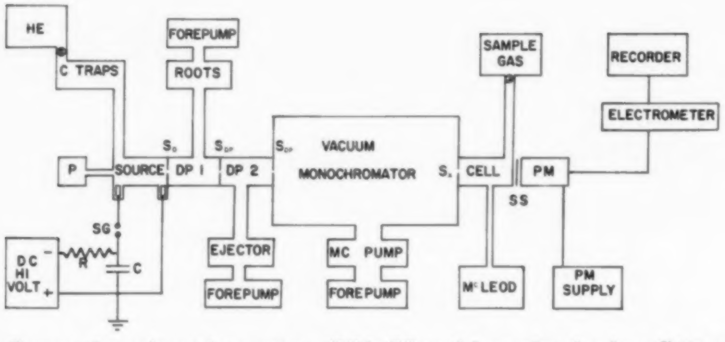

Fig. 1. Schematic block diagram of experimental apparatus. DP is differential pumping chamber; C traps are charcoal traps cooled with liquid nitrogen; SS is sodium salicylate phosphor; PM is photomultiplier; P is pressure gauge.

A more complete description of the light source itself will be published elsewhere in the near future.[5]

A normal incidence McPherson vacuum monochromator, equipped with differential pumping between the entrance slit and the main chamber was used with a 1200 line/mm, $MgF_2$ coated, Bausch & Lomb concave replica grating (radius 2.218 m, blazed at approximately 1500 Å). The differential pumping enabled the discharge tube to be operated without a window at pressures of up to 1 atm with about 1-$\mu$ Hg pressure in the monochromator.

The absorption cell and photomultiplier are mounted behind the monochromator exit slit. Tubing connections through the cell wall provide for sample gas flow into the cell and for pressure measurement with a suitably trapped McLeod gauge. No window is used in the entire light path, and the cell is constructed in such a way that the sample gas can only flow through the exit slit into the monochromator. The combination of the narrow slit and the high-speed pumping of the monochromator enables pressures of up to 2 mm Hg to be maintained in the cell, although in the present case the highest pressure used was 0.2 mm Hg. The residual sample gas pressure in the monochromator was not large enough to cause a significant error in the absorption coefficient measurement, and it was neglected in the calculation. The absorption cell pressure calibration necessary due to gas flow is described later in this section. The light path through the cell was 10.25 cm. The end of the absorption cell was sealed with an O-ring held by a glass disk coated on the front surface with sodium salicylate, which fluoresces under vacuum ultraviolet radiation. An end window photomultiplier (EMI 9514B) located immediately behind the glass window detects this fluorescent radiation. The photocurrent from the multiplier was measured with a Victoreen electrometer, Model VTE-1, and displayed on a Sargent MR potentiometric recorder. The sample gas used was assayed reagent grade krypton (impurities less than 130 ppm) prepared by the Air Reduction Company.

## Procedure

The data were obtained using the following procedure. The light source and detection equipment were allowed to warm up for about two hours. Then, an incident intensity ($I_0$) scan was made over the wavelength region of interest at a suitably slow monochromator scanning rate. Next, krypton was allowed to flow through the sample cell until the desired equilibrium pressure was obtained. Then the previous wavelength region was rescanned on the same recorder chart using a different colored pen to record the transmitted intensity ($I$). Pressure measurements were made several times during this scan to check on possible variations in the flow rate. After this scan the gas flow was stopped and a second incident intensity ($I_0$) trace in a third color was placed on the chart. The entire procedure required about 90 min, and only recorder charts showing little or no drift between the two $I_0$ scans were analyzed. There was no significant wavelength shift among the scans. The multiplier signal was placed at zero on the chart between successive scans by means of a bucking current, which effectively removes the photomultiplier dark current from the recorded trace.

## Calculations

The absorption coefficient $k$, in cm$^{-1}$, was calculated from the preceding data by use of the familiar equation

$$k = (1/L)(760/P)(T/273)\ln(I_0/I), \qquad (1)$$

where $I_0$ and $I$ are the incident and transmitted light intensity, respectively, $L$ is the absorption path length in cm, $P$ is the gas pressure in mm Hg, and $T$ is the gas temperature in °K. The total absorption cross section $\sigma$, in cm$^2$, is a frequently used equivalent expression for absorption data and is equal to $k/n_0$, where $n_0$ is Loschmit's number, $2.69 \times 10^{19}$ cm$^{-3}$. The $I_0$ and $I$ values on the recorder scans were read at equal divisions along the chart and placed on punched cards. These divisions were spaced close enough so that several readings were taken in each resolution interval of 0.5 Å. This close spacing of the readings reduces the effects of random noise and enables the structure of the autoionized lines to be readily obtained. The absorption coefficients, $k$, were calculated, averaged, and plotted automatically from the punched cards. It was found that the data obeyed the absorption law shown in Fig. 2. The three wavelengths shown in this figure were located in the structureless region of the ionization continuum. In the region where the autoionized lines appear (845–886 Å), the measured points were more scattered than in Fig. 2, but the results were generally satisfactory.

The wavelength scale was obtained from impurity lines of Ne I and H primarily, which are superimposed on the helium continuum traces. A least-squares calculation of the chart locations and the known wavelengths of these lines showed that the wavelength drive was linear with time and provided the necessary conversion factors from chart position to wavelength. From the results of these calculations, it is estimated that the wavelengths are located to about ±0.1 Å.

### Scattered Light Correction

A small correction for scattered light was made. This correction was approximated with an empty cell by scanning with an LiF filter placed directly in front of the sodium salicylate phosphor, while operating the light source under exactly the same conditions as used in the absorption measurements. The scattered light thus found is small and almost constant in intensity as a function of wavelength. Over most of the present range it is less than 2% of $I_0$. Since a windowless system is used, there is the possibility that higher orders of lower wavelength radiation may cause errors in using the present technique. With grazing incidence monochromators the problem would be especially acute. However, in using a normal incidence-type instrument such radiation would be very weak, particularly in using the present light source because helium strongly absorbs radiation below 504 Å, the He ionization threshold. This expectation is confirmed by photoelectric scans as well as spectra taken below 500 Å.

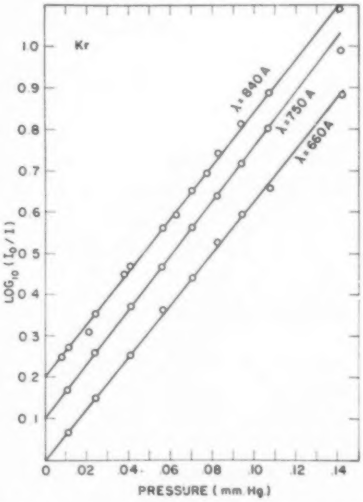

Fig. 2. Plot of $\log_{10}(I_0/I)$ against krypton sample pressure showing agreement with absorption law. Data for wavelengths in ionization continua below 845 Å. In order to separate data, ordinate zero shifted by 0.1 and 0.2 for 750 and 840 Å curves, respectively. Pressures are as recorded before correction.

### Pressure Correction

Probably the largest source of error in the present measurements results from the pressure gradient which occurs along the absorption path in the flow cell. A correction for this pressure gradient has been made by obtaining absorption data with this flow cell for gases having known absorption coefficients. The correction was made by measuring the absorption coefficients of oxygen throughout the well-known Schuman-Runge continuum[6] using impurity lines in the helium discharge as the background light source. Measurements were made at twelve wavelengths between 1350 and 1550 Å and at several pressures. As a check at the lower pressures, measurements were also made of an intense band of $CO_2$ at 1122 Å[7] using the argon continuum as background. Absorption coefficients obtained by Watanabe and associates[6,8] using cells sealed with LiF windows were used as a reference. As a result of the correction, the calculated absorption coefficients were all increased by the factor 1.15. It is thought that the pressure error after this correction is reduced to around 5%.

## Results

### Autoionized Lines: 845–886 Å

The absorption coefficient plot of the autoionized diffuse lines of krypton in the region between the two ionization thresholds, ($Kr^+$), $4p^5\,{}^2P_{3/2}$ (885.62 Å) and ($Kr^+$), $4p^5\,{}^2P_{1/2}$ (845.07 Å) is shown in Fig. 3. An absorption spectrum of krypton in the same region is also reproduced in Fig. 4. These lines* have been previously assigned to the series $4p^6\,{}^1S_0 - 4p^5({}^2P_{1/2})ns'$ and $4p^6\,{}^1S_0 - 4p^5({}^2P_{1/2})nd'$.[2,9] The two series overlap and only the first three autoionized "lines" are partially resolved. The "lines" are asymmetrically broadened, that is, broadened much more on the short wavelength side of the peak than on the long wavelength side. On close inspection of the curve, as well as the spectrograms, it appears that the $d'$-series is broadened very much more than the $s'$-series. This is clearly observable in Fig. 4. The appearance of the ${}^2P_{3/2}$ threshold at 886 Å is interesting. The absorption curve does not level out into the relatively flat plateau as expected for ionization continua and observed in the other continuum associated with the ${}^2P_{1/2}$ threshold at 845 Å. Instead, it rises sharply and then falls rapidly as it approaches the first autoionized peak.

---

* Moore's designation (see ref. 9) for these levels are $ns'\,[0\tfrac{1}{2}]^{\circ}_{1}$ and $nd\,[1\tfrac{1}{2}]^{\circ}_{1}$, respectively.

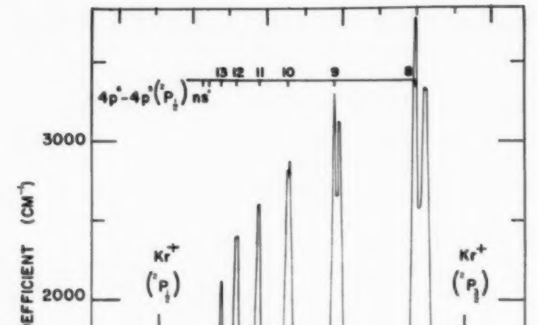

Fig. 3. Absorption coefficients of krypton between 840 and 886 Å showing two overlapping series of autoionized lines converging to the $^2P_{1/2}$ threshold of $Kr^+$. Resolution is 0.5 Å. Average of five measurements over range 0.008 to 0.080 mm Hg. The symbol $m$ in $d'$ series refers to principal quantum number.

Figure 3 is the averaged curve based on five scans over an observed pressure range of 0.080 to 0.008 mm Hg. The charts were read every 0.086 Å, making a total of six readings per bandwidth of 0.5 Å. A pressure effect was noticed only on the first few members of the $s'$-series. In fact, at the higher pressures, the $n = 8$ member of the $s'$-series was not as strong as the nearby $n = 6$ member of the $d'$-series lines, while at lower pressures it became stronger. The $d'$-series lines showed no pressure effect. Thus, the maximum $k$ values of the $s'$-series lines are not known as accurately as the rest of the curve. With the exception of these peaks, the absorption coefficients are estimated to be known within 10%, as discussed more fully in the next section.

Although the autoionized peaks are much broader than the instrumental bandwidth, it is difficult to obtain meaningful oscillator strengths because of the superimposed ionization continuum. Also, configuration interaction effects (see Discussion) may significantly lower the continuum level between the peaks. For these reasons, two types of measurements were done. In the first set of measurements the autoionized peaks were separated from the continuum by drawing straight lines between the minima. This is the most logical intuitive procedure in the absence of further information, and it provides values which may be compared with earlier measurements done in a similar manner.[3] These oscillator strength values are shown in Table I. In addition, a total oscillator strength measurement was made which is more suitable for theoretical analysis. In this case the wavelength region was divided into sections by drawing lines from the absorption minima to the base line in the $k$-value curves. The measurements and wavelength limits are given in Table II. The values given in Tables I and II were obtained from the usual expression[10]

$$f = 4.19 \times 10^{-8} \int_{\nu_1}^{\nu_2} k_\nu d\nu, \qquad (2)$$

with $k$ and $\nu$ measured in $cm^{-1}$. The integral was evaluated by measuring the areas under the peaks previously described with a planimeter.

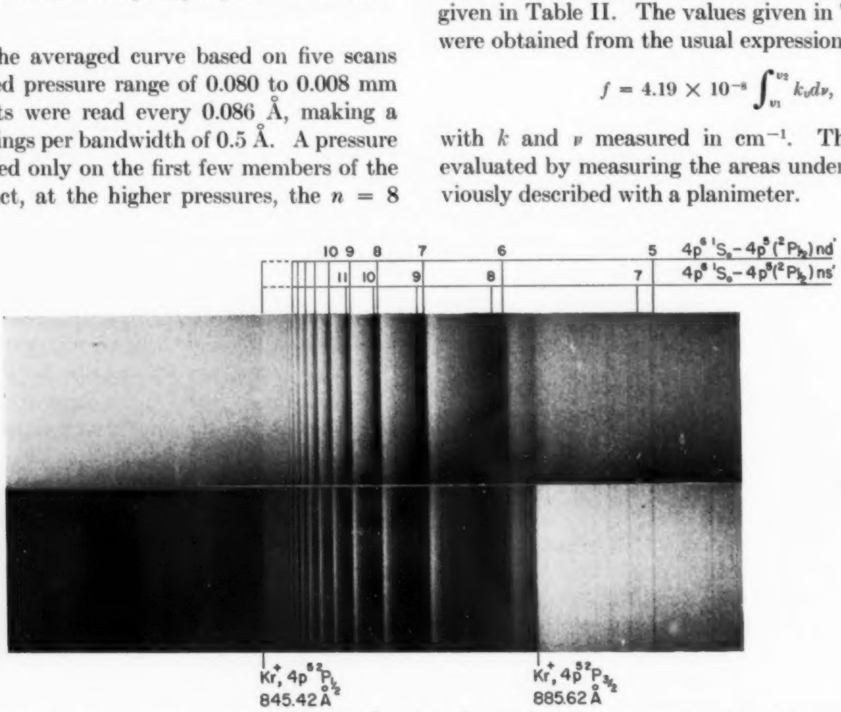
10 9 8 7 6 5
$4p^6\,{}^1S_0-4p^5(^2P_{1/2})nd'$
11 10 9 8 7
$4p^6\,{}^1S_0-4p^5(^2P_{1/2})ns'$
$Kr^+, 4p^5\,{}^2P_{1/2}$
845.42 Å
$Kr^+, 4p^5\,{}^2P_{3/2}$
885.62 Å

Fig. 4. Absorption spectrum of Kr in the region between 900 Å and 800 Å. This spectrum was taken with a 2-m normal incidence type spectrograph equipped with a 600 lines per mm grating. The background is He-continuum. Pressure of Kr in the spectrograph; top: ~ 0.5 $\mu$; bottom: ~ 10 $\mu$.

Approximate lifetimes for the autoionized states are given in Table III. The lifetimes are between 1 and $4 \times 10^{-14}$ sec and increase toward higher members of the series. The values given are quite approximate, due to the asymmetrical shape of the lines, and are more representative of the broader *d*-series.

## Ionization Continua: 600–845 Å

At wavelengths below 845 Å, absorption continua associated with the $^2P_{3/2}$ and $^2P_{1/2}$ states of $\mathrm{Kr}^+$ are superimposed. The absorption coefficients in this region are shown in Fig. 5, where individual measurement points are used. These points are the average values of 8 measurements over a pressure range of 0.021 to 0.14 mm Hg. The absorption coefficients shown in Fig. 5 begin at the $^2P_{1/2}$ threshold and fall on a smooth, almost constant curve. There is a broad maximum at about 725 Å and then the curve falls slowly toward the lowest wavelengths available. Points measured near emission lines generally tend to be more scattered, because of slight misalignments between the $I_0$ scans, and these points have not been included in Fig. 5. Consequently, in Fig. 5, one can see several gaps where impurity emission lines in the source are located, for example, the neon resonance lines at 736 and 744 Å. It appears in the figure that there are two broad absorption peaks at about 605 and 613 Å. However, the background helium continuum is weak in this region, making the possible error in each point about as large as the observed peaks. Also it is difficult to identify these broad peaks from the original recorder charts, possibly because they are diffuse and background intensity is weak. Therefore, it is possible that these peaks are caused by series of fortuitous random errors. With this possible exception, no discrete absorption or threshold could be observed on the original recorder charts or in the reduced data. The small irregularities in Fig. 5 are thought to be due to random scatter.

**Table I. Krypton Oscillator Strengths Obtained by Drawing Straight Lines between Minima in *k*-Value Curves (Fig. 3)**[a]

| λ av (Å) | *ns′* | *nd′* | *f* | Measurement precision |
|---|---|---|---|---|
| 880 | 8 | 6 | 0.0666 | 0.0027 |
| 869 | 9 | 7 | 0.0378 | 0.0017 |
| 863 | 10 | 8 | 0.0227 | 0.0012 |
| 858 | 11 | 9 | 0.0130 | 0.0011 |
| 856 | 12 | 10 | 0.0083 | 0.0008 |
| 854 | 13 | 11 | 0.0052 | 0.0009 |
| 852 | 14 | 12 | 0.0030 | 0.0005 |
| 851 | 15 | 13 | 0.0017 | 0.0005 |
| Σ | | | 0.158 | 0.009 |

[a] Peaks are autoionized lines in the overlapping series $4p^6\,{}^1S_0 - 4p^5({}^2P_{1/2})nd'$ and $4p^6\,{}^1S_0 - 4p^5({}^2P_{1/2})ns'$. Values given are averages from five experiments at observed pressures of 0.008, 0.021, 0.038, 0.063, and 0.080 mm Hg.

**Table II. Krypton Total Oscillator Strength Values Obtained by Drawing Lines from Minima to Base Line in Fig. 3**

| λ av (Å) | Upper λ of region | *f* | Remarks |
|---|---|---|---|
| — | 886.5 | 0.0087 | $^2P_{3/2}$ threshold maximum |
| 880 | 883.2 | 0.0934 | |
| 869 | 871.1 | 0.0529 | |
| 863 | 864.0 | 0.0341 | |
| 858 | 859.5 | 0.0237 | |
| 856 | 856.4 | 0.0180 | |
| 854 | 854.3 | 0.0121 | |
| 852 | 852.6 | 0.0077 | |
| 851 | 851.5 | 0.0060 | |
| — | 850.6<br>845.9 | 0.0300 | Unresolved region to $^2P_{1/2}$ threshold |
| Σ | | 0.287 | |

## Discussion

It is estimated that all absorption coefficient values given in this paper are known to ±10% on the basis of the following considerations: The two significant errors are caused by the fluctuations in the light source intensity and by the pressure gradient along the absorption path length. The sample pressures were chosen so that $I/I_0$ was generally between about 0.65 and 0.15, which is roughly the optimum range for spectrophotometry from published error curves.[11] Also from these curves, it can be determined that the fluctuation of roughly ±1.5% observed for $I_0$ would give an uncertainty of ±5% after taking the logarithm of $I_0/I$. The pressure error is more difficult to estimate and is probably larger. As mentioned in the experimental section, a correction for the pressure gradient was made using gases of known absorption coefficient. This certainly reduces the pressure uncertainty, but it still is felt to be roughly ±5%. Thus, the total estimated error is about ±10%. The precision is considerably better, ranging from 1.5% between 700 and 845 Å to 5% at wavelengths near 600 Å, based on data at fixed wavelengths from the 8 scans used in Fig. 5.

The results of this investigation can be compared with the measurements of Pery-Thorne and Garton.[3] They obtained *f* values of the autoionized lines by

**Table III. Lifetimes of Autoionized Krypton Levels**

| λ av (Å) | Upper states and transitions | Half-width (Å) | $\tau (10^{-14}\,\mathrm{sec})$ |
|---|---|---|---|
| 880 | $4p^6\,{}^1S_0 - 4p^5\,6d'$<br>$4p^6\,{}^1S_0 - 4p^5 8s'$ | 2.7 | 1.5 |
| 869 | $4p^6\,{}^1S_0 - 4p^5 7d'$<br>$4p^6\,{}^1S_0 - 4p^5 9s'$ | 2.0 | 2.0 |
| 863 | $4p^6\,{}^1S_0 - 4p^5 8d'$<br>$4p^6\,{}^1S_0 - 4p^5 10s'$ | 1.3 | 3.0 |
| 858 | $4p^6\,{}^1S_0 - 4p^5 9d'$<br>$4p^6\,{}^1S_0 - 4p^5 11s'$ | 1.0 | 3.9 |

photographic photometry using the Hopfield helium continuum as the source. They did not include the observed ${}^2P_{3/2}$ continuum in their measurements, and so their values can be compared with our measurements in Table I, where the peaks were defined by drawing straight lines between the minima. The total $f$ values for the autoionized lines (first 8 peaks) found by them was 0.101, which is to be compared with the present value of 0.158. Considering the experimental errors and the usually large differences in this type of measurement, this is thought to be fairly good agreement. Both $f$-value measurements are uncertain, however, because of the effects of configuration interaction between the autoionized lines and the continuum, as discussed recently by Fano.[12] This theory predicts that autoionized lines in general will be quite asymmetrical in shape and that in the vicinity of such lines the absorption coefficient curve will have deep minima (or even become zero in some other cases). It is apparent that the absorption coefficient curve presently measured (shown in Fig. 3) exhibits qualitatively the behavior predicted by the theory. If configuration interaction effects are strong, the minima between the autoionized peaks will not be the ${}^2P_{3/2}$ continuum, and the oscillator

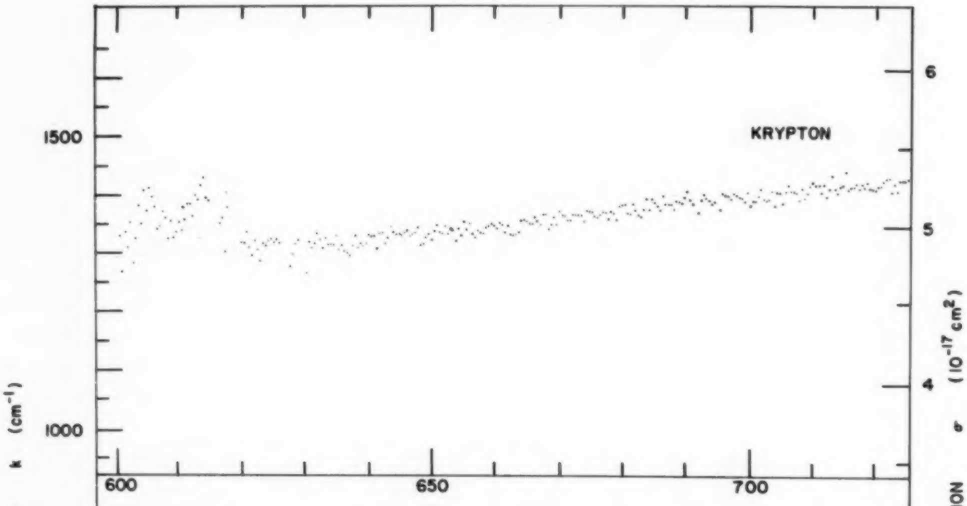

Fig. 5. Absorption coefficients of krypton between 600 and 845 Å (${}^2P_{1/2}$ threshold). Resolution is 0.5 Å. Average values from eight measurements over pressure range 0.021 to 0.14 mm Hg. Diffuse peaks at 605 and 613 Å are roughly within precision of measurement and may be fortuitous errors.

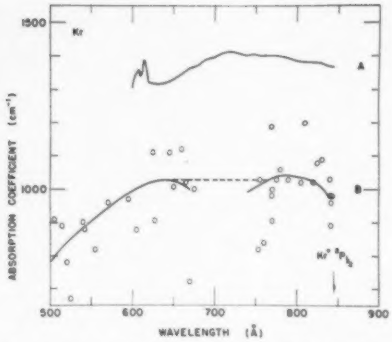

Fig. 6. Comparison of absorption coefficients in ionization continua. Curve A, this investigation; curve B and points, Pery-Thorne and Garton.[3]

strengths will be in error. Because of this possibility, the total oscillator strengths between the absorption minima are also given (Table II). Further measurements over different wavelength ranges may of course be obtained from Fig. 3. It is anticipated that the data given here may be analyzed further theoretically to provide more insight into this problem.

Using a photoelectric technique and the flashtube continuum as background, Pery-Thorne and Garton[3] measured absorption coefficients of the ionization continuum of Kr at a number of points between 845 and 500 Å. Our measurements of the same continuum reported here are larger than their values. The two sets of absorption coefficient measurements are shown in Fig. 6 for comparison purposes. At the $^2P_{1/2}$ threshold edge, the previous measurement was $1120 \pm 200$ cm$^{-1}$, while in the present case the best average value of all data is $1370 \pm 140$ cm$^{-1}$. Over the range 845 to 600 Å they find that the absorption coefficient is constant and equal to about 1050 cm$^{-1}$, which can be compared with the higher values in Fig. 5. There is a gap in their measurements between 660 and 750 Å, where the light intensity was too weak for good measurements. Because of this gap and the scatter in the points, it is not possible to observe in their data the broad maximum at about 725 Å which we observed. Their absorption coefficients decrease monotonically at wavelengths below 600 Å. This is compatible with the slowly decreasing absorption coefficients observed in our data (Fig. 6). In addition, we observed the two peaks at 605 and 613 Å which were not observed by them.

Calculations of $n - 1$ ($n$ is refractive index) at 2303 Å from the vacuum ultraviolet absorption data made by Pery-Thorne and Garton[3] accounted for only about 70% of the measured $n - 1$ value. Only an approximate calculation is feasible with our data because of the present wavelength range, but using our larger absorption coefficients given here such an approximate calculation gives almost 90% of the observed $n - 1$ value.

Recently, theoretical calculations of the krypton absorption coefficients have been given by Cooper.[13] The calculation extends from the $^2P_{1/2}$ threshold at 845 to 100 Å. At the $^2P_{1/2}$ threshold his value is about two times larger than our measurement. At shorter wavelengths the calculated values drop abruptly and at 600 Å are roughly half our values. It is difficult to speculate about the shape of the continuum between the two ionization thresholds because of strong interaction between the $d'[1^1/_2]^\circ$ states and the continuum state associated with the $^2P_{3/2}$ state of Kr$^+$. The absorption maximum observable in Fig. 3 near 886 Å is possibly the result of configuration interaction involving the $n = 5$ member of the $d'$-electron series located at a wavelength of 903.06,[9] or slightly longer than the $^2P_{3/2}$ ionization threshold. This peak would thus be the "tail" of the broadened line. Another possibility is that the maximum is the result of configuration interaction with the first autoionized peak.

The rare gases are monatomic rather than molecular, and it is usually considered that the only absorption process contributing to the rare-gas continua is photoionization. Thus, the photoionization efficiency, or the number of electrons formed per photon absorbed, is assumed to be unity in these continua. It is, therefore, possible to make convenient absolute intensity measurements by using the rare gases in an ionization chamber and the measured total absorption cross sections (such as given here) rather than by using the difficult thermocouple technique. It is possible that the efficiency is less than unity in the region of the autoionized lines. However, thermocouple measurements of xenon in the 1023 to 850 Å region[8] have indicated that the efficiency is unity to within 10% in the autoionized lines also.

## References

1. C. Cuthbertson, Proc. Roy. Soc. (London) **A114,** 650 (1927).
2. H. Beutler, Z. Phys. **93,** 177 (1935).
3. A. Pery-Thorne and W. R. S. Garton, Proc. Phys. Soc. (London) **76,** 833 (1960).
4. J. J. Hopfield, Astrophys. J. **72,** 133 (1930); Y. Tanaka, Sci. Papers Inst. Phys. Chem. Res. (Tokyo) **39,** 465 (1942); Y. Tanaka, A. S. Jursa, and F. J. LeBlanc, J. Opt. Soc. Am. **48,** 304 (1958).
5. R. E. Huffman, Y. Tanaka, and J. C. Larrabee, Appl. Opt. **2,** 617 (1963).
6. E. C. Y. Inn, K. Watanabe, and M. Zelikoff, J. Chem. Phys. **21,** 1648 (1953).
7. Y. Tanaka, A. S. Jursa, and F. J. LeBlanc, J. Chem. Phys. **32,** 1199 (1960). Two very strong absorption bands (1129 Å and 1122 Å) have been observed.
8. K. Watanabe and F. F. Marmo, J. Chem. Phys. **25,** 965 (1956).
9. C. E. Moore, "Atomic Energy Levels," Natl. Bur. Std. Circ. 467, Vol. 2 (1952).
10. V. J. Hammond and W. C. Price, Trans. Faraday Soc. **51,** 605 (1955).
11. T. R. Hogness, F. P. Zscheile, Jr., and A. E. Sidwell, Jr., J. Phys. Chem. **41,** 379 (1937).
12. U. Fano, Phys. Rev. **124,** 1866 (1961), and references given therein.
13. J. W. Cooper, Phys. Rev. **128,** 681 (1962).

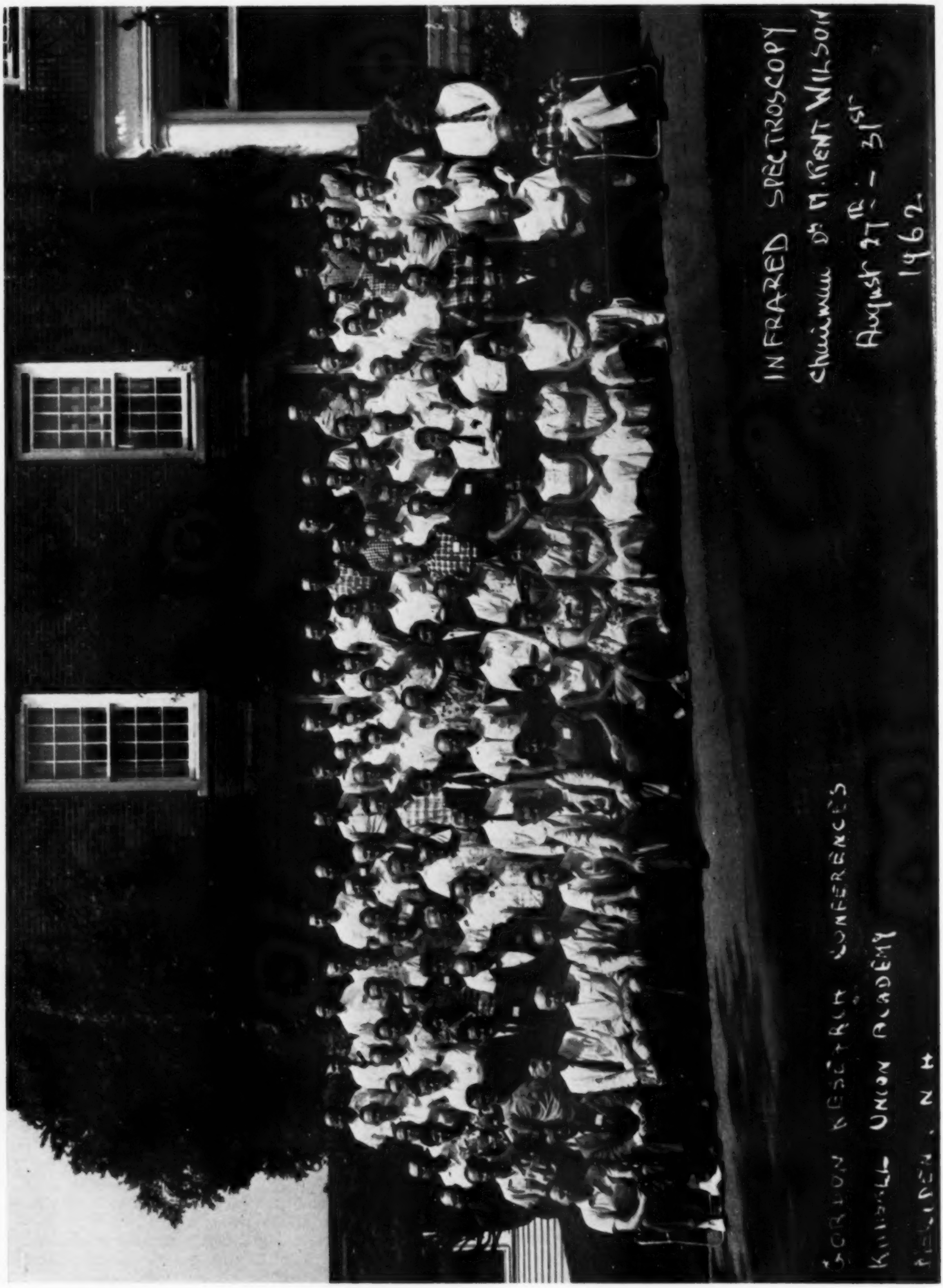
INFRARED SPECTROSCOPY
Chairman Dr. M. Kent Wilson
August 27th – 31st
1962
GORDON RESEARCH CONFERENCES
KIMBALL UNION ACADEMY
MERIDEN, N.H.

# Performance of Curved Crystals in the Range 3 to 12 A

J. L. Jones, K. W. Paschen, and J. B. Nicholson

A number of diffracting crystals are available for use in x-ray fluorescence spectroscopy. The choice of those best suited for any given analytical problem depends upon the reflectance for the wavelength of interest, and, also, upon the ability to discriminate against unwanted radiation. These characteristics were explored experimentally, and the results are presented in a form which can be interpreted readily for use with curved crystal spectrometers.

## Introduction

X-ray fluorescence spectroscopy has been in use for a number of years and has become a standard tool, rivaling optical emission techniques for many types of work. Nondispersive methods are useful for many problems,[1] but the analysis of reasonably complex materials is best carried out with spectrometers employing large single crystals as x-ray gratings.

Although some use has been made of crystals in transmission,[2] opacity to long wavelengths has made the reflection technique by far the most used. Flat crystals,[3] having collimators to parallelize x rays, and curved crystals, providing focusing geometry, are both in general use.

Curved crystals of the Johansson[4] type provide some real advantages in instruments to be used for routine analytical work. A large number of crystal spectrometers can be nested to provide simultaneous study of a number of elements,[5] allowing optimum choice of crystals for each wavelength of interest. Also, for use in the electron microprobe x-ray analyzer, the use of curved crystals becomes essential.[6–8]

For more comprehensive discussions of the use of crystals for x-ray spectroscopy, the reader should refer to the books by Liebhafsky *et al.*[9] and by Birks.[10]

Limitations on the resolution and reflectivity of curved crystals have been discussed by Johansson,[4] Wilsdorf,[11] and others, but the need of the spectroscopist for a readily interpreted means for choosing crystals has not been met. The purpose of this paper is to present data representative of a number of crystals in a form appropriate to the conditions under which they are used.

## Curved Crystal Spectrometer

The Johansson type of crystal spectrometer is illustrated in Fig. 1. The planes of the crystal are curved to radius $R$ and the surface is ground to half of $R$ or $r$. Radius, $r$, describes a circle similar to the Rowland circle of spherical grating geometry. A point source at A, if considered only in the plane of the figure, will be perfectly imaged at C, in accordance with the Bragg relationship,

$$\sin\theta = n\lambda/2d,$$

in which $\theta$ is the complement of the angle of incidence to the *crystal planes*, $n$ is the order number, $\lambda$ is wavelength, and $d$ is the spacing of the planes in depth.

In the practical situation, there are a number of factors which prevent the realization of perfect focus. We will discuss these briefly, since they are responsible for some of the characteristics observed in the present study. The effect of transparency of the crystal is illustrated in Fig. 2. Any ray which, instead of being diffracted at the surface at point, p, is diffracted at p′ within the crystal and returns to C, must have a longer wavelength than that calculated for A, p, and C. In other words, if a line is scanned, which has the calculated wavelength, the peak will be broadened asymmetrically on the short wavelength side. The importance of this effect is limited to the shorter wavelengths and the more transparent materials. If the depth of penetration does not exceed about 0.1% of the focusing circle radius, the effect upon line shape is difficult to measure. On the other hand, it is a factor which does contribute to the minimum line-width obtainable.

The use of cylindrical optics and slits of finite length imposes an additional limit on the resolution. So far, the discussion has been confined to rays which proceed

---

The authors are with Applied Research Laboratories, Inc., Glendale 7, California.

Received 31 January 1963.

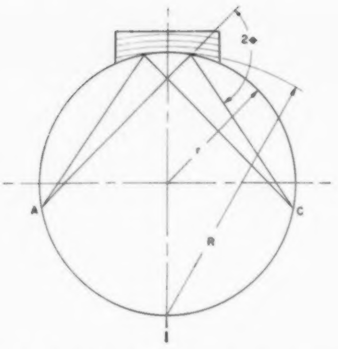

Fig. 1. Optical diagram of Johansson curved crystal spectrometer.

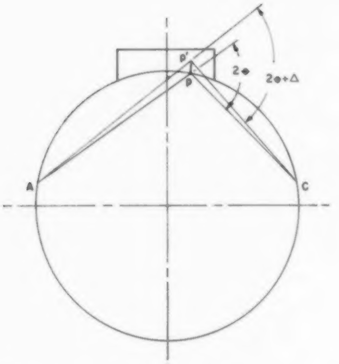

Fig. 2. Effect on resolution caused by transparency of crystal to radiation.

parallel to the optical plane. Since radiation passing through the primary slit is not restricted to this parallel direction, rays which make an angle to this plane must be considered. Figure 3 illustrates a somewhat generalized case of such a ray. The ray *ApC* is representative of the original parallel case. If a ray originates at A′ and strikes the crystal at a point p′, directly over p, it can then fall on point C′, directly over C. The Bragg angle, in this case, will be smaller than for the parallel ray, since the points A′ and C′ are farther apart than A and C.

The aberrations discussed thus far can occur for a crystal in which the structure is exactly that specified in the Johansson arrangement. In other words, all elements of the crystal are assumed to be in perfect alignment with each other, and the crystal planes are assumed to have common centers of curvature along the cylindrical axis. A real crystal, on the other hand, possesses a "mosaic" structure, in which the microscopic elements are slightly misoriented with respect to each other in a random fashion, but having a maximum displacement which can be measured as the "rocking angle". The magnitude of the mosaic effect varies considerably from one type of crystal to another. In addition to this, macroscopic portions can be misoriented, due to growth imperfections or defects introduced in the bending and grinding operations.

The presence of the mosaic structure introduces another variable which affects resolution. In Fig. 3, one of the conditions for reflection is that the normal to the crystal plane at point p′ is parallel to the optical plane. The presence of the mosaic structure makes it possible for this normal to fall at an angle to the optical plane. Consequently, the ray returning to the secondary slit may now fall at some point other than C′, for example, below C. Thus, the range of wavelengths which can simultaneously be diffracted into the secondary slit is increased. Another effect of the mosaic structure concerns the use of slits which are finite in width.

In Fig. 4, let *ApC* represent the path which would be traced by a ray of a certain wavelength. In a perfect crystal a ray originating at some other point, such as A′, would fall at C′, and would have to have a wavelength differing from that of *ApC*. In the presence of a mosaic structure, however, the ray could begin at A′ and still return to point C. The wavelength for this ray will also be different from that of *ApC*. In addition to this, a ray of the same wavelength as *ApC*, but originating at A′, can return to point C″. If the secondary slit-width is great enough, all of these rays can pass through the system. Aside from the

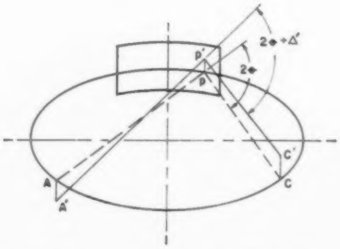

Fig. 3. Effect on resolution caused by vertical divergence in a cylindrical x-ray spectrometer.

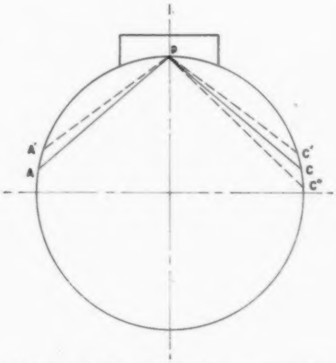

Fig. 4. Effect of finite slit-width on crystal resolution.

### NEW SUBSCRIPTION ORDER

## APPLIED OPTICS

Please enter my/our subscription* and continue until countermanded:

- ☐ OSA member rate $6.00 per year
- ☐ Other AIP Societies' rate $8.00 per year
- ☐ Regular rate $10.00 per year
- ☐ Please send OSA membership information
- ☐ check enclosed ☐ bill me
- ☐ Single copy of issue ........................................ $2.00

Name ........................................................ Membership No. ..............................

Address ...................................................................................................

...................................................................................................

*Subscriptions entered for calendar year only.

**Please allow eight weeks for order processing.**

NEW SUBSCRIPTION ORDER

APPLIED OPTICS

Please enter my/our subscription* and continue until countermanded:

- ☐ OSA member rate $6.00 per year
- ☐ Other AIP Societies' rate $8.00 per year
- ☐ Regular rate $10.00 per year
- ☐ Please send OSA membership information
- ☐ check enclosed ☐ bill me
- ☐ Single copy of issue ........................................ $2.00

Name ........................................................ Membership No. ..............................

Address ...................................................................................................

...................................................................................................

*Subscriptions entered for calendar year only.

Please allow eight weeks for order processing.

**FIRST CLASS**
Permit No. 18297
New York, N. Y.

**BUSINESS REPLY MAIL**
No postage stamp necessary if mailed in the U. S. A.

POSTAGE WILL BE PAID BY

**APPLIED OPTICS**
American Institute of Physics
335 E. 45th Street
New York 17, N. Y.

**FIRST CLASS**
Permit No. 18297
New York, N. Y.

**BUSINESS REPLY MAIL**
No postage stamp necessary if mailed in the U. S. A.

POSTAGE WILL BE PAID BY

**APPLIED OPTICS**
American Institute of Physics
335 E. 45th Street
New York 17, N. Y.

n a

loss of
that th
wavel
flectio
The
used i
ment.
of the
tends
Althou
values
crysta
consta
Fro
resolu
crimi
width
its spe
but is
stand
maxi
merit
pends
and
crysta
metho
In
cienc
impo
feren
frequ
be pu
cryst
a gre
this,
able
prov
cryst
They
after
cryst
depe
For
proc
As
betw
the r
pare
This
crys
requ
leng
rela
line
choi

loss of resolution resulting from this, it is also evident that the acceptance of a finite bundle of rays of a single wavelength is a necessary condition for having a reflection intensity greater than zero.

The degree of monochromaticity of the radiation used in making measurements also affects the measurement. In other words, the natural spectral line-width of the x-ray lines used is an additional factor which tends to set a lower limit to the measured line-width. Although it would be possible to subtract the known values from the measurements, the comparison of two crystals at the same wavelength contains this as a constant factor.

From the standpoint of the analyst, measurement of resolution becomes a question of the degree of discrimination against a nearby wavelength. The total width of a peak produced by a crystal, as mounted in its spectrometer, provides information of the same sort, but is difficult to measure directly. From a practical standpoint, the Rayleigh criterion (width at half-maximum) provides a readily measurable "figure of merit". The absoluteness of this measurement depends upon the nonexistent qualities of ideal line shape and equal intensities, but unless choices between crystals need to be made with extreme precision, this method provides a usable yardstick.

In choosing crystals for spectroscopy, relative efficiency of diffraction, or speed, may assume a greater importance than resolution. Unless particular interferences exist, the ultimate sensitivity of the analysis frequently depends upon the total radiation which can be put through the system. The basic structure of a crystal, and the reflecting planes chosen for use, have a great deal of influence upon speed. In addition to this, the dislocation pattern affects speed to a remarkable degree. Birks and Seal[12] have studied the improvement due to the introduction of strains in LiF crystals when they are quenched, abraded, or bent. They found intensity increases as high as factors of 10 after plastic bending. Treatment of the surface of a crystal, as by etching, affects speed to a degree which depends upon the transparency of the layer removed. For longer wavelengths, the removal of the effects of processing becomes very important.

Aside from differences of reflectivity which occur between any two individual crystals of a single type, the relative efficiency of crystals of different types, compared to each other, varies as the wavelength changes. This variation results in the need for matching the crystal to the problem wherever optimum results are required. The ability of crystals to diffract wavelengths of higher orders ($n = 1, 2$, etc., in the Bragg relationship), which may be direct interferences on lines of interest, provides another variable in the crystal choice problem. The intensity of reflection of a given higher order, relative to the first, is usually quite different for one type of crystal than for another.

The ease with which the width of the primary and secondary slits may be changed in a curved crystal spectrometer makes it desirable to know not only how resolution varies with slit-width, but also how intensity varies in relation to resolution. This function is, of course, controlled by the variables already discussed. The magnitudes of the vertical divergence and mosaic effects are further modified by the "$d$" spacing of the crystal. This is because the positions of the slits on the focusing circle and, therefore, the distances from slits to crystal, are determined by the "$d$" spacing, as larger "$d$" spacing requires the slits to be closer to the crystal.

Qualitatively, line-width, as measured with a practical spectrometer, will have a definite lower limit, as determined by the factors discussed above. As slit size is increased, these factors will assume a decreasing role and, eventually, the line-width will be largely a function of slit size. Intensity, on the other hand, will have a lower limit of zero. With increased slit-width, intensity will increase, but will reach a finite maximum value determined by the reflectivity of the crystal. The actual slit size at which the maximum is reached will depend upon the magnitude of the rocking angle of the crystal.

So far, the discussion has been confined to the diffraction of specific wavelengths, either that of primary interest or of higher orders. However, the importance of the spectrum background level must not be overlooked. The source of such background lies in the x-ray tube used for excitation and in the nature of the analytical samples, but the ability of the crystal to reject it must be taken into consideration. One component of the background is a combination of "white" and line radiation generated in the x-ray tube and scattered by the sample. The portion of this, which is of the same wavelength as that of primary interest, will, of course, be diffracted as though it originated in the sample, and will not be affected by crystal choice. That portion which is of higher order than the first will be discriminated against in the same way as lines of that wavelength originating in the sample. Another component of the background is radiation of all wavelengths which is directly scattered by the crystal into the secondary slit. The amount of such scatter is a function of the crystal material and its surface treatment. This should not be considered a major factor, since the majority of crystals in use are likely to be very similar in scattering ability, with the possible exception of germanium. A third component of the background is the characteristic fluorescence of the elements composing the crystal. Radiation from the sample of wavelength shorter than the absorption edges of the elements in the crystal will cause excitation of these

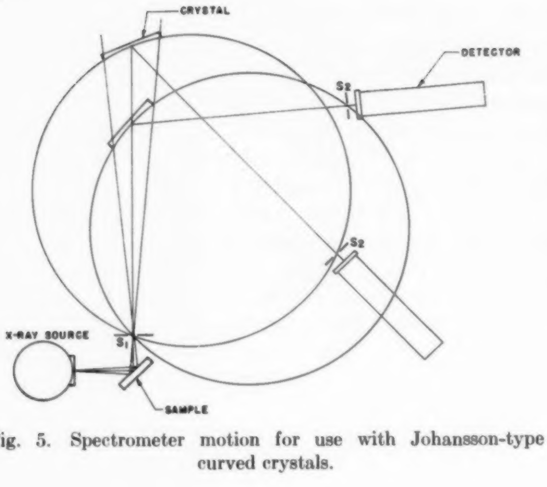

Fig. 5. Spectrometer motion for use with Johansson-type curved crystals.

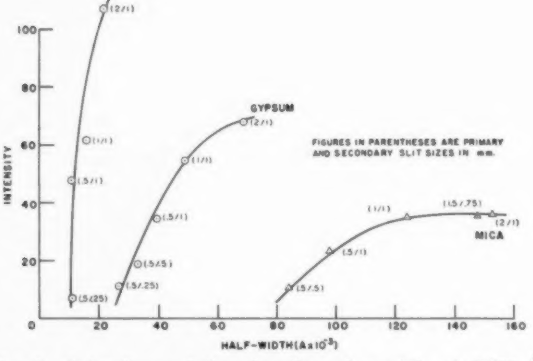

Fig. 6. Intensity-resolution function of crystals at 9.889 Å (Mg$K\alpha$).

elements. The wavelengths from elements of atomic number 9 and below cannot be observed with detectors in routine use at present, and do not constitute a problem. On the other hand, Cl and Si in the crystals can cause a serious rise in background level when a light element is to be analyzed in a matrix of somewhat higher atomic number.

Since the components of the background particularly affected by crystal characteristics consist either of the excitation of the known elements in the crystal, or of higher order reflections, the present study was confined to intensity-resolution comparisons, and to comparisons at higher orders.

## Apparatus and Procedure

The investigations were carried out with a scanning spectrometer of the type shown in Fig. 5. The x-ray tube, sample, and primary slit remain stationary, while the crystal and secondary slit are moved so as to remain on the focusing circle at all times. A lead screw moves the crystal and provides a linear wavelength scale. For scanning, a constant speed motor drive provides a direct wavelength correlation with the trace on a recorder which, coupled with suitable amplifiers, shows a deflection proportional to the output of the detector. Two modes of readout are available, i.e., ratemeter and integration. In the integration mode, the current output of the detector charges a capacitor for a fixed interval of time, after which the voltage on the capacitor is read by an electrometer amplifier. A flexible boot flushed with helium was used to reduce the absorption of the x rays in the optical path.

For the intensity-resolution phase of the experiment, the $K\alpha$ lines of each of the elements, 12 through 22, (except 18, Ar, and 21, Sc) were taken in turn. Each crystal of interest at a given wavelength was aligned, and a scan was made of the characteristic wavelength with each combination of slit sizes used in the experiment. Although it is known that variations occur between individual crystals, one representative crystal

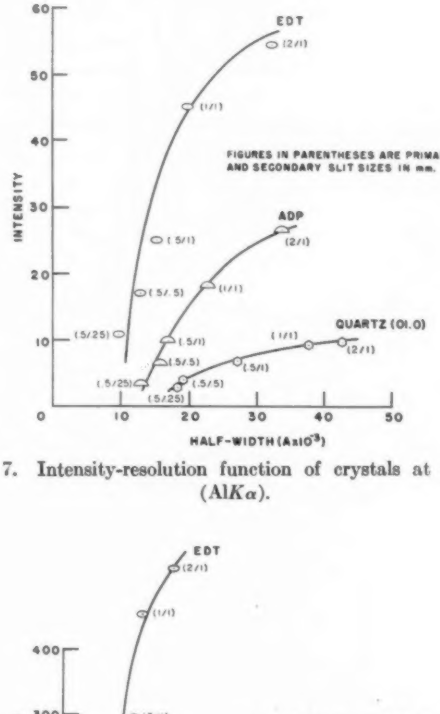

Fig. 7. Intensity-resolution function of crystals at 8.339 Å (Al$K\alpha$).

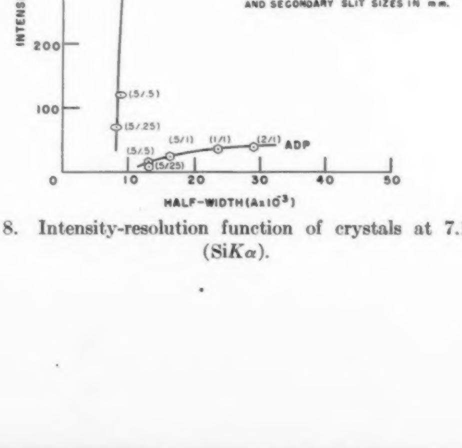

Fig. 8. Intensity-resolution function of crystals at 7.126 Å (Si$K\alpha$).

of each type was chosen for these studies. The range of slit sizes covers those most commonly in use. Peak height above background and width of peak at the half-height (half-width), were plotted. These curves are shown in Figs. 6-14. Figures in parenthesis are primary and secondary slit-widths in millimeters. Experience has shown that the primary slit can be either larger or smaller than the secondary without affecting the results. Consequently, both relationships, as well as equal sizes, were used throughout the experiment. The same sample was used for all runs on any given element, and the excitation conditions were maintained the same where possible. When the dynamic range of the intensity was too great to maintain linearity, or accuracy of measurement, the excitation was modified by a measured amount and the results were normalized by application of the measured ratio. A comparison of crystals at 11.909 Å (Na$K\alpha$) and at 9.889 Å (Mg$K\alpha$) was also made in the electron microprobe x-ray analyzer with one set of conditions only. In this case, the point of impact of the electron probe upon the sample acted as the primary slit ($\sim$1-$\mu$ diam). The secondary slit was 0.25 mm. The results of this study are given in Table I. The results for KAP are the average of values obtained with two crystals.

**Table I. Performance of Crystals at 9.889 Å (Mg$K\alpha$) and at 11.909 Å (Na$K\alpha$) in the Electron Microprobe X-Ray Analyzer**

| Crystal | λ(Å) | Intensity (P − B) | Half-width (A) |
|---|---|---|---|
| ADP[a] | 9.889 | 100 | 0.012 |
| KAP[b] | 9.889 | 275 | 0.016 |
| Mica | 11.909 | 100 | 0.025 |
| KAP | 11.909 | 530 | 0.014 |

[a] Ammonium dihydrogen phosphate.

[b] Potassium acid phthalate.

For the comparison of higher-order reflections, wavelengths were chosen which would provide lines as close as possible to the first-order line without giving a direct interference. For each wavelength studied, a synthetic sample was prepared with enough of each of the chosen elements to provide a measurable intensity. Each crystal, in turn, was mounted, and duplicate integrations were taken of the intensity of each peak and of background. Slit sizes were chosen in the vicinity of the "knee" of the previously taken resolution curves. The peak minus background for each higher order was ratioed to that for the first order. One crystal in each group was chosen as a standard, and all ratios were normalized to those for this crystal, thus, providing a comparison between crystals. These normalized values are given in Table II, as "discrimination factors". A high value indicates a high rejection for this order, compared to a crystal with a lower factor. In some cases, the intensities available under the experimental conditions resulted in no measurable intensity for a particular line. In these cases, the factors are listed as "less than" or "more than" values. Ge and Si are typical examples of this. Rejection of second order is so complete that even a pure sample produces no measurable intensity.

All crystals used in this study were of the Johansson type, except for mica, and were made for use with a focusing circle of 10-cm radius. The mica was a thin plate with a radius of curvature of 20 cm. (Johannsson type[13]).

## Discussion of Results

An examination of the curves of Figs. 6–14, shows a definite lower limit to the half-width for each crystal, as would be expected. As the slits are increased in size, the intensity increases at a relatively rapid rate with very little change in the resolution. At the upper end, however, the curves tend to level off to a maximum intensity. In general, the crystals giving the most intense diffraction, for example, ADP in Fig. 6, show very little leveling off in the range of slit-widths used in this study.

The shape of these intensity-resolution curves can be related in a qualitative sense to the aberrations discussed in the introductory section. The lower limit of half-width for each crystal is chiefly determined by two effects; the nonparallel rays, whose angularity is a function of the distance from slit to crystal,* and the mosaic line broadening. As the slit sizes are increased, the apparent line-width produced by the scanning motion increases without limit.

The intensity function has an obvious lower limit of zero when the slit-widths approach the minimum. The slit sizes at which the upper limit of intensity is reached is dependent upon the relation of the angular

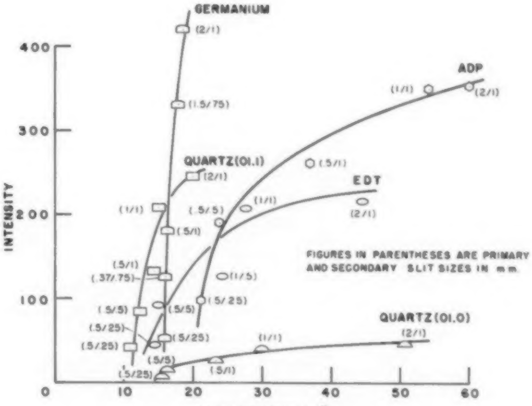

Fig. 9. Intensity-resolution function of crystals at 6.155 Å (P$K\alpha$).

---

* Determined by the crystal "$d$" spacing.

**Table II. Discrimination Factors of Crystals for Orders Greater than $n = 1$**

| Crystal | Plane | λ(Å) | Discrimination factor $n = 2$ | $n = 3$ | $n = 4$ | $n = 5$ |
|---|---|---|---|---|---|---|
| ADP | (101) | 9.889(Mg$K\alpha$) | | | 1.0 | 1.0 |
| Gypsum | (020) | | | | 4.6 | 1.7 |
| Mica | (002) | | | | <1.0 | <0.1 |
| ADP | (101) | 8.339(Al$K\alpha$) | | 1.0 | 1.0 | |
| EDT | (020) | | | 4.0 | 6.0 | |
| ADP | (101) | 7.126(Si$K\alpha$) | | 1.0 | 1.0 | |
| EDT[a] | (020) | | | 3.2 | 8.8 | |
| $SiO_2$ | (01.0) | | | 0.9 | 1.6 | |
| ADP | (101) | 6.155(P$K\alpha$) | 1.0 | 1.0 | 1.0 | |
| EDT | (020) | | 1.7 | 2.8 | 8.6 | |
| $SiO_2$ | (01.0) | | 0.13 | 0.6 | 0.6 | |
| $SiO_2$ | (01.1) | | 0.63 | 21.0 | 18.0 | |
| Ge | (111) | | >38.00 | 0.8 | 1.7 | |
| ADP | (101) | 5.373(S$K\alpha$) | 1.0 | 1.0 | | |
| EDT | (020) | | 3.2 | 6.4 | | |
| $SiO_2$ | (01.0) | | 0.3 | 1.2 | | |
| $SiO_2$ | (01.1) | | 1.4 | >46.0 | | |
| Si | (111) | | >43.0 | 1.6 | | |
| NaCl | (200) | | 4.5 | 15.0 | | |
| Ge | (111) | | 19.3 | 1.1 | | |
| NaCl | (200) | 4.729(Cl$K\alpha$) | 1.0 | 1.0 | 1.0 | |
| Ge | (111) | | >13.0 | 0.12 | 0.3 | |
| $SiO_2$ | (01.1) | | 0.4 | 6.2 | >0.7 | |
| LiF | (200) | 3.744(K$K\alpha$) | 1.4 | 3.6 | | |
| NaCl | (200) | | 1.0 | 1.0 | | |
| Ge | (111) | | >80.0 | 0.5 | | |
| $SiO_2$ | (01.1) | | 1.3 | 2.1 | | |
| LiF | (200) | 3.360(Ca$K\alpha$) | 1.0 | 1.0 | 1.0 | 1.0 |
| NaCl | (200) | | 0.9 | 0.4 | 0.2 | 0.8 |
| Ge | (111) | | >60.0 | 1.1 | 0.1 | 13.0 |
| LiF | (200) | 2.750(Ti$K\alpha$) | 1.0 | 1.0 | | |
| NaCl | (200) | | 0.7 | 0.3 | | |
| Ge | (111) | | >100.0 | 0.67 | | |
| $SiO_2$ | (01.1) | | 0.8 | 0.7 | | |

[a] Ethylenediamine-*d*-tartrate.

slit-width to the rocking angle of the crystal. When the limit imposed by this angle has been reached, the intensity cannot increase further.

Examination of these curves shows a dramatic difference, at each wavelength, between the best crystal and the others which could be used. In nearly all cases, that which provides the best intensity also gives the best resolution. These differences serve to emphasize the importance of the use of multiple fixed spectrometers, which allows choice of the best crystal for each wavelength.

The data in Table II reveal rather large differences in the relative rejection of higher orders. This information becomes useful in those special cases where interference from a specific high-order line may make it desirable to choose a crystal for its discrimination against this order. An obvious example of this would be the use of germanium where a direct second-order interference exists. Another similar example is the high rejection of third order by the (01.1) plane of quartz in the vicinity of the S$K\alpha$ line at 5.373 Å.

These results can provide a guide to the choice of the best crystal, when the nature of the analytical problem is well known. Although some complex problems may require a special study in order to reach a final decision, the choices are considerably narrowed down by an examination of the data presented.

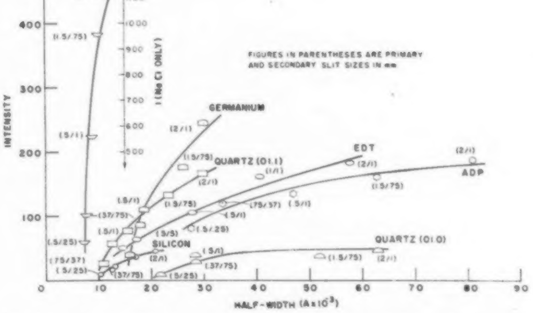

Fig. 10. Intensity-resolution function of crystals at 5.373 Å (S$K\alpha$).

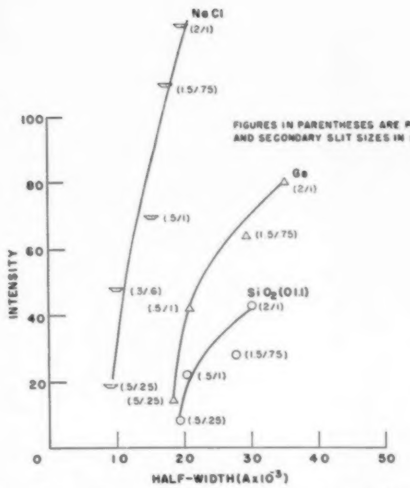

Fig. 11. Intensity-resolution function of crystals at 4.729 Å (Cl$K\alpha$).

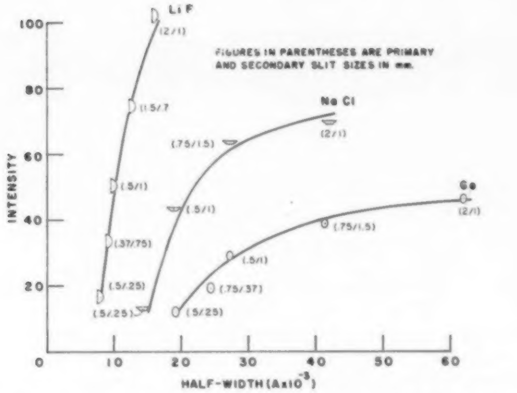

Fig. 13. Intensity-resolution function of crystals at 3.360 Å (Ca$K\alpha$).

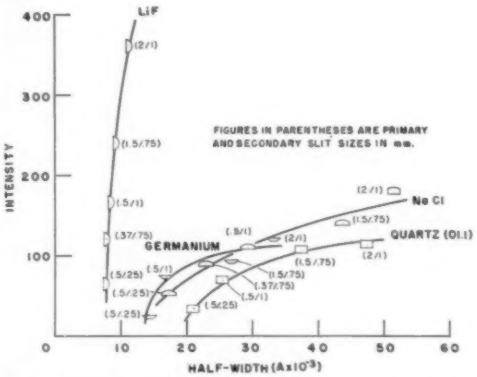

Fig. 12. Intensity-resolution function of crystals at 3.744 Å (K$K\alpha$).

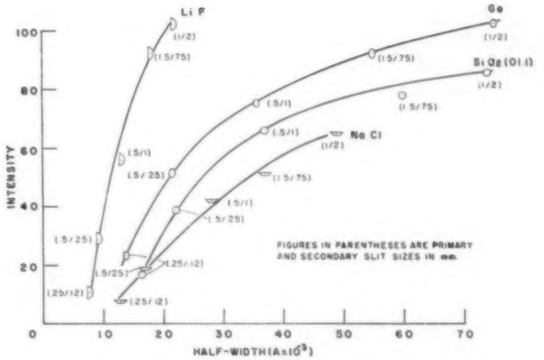

Fig. 14. Intensity-resolution function of crystals at 2.750 Å (Ti$K\alpha$).

The authors would like to express appreciation to M. F. Hasler for his valuable criticisms and discussions.

## References

1. R. M. Dolby, Proc. Phys. Soc. (London) **73,** 81 (1959).
2. Y. Cauchois, J. Phys. Radium **3,** 320 (1932).
3. N. Spielberg, W. Parrish, and K. Lowitsch, Spectrochim. Acta **15,** 564 (1959).
4. T. Johansson, Z. Physik **82,** 507 (1933).
5. G. Andermann, J. L. Jones, and E. Davidson, *Proc. 7th Ann. Conf. on Ind. Appl. of X-Ray Anal.* (Metallurgy Division, Denver Research Institute, Univ. of Denver, Col., 1959), p. 215.
6. D. B. Wittry, *Advances in X-Ray Analysis* (Plenum Press, New York, 1960), Vol. 3, p. 185.
7. L. S. Birks and E. J. Brooks, Rev. Sci. Instr. **29,** 425 (1958).
8. L. S. Birks and E. J. Brooks, Rev. Sci. Instr. **28,** 709 (1957).
9. H. A. Liebhafsky, H. G. Pfeiffer, E. H. Winslow and P. D. Zemany, *X-Ray Absorption and Emission in Analytical Chemistry* (Wiley, New York, 1960).
10. L. S. Birks, *X-Ray Spectrochemical Analysis* (Interscience Publishers, New York, 1959).
11. H. Wilsdorf, Naturwissenschaften **11,** 250 (1951).
12. L. S. Birks and R. T. Seal, J. Appl. Phys. **28,** 541 (1957).
13. H. H. Johann, Z. Physik **69,** 185 (1931).

## October Issue Features Bubble Chamber Optics

# Meeting Reports

## Second Hungarian Optical Conference, Budapest, 6–9 May 1963

Reported by W. Lewis Hyde, Rochester

The Second Hungarian Optical Conference was held in Budapest 6–9 May 1963 under the sponsorship of the Hungarian Society for Optics, Acoustics, and Film Technology. About 75% of the 112 participants were from Hungary and 16 from East Germany. The rest came from France, Poland, Czechoslovakia, Rumania, Italy, and the U.S.A.

Twenty-eight papers were read, mostly in German. The principal optical activity in Hungary is at the Hungarian State Optical Works (M.O.M). in Budapest, but interesting work on coherence in the Michelson interferometer is being carried out in the Central Research Institute for Physics where Janossy is Director, and there is a lively interest in optics in the television, motion picture, spectrographic, and medical fields.

Papers concerning thin films, measurement of modulation transfer functions, tolerancing of optical systems, instruments design, etc. were read. Sandor Majoros, who published a paper last year in *J. Opt. Soc. Am.* on his investigations of "Statoptics" (a mathematical formalism for lens design based on an analogy with statics), described further investigations, particularly on the design of "polyachromats". Majoros is Technical Director of M.O.M. in Budapest.

The Eastern European countries are coordinating their economic activity, and there is an active program to concentrate the production of particular classes of optical instruments in different countries: the Hungarians are specializing in geodetic instruments (theodolites, levels, etc.), the Czechs are making microscopes in the Meopta factory in Prerov, and the East Germans are making cameras in Jena and Dresden.

Hungarians do not appear to travel outside of Hungary under the present regime, but they are eager to establish technical and personal contact with other scientists. Foreigners visiting Hungary will find a cordial and personal welcome everywhere from a proud, talented, and worldly people working hard to rebuild their country. The increased personal freedom and improved standard of living in the last few years have resulted in general optimism, and the extensive damage of 1956 is being rapidly repaired. Two of us from the United States rented a car in Vienna and drove to Budapest (200 km). Even though we used the car all week, the cost was less than airline fare, and it greatly facilitated social activity. Another alternative worth considering for visitors to Budapest is the new hydrofoil boat traveling daily from Vienna on the Danube. It is valuable to be able to speak German, the most common second language, but English is widely spoken.*

Endre Hódi, Secretary of the Organizing Committee, Second Hungarian Optical Conference.

Sandor Majoros, Technical Director, Hungarian Optical Works (Magyar Optikai Muvek), Budapest.

## IRIS

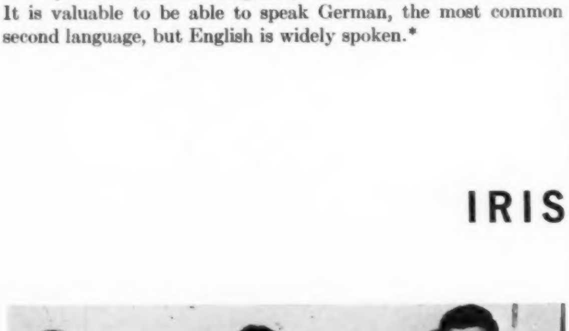

Top—left to right—Jack Connell *Boeing-Seattle*, J. William Grady *Army Chief of Staff for Intelligence*, J. M. Dempsey, Jr. *Baird-Atomic*. Bottom—left to right—William Langton *Baird-Atomic*, George Roberts *Missile Electronic Warfare Division White Sands Missile Range*, and Walter Baird *Baird-Atomic*.

---

* Another report of this meeting may appear in a later issue.

# Predisperser for High-Resolution Grating Spectrographs

Joseph Reader, Louis C. Marquet, and Sumner P. Davis

A predispersing device designed for use with grating spectrographs used in high orders is described Some basic considerations are pointed out, and the uses of the predisperser with Fabry-Perot interferometers and as an order sorter are discussed.

The necessity for accurate spectral line measurements has led to the development of well-blazed, accurately ruled, plane diffraction gratings, and to their utilization in specially designed instruments. In particular, the simple mirror monochromator has proved to be of great usefulness. One of the problems associated with this type spectrograph is that of overlapping orders, which must be separated or eliminated before the desired spectral information can be obtained. We have constructed a predispersion instrument particularly suited to our problems in the examination of rare-earth spectra under high resolution and dispersion.

## I. Predisperser for Fabry-Perot Interferometry

### A. Introduction

In using Fabry-Perot interferometers for high-resolution spectroscopic investigations, the interferometer is generally crossed with an auxiliary stigmatic spectrograph. In the case of complex spectra of the rare-earth and heavy elements, it is desirable that the auxiliary spectrograph have a plate factor of 1 Å/mm or less, depending on the specific situation. This high dispersion is necessary not only to distinguish the different spectrum lines, but also to separate the overlapping interferometer orders so as to remove any ambiguities in the interpretation of hyperfine structure patterns. The wide slit used in Fabry-Perot interferometry imposes more severe requirements on the spectrograph dispersion than is normally required with line spectra. It is also desirable that the spectrograph be relatively free from major light losses, such as the loss of light to unwanted grating orders.

These requirements have led to the use of plane grating spectrographs (mirror monochromators) employing highly blazed gratings which are designed to be used in high orders for the photographic region.[1,2] For example, a plane grating instrument recently installed in this laboratory utilizes a 300 groove/mm grating blazed at 64°, and 305-cm focal length mirrors. A schematic diagram is shown in Fig. 1. With this instrument a spectrum line at 4000 Å appears in the region of the blaze in the 14th order; the plate factor is 0.4Å/mm with a 305-cm camera mirror.

Although this high auxiliary dispersion is ideal for hyperfine structure studies with etalons, the overlapping grating orders present a serious problem. The free-spectral range (region without overlap) is given by:

$$\Delta\lambda = (\lambda^2/2d)/(\sin\theta + \sin\phi) = (\lambda^2/2d)f(\theta,\phi), \qquad (1)$$

where $d$ is the grating spacing and $\theta$ and $\phi$ are the angles of incidence and diffraction, respectively. If only a fixed position in the camera is being considered, the angular function $f(\theta, \phi)$ is a constant. For the above grating, the free-spectral range is approximately 110 Å at 2500 Å, and 1160 Å at 8000 Å. In the long-wavelength region the orders can be separated easily by a suitable filter, taking into account emulsion sensitivities. However, at short wavelengths the use of filters to separate the grating orders is not possible in general. Furthermore, the appreciable absorption and reflection losses of filters make them poor choices for isolating the grating orders.

These circumstances lead to the desirability of a predispersing element for obtaining spectrograms free from overlapping orders. Various instruments have been constructed in other laboratories. One such instrument is in use at the University of Michigan.[1] At the present time, however, there are no commercial "order sorters" which are suitable for use with interferometers. This section of the paper describes a convenient predisperser which is simple in design and

---

The authors are with the Physics Department, University of California, Berkeley, California. The present address of Joseph Reader is Chemistry Division, Argonne National Laboratory, Argonne, Illinois.

Received 4 February 1963.

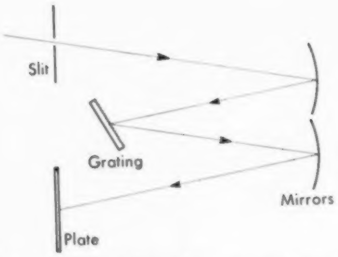

Fig. 1. Plane grating mirror monochromator.

construction, and which has been used with considerable success in examining rare-earth hyperfine structures, particularly of promethium[3] and erbium.

## B. Basic Principles and Construction of Predisperser

In the most common applications of an external mounting of the Fabry-Perot interferometer, the interferometer is illuminated with collimated light, and the fringes are focused on the spectrograph slit by a long focal length projection lens. The circular fringes are centered on the slit by tilting the interferometer so that the normal to the reflecting surfaces is parallel to the spectrograph axis. The requirement that the fringes be centered on the slit makes it clear that any predispersing element must be placed between the light source and the interferometer.

The selection of a predispersing element can be guided by considering the properties of the spectrograph. According to the above equation, the free-spectral range is proportional to $\lambda^2$. The amount of predispersion required is inversely proportional to the free-spectral range, making it desirable that the predisperser have a dispersion proportional to $1/\lambda^2$. Taking account of the facts that the dispersion of a grating is approximately independent of wavelength, and that of a prism approximately proportional to $1/\lambda^3$, the use of a prism as a predispersing element more nearly fulfills the requirements of the spectrograph than does the use of a grating.

Another property of external interferometer mountings can play an important role. Fabry-Perot plates are made with small wedge angles between the coated and uncoated surfaces in order to separate the primary pattern from the secondary patterns. The secondary patterns result from reflections off the uncoated surfaces. The interferometer is assembled so that the secondary patterns are thrown to the sides of the spectrograph slit. However, if the light source is large in extension, it may not be possible to prevent the secondary images from entering the spectrograph slit without the use of an auxiliary slit placed between the source and the interferometer. It is logical to use the slit of the predisperser as this auxiliary slit.

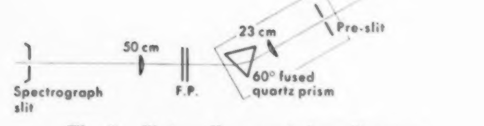

Fig. 2. Externally mounted predisperser.

The predisperser which we have constructed has three optical components: a bilateral slit (pre-slit), a 23-cm fused-quartz collimating lens, and a 60° fused-quartz prism. The pre-slit and the refracting edge of the prism are parallel to the spectrograph slit. A diagram is shown in Fig. 2. Light from the source is focused onto the pre-slit with a lens of suitable focal length. The light emerging from the pre-slit is collimated by the 23-cm lens, and in passing through the prism is dispersed in a direction perpendicular to the spectrograph slit. After traversing the interferometer, the light is focused onto the spectrograph slit by the 50-cm projection lens. Both the pre-slit and the interference rings are simultaneously in focus at the spectrograph slit.

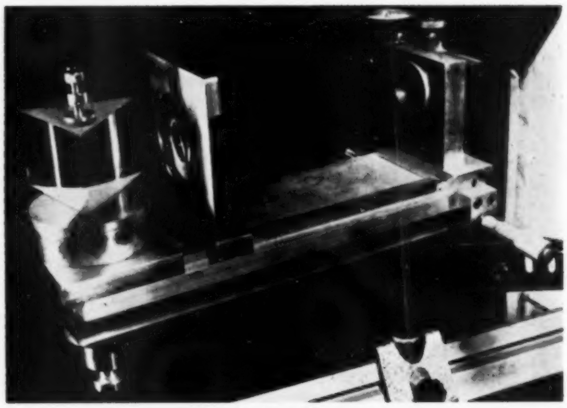

Fig. 3. Predisperser.

A photograph of the instrument is shown in Fig. 3. Each predisperser component is mounted on an aluminum rider which can move back and forth along a solid aluminum base. The position of the rider can be fixed by tightening a set screw against a rectangular guide. The aluminum base consists of two plates, one above the other. The upper plate can be rotated with respect to the lower about a vertical axis coinciding with the effective center of the prism. This rotation is spring loaded and controlled by a micrometer screw. The lower plate of the base is supported by two rods which are held in conventional triangular bench riders. The support under the pre-slit is not centered in the width of the base. This permits the base to be leveled. The prism is mounted on a table which allows an independent, calibrated rotation of the prism. The pre-slit mount is designed to allow a 180° rotation about the optic axis. The width of the pre-slit can be read directly from a micrometer dial indicator actuated by one of the slit jaws. The maximum slit opening is 5 mm.

### C. Optical Adjustments

Although the essential features of this predisperser are not complicated, the instrument must be very carefully adjusted before actual use. An indication of the necessary adjustments follows. These procedures are based on the assumption that the projection lens has been properly aligned. The interferometer is usually removed from the system during adjustment of the predisperser.

1. The base is leveled and adjusted so that the center of the pre-slit is at the same height as the spectrograph axis.
2. The axis of rotation of prism and base is made to intersect the spectrograph axis. This adjustment is checked by setting the prism at minimum deviation for a particular spectrum line and rotating the base so that the line falls on the spectrograph slit. The beam should then be centered in the spectrograph optics. No adjustment for making the axis of rotation strictly vertical is needed, because of accurate machining of the base and prism table, and careful leveling.
3. The 23-cm collimating lens is positioned so that the pre-slit is imaged sharply on the spectrograph slit jaws. In our instrument, this lens is not an achromat, and must be reset for each spectral region. In the ultraviolet, a photomultiplier placed in the center of the spectrograph camera is used to determine the position of best focus. Once a graph of the lens position vs wavelength is obtained, the lack of an achromatic lens is not an inconvenience. Nevertheless, a high quality quartz-fluorite achromat would certainly be more suitable for this purpose. In making visual settings of the focus, a false focal position can arise from spherical aberration, if the collimating lens is not stopped down to the useful diameter of the beam.
4. The pre-slit is rotated so that its image is parallel to the spectrograph slit. Since the image is slightly curved, this adjustment has only a limited precision. In practice, the pre-slit is rotated until its image appears symmetrically placed about the center of the spectrograph slit.

This outline is not intended as a comprehensive, step-by-step procedure for obtaining a satisfactory adjustment of the instrument. It is clear that the above steps are not completely independent, and that a certain amount of iteration is required.

Prior to each exposure, the spectrograph grating is first set for the desired spectral region, and the prism set approximately at minimum deviation for the center of this region, using a mercury lamp as a source. The ultraviolet lines can be satisfactorily observed by placing a fluorescent screen in the focal plane of the 50-cm projection lens. Next, a source giving a continuous spectrum (high-pressure xenon arc in most instances) is focused on the narrowed pre-slit, and the radiation traversing the entire optical system—predispersion and spectrograph—is monitored with a photomultiplier tube placed at the center of the plate holder. The axis of the predispersion system is rotated to the position where the photomultiplier signal is a maximum. The pre-slit is then widened to allow the desired range of wavelengths to pass through the spectrograph slit. Finally, the light source is aligned with the axis of the predispersion system and focused on the pre-slit.

### D. Performance

With a 50-cm projection lens, the 60° fused-quartz prism gives a reciprocal linear dispersion of 50 Å/mm at 3000 Å, 100 Å/mm at 4000 Å, and 300 Å/mm at 5000 Å. The width of the pre-slit required to separate the grating orders is about 0.8 mm throughout the spectrum for the Berkeley plane-grating. The optic axis undergoes a deviation of about 34°. The light-transmitting efficiency was photoelectrically measured to be close to 70%. Of the 30% of the light not transmitted, 10% was due to the prism and 20% was due to the collimating lens. If the present collimator were replaced by a high-quality lens, and the prism and lens surfaces coated with antireflection coatings, we estimate that a net efficiency of about 90% would be possible.

It should be mentioned that the predisperser was tested with a transmission grating replacing the grating as the dispersing element. The grating was purchased specifically for this purpose from Bausch & Lomb Company. The grating has 200 grooves/mm and is strongly blazed for 5000 Å in the first order. It is mounted on a fused-quartz backing plate. The use of this grating produces a reciprocal linear-dispersion of about 100 Å/mm thoughout the spectrum, and a deviation of the optic axis of about 5°. Measurements of the net efficiency gave results which varied from about 56% at 5500 Å (region of blaze) to 25% at 3600 Å. Because of the lower efficiencies, the predisperser has not been used in any actual applications with the grating as the dispersing element.

The appearance of the Fabry-Perot interference rings at the spectrograph slit is shown in Fig. 4. Although the fringes are centered in the spectrograph slit, they are not centered in the image of the pre-slit. The only exception is a spectrum line in the

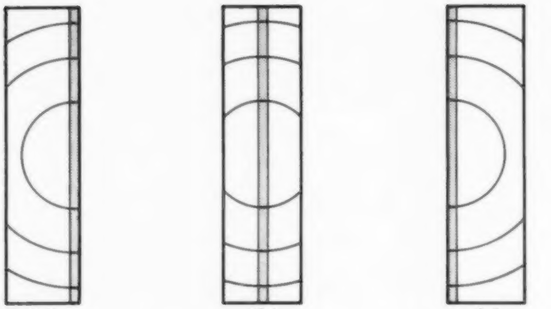

(a) (b) (c)

Fig. 4. Schematic appearance of Fabry-Perot rings at the slit for (a) the longest wavelength in the region of interest; (b) the central wavelength in the region of interest; and (c) the shortest wavelength in the region of interest. The heavy outline represents the image of the pre-slit; the shaded region represents the spectrograph slit.

center of the wavelength region of interest. The fringes of this line are centered in both slits.

With the predisperser, a certain amount of difficulty is encountered in trying to eliminate the secondary interference patterns. If the secondary patterns are thrown as far as possible to each side of the spectrograph slit, it is likely that the secondary patterns of spectrum lines in the next higher and lower overlapping grating-orders will pass through the slit. Similarly, if the interferometer-plate wedge-angles are positioned so that the secondary patterns of the central wavelength just miss the slit, the secondary patterns from other wavelengths in the region of interest will pass through the slit. The range of wavelengths covered by the spectrograph camera determines whether or not it is possible to prevent all secondary patterns from entering the spectrograph slit. For the full 25.4-cm plate which the Berkeley spectrograph accepts, it is not possible to obtain spectrograms completely free from secondary patterns when the predisperser is employed. However, a compromise is possible whereby one-sixth of the plate at each extremity receives secondary patterns, both from lines which fall on that part of the plate and from lines in the next higher or lower overlapping grating order. This leaves the center two-thirds of the plate completely free from secondary patterns.

A section of plate from a $Pm^{147}$ interferogram using the optical system of Fig. 2 is reproduced in Fig. 5. For this picture, a hollow cathode light source containing a few milligrams of $Pm^{147}$ was operated at a current of 75 mA. The Fabry-Perot spacer was 10.01 mm and the exposure time 15 min. The spectrograph plate factor is 0.7 Å/mm. An effective resolution of over $10^6$ is indicated here. The resolving power in this case is limited by Doppler broadening in the source, rather than by the optics. The use of the high spectrograph dispersion to distinguish the overlapping interferometer orders is well illustrated by this figure.

## II. Predisperser for Order Sorting

### A. Introduction

The plane-grating spectrograph by itself is not a convenient instrument to use in the investigation of a complex line spectrum over an extended wavelength region, owing to the high blaze angle of the grating and the small spectral region covered in a single exposure (about 100 Å in the 14th order of 4000 Å in our instrument). The predisperser described above can be utilized as a bandpass filter of variable bandwidth to select a wavelength region encompassing one or more of the grating orders, but a large number of separate exposures is necessary to cover even a relatively small region of the spectrum.

To reduce the number of exposures, cross dispersion

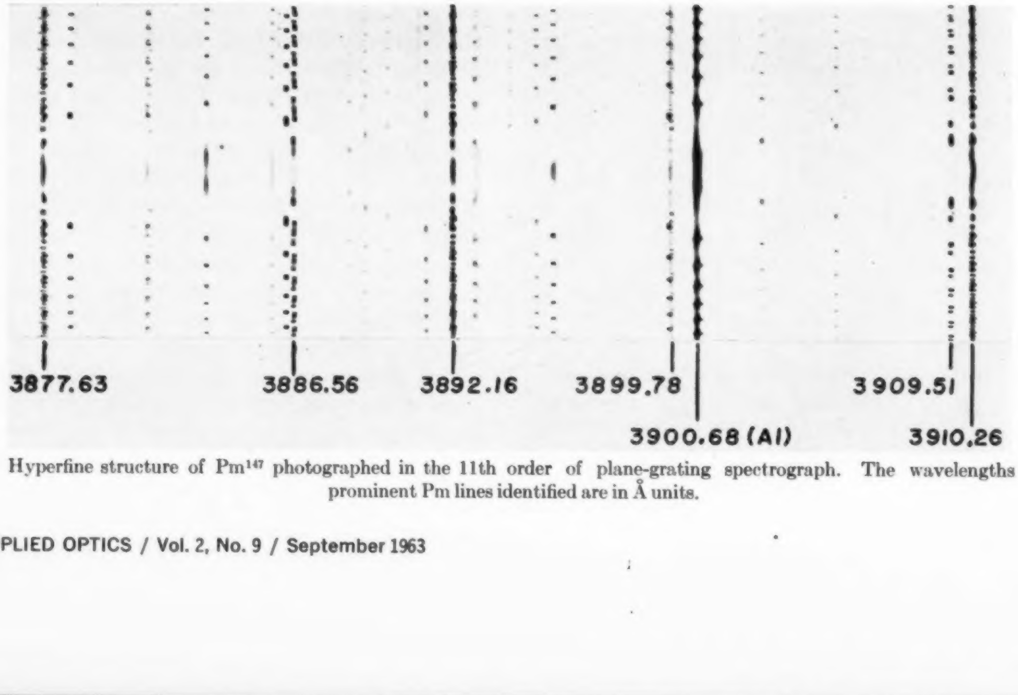

Fig. 5. Hyperfine structure of $Pm^{147}$ photographed in the 11th order of plane-grating spectrograph. The wavelengths of the prominent Pm lines identified are in Å units.

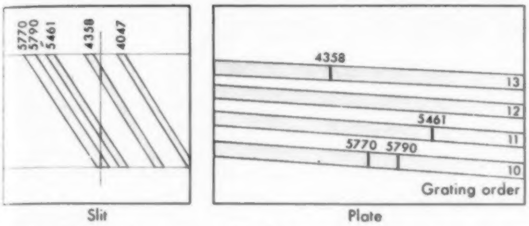

Fig. 6. Schematic appearance of the mercury spectrum at the slit and on the plate. The grating dispersion has been made much smaller than is actually the case, in order to show all the lines on the same plate.

is introduced. This can be done internally as with the echelle of Harrison *et al.*[4] or externally as in variations of the echelle spectrograph or with the Jarrell-Ash Order Sorter.[5] In an external mounting, an order-sorting device produces vertical dispersion at the spectrograph slit. A corresponding vertical dispersion is obtained at the plate since the plane grating is a stigmatic instrument. The lines orginating from different orders appear displaced vertically from one another. With the predisperser described in Sec. IB, for which the dispersion is normally horizontal, it is only necessary to rotate the pre-slit about the optic axis to achieve this vertical dispersion.

## B. Method of Use

The method of using the predisperser as an order sorter can best be visualized by considering light from a monochromatic source to be focused onto the pre-slit. When the pre-slit is vertical, its image at the spectrograph slit is vertical and slightly curved. If the pre-slit is rotated, its image at the spectrograph slit becomes inclined. If a source is used which contains several wavelengths, there is an inclined image for each wavelength present. These images are dispersed horizontally by the prism. Figure 6 shows a schematic diagram of the mercury spectrum at the spectrograph slit and at the plate. It can be seen that the horizontal dispersion of the prism, together with the inclination of the images, produces a vertical dispersion along the length of the spectrograph slit. Wavelengths appearing in different orders of the grating are imaged at different positions along the slit.

The number of orders appearing on the plate is controlled by varying the angle of rotation of the pre-slit. The vertical distance between orders varies inversely with the number of orders. The length of the spectrum lines depends upon the width and angle of the pre-slit. The desired amount of vertical overlap between lines in adjacent orders is obtained by choosing an appropriate pre-slit width, once the angle has been set.

All lenses between the pre-slit and spectrograph should be achromatic over the range of wavelengths being photographed. If all lines are not simultaneously in focus at the spectrograph slit, the ends of those lines not in focus will be poorly defined on the plate.

The predisperser used in the above way has proved invaluable in our research on rare-earth spectra. Wavelength measurements are being made using thorium standards. In photographing these spectra, it is possible to employ standards in the same order as the rare-earth lines, or, in regions where there is an insufficient number of standards, several orders of standards can be made to overlap the rare-earth lines by increasing the pre-slit width.

# III. Other Uses

We have successfully used the predisperser to obtain hyperfine structure patterns of weak lines which are very close to extremely strong lines, such as the aluminum resonance doublet in a hollow cathode. Ordinarily, the scattered light from the intense lines provides a back-ground stronger than the patterns of the weak lines. With the predisperser, light from a strong line can be kept out of the spectrograph to a large extent, while the light from a neighboring weak line can be transmitted with almost undiminished intensity. Scattering within the projection lens, interferometer, and predisperser prevent the complete elimination of a very strong line.

It has also been possible to eliminate intense light from band spectra originating from impurities in a light source containing minute quantities of radioactive materials, enabling observation of weak atomic line spectra.

Another application is the photographing of molecular band spectra in high orders of either plane- or concave-grating spectrographs, allowing utilization of very high resolution without the presence of overlapping orders. Conventional order sorters with dispersion in a direction parallel to the spectrograph slit cannot be used with concave grating instruments.

We gratefully acknowledge partial support of this work by a grant from the National Science Foundation. We express our appreciation to Cliff Grandt of the Physics Department Shop for his valuable contributions in the mechanical design and fabrication of the predisperser.

# References

1. A. K. Pierce, J. Opt. Soc. Am. **47,** 6 (1957).
2. H. H. Stroke and K. K. Y. Li, J. Opt. Soc. Am. **51,** 678 (1961).
3. J. Reader and S. P. Davis, J. Opt. Soc. Am. **53,** 431 (1963).
4. G. R. Harrison, J. E. Archer, and J. Camus, J. Opt. Soc. Am. **42,** 706 (1952).
5. R. F. Jarrell, J. Opt. Soc. Am. **45,** 259 (1955).

# Papers to appear in subsequent issues

We have had almost 500 papers submitted for publication during the past two years, and we have already built up a backlog which is as embarrassing for a new publication as it is a demonstration of the need for this journal. We have done our best to publish papers as quickly as we can by bringing out bigger issues than had originally been intended last year, by **becoming a monthly in 1963** and by occasionally dropping some of the "filler" departments. The Editors wish to express their sincere appreciation to all contributors who have thus demonstrated their faith in **Applied Optics.**

Interferometric Measurement of Vibration Amplitudes—*Bowie*

Infrared Transmission through Fogged Salt Windows—*Morrow and Turk*

A Simple Grating Calibrator for the Visible and Vacuum Ultraviolet—*Hammer, Arakawa, and Birkhoff*

Photorefractometer II Measurement of N and K—*Kapany and Pontarelli*

The Use of Polarized Infrared Radiation in Magneto-optical Studies of Semiconductors—*Palik*

An Optical Null Double-Beam Double-Pass IR Spectrophotometer—*Minami*

A Photomultiplier Circuit for Precision Spectrophotometry—*Budde*

Large-Scale Photoelectric Planimeter for Leaves—*Carman*

A New Method for High-Speed Motion Picture Photography of Transparent Drops—*Pfeiffer*

Photometric Accuracy of Infrared Spectrophotometers—*Stewart*

Study of the Fabrication of Aspherical Surfaces—*Sakurai and Shishido*

Transmission of Isotropic Radiation Across an Interface Between Two Dielectrics—*Stern*

Isosceles Total Internal Reflectors as Optical Elements—*Rothstein*

Test of Theoretical Absorption Band Model Approximations—*Burch and Williams*

Optics in Norway—*Hisdal and Omholt*

Use of an Analog Computer in Side-on Arc Spectroscopy—*Shumaker and Yokley*

The Evaporation Rate of Filament Material from Alternating Current Heated Filaments—*Wilson*

Attenuation by Ozone and the Earth's Albedo in the Middle Ultraviolet—*Green*

Double Monochromator Systems—*Christensen and Potter*

Experiments with the Optical Excitation of Mercury Vapor for the Production of Isolated Fluorescence—*Zito and Schraeder*

Observations of Near Infrared Radiation from the Solar Atmosphere—*Taylor and MacQueen*

Irradiance on a Flat Object Underwater—*Tyler and Shaules*

Kirchhoff Diffraction Pattern Calculations—*Moore*

Electronic Flash Illumination of a Large Wilson Cloud Chamber—*Edgerton*

Interference Filter Spectrometer for Low Intensity Extended Sources—*Carter, MacRae, Nelson, Birkhoff, and Arakawa*

A Universal Spectrophotometer—*Kaye*

The Stressed-Plate Shutter: A New Moderate-Speed Electro-Optical Light Modulator—*Hauser, Smith, and Marlowe*

Measurement of Energy Flux Density Distribution in the Focus of an Arc Image Furnace—*Beyer, McCulley, and Evans*

Irradiance Linearity Corrections for Multiplier Phototubes—*Baker and Wyatt*

Optics in Australia—*Steel*

Slit-Induced Errors in Pressure-Broadened Line Measurements—*Dalton*

Variation of Lead Sulfide Response with Incident Angle and Orientation in Detector Plane—*Groner and Stoliar*

A Continuously Variable Optical Beam Splitter and Intensity Controller—*Harrick*

A New Family of Flat-Field Cameras—*Gelles*

Dispersion in the Vicinity of an Optical Resonance—*For and Bradley*

Design for a Wide-Angle, Linear-Output, Horizon-Sensor Optica System—*Palser*

A Redetermination of Some Optical Properties of Calcium Fluoride—*Malitson*

Test Methods in Spectrophotometry: Stray Light Determination—*Poulson*

The Scattering of Infrared Radiation from Clouds—*Bauer*

Temperature Measurements with an Optical Pyrometer under Adverse Conditions—*Paul*

An Absolute Reflectometer for Use at Low Temperatures—*Hartman and Logothetis*

Field Photometer with Nine-Element Filter Wheel—*Frentress, Young, and Edwards*

On the Astrophysical Work of W. W. Coblentz—*Strong*

Jet-Controlled Arc II: Excitation of Third Spectra—*Moore, Thygesen, Derwin, and Eward*

Illumination of the Slit Source of the Hough-Powell Digitizer—*Rosin*

Bubble Chamber Optics—*Welford*

Illumination of the 80-in. Bubble Chamber—*Rosin*

A Flying Spot Measuring Machine Employing Crossed Glass Fibers—*Palmer*

Optical Properties of "Liumogen": A Phosphor for Wavelength Conversion—*Kristianpoller and Dutton*

Optical and Mechanical Properties of Bubble-Chamber Windows—*Reitmayer and Deeg*

Exfocal Pumping of Optical Masers in Elliptical Mirrors—*Roess*

Optical Harmonic Generation in Two Ferroelectric Crystals—*Smith*

Spectroscopy Applied to Hypersonic Atmospheric Penetration—*Planet*

A New Grazing Incidence Spectrometric Mounting—*Landon*

Coblentz's Contribution to Infrared Spectroscopy—*Jones*

Spectral Emittance of Refractory Materials—*Blau and Jasperse*

The Influence of W. W. Coblentz on Radiometry—*J. A. Sanderson*

The Trigger Circuit for the 80-in. Bubble Chamber Light Source—*Yamamoto and Sims*

The Infrared Transmittance of Carbon Dioxide—*Stull, Wyatt, and Plass*

An Automatic Calibrating Apparatus for Standard Scales by Counting Interference Fringes—*Doi, Shimizu, Tsuboi, and Kouno*

Data Processing System for the Automatic Transformation of Observed Plasma Intensities into Their Radial Distribution—*Paquette and Wiese*

Characterization of Bolometric Detectors—*Hoffman*

Push-Pull Optical Modulators and Demodulators—*Sterzer*

# A Two-Wavelength Two-Frequency Ratio Recording Infrared Spectrometer Analyzer

A. M. Bartz and H. D. Ruhl

An infrared plant stream analyzer is described which records as its output the ratio of two wavelengths; one the measuring and the other the reference wavelength. The two wavelengths are obtained by using two entrance slits in a grating spectrometer and chopping the radiation passing through each slit at a different frequency, permitting the use of electrical bandpass filters for wavelength separation and recording.

The rapidly expanding field of chemical process control is constantly demanding composition analyzers of improved sensitivity, specificity, time lag, and most important, reliability. For many applications, particularly where a continuous measurement of a specific component in a multicomponent stream must be made, an infrared analyzer is well suited. Commercial infrared process analyzers are generally either of the nondispersive type or use narrow bandpass transmission filters to select wanted wavelengths. The nondispersive analyzers require a proper sensitizing gas and cannot usually be used for a liquid sample with a complicated infrared spectrum. The bandpass filter analyzers are fine except that they are commercially available for only the near infrared. One of the reasons for this is that at the present time filters for wavelengths beyond 5 or 6 $\mu$ are very expensive and are frequently not sufficiently selective, i.e., their bandwidth is too wide to remove unwanted radiation adjacent to a narrow absorption band. An obvious additional disadvantage is that each filter is usually suited for only a specific analysis so, if the need for a plant stream analysis is terminated, the only way the instrument can be adapted to a new problem is to replace the filter.

The Dow Chemical Company has, for many years, built its own infrared plant stream analyzers simply because the instruments we need are not commercially available. Our most recent version of what we think is a versatile, reliable instrument, is described in this paper.

The desirability of recording the ratio of two wavelengths in an infrared plant stream analyzer is well established.[1-4] This eliminates the effect of a reduction (or increase) in size of the optical signal common to both wavelengths. Changes in signal size could be caused by source fluctuations, sample changes (bubbles pressure, temperature, particles), cell windows, transmission drift (fogging, dirt), detector sensitivity loss, or reflectivity variations in the common optical path. The method of obtaining this ratio varies, and we think the method described in this paper has some advantages in optical and mechanical simplicity.

The operation of the analyzer can be followed by observing the optical diagram in Fig. 1. The light from the coiled nichrome wire source SO fills out spherical mirrors $M_1$ and $M_4$ which focus it on entrance slits $S_1$ and $S_2$, respectively, by means of plane mirrors $M_2$, $M_3$ and $M_5$, $M_6$. The rotating chopper interrupts the light passing through $S_1$ at 6 cps and that passing through $S_2$ at 12 cps. The radiation passing through $S_1$ and $S_2$ falls on two different portions (slightly displaced) of the spherical collimating mirror $M_7$ which illuminates the reflection grating G from two different angles. The grating disperses the light from each angle of incidence into two spectra (displaced in wavelength) which the second collimator presents at the exit slit $S_3$. The interference cut-on filter F removes light of higher grating orders. The grating is usually used in the first order only. The exit slit simultaneously transmits radiation chopped at both 6 and 12 cps corresponding to two wavelengths which after traversing the sample cell is focused on the thermocouple detector D by ellipsoid mirror $M_9$. By using two entrance slits each with full aperture, an improvement of two in signal-to-noise is obtained over the in-

---

The authors are with the Dow Chemical Company, Chemical Physics Research Laboratory, 1603 Building, Midland, Michigan. Received 30 January 1963.

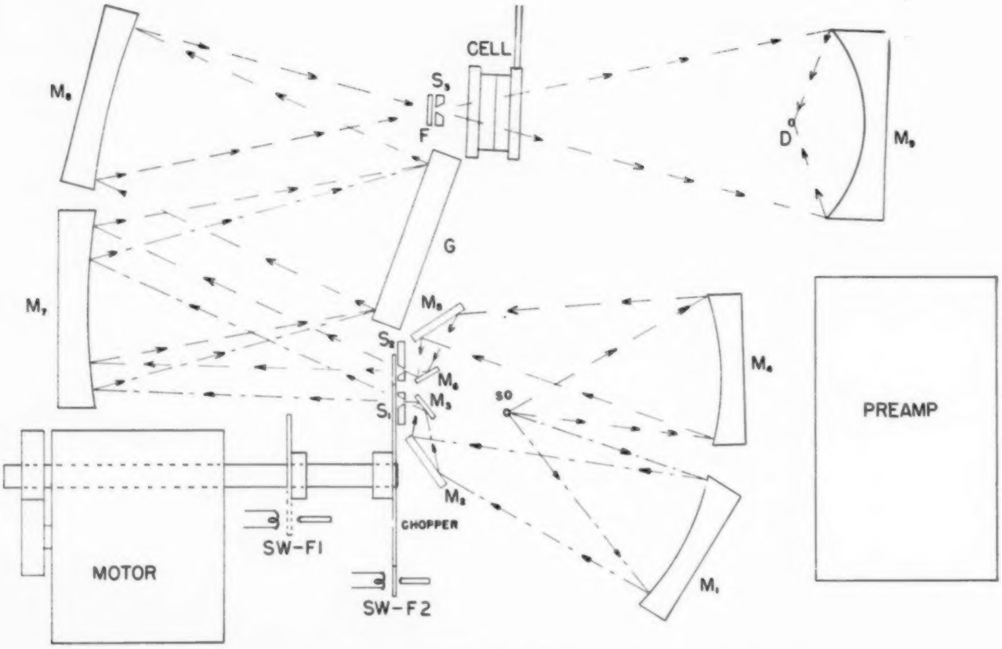
$M_8$
CELL
$S_3$
F
D
$M_9$
G
$M_7$
$M_5$
$S_2$
$M_6$
$M_3$
$S_1$
SO
$M_4$
PREAMP
$M_2$
CHOPPER
SW-F1
MOTOR
SW-F2
$M_1$

Fig. 1. Optical diagram.

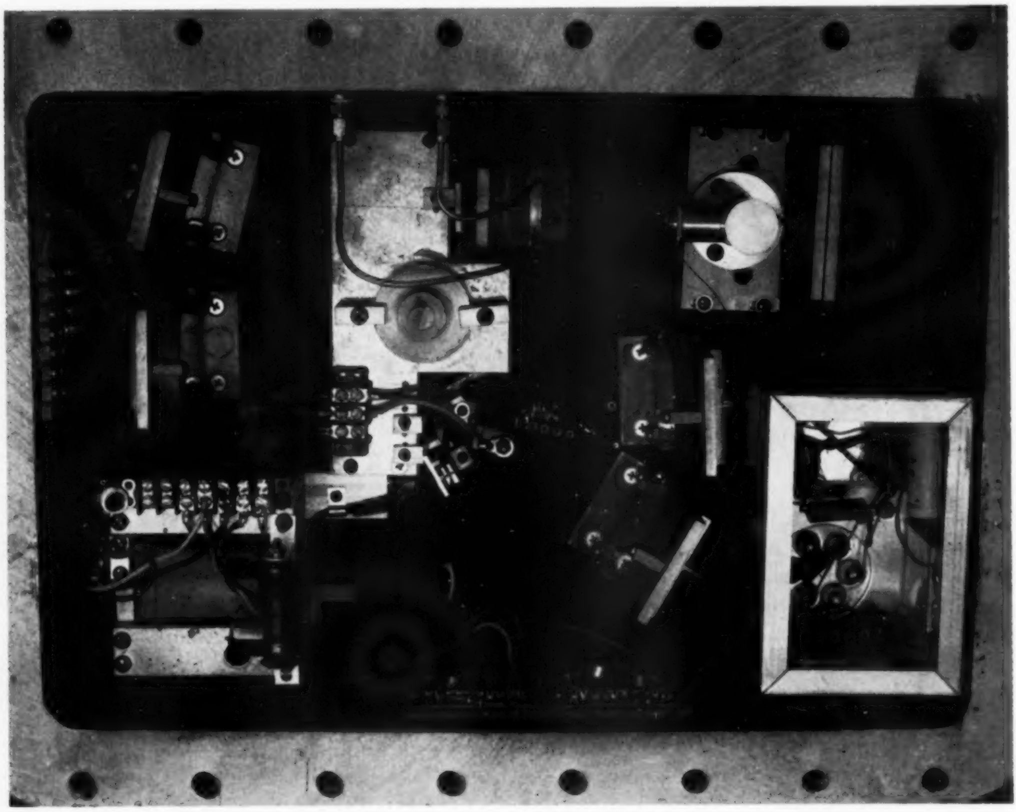

Fig. 2. Analyzer in explosion-proof housing.

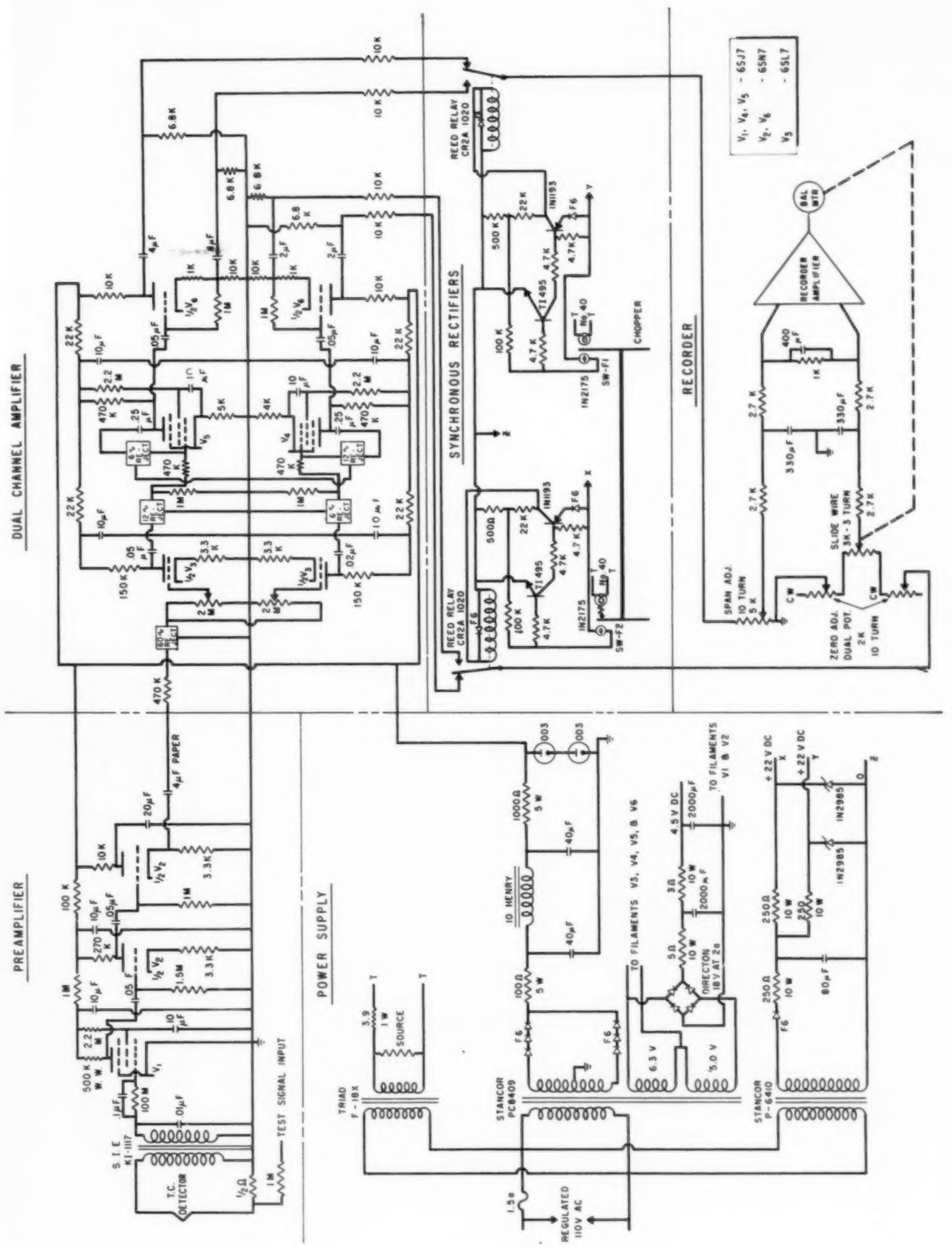
DUAL CHANNEL AMPLIFIER
PREAMPLIFIER
SYNCHRONOUS RECTIFIERS
RECORDER
POWER SUPPLY
T.C. DETECTOR
S.I.E. KI-1117
TEST SIGNAL INPUT
REGULATED 110V AC
TRIAD F-18X
STANCOR PC8409
STANCOR P-6410
10 HENRY
SOURCE
TO FILAMENTS V3, V4, V5, & V6
TO FILAMENTS V1 & V2
DIRECTON 18V AT 2a
6.3 V
5.0 V
+22 V DC
4.5 V DC
1N2985
REED RELAY CR2A 1020
1N1193
T1495
1N2175
SW-F1
SW-F2
CHOPPER
No. 40
60 ~ REJECT
12 ~ REJECT
6 ~ REJECT
RECORDER AMPLIFIER
BAL MTR
SLIDE WIRE 3K-3 TURN
SPAN ADJ. 10 TURN 5 K
ZERO ADJ. DUAL POT. 2K 10 TURN
CW
V1, V4, V5 - 6SJ7
V2, V6 - 6SN7
V3 - 6SL7

Fig. 3. Electrical schematic.

strument described in ref. 3. The liquid sample cell has a representative plant sample continuously flowing through it such that any change in the concentration of the measured component is immediately detected with only the piping velocity-distance time lag. The measuring wavelength, where the sample component of interest has a satisfactory infrared absorption band, is found by rotating the grating about a vertical axis while the reference wavelength is determined by the separation between the two entrance slits. The reference wavelength can be selected to eliminate also the effect of interference by an unwanted sample component which absorbs at the measuring wavelength. By selecting the reference wavelength such that the absorption due to the interfering component is equal at both wavelengths and recording the ratio, the output will be independent of changes in concentration of the interfering component. The reference wavelength, which is on the side of a large band, is found experimentally by incrementally moving the reference entrance slit until no interference is observed. For our standard size collimator ($M_7$) and grating the reference wavelength may be as much as 4 $\mu$ and as little as 0.1 $\mu$ on either side of the measuring wavelength. This is usually an adequate range in which to select the reference wavelength. The chopper, designed so that it can be used with any wavelength separation possible with collimator $M_7$, is physically symmetrical for dynamic balance, and is driven by a gearless low rpm motor coupled by a rubber-fabric belt for exceptionally quiet operation. Figure 2 is a top-view photograph of the analyzer in an explosion-proof housing.

The analyzer electronics are shown schematically in Fig. 3. A preamplifier having a gain of approximately $10^5$ is located next to the detector inside the analyzer housing. The preamplifier output signal, which contains both frequencies, is transmitted to the amplifier where the six- and twelve-cycle signals are separated and further amplified. Twin-tee networks are used in each channel to obtain band-reject and band-select filter characteristics. The bandpass of each channel is two cycles. The six- and twelve-cycle output signals are synchronously rectified, which provides additional frequency discrimination.

The synchronous rectifier represents a departure from normal systems. We sought a system which was stable, linear, hermetically sealed, and reliable. The present system consists of a pilot lamp, rotating shutter, photoduodiode, transistorized bistable trigger circuit, and relay.

The life of the pilot lamp is prolonged by operating it at 50% of its rated voltage. A shutter is mounted on the chopper shaft to maintain synchronism. It alternately blocks or passes light to the photoduodiode, which in turn changes the trigger circuit from one stable condition to the other and operates the relay. This particular analyzer uses two such systems, one for six-(SW-F1) and one for twelve-(SW-F2) cycle rectification.

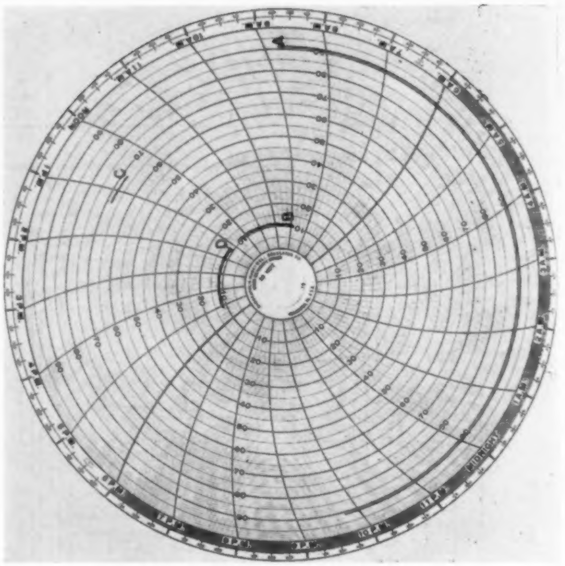

Fig. 4. Recorder chart showing span, noise and stability.

The rectified twelve-cycle signal from the reference channel is placed across the slidewire and zero adjust potentiometers. The rectified six-cycle signal from the measuring channel appears across the Span adjust potentiometer. A part of each signal is filtered and applied to the recorder amplifier. When the recorder is at balance, the pen position is a function of the ratio of the six-cycle signal to the twelve-cycle signal.

The "Span" potentiometer provides convenient control over scale expansion. For example, by adjusting the "Span" control one can obtain full-scale pen deflection for various concentration ranges, such as 0–0.5% or 0–1%. The "zero" potentiometer allows a scale shift. For example, by adjusting the "zero" control one can record the 0.5% concentration range from 0–0.5% or 0.5–1%.

The first application of this analyzer was to measure 0–1% ethyl hydrogen dichlorosilane in dimethyl dichlorosilane. The measuring wavelength selected for this problem was 4.5 $\mu$ while the reference wavelength was 4.1 $\mu$. This band gives an 88% change in transmission in a 1-mm NaCl cell for a 0–1% change in concentration of $EtHSiCl_2$. This huge sensitivity makes it an unusually simple problem for infrared. Figure 4 is a photograph of a recorder chart of the analyzer with the following conditions: (A) 1% $EtHSiCl_2$; (B) 0% $EtHSiCl_2$; (C) 0% $EtHSiCl_2$ plus wire screen in measuring wavelength beam; (D) 0% $EtHSiCl_2$ plus wire screen in combined beams (in front of sample cell).

The difference between (A) and (B) is, of course, the span for maximum and minimum sample component concentration. This, as well as the pen position (zero), is adjustable as described previously. Tracings (C) and (D) are intended to show the insensitivity of the instrument to a gross loss in signal size at both wavelengths. Tracing (C) shows that a wire screen removes 63% of the available light from a beam. Tracing (D) shows that even with a 63% loss of signal (in this case due to the screen) the recorder deflection is about 0.5% of scale or equivalent to an error in component concentration reading of less than 50 ppm.

## References

1. G. J. Hecht, J. A. Edinborgh, and V. N. Smith, paper presented at the Instrument Society of America Conference, Sept. 1959.
2. A. M. Bartz and L. W. Herscher, ISA Trans. **1**, 39 (1962).
3. A. Savitsky and D. R. Bresky, Ind. Eng. Chem. **46**, 1382 (1954).
4. H. G. Conner, W. M. Trippeer, and D. J. Troy, paper presented at the Optical Society of America meeting, Washington, D.C., March 14–17, 1962.

**Applied Optics**

# Of Optics and Opticists

***This column is compiled partly from information sent by our Reporters in various centers of optics across the continent, but the Managing Editor welcomes news from any source***

God grant there never is a paper
So good that even I
Without a stroke from my pencil
Will have to let it by. *R. W.*[*]

This column this month reprints, by kind permission of the author, and of the editor of *Scholarly Books in America*, a discussion by Mark Carroll, associate director of the Harvard University Press, of Authors' Alterations:

It is a bright golden morning when your first galley proofs arrive and you secrete yourself in your study to spend the first of many productive hours in reading your stately prose, set in type for the first time. Admiring what the printer hath wrought, and even more, what thou hast wrought, you hum a merry hum as you savor the intoxicating flavor of your typeset ideas. Chances are your manuscript had your complete and unqualified approval before your editor released it for the printer's attention, so your proofreading task will be a routine one, confined to catching the compositor and the printer's proofreader off base in a missed capitalization, an overlooked broken letter, or a wrong sized numeral. Not wishing to improve on perfection, you resolve (having been warned of the high cost of author's alterations) not to change a jot or tittle of your text. But stop, here is a "that" that better be replaced by a "which", and there is a "which" which would make a singing sentence absolutely lyrical if it were neatly excised and replaced by "that". And there your downfall begins, gentle author, for the unnecessary correction of typeset matter adds to the manufacturing cost of books, multiplies the possibility of error, and subtracts from the expected life span of editors and publishers.

Perhaps we should pause here for definitions. For centuries, printers' compositors have been admonished to follow copy "out the window", and what the compositor reads, he sets. For any author's corrections, i.e., changes in the type he has set that cause it to differ from the original copy given him, the printer charges, whether the changes are to be made by hand or on a fancy typesetting machine, "not less than the hour cost of these operations plus a profit", as a manual of the Book Manufacturers Institute instructs him to do. Permit me to quote, since it states the problem quite well, from a concise discussion of manufacturing procedures.

"With regard to the corrections in the proofs it must be remembered that the more carefully a book is written, the less expense will be incurred for 'author's corrections'. This charge is often a great source of contention between the author, publishers, and printer, and altogether is an unsatisfactory item. A printer is bound, with certain reservations, to follow the copy supplied, and if he does that, and the author does not make any alterations, there is no charge, and nothing to wrangle about. But should there be many emendations in the proof, they may prove disastrous as regards trouble and expense.

"A page of type may contain two or three thousand letters, every word being built up letter by letter and line by line till the page is complete. A small correction, trivial as it may seem to the inexperienced, will possibly involve much trouble to the printer, and the labour on it is not apparent and is only appreciated by a practical man.

"A word inserted or deleted may cause a page to be altered throughout line by line, and a few words may possibly affect several pages. The charges made for corrections are based on the time consumed in making the alterations or corrections, and are very difficult to check, even by an expert."

This admirable statement was made by Charles T. Jacobi, manager of the Chiswick Press in London, in *Some Notes on Books and Printing: A Guide for Authors and Others*, published in 1892. Not much progress has been made since in licking this problem.

To put it another way, this is what Séan Jennett has to say on the subject in *The Making of Books* (Pantheon): "Authors, who, in the printer's eyes, are often the most inconvenient of people, sometimes take it into their heads to add three or four words, or delete them, here and there throughout the proofs. No doubt the alteration changes what was before ordinary and mediocre English into great and memorable language, ensuring the author's fame to furthest posterity, but when it comes to paying for it he is apt to argue. Now adding a word or more in a line means, since all the lines must be of the same length, that the word at the end of the line must come out and be placed at the beginning of the next; while the word at the end of that line is in turn transposed to the beginning of the following one; and so on to the end of the paragraph, every line affected having to be respaced. If the correction occurs at the beginning of a paragraph it may be necessary to reset the entire paragraph. The cost of adding a single word may thus amount to more shillings than there are letters in the word, and the question whether it is really worth while should be carefully considered."

---

[*] Reprinted by kind permission of the Editor of The Chemical Society.

True, there are unavoidable alterations such as the insertion of page numbers on the contents page and in cross-references, the addition of the Library of Congress number, a respacing of the title page or chapter headings. For this reason, to avoid penalizing the author for necessary alterations inherent in the bookmaking process, the publisher usually assumes a percentage of the cost for corrections and additions: beyond this it is usually the author's responsibility.

The practices of individual university presses, as reported by Richard G. Underwood in his excellent 1960 survey on production and manufacturing problems of university presses ranges from the permissive to the punitive. Underwood's breakdown of these practices is pretty sordid reading, but the commonly accepted policy is that the author shall be charged for all costs of alterations exceeding 10 (in some cases 5) percent of the cost of the original composition or typesetting.

Whatever a press's policy, its practice often differs, for it is a known fact that some presses don't charge their embellishing authors anything while others spend countless hours in management overhead time trying to decide just how much (or how little) an author should be charged for rewriting his book in proof. To be sure, in a book on current events, there is some justification (and probably encouragement from the publisher) for changes to make the book as up to date as possible, but in the usual serious university press book, there is no excuse for adding material in proof that could have been added to the typescript. Sometimes a knowledgeable author will cite Sir Winston Churchill's well-publicized practice of treating his proofs as manuscript and running rampant with his pen, but this clearly calls for a rebuttal speech pointing out certain subtle differences in the circumstances surrounding his books and yours.

You may have gathered by now that publishers are unhappy about authors who make unnecessary or excessive changes, and if so, you may go to the head of the class. One publisher's production man I know says flatly, "There should be no author's alterations", and he is probably right, but I point out to him that authors, too, are human and prone to error, and cannot help wanting to better their lot by improving their product. He then trumps me by saying that there is no excuse whatsoever for changing tabular matter (which costs the most to set, and, consequently, to change). He pounds his desk and says, "The copy is either right or wrong and if the latter it should not be put into type." Hear, hear! Editors take notice. Authors, beware.

We have kicking around our offices, used for paperweights or window props, a number of Linotype slugs which read, "Changing even a comma means resetting this entire line, at a cost of 75¢" but we no longer use them to threaten authors since the price has now gone up.

If it cost $2000 to set your 256-page monograph and the compositor making the corrections and changes specified on the proof earns more per hour than you do, it is easy to see how alteration costs quickly mount, particularly since correction is a piecework process, costing more then the original setting by machine. Correction of newly discovered error is permissible: polishing and additions as a result of second thoughts are not. Nor is belated verification of quoted matter. One author I know swore that his poetry quotations were perfect, but on checking the proof an anxious editor quickly proved that they were not: his book is a 274-page study, costing $1575 to set in type, and he was billed $114.46 for excess author's alterations, after the publisher had paid his own part of the bill. Such cases are legion and make publishers gray and authors poorer. Nothing is more plaintive than an author's justification of the afterthoughts that caused him to tinker too much with his proof, and though he is willing to have the changes made at any price, he might well have saved himself money. It should be realized that type is not rubber, that a "w" takes up more space than an "l", thereby complicating the replacement of typeset words with different words containing the same number of characters, and changing even punctuation or capitalization can quickly run up a healthy bill. If authors and editors were tougher on themselves and on each other in making sure that the final approved typescript was as final and as correct as it should be and could be, then time and money, both publishers' and authors', might be saved on every book published. And that could mean more books published and consequently more reviews, more promotions, more foundation grants, more leaves to write more books. Editors, be tough! Authors, be vigilant!

P. Fleury *Paris* and Mrs. Ballard, wife of the OSA President, during an ICO reception at the Pinakothek in Munich August 1962.

Dr. K. Greenland *England* and Dr. and Mrs. E. Ingelstam *Sweden* during a musical interlude in Munich 1962.

# The Optical Society of America

## Officers of the Society

| | |
|---|---|
| *President* | Stanley S. Ballard, Department of Physics, University of Florida, Gainesville, Fla. |
| *President-Elect* | Richard C. Lord, Spectroscopy Laboratory, MIT, Cambridge 39, Mass. |
| *Past President* | David L. MacAdam, Research Laboratories, Eastman Kodak Company, Rochester 4, N.Y. |
| *Executive Secretary* | Mary E. Warga, OSA, 1155 16th Street N.W., Washington 6, D.C. |
| *Treasurer* | Archie I. Mahan, Applied Physics Laboratory, 8621 Georgia Avenue, Silver Spring, Md. |
| *Editor of the Journal of the Optical Society of America* | Deane B. Judd, National Bureau of Standards, Washington 25, D.C. |
| *Editor of Applied Optics* | John N. Howard, AFCRL, Bedford, Mass. |

## Directors-at-Large

** Term expires December 31 of the indicated year.*

Rudolf Kingslake (63)* Eastman Kodak Company, Rochester 4, N.Y.
Earle K. Plyler (63)* Department of Chemistry, Florida State University, Tallahassee, Fla.
David Richardson (63)* Bausch & Lomb, Inc., Rochester 2, N.Y.
Georg H. Hass (64)* ERDL, Fort Belvoir, Va.
R. Clark Jones (64)* Polaroid Corp., Cambridge, Mass.
E. D. McAlister (64)* Scripps Institution of Oceanography, La Jolla, Calif.
W. Lewis Hyde (65)* University of Rochester, Rochester 20, N.Y.
John A. Sanderson (65)* Naval Research Laboratory, Washington 25, D.C.
George Wald (65)* Biological Laboratories, Harvard University, Cambridge 38, Mass.

## Local Sections

*Rochester*
Joseph L. Rood *President*
Robert M. Blakney *President-Elect*
Joseph H. Altman *Secretary*
Research Laboratories
Eastman Kodak Co.
Rochester 4, N.Y.
Vernon L. Parks *Treasurer*

*Detroit*
Richard Majkowski *President*
Carl Leistner *President-Elect*
Daniel L. Harmon *Secretary*
16152 Parkside, Detroit 21, Mich.
Samuel Cohen *Treasurer*

*Niagara Frontier*
E. Schustik *President*
Thomas Frost *President-Elect*
Calvin W. Young *Secretary*
Carborundum Metals Co.
Box 32, Akron, N.Y.
Ray Annino *Treasurer*

*New England*
David S. Gray *President*
Charles Koester *Vice-President*
Geoffrey Harvey *Secretary*
Itek Corporation
10 Maguire Rd.
Lexington, Mass.
William J. Davis *Treasurer*

*Texas*
P. O'B. Montgomery *President*
Harry J. Auvermann *President-Elect*
Norman C. Allen *Secretary-Treasurer*
Texas Instruments, Inc.
Box 6015
Dallas 22, Tex.

*Delaware Valley*
F. J. Warzak *President*
J. E. Tudor *Secretary*
General Electric Company MSVD
3316 Spring Garden Street
Philadelphia, Pa.
M. Consherry *Treasurer*

*Pittsburgh*
Thomas P. Vogl *President*
Jerome J. Wolken *President-Elect*
George L. Buc *Secretary*
Fisher Scientific Company
717 Forbes Street
Pittsburgh 19, Pennsylvania
Irving S. Stapsy *Treasurer*

*Chicago*
Fred Clarke *President*
Donald Pontarelli *Vice-President*
Richard Steck *Secretary*
4556 North Oakview
Chicago 31, Ill.
Howard Padgitt *Treasurer*

*Southwestern Connecticut*
Leonard Eisner *President*
Robert C. Gore *Vice-President*
Martin Rome *Secretary*
Machlett Laboratories, Inc.
1063 Hope Street
Springdale, Connecticut
Edward Speyer *Treasurer*

*Southern California*
Ernest Davidson *President*
Wm. S. Gallaway *Vice-President*
Milton Laikin *Secretary*
1913 Preuss Road
Los Angeles 34, Calif.
Jerome J. Rosenblatt *Treasurer*

*Northern California*
Andrew L. Jorgensen *President*
Clyde C. Shaw *Vice-President*
Harvey Morton *Secretary-Treasurer*
Tinsley Laboratories
2448 Sixth Street
Berkeley, Calif.

*National Capital*
Matthew P. Thekaekara *President*
Frederick W. Paul *First Vice-President*
Harry K. Hammond, III, *Secretary*
National Bureau of Standards
Washington 25, D.C.
Richard S. Hunter *Treasurer*

*San Diego*
John E. Tyler *President*
John H. Taylor *Vice-President*
John M. Hood *Secretary-Treasurer*
Bldg. 4, U.S. Navy Electronics
Laboratory
San Diego 52, Calif.

*Detroit*
Carl J. Leistner *Chairman*
W. K. Lesnick *Chairman-Elect*
D. L. Harmon *Secretary*
University of Detroit
Detroit, Mich.
Samuel Cohen *Treasurer*

**The Optical Society of America was organized in 1916 "to increase and diffuse the knowledge of optics in all its branches, pure and applied, to promote the mutual interests of investigators of optical problems, of designers, manufacturers and users of optical instruments and apparatus of all kinds and to encourage cooperation among them."** The Society invites to membership all who are interested in any branch of optics, either in research, in instruction, in optical or illuminating engineering, in the manufacture and distribution of optical goods of all kinds, or in physiological and medical optics. Further information may be obtained from the Executive Secretary of the Society. **Annual Dues:** Regular members and Fellows, $17.00; Associate members, $13.00; Corporate members, $125.00. These dues include subscription to the Society's official journal, the **Journal of the Optical Society of America**, but not to its other publications.

## editorial . . .

# Wanted: Optical Engineers

A NUMBER OF little-known facts about what is actually a little-known industry were revealed in a special report on optics in Missiles and Rockets' Aug. 22 issue.

The manufacture of precision optics had grown into a significant industry in this country after World War I, when we first discovered that Americans could build optics which were just as good as those built by the Germans and the Swiss, who theretofore had monopolized the field.

M/R's report revealed that the optics share of the missile/space industry will reach $75-85 million next year and is likely to double in the three to five years following; that the American industry is no longer dependent on European techniques; that the optics industry is getting more sophisticated, more competitive—and much larger.

The report also revealed that there is an acute and shocking shortage of trained optical engineers and of optical and photographic scientists in the United States.

There is an almost complete (one industrialist called it "shameful") lack of interest on the part of engineering schools in establishing good courses in optics. Moreover, the few good physicists in the field are not interested in everyday optical engineering.

Thus, just at the time when the Missile/Space Age is levying greater demands on an expanding industry, that expansion is almost certain to be held back and limited by the lack of people trained in optics.

Why? Blessed with 20/20 hindsight, we can easily spot the answer: almost complete lack of foresight and preparedness on the part of both educators and the industry.

For education is, of course, the solution. To educate, however, you must first have teachers. Then you must have students supplied with adequate courses and laboratories.

It seems apparent that the optics industry itself will have to provide these essentials if it is to have the trained people it needs. This can be done in part by financial support to the universities to set up and staff facilities. By means of scholarships promising students can be aimed in the right direction. Cooperative programs, which cost participating companies little, could produce relatively soon the beginning of the needed stream of competent personnel.

The textile industry in the South has followed such programs for years—with scholarships, school facilities and equipment—to provide the bright young men and women to meet the challenge of synthetics. Without the new ideas in manufacturing, industrial management and engineering contributed by these trained new minds, our natural-fiber textile industry probably would not exist at all today.

But this is still not enough. In the case of optics, education must go a step further. Pre-education is necessary, as well as advanced training. The industry must make our high school and early college students aware of the opportunities that exist in optics. The general public, too, should be educated to the importance of optics, its challenges and rewards.

A PARTIAL remedy for the present might be a higher development of computer techniques for optical design. Already finding limited use, computers can solve difficult lens problems and probably can be used for more complex design configurations. The immediate effect of this would be to free optics specialists from routine tasks, and permit them more time for advanced problems.

Optics is not the only industry which should take heed of the manpower shortage. Almost every other business in this Missile/Space Era of leap-frogging technological advancement would do well to look to its own house. Many have already found that lack of skilled technicians is their greatest problem. Obviously, this situation will spread in the future—if individual industries don't start to do something about it now.

**Clarke Newlon**

Reprinted with
the kind permission of the Editor of
**missiles and rockets, August 29, 1960**
**American Aviation Publications**

**Applied Optics**

# Letters to the Editor

*Letters to the Editor should be addressed to the Editor,*
*APPLIED OPTICS, 1155 16th St., N.W., Washington, D.C. 20036*

## Far-Infrared Absorption of Ruby at Liquid Helium Temperature

Armand Hadni

Faculté des Sciences de Nancy, France.

Received 6 May 1963.

At room temperature, the transmission of ruby is relatively low in the far infrared and this would be a common fact resulting from the combination of one photon with a phonon to give another phonon of the same wave vector (vertical transition). At liquid helium temperature, there are not enough phonons to give this absorption, and we have seen that many materials become transparent.[1] This allows absorption studies of ions imbedded in crystals at liquid helium temperature, and we presented recently some spectra which seem to reveal electronic transitions in the far infrared.[2]

We have obtained (Fig. 1) a far-infrared absorption line at 260 μ (38.5 cm$^{-1}$) in concentrated ruby (1.1%). The line disappears when the temperature is raised up to 77°K, but the general transmission is still high. At room temperature the transmission is much lower. The spectrometer is described elsewhere.[3]

Schawlow[4] and Wieder[5] have obtained pulsed maser oscillations simultaneously at wavelengths of 7009 and 7041 A in concentrated ruby. These lines would terminate on states above the ground states at about 40 and 100 cm$^{-1}$, respectively, and they are ascribed to two distinct types of coupled ions of $Cr^{3+}$ in $Al_2O_3$.[4] We have not found any absorption near 100 cm$^{-1}$. However, it has been suspected that the polarized 7041 Å line has an origin not closely connected with the nonpolarized 7009 Å and other neighboring lines. Its intensity, for instance, is not directly related to the concentration of $Cr^{3+}$ ions.[4]

A study of the dependence of the line intensity on concentration is needed to give real evidence that the line is associated with chromium ion pairs.

We plan experiments where chopped far-infrared 260-μ radiation would modulate the population of the 38.5-cm$^{-1}$ level. A partial modulation of a beam of 7009 Å would result and could be detected with a photocell if the relaxation time of the upper state of the far-infrared transition is not too short. This would be a version of Bloembergen's infrared quantum counter proposal.[6]

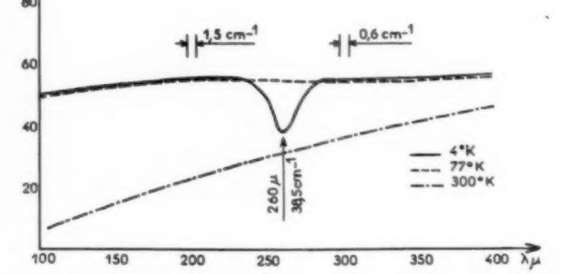

Fig. 1. Far-infrared absorption spectrum of ruby containing 1% Cr. Sample thickness 4 mm.

### References

1. A. Hadni, J. Claudel, E. DeCamps, X. Gerbaux, and P. Strimer, Compt. Rend. **255,** 1595 (1962).
2. A. Hadni, B. Wyncke, P. Strimer, E. DeCamps, J. Claudel, and X. Gerbaux, 3rd Internatl. Symp. on Quantum Electronics, Paris, France, Feb. 1963.
3. A. Hadni, "Instrumentation in the Far-Infrared and Applications of Far-Infrared Spectra", Internatl. Symp. on Far-Infrared Spectroscopy, Cincinnati, Ohio, Aug. 1962; Spectrochim. Acta **79,** 793 (1963).
4. A. L. Schawlow and G. E. Devlin, Phys. Rev. Letters **6,** 96 (1961).
5. I. Wieder and L. R. Sarles, Phys. Rev. Letters **6,** 95 (1961).
6. N. Bloembergen, Phys. Rev. Letters **2,** 84 (1959).

## Feasibility of a Reflecting Coronagraph

H. Zirin and Gordon Newkirk, Jr.

High Altitude Observatory of the National Center for Atmospheric Research, Boulder, Colorado.

Received 25 February 1963.

The Lyot Coronagraph[1] with a single-element objective lens has one serious disadvantage—chromatic aberration. As a result the solar image is precisely focused on the occulting disk, which blocks the image of the solar photosphere, at only one wavelength. Moreover, spectrographic analysis of the chromatic image of the chromosphere or of prominences at the limb of the sun is made extremely difficult by the fact that the slit of the spectrograph receives radiation from a range of different heights above the solar limb. Although achromatic objective lenses of two or three elements reduce these difficulties considerably, such achromats also increase the amount of stray light in the coronagraph. The use of a Mangin mirror to remove the chromatic aberration of a single-element coronagraph lens can produce an accurately achromatic image of the sun on the spectrograph slit; however, the occulting disk must still be placed in the chromatic image of the primary objective. Light of wavelengths other than that focused on the occulting disk is thus vignetted by various amounts. A coronagraph with an objective mirror would obviously have none of the difficulties outlined above.

Although the reflecting coronagraph has long been considered desirable, the pinholes and granular structure, which have always been regarded as inevitable in metals deposited on glass, scatter so much light that such an instrument has always been deemed impractical. (We have, however, been unable to locate published measurements of the scattering from any proposed coronagraph mirror.) Fortunately, the techniques of depositing aluminum on glass appear sufficiently advanced at the present time that a reflecting coronagraph appears feasible.

We have recently tested in the laboratory a prototype coronagraph mirror of fused quartz of 5-cm aperture and 50-cm focal length. The mirror had been coated with aluminum and a thin overlay of quartz for minimum scatter (a proprietary process—Front Surface Aluminum Mirrors No. 749) by Liberty Mirror Division of Libbey-Owens-Ford Glass Company. Our tests show that the light scattered by this objective mirror has a radiance of approximately $1.2 \times 10^{-5}$ that of a source subtending a solid angle approximately equal to that of the sun. The measurement refers to the average radiance of scattered light from approximately 1.1 to 2.0 solar radii from the center of the solar disk.

The scatter from the same mirror before coating was about the same; evidently aluminizing produced an increase in scattering of roughly the same amount as the increase in reflected intensity. This level of scattered light is greater than the radiance of about $10^{-6}$ encountered in the best single-element coronagraph lenses measured in the same manner.[2] (Such lenses usually show an angular dependence of scattering which leads to a radiance of $5 \times 10^{-6}$ at 1′ above the solar limb.) On the other hand, the scattered light from our prototype mirror is similar to the radiance of $\sim 10^{-5}$ characteristic of the best skies at high-altitude mountain observatories.

Our tests indicate, therefore, that the construction of a completely achromatic, reflecting coronagraph is feasible. We are presently building a small prototype instrument to test its practicality.

This research was carried out under an Office of Naval Research contract and a National Aeronautics and Space Administration contract. , We wish to thank J. C. Ogle, Jr. of Liberty Mirror for his assistance.

## References

1. B. Lyot, Compt. Rend. Acad. Sci. Paris **191**, 834 (1930).
2. G. Newkirk, Jr., and D. Bohlin, Appl. Opt. **2**, 131 (1963).

---

# Applied Optics
# Optical Activities in Industry

*reported by FRANK COOKE, 66 Summer Street, North Brookfield, Mass.*
*Mr. Cooke welcomes news and comments for this column which should be sent to him at the above address*

**Problem:** To hold thin glass pieces solid enough for grinding, lapping, and polishing, but without appreciable strain.

One convenient solution is to use double-coated pressure contact tape. Every optical worker has experienced the disappointment of having a flat surface warp beyond tolerance upon being unmounted. Strain introduced by the mounting media, generally wax, causes this twisting. Differences of expansion ratios between the base plate and the work also cause warping because of the "bi-metal thermostat" effect. The double-tape technique functions well for most moderately accurate parts.

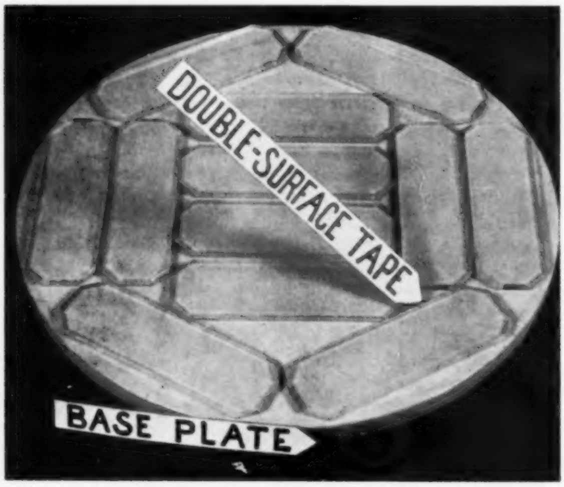

Thin front surface mirrors are shown mounted on a glass base plate. After being pressed down, the edges are sealed with shellac to preclude infiltrating of the lapping and polishing liquids. A surface flatness of four fringes in the 15.2-cm length is obtained. Usual parallelism of 15 sec can be held.

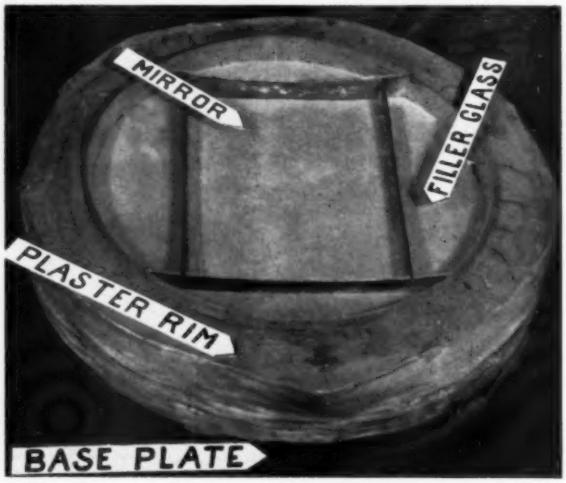

A large 25 cm × 30 cm front surface spherical mirror mounted for diamond wheel roughing in and subsequent polishing. Base plate is of the same glass type to mitigate expansion warping. Edge fillers make up a round form and permit symmetrical polishing pressures.

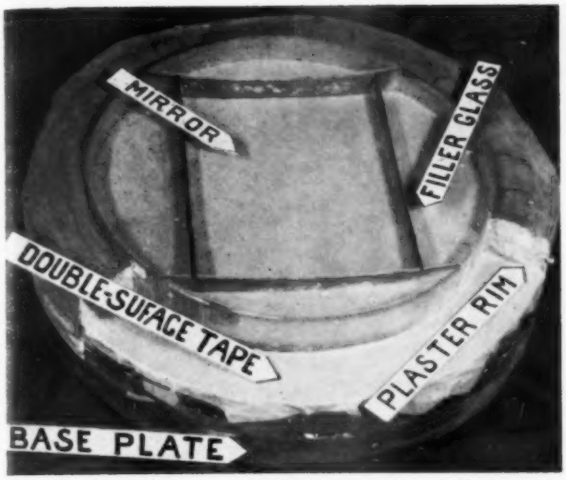

Plaster rim reinforces the assembly so that side thrust of grinding is counteracted. Modeling clay is inserted between mirror and fillers to prevent entrance of liquid. Clay's top is smoothed slightly below working surface, and shellacked.

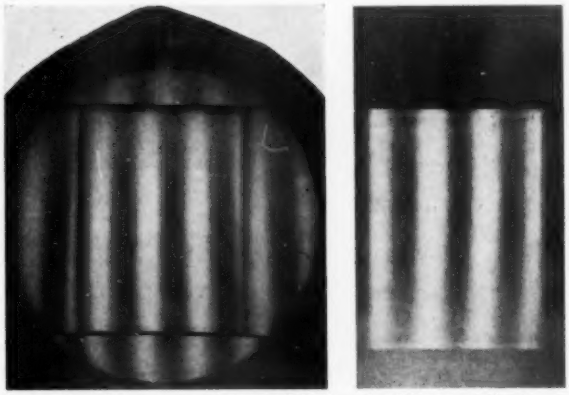

*Left:* Ronchi pattern of the polished and still mounted mirror. Spherical accuracy of $^1/_4$ wave shown. *Right:* After unmounting, the sphere showed not more than $^1/_4$ wave change. Note the lack of rolled edge. Very likely, had this mirror been made in one piece and then sawed out, much more warping would have occurred. Only very well annealed glass would have given this result. Our blank was only commercially annealed.

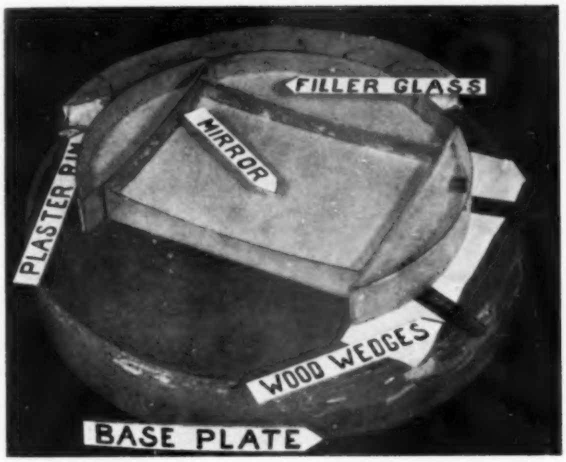

Disassembly shown. Acetone is seeped between the piece and the tape. Thin wooden wedges are used to lift off the pieces.

---

Richard C. Lord *1964 OSA President* (left) and John Sanderson *member of OSA Board of Directors.*

*photo D. L. MacAdam*

## LASER ABSTRACTS

Covering approximately 65 foreign and domestic journals, U.S. and foreign patents, and pertinent technical papers offered at meetings, Lowry-Cocroft Abstracts, 516 Main Street, Evanston, Illinois, is now issuing, on a semimonthly basis, coded 5 × 8 Uniscrt punched cards abstracting the numerous areas of laser technology. The cards contain such information as application, whether theoretical or experimental, and the type of publication—journal article, patent, or government or private report. Preparation of **Laser Abstracts** is directed by Robert L. Pasek, with Lowry-Cocroft Abstracts handling the printing and distribution. The cost is 30¢ per card, and it is expected that subscribers will receive 10 to 20 abstracts in each semimonthly mailing.

# Meetings Calendar

**September**

| | |
|---|---|
| — | Internatl. Commission on Glass, 14th Ann. Mtg., Lausanne *R. Günther, Bockheimer Landstr. 126, Frankfurt am Main, Germany* |
| — | British Assoc. for the Advancement of Science, 125th Ann. Mtg., Aberdeen, Scotland *G. Allen, Burlington House, London, W. 1, England* |
| 2–7 | Internatl. Symp. on Space Technology and Science, Tokyo *I. Tani, Japanese Rocket Soc., Yomiura Newspaper Bldg., 1–3 Ginza-Nishi, Tokyo, Japan* |
| 4–6 | Internatl. Conf. on Information Theory, Sendai, Japan *G. L. Turin, U. of Calif., Berkeley, Calif.* |
| 5–6 | Symp. on the Ellipsometer and its Use in the Measurement of Surfaces and Thin Films, Sheraton-Park Hotel, Wash., D.C. *E. Passaglia, NBS, Wash. 25, D.C.* |
| 8–13 | Illuminating Engin. Soc., Natl. Technical Conf., Detroit, Mich. *W. P. Lowell, Jr., Sylvania Electric Prod., Inc., 60 Boston St., Salem, Mass.* |
| 8–13 | ACS Natl. Mtg., New York City *ACS, 1155 16th St. N.W., Wash. 6, D.C.* |
| 8–15 | Thin Film Optics Colloq., Marseilles *P. Rouard, Faculté des Sciences de Marseille, Pl. Victor Hugo, Marseille 3, France* |
| 9–14 | Union of German Physical Societies, Fall Mtg., Hamburg *Verband Deutscher Physikalischer Gesells., Bundesalle 100, Braunschweig, Germany (Fed. Rep.)* |
| 9–18 | IUCr, Gen. Assembly and Internatl. Cong., Rome, Italy *D. W. Smits, c/o Math. Inst., U. of Groningen, Reitdiepskada 4, Groningen, Netherlands* |
| 9–20 | Microscopic Fusion Methods, McCrone Res. Inst. *J. A. Reffner, McCrone Res. Inst., 451 E. 31 St., Chicago 16, Ill.* |
| 16–18 | 10th Ottawa Symp. on Applied Spectroscopy, Ottawa *J. Kelly, The Steel Co. of Canada Ltd., Wilcox St., Hamilton, Ont., Canada* |
| 15–19 | Internatl. Scientific Radio Union, 14th Gen. Assembly, Tokyo, Japan |
| 23–27 | ISA Instrument-Automation Conf. and Exhibit, Philadelphia *W. H. Kushnick, 313 6th Ave., Pittsburgh 22, Pa.* |
| 23–Oct. 5 | Photomicrography, McCrone Res. Inst. *J. A. Reffner, McCrone Res. Inst., 451 E. 31 St., Chicago 16, Ill.* |
| 24–28 | Photoluminescence of Solids and Liquids Mtg., Toruń *M. Frackowiak, Physics, Nicholas Copernicus U. of Toruń, Grudziadzka 5, Toruń, Poland* |
| 30–Oct. 4 | 11th Internatl. Conf. on Spectroscopy, Belgrade *Sekretarijat, Prirodno-matematički fakultet, Fizičkohemijski zavod, Beograd, Studentski trg 16, Blok C, Yugoslavia* |

**October**

| | |
|---|---|
| — | Internatl. Conf. on the Science of Photography, Turin, Italy |
| — | 4th Internatl. Color Conf., Budapest *M. K. Egyesülete, Szabadság-tér 17, Budapest 5, Hungary* |
| — | IAU, 23rd Exec. Comm. Mtg., Erevan, Armenia, U.S.S.R. *D. H. Sadler, c/o Royal Greenwich Observatory, Herstmonceux Castle, Hailsham, Sussex, England* |
| — | IUPAP, 11th Gen. Assembly, Warsaw, Poland |
| 1–6 | Internatl. Soc. of Photogrammetry, Commissions 1–4 Mtg., Milan *A. L. Nowicki, c/o Army Map Service, 6009 Mass. Ave. N.W., Wash., D.C.* |
| 9–12 | Am. Ceramic Soc. Glass Div., Bedford Springs, Pa. *J. Rood, Bausch & Lomb, Rochester 2, N.Y.* |
| 11–12 | Elementary Particles and the Nucleus, Symp. & Fall Mtg. APS N.Y. State Sect., Olean, N.Y. *J. M. Geiger, Physics, St. Bonaventure U., St. Bonaventure P.O., Allegany, N.Y.* |
| 13–18 | SMPTE, 94th Semiann. Conv., Boston, Mass. *SMPTE, 55 W. 42 St., New York 36, N.Y.* |
| 14–18 | Soc. for Appl. Spectroscopy, El Cortez Hotel, San Diego *E. P. Wadsworth, Jr., Chemistry, San Diego State Col., San Diego 15, Calif.* |
| 16–18 | Am. Vacuum Soc., Boston *AVS, P.O. Box 1282, Boston, Mass.* |
| 17–19 | SPSE Color Photographic Systems Symp., Marriott Motel, Washington, D.C. *SPSE, P.O. Box 1609, Wash., D.C.* |
| 21–23 | 11th Detroit Anachem Conf., Wayne State U., *C. M. Gambrill, Ethyl Corp., 1600 W. Eight Mile Rd., Detroit 20, Mich.* |
| 23–25 | **Optical Society of America Annual Meeting, Sherman House, Chicago** *M. E. Warga, OSA, 1155 16th St. N.W., Wash. 6, D.C.* |
| 28–Nov. 1 | Internatl. Symp. on Plasma Phenomena and Measurements, San Diego *AFOSR, Attn: Lt. Col. C. D. Colchagoff, SRE, Wash. 25, D.C.* |

**November**

| | |
|---|---|
| 7–9 | Acoustical Soc. of Am., Ann Arbor *G. Peterson, U. of Mich., Ann Arbor, Mich.* |
| 12–15 | Magnetism and Magnetic Materials Conf., Atlantic City, N.J. *J. D. Blades, Burroughs Corp. Res. Center, Paoli, Pa.* |
| 12–14 | AFIPS, Fall Joint Computer Conf., Los Angeles, Calif. *P. Huggins, AFIPS, P.O. Box 55, Malibu, Calif.* |
| 13–15 | 5th Ann. Eastern Analytical Symp., Statler Hilton Hotel, NYC *R. F. O'Connell, Sperry Rand Research Center, Sudbury, Mass.* |
| 19–21 | APS, Norman, Okla. *W. A. Nierenberg, U. of Calif., Berkeley 4, Calif.* |

**December**

| | |
|---|---|
| 19–21 | APS, Pasadena *W. A. Nierenberg, U. of Calif., Berkeley 4, Calif.* |
| 26–31 | AAAS, 130th Ann Mtg., Cleveland, Ohio *AAAS, 1515 Mass. Ave. N.W., Wash. 5, D.C.* |

**1964**

| | |
|---|---|
| — | Colloquium on Magnetism, Nottingham, England *IUPAP, Institut d'Optique, 3 boul. Pasteur, Paris 15e, France* |

**January**

| | |
|---|---|
| 19–24 | ACS Natl. Mtg., Denver, Colo. *ACS, 1155 16th St. N.W., Wash. 6, D.C.* |
| 29–31 | Am. Meteorological Soc., ann. mtg., Los Angeles *AMS, 45 Beacon St., Boston 8, Mass.* |

**March**

| | |
|---|---|
| 2–6 | 15th Pittsburgh Conf. on Analytical Chem. and Appl. Spectroscopy, Pittsburgh, Pa. |
| 15–21 | Am. Soc. of Photogrammetry, Am. Cong. on Surveying and Mapping, Washington, D.C. |

**April**

| | |
|---|---|
| — | Am. Ceramic Soc. Glass Div. Chicago *J. Rood, Bausch & Lomb, Rochester 2, N.Y.* |
| — | Internatl. Measurements and Instruments Conf., 3rd, Stockholm *G. Ljungberg, Royal Swedish Acad. of Engin. Science, Box 5073, Stockholm, Sweden* |

## ANNUAL SUBSCRIPTIONS

| | |
|---|---|
| OSA members | $ 6.00 |
| Other AIP societies' members | $ 8.00 |
| Non-members and libraries | $10.00 |
| Single copies | $ 2.00 |

**Subscriptions should be addressed to** Applied Optics **Subscription Handling, American Institute of Physics, 335 East Forty-Fifth Street, New York 17, New York. Eight weeks should be allowed for order processing.**

## ADVERTISING

**Advertising inquiries, orders, plates, and correspondence should be addressed to the APPLIED OPTICS Advertising Office, 1155 Sixteenth Street, N.W., Washington, D.C. 20036 • 202-DI 7-4131 • Mrs. Boraks**

# STRETCHING THE RANGE OF TIME RESOLVED SPECTROSCOPY

*BECKMAN & WHITLEY*
*introduces*

# MODEL 1500 SPECTROGRAPH

For time resolved spectroscopy Model 1500 is a nearly universal instrument. In combination with a high speed streak camera or with an electronic detector, Model 1500 provides a time resolved spectroscopy system that will record information at rates up to $10^{11}$ bits per second with time resolution compatible with electron transition times.

Model 1500 has a wavelength range of from 1500 angstroms to 60,000 angstroms. It is capable of temperature measurement up to 1,000,000° Kelvin and time resolution down to $3 \times 10^{-7}$ seconds when used with Beckman & Whitley high speed sweeping image cameras. The instrument employs all mirror optics which extend its range from the vacuum ultraviolet to medium infrared wavelengths.

Typical applications include the study of aerodynamic heating, hypersonics, gas dynamics, shock tube phenomena, high-speed radiated transients and composition of molecular species.

For complete information about Model 1500 or Beckman & Whitley's photo-recording instruments, write or phone Jack Patterson, Field Sales & Service Manager.

Field Offices: Ridgewood, N.J.; Los Angeles, Calif. Foreign Offices: Tokyo, Japan; Soest, Holland; Karlskrona, Sweden.

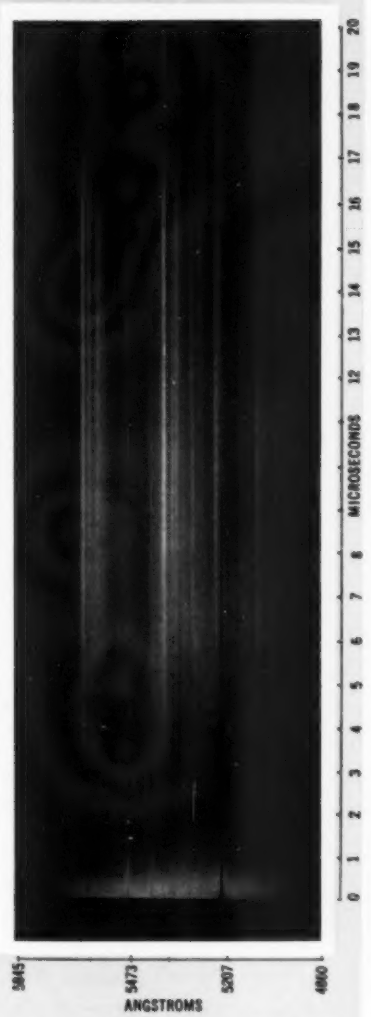

Time resolved spectrographic record of a nichrome bridgewire exploded in air by a 100 joule discharge with an initial voltage of 5000 V. Time resolution: $0.6 \times 10^{-7}$ seconds: spectral resolution: 4.7 angstroms. Recorded with Model 1500 combined with Beckman & Whitley Model 339 Streak Camera.

**Beckman & Whitley**
*a subsidiary of Technical Operations Inc.*
**SAN CARLOS, CALIFORNIA**
**591-8241 Code 415**

In Outer Space
OR AT OCEAN DEPTHS

**lenses give you GREATER DETAIL**

Diffraction Limited offers you a one source responsibility from **research** to computer to finished optics.

**DL for custom design and fabrication for . . .**

- **INDUSTRIAL**
- **EDUCATIONAL AND**
- **DEFENSE APPLICATIONS**

**of all types — includes large optics, aspherics, infrared optics and instrumentation.**

*For a solution to your optical problems call or write:* Tel: 617 275-8212.

Facilities brochure on request.

Diffraction Limited INC.
OPTICS

MIDDLESEX TURNPIKE • BEDFORD, MASS.

## THE SCIENCE OF COLOR

**THIS DEFINITIVE BOOK ON COLOR,** prepared by OSA's Colorimetry Committee and setting forth the history, physics, physiology, psychology, and technology of color vision and color measurement, will be reprinted later this year by OSA.

**LIMITED EDITION.** Twenty-five color plates make this book uniquely beautiful, and, when the original supply of color sheets is exhausted, they cannot be reproduced. Therefore, this edition is limited.

**AUTHORITATIVE DATA,** mostly unavailable in other books, 39 tables, 102 figures, 340 pages of text, 22 pages of bibliography, and 23 pages of glossary-index have all been critically re-examined and corrected. The new **SCIENCE OF COLOR** is therefore the most up-to-date as well as the most complete source book for color science.

**ORDER NOW**
**SEND CASH WITH ORDER**
**PRICE $10.00; OSA MEMBERS $8.50**

**Order Form**

Optical Society of America
Room 101, 1155 16th Street N.W.
Washington, D.C. 20036

Please send one ....... copy of SCIENCE OF COLOR.

☐ Cash/check herewith
☐ $10.00
☐ $8.50 (OSA Member price)

Name ..............................................

OSA Membership # ..............................................

Address ..............................................

Kodak IRTRAN 2 f/1 Lenses for 1-14μ seem to be permeating infrared technology, probably for their thermal, mechanical, and chemical ruggedness. There is no chance of getting a poorly annealed one because they simply don't require annealing. If you can use any on this page, just send the purchase order to Eastman Kodak Company, Apparatus and Optical Division, Rochester 4, N.Y. We can probably ship in a week. If you need more data or more special lenses, phone 716-562-6000, Ext. 5166.

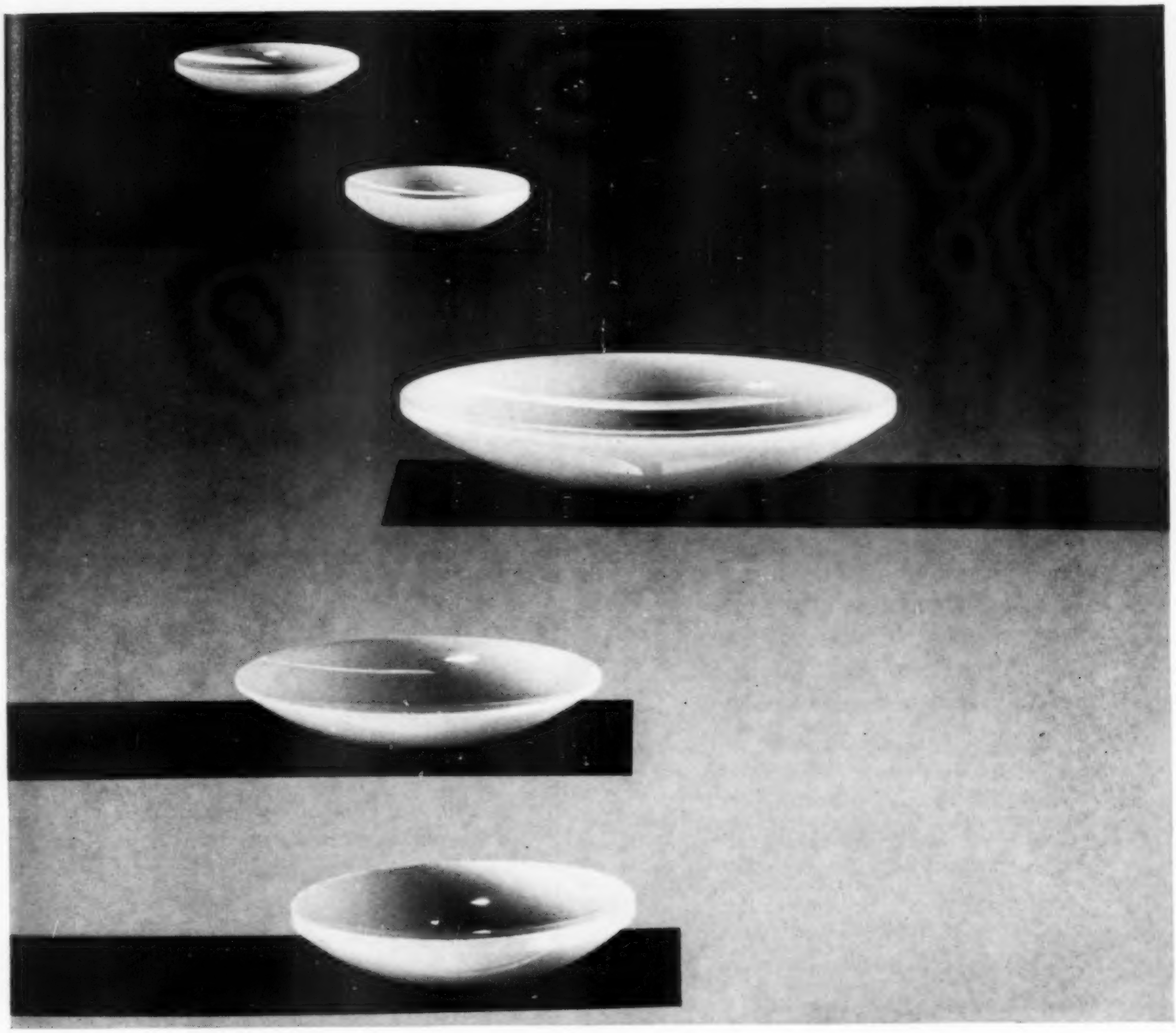

1. **IR-100** equivalent focal length: 25.2mm computed at 1.5μ; 26.4mm computed at 10μ; measured blur circle: 0.36mm*; $77.**

2. **IR-101** equivalent focal length: 25.4mm computed at 3μ; 26.7mm computed at 10μ; measured blur circle: 0.15mm*; $235.**

3. **IR-301** equivalent focal length: 76.2mm computed at 4.26μ; 79.5mm computed at 10μ; measured blur circle: 0.38mm*; $395.**

4. **IR-200** equivalent focal length: 50.6mm computed at 1.5μ; 53.8mm computed at 10μ; measured blur circle: 0.61mm*; $168.**

5. **IR-201** equivalent focal length: 48.8mm computed at 4.26μ; 50.9mm computed at 10μ; measured blur circle: 0.20mm*; $325.**

*diameter of axial image of point source at which measured intensity drops to 5% of center peak intensity, for 2-4.5μ range.

**net price each in 1-10 quantities, subject to change without notice.

30°K
IR COOLING

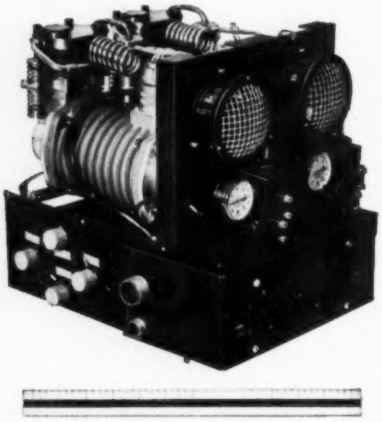

This compressor package is part of a closed-cycle refrigerator capable of cooling a long-wavelength IR detector to 30°K.

Simplified aircraft installation is achieved through the use of quick disconnect couplings and flexible lines between compressor package and cooling head. Complete system weighs only fifty pounds and occupies one cubic foot. Compressor package can be remotely located with only a 12-ounce cooling head at the detector interface.

Vibration, in the infrared system, is avoided by the use of Joule-Thomson refrigeration which requires no cold moving parts.

Air Products manufactures a complete line of critical performance cryogenic refrigeration systems matched to your needs.

For more information, write:

CRYOGENIC REFRIGERATION SYSTEMS
DEFENSE AND SPACE DIVISION

Air Products and Chemicals INC.
ALLENTOWN, PENNSYLVANIA

LASER
GIANT PULSE SYSTEM

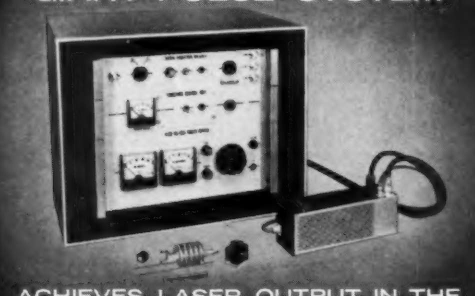

ACHIEVES LASER OUTPUT IN THE 100 MEGAWATT RANGE—AND UP.

Kappa Scientific's Kerr Cell LASER Control System is a precision apparatus for controlling the pulse shape, timing and amplitude of a LASER to achieve a single intense pulse output in the multi-megawatt range.

This system is part of a growing line of LASER products and accessories covered in our new catalog. Write for your copy today.

KAPPA SCIENTIFIC CORPORATION
49 South Baldwin Ave. / Sierra Madre, Calif. / EL 6-1614

MINIATURE LAMPS
Unusual configurations, including filaments, in small or medium quantities

We can produce small or medium production runs of miniature incandescent lamps to your specifications, in unusual configurations, including filaments.

You may also be able to use some of our 14 standard types of miniature lamps, as designed by us for use in our medical diagnostic instruments. A free bulletin is available showing their essential dimensions and electrical characteristics.

Please send for this free bulletin, or write us in detail about your special requirements.

Welch Allyn, Inc., 100 Jordan Rd., Skaneateles Falls, N.Y.

WELCH ALLYN
LIGHTS THE WAY

**OPHTHOS INSTRUMENT COMPANY**

**9600 Overlea Drive, Rockville, Maryland**

- **BROMINE AND CHLORINE ABSORPTION FILTERS**
- **METALLIC HALIDE—WAVELENGTH STUDIES**
- **Th, Fe, NOBLE GASES—CALIBRATION**
- **ELECTRODELESS DISCHARGE LAMPS**

---

*interferometrically controlled Gratings*

*PLANE · CONCAVE · MASTER · REPLICA*

*Write for Particulars*
**DIFFRACTION PRODUCTS, INC.**
*344 Lathrop Ave., River Forest, Ill.*
*Zip Code 60305*

# OCLI ALL-DIELECTRIC ULTRAVIOLET FILTERS

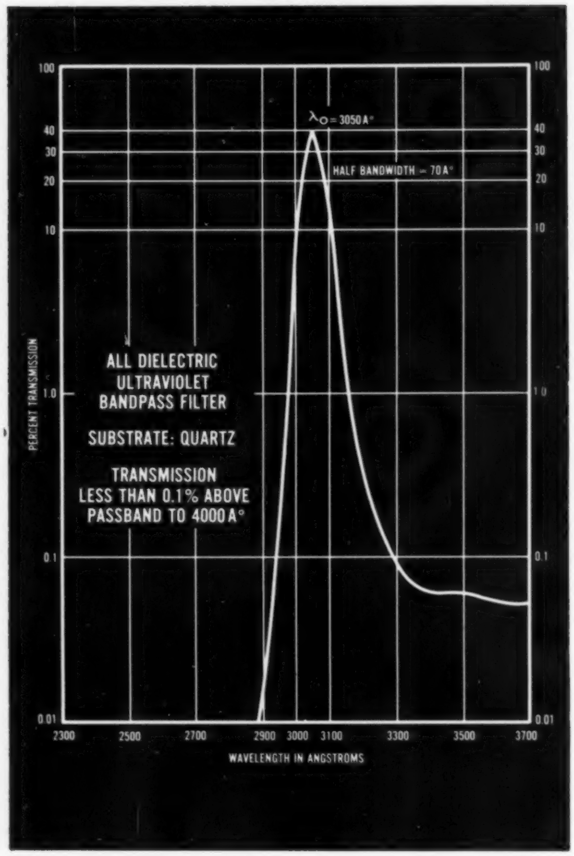

New all-dielectric ultraviolet filters developed by Optical Coating Laboratory offer many advantages over the conventional metal-dielectric ultraviolet filters.

- **Higher transmission in the bandpass.**
- **Narrower bandwidths.**
- **Stronger sideband rejection.**
- **Increased optical stability.**
- **Greater environmental resistance.**

For detailed information about OCLI all-dielectric ultraviolet filters—or improved metal-dielectric ultraviolet filters—contact:

OCLI

OPTICAL COATING LABORATORY, INC.
2789 GIFFEN AVENUE, SANTA ROSA, CALIFORNIA, U.S.A.
Teletype 707-546-4959 Telephone (707) LI 5-6440

**IBM** FEDERAL SYSTEMS DIVISION

## SPACE GUIDANCE CENTER

### Optical Engineers and Lens Designers

The IBM Space Guidance Center is expanding its optical capabilities in the field of airborne and space vehicle instrumentation. This includes applied research and instrument development, and image evaluations.

Specific areas where openings are now available include: Design of projection, optical relay, and photographic systems . . . Sensor development and evaluation for airborne use . . . Semiautomatic image evaluation.

To arrange for a confidential interview with IBM, an Equal Opportunity Employer, please write:

**F. P. Longwell, Dept. 619J**
**Manager, Displays and Optics**
**IBM Space Guidance Center**
**Owego, N. Y.**

**IBM**® INTERNATIONAL BUSINESS MACHINES CORPORATION

## FUTURE MEETINGS

## OPTICAL SOCIETY OF AMERICA

**1963 23–25 October, 48th Annual Meeting,**
**Sherman House Hotel,**
**Chicago, Ill.**

**1964 1–3 April, Spring Meeting,**
**Sheraton Park Hotel,**
**Washington, D.C.**

**7–9 October, 49th Annual Meeting,**
**Statler-Hilton Hotel,**
**New York, N.Y.**

**1965 31 March, 1 and 2 April,**
**Spring Meeting,**
**Statler-Hilton, Hotel,**
**Dallas, Tex.**

Executive Office
1155 16th Street, N.W. Washington, D.C. 20036

NO GUESSWORK HERE

■ Peak image sharpness—without guesswork or estimates—is insured in the new Statimatic* reprographer by calibrating the optical system with LogEtronic's Model C Focatron** Meter. According to Arnold Wheelock of The Plastic Coating Corp., "High quality in offset duplicating masters produced in the reprographer depends critically on sharpest possible focus—we just cannot count on the human eye in unit after unit. The positive, unambiguous indication we get on the Focatron meter does the job far more accurately and quickly."

■ The inspector simply places the target in the copy position, spots the Focatron probe in the projected image on the glass platen, and adjusts the optical system until he gets a peak reading on the meter. That's all.

■ **If you can't afford guesstimates in focusing either, the Focatron Image Sharpness Meter may help you, too. Drop us a line, and we'll send you a Focatron technical bulletin which will tell you the whole story.**

*Reg. Trade Mark **Reg. Trade Mark

LogE Focatron® BY LogEtronics Inc.

500 E. Monroe Ave., Alexandria, Va. TE 6-5180

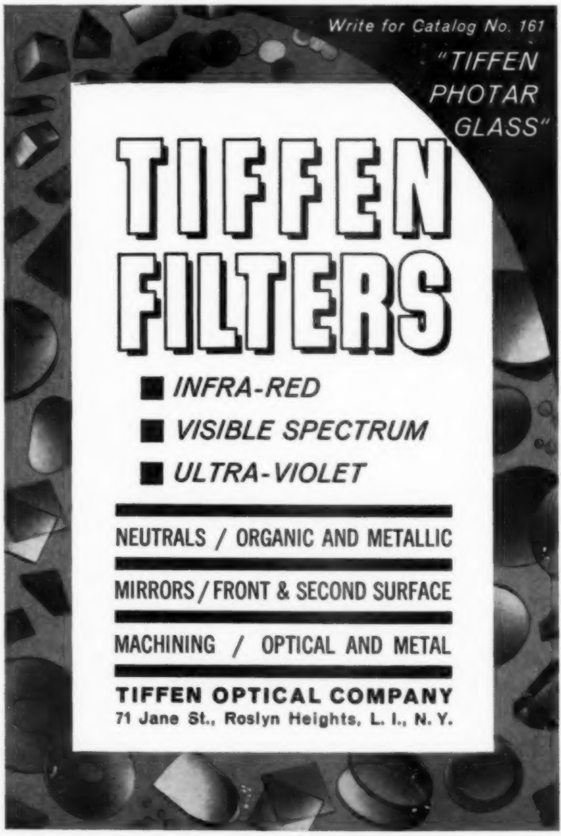

Write for Catalog No. 161 "TIFFEN PHOTAR GLASS"

TIFFEN FILTERS

- *INFRA-RED*
- *VISIBLE SPECTRUM*
- *ULTRA-VIOLET*

NEUTRALS / ORGANIC AND METALLIC

MIRRORS / FRONT & SECOND SURFACE

MACHINING / OPTICAL AND METAL

**TIFFEN OPTICAL COMPANY**
71 Jane St., Roslyn Heights, L. I., N. Y.

*New Catalog . . .*

OPTICAL BENCHES

☐ triangular benches

☐ lathe bed benches

☐ research benches

☐ non-magnetic and student-teaching benches

*Free catalog . . . just ask*

THE Ealing CORPORATION

2239 Massachusetts Avenue
Cambridge 40, Massachusetts

1923 1963

## 40th ANNIVERSARY

Steady growth during the past 40 years, finds us today with an extremely wide variety of essentials that meet the exacting requirements of modern technology.

Our plant, which covers over 20,000 square feet, is producing an ever increasing number of products for both science and industry. It includes an optical division with unsurpassed facilities for grinding, polishing and surfacing, an instrument shop with modern machinery, a high-vacuum coating laboratory as well as a section for the manufacture of diamond-impregnated tools using a sintering process for metal matrix only for working of quartz, glass, ceramics or other hard, brittle material. We also import and distribute the finest optical glass. We'll be glad to study your requirements and give you our recommendations.

## MULTI-LAYER INTERFERENCE FILMS

Made in our New Rochelle High Vacuum Coating Laboratory

For dichroic and achromatic beam splitters and filters. High efficiency. . .Relatively wide band

**Our coatings were used in the first TELSTAR color TV transmission**

**For lasers and masers**

Over 99% reflectivity

| | |
|---|---|
| #530–630 | reflects 530 mμ to 660 mμ |
| #N-6343 | reflects 610 mμ to 710 mμ |
| #N-680 | reflects 670 mμ to 750 mμ |
| #N-1064 | reflects 980 mμ to 1120 mμ |
| #N-1150 | reflects 1120 mμ to 1220 mμ |

Coatings are also available with peak reflectivity at any other desired wavelength.

Unaffected by immersion in liquid nitrogen. Can easily be cleaned with Acetone, Alcohol, or normal detergents.

## ABSORPTION TYPE COLORED OPTICAL FILTER GLASS

Processed in our New Rochelle Optical Shop in about 100 types for the ultra-violet (from 250 mμ), visible, and infrared (to 3000 mμ) spectral regions. Available in flat or as solid bars for the manufacture of tubing for liquid laser excitation.

**Also Anti-Laser Eye-Protection Filter Glass BG-18**

●

## NEODYMIUM DOPED GLASSES
### FOR SOLID STATE LASERS

| Type | LG-2 | LG-4 |
|---|---|---|
| Basic Glass | Borosilicate glass | Lanthanum-Borosilicate glass |
| Doping | 2 weight % $Nd_2O_3$ | 2 weight % $Nd_2O_3$ |

Emission wavelength: 1.06 μ

**FISH-SCHURMAN CORPORATION**
**90 Portman Road, New Rochelle, N. Y.**

## LIGHT BEAM SPLITTERS

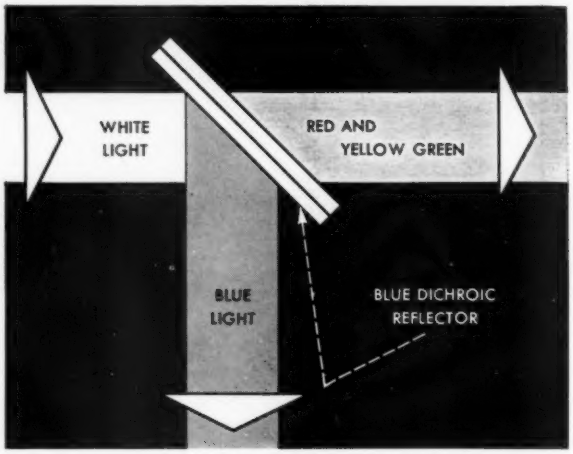

## *Dichroic reflectors can put light and heat to work as you specify*

What do you want to do with a light beam? In millimicrons, what wave lengths do you want reflected? Where do you want spectrophotometric reflection to peak?

Liberty Mirror offers a standard line of dichroic coatings that reflect 90% or more of incident light in wave lengths from as low as 350 millimicrons up to 1,000 millimicrons. If a Hi-Efficiency dichroic coating hasn't already been pinpointed to meet your specifications, Liberty Mirror will develop one that does.

Vacuum-deposited coatings of various metals are used to make front-surface mirrors, neutral filters, transparent mirrors, high-efficiency beam splitters, beam-splitting dichroic mirrors and filters. Metallic and transparent electrically conducting coatings are available for resistance heating. Static-dissipating and high-frequency shielding coatings are also available.

Applied to all types of glass, metal or plastic, the coatings are used in such varied products as scientific and optical instruments, cameras, toys, pin setters, wheel-aligning equipment, aircraft and missiles. Free data sheets are available on all coatings.

Write L·O·F, Liberty Mirror Division, 5593 Libbey·Owens·Ford Building, Toledo 2, Ohio.

LIBERTY
MIRROR DIVISION
LIBBEY·OWENS·FORD

MADE IN U.S.A.
LOF
GLASS

When
you
think
of

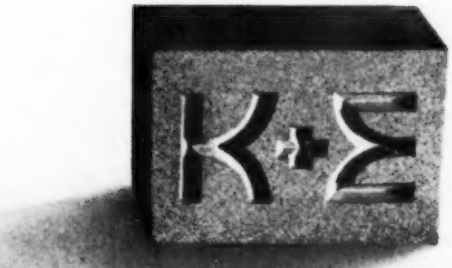

Undoubtedly you think of slide rules . . . transits . . . tracing paper. Correct? But to round out the picture, please enter K&E in your file for these highly advanced space-age instruments . . .

SPACE AND MISSILES SYSTEMS

Solar and Star Simulators • Cine and Special Theodolites • Antenna Contour Checking Instruments • Contour Probing Instruments • Polaris Guidance and Fire Control Instruments • Collimation Test Instruments • Deviators • Borescopes — Electronic and Visual

R&D AND LABORATORY INSTRUMENTS

Auto-Collimators — Electronic and Visual • Electronic Levels • Gravity Reference Instrument • Jig Theodolite • Angle Index Tables and Read-out Devices • Gratings • Targets and Special Scales

INSTRUMENTS FOR MANUFACTURING, INSPECTION, QUALITY CONTROL

A complete line of alignment instruments and accessories

Want specific product information? Write K&E today. Our O&M Division can assist you with R&D.

OPTICS AND METROLOGY DIVISION

**KEUFFEL & ESSER CO.**
HOBOKEN, NEW JERSEY

3704

# HIGH RESOLVING POWER APPARATUS

The development of the maser and laser has substantially broadened the use of high resolving power apparatus. Hilger & Watts now provide a comprehensive selection of equipment to meet the increased requirements.

Among the more important are etalon and interferometer plates — ranging from 20 mm. aperture to 100 mm. aperture; with flatnesses to 1/200 of a wavelength. Mounts for these plates, as well as wave length spectrometers designed to accommodate etalons within the instrument, are standard stock items.

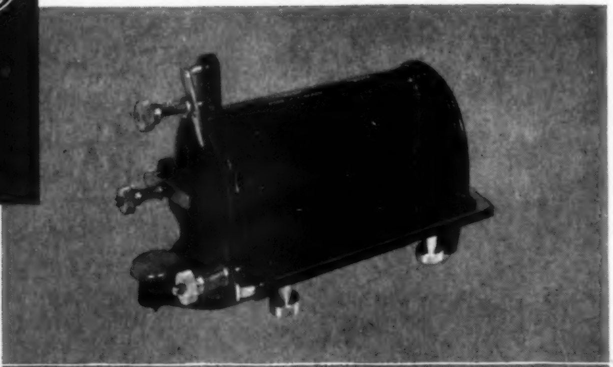

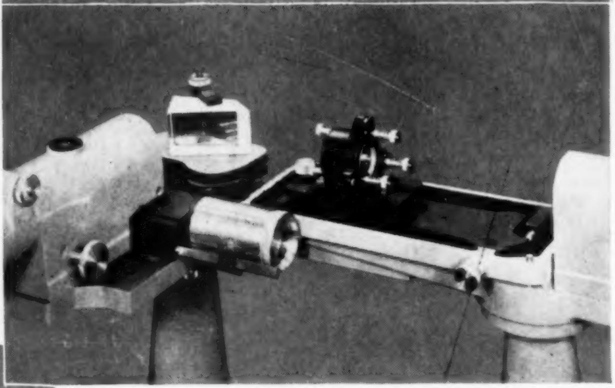

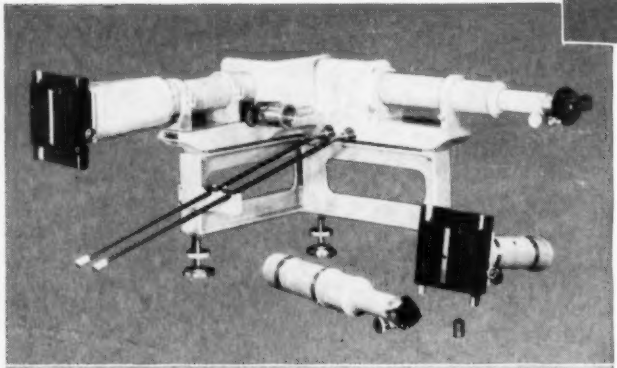

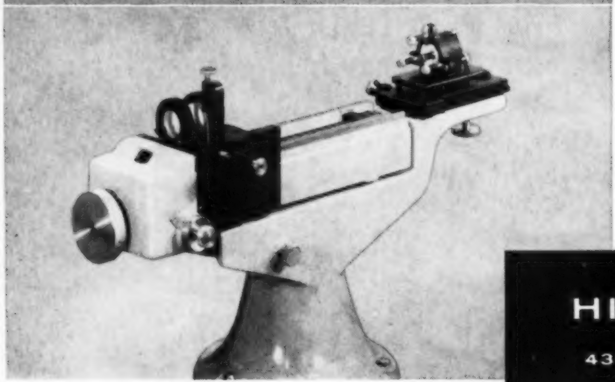

Other new developments include: motor driven Fabry-Perot and Michelson interferometers with fringe counting and amplitude measuring equipment; dielectric coatings for all plates. Lummer-Gehrcke plates and transmission echelon gratings are also available.

*Illustrated Top Right—*
B345 100 mm. Aperture Etalon

*Illustrated Center Right—*
D186 Spectrometer with Etalon mounted

*Illustrated Center Left—*
D260 Large Aperture Spectrometer with Etalon

*Illustrated Bottom Left—*
N34 Interferometer with Etalon

**HILGER & WATTS, INC.**

431 SOUTH DEARBORN ST. CHICAGO 5, ILL.

Sales, Service, Parts by

**ENGIS EQUIPMENT COMPANY**

CHICAGO 5, ILL.

• *Ask for individual catalog sheets and for complete instrument listing.*